行政院國家科學委員會專題研究計畫 期末報告

典型抽水所引致三維壓密沉陷解析

計 畫 類 別 ：個別型
計 畫 編 號 ：NSC 100-2221-E-216-025-
執 行 期 間 ：100 年 08 月 01 日至 101 年 10 月 31 日
執 行 單 位 ：中華大學土木工程學系

計 畫 主 持 人：呂志宗

計畫參與人員：碩士班研究生-兼任助理人員：謝適任

公 開 資 訊 ：本計畫可公開查詢

中 華 民 國 102 年 01 月 31 日

中 文 摘 要 ： 本研究旨在探討週期性抽水、非點狀抽水及瞬時抽水等所引致之地表位移、地層有效應力變化及地層超額孔隙水壓等，數學模式中，擬引用 Biot 之三維壓密理論，將地層模擬為均質等向或橫向等向性之多孔隙的彈性半無限域，本研究擬採用符號運算軟體 Mathematica 與積分轉換方法，推導出各種典型抽水速率所引致的暫態暨長期之地層反應的閉合解。各項研究成果均將進行參數影響分析，並將所獲得之研究成果製作成容易應用之工程圖表，以利於其在工程上之應用。

中文關鍵詞： 抽水，孔彈性力學，積分轉換，半無限域，閉合解。

英 文 摘 要 ： This study presents the ground surface displacements, effective stresses and excess pore water pressures induced by periodic groundwater withdrawal, non-point groundwater withdrawal, and transient groundwater withdrawal, etc., in a homogeneous isotropic/cross-anisotropic poroelastic half space. The formulation of the mathematical model is based on Biot’s three-dimensional consolidation theory of porous media. Using symbolic computation with Mathematica and integral transforms, the closed-form solutions of the transient and long-term responses of the stratum subjected to some typical pumping rates are derived. The consolidation affected by the critical consolidation parameters are illustrated and discussed. Appropriate figures are constructed for the engineering applications.

英文關鍵詞： Groundwater Withdrawal, Poroelasticity, Integral Transform, Half Space, Closed-form Solution.

行政院國家科學委員會補助專題研究計畫 □期中進度報告 ☑期末報告

典型抽水所引致三維壓密沉陷解析

計畫類別：☑個別型計畫　□整合型計畫
計畫編號：NSC100－2221－E－216－025－
執行期間：100 年 8 月 1 日至 101 年 10 月 31 日

執行機構及系所：中華大學土木工程學系

計畫主持人：呂志宗
共同主持人：
計畫參與人員：謝適任

本計畫除繳交成果報告外，另含下列出國報告，共 1 份：
□移地研究心得報告
☑出席國際學術會議心得報告
□國際合作研究計畫國外研究報告

處理方式：除列管計畫及下列情形者外，得立即公開查詢
□涉及專利或其他智慧財產權，□一年□二年後可公開查詢

中　華　民　國　102　年　1　月　31　日

摘　　要

本研究旨在探討週期性抽水、非點狀抽水及瞬時抽水等所引致之地表位移、地層有效應力變化及地層超額孔隙水壓等，數學模式中，擬引用 Biot 之三維壓密理論，將地層模擬為均質等向或橫向等向性之多孔隙的彈性半無限域，本研究擬採用符號運算軟體 Mathematica 與積分轉換方法，推導出各種典型抽水速率所引致的暫態暨長期之地層反應的閉合解。各項研究成果均將進行參數影響分析，並將所獲得之研究成果製作成容易應用之工程圖表，以利於其在工程上之應用。

關鍵詞：抽水，孔彈性力學，積分轉換，半無限域，閉合解。

ABSTRACT

This study presents the ground surface displacements, effective stresses and excess pore water pressures induced by periodic groundwater withdrawal, non-point groundwater withdrawal, and transient groundwater withdrawal, *etc.*, in a homogeneous isotropic/cross-anisotropic poroelastic half space. The formulation of the mathematical model is based on Biot's three-dimensional consolidation theory of porous media. Using symbolic computation with Mathematica and integral transforms, the closed-form solutions of the transient and long-term responses of the stratum subjected to some typical pumping rates are derived. The consolidation affected by the critical consolidation parameters are illustrated and discussed. Appropriate figures are constructed for the engineering applications.

Keywords: Groundwater Withdrawal, Poroelasticity, Integral Transform, Half Space, Closed-form Solution.

目　　錄

摘要 …… I

ABSTRACT …… II

目錄 …… III

一、前言 …… 1

二、研究目的 …… 2

三、文獻探討 …… 2

四、研究方法 …… 3

五、結果與討論 …… 4

參考文獻 …… 5

附錄 1　研究成果投稿後已被接受之 EI 等級期刊論文一篇 …… 附 1

附錄 2　研究成果投稿後依審查意見修訂中之 EI/SCI 等級期刊論文一篇 …… 附 30

附錄 3　研究成果投稿後已發表於 EI 等級之國際會議論文(第一篇) …… 附 61

附錄 4　研究成果投稿後已發表於 EI 等級之國際會議論文(第二篇) …… 附 74

附錄 5　出席國際會議並擔任會議主持人之心得報告 …… 附 86

附錄 6　初步整理後擬進行投稿之其他相關研究成果(1) …… 附 95

附錄 7　初步整理後擬進行投稿之其他相關研究成果(2) …… 附 104

附錄 8　初步整理後擬進行投稿之其他相關研究成果(3) …… 附 111

附錄 9　參與本計畫案之兼任研究助理謝適任同學的碩士論文：單井抽水所引致軸對稱彈性沉陷之研究 …… 附 119

一、前言

歷年來超抽地下水所引起的地層下陷問題一直廣受國人重視，審視民國 101 年以來與該主題相關之研究計畫案發現，除本計畫案以外，至少仍有 16 個相關之研究計畫案仍獲得各界之經費支持[1-16]，其中有 12 個研究計畫案[1-12]是由國科會予以經費支持、3 個研究計畫案[13-15]是由水利署給予經費補助、另有 1 個研究計畫案[16]是由農委會給予經費補助。這些計畫案[1-16]與本計畫案[17]所欲探討之研究主題，均是當今各界相當關注之抽水所引致的地層下陷之相關議題。

如圖 1 所示，計畫申請人自服務於教職以來，即兢兢業業從事於研究工作，並擬訂適合個人之研究主題，曾多次獲得國科會之經費補助，對累積個人之研究潛能，提昇個人之研究水平，助益甚大。今本研究計畫案能順利執行完畢，最重要的就是能獲得國科會之經費補助，謹致個人萬分之謝忱。

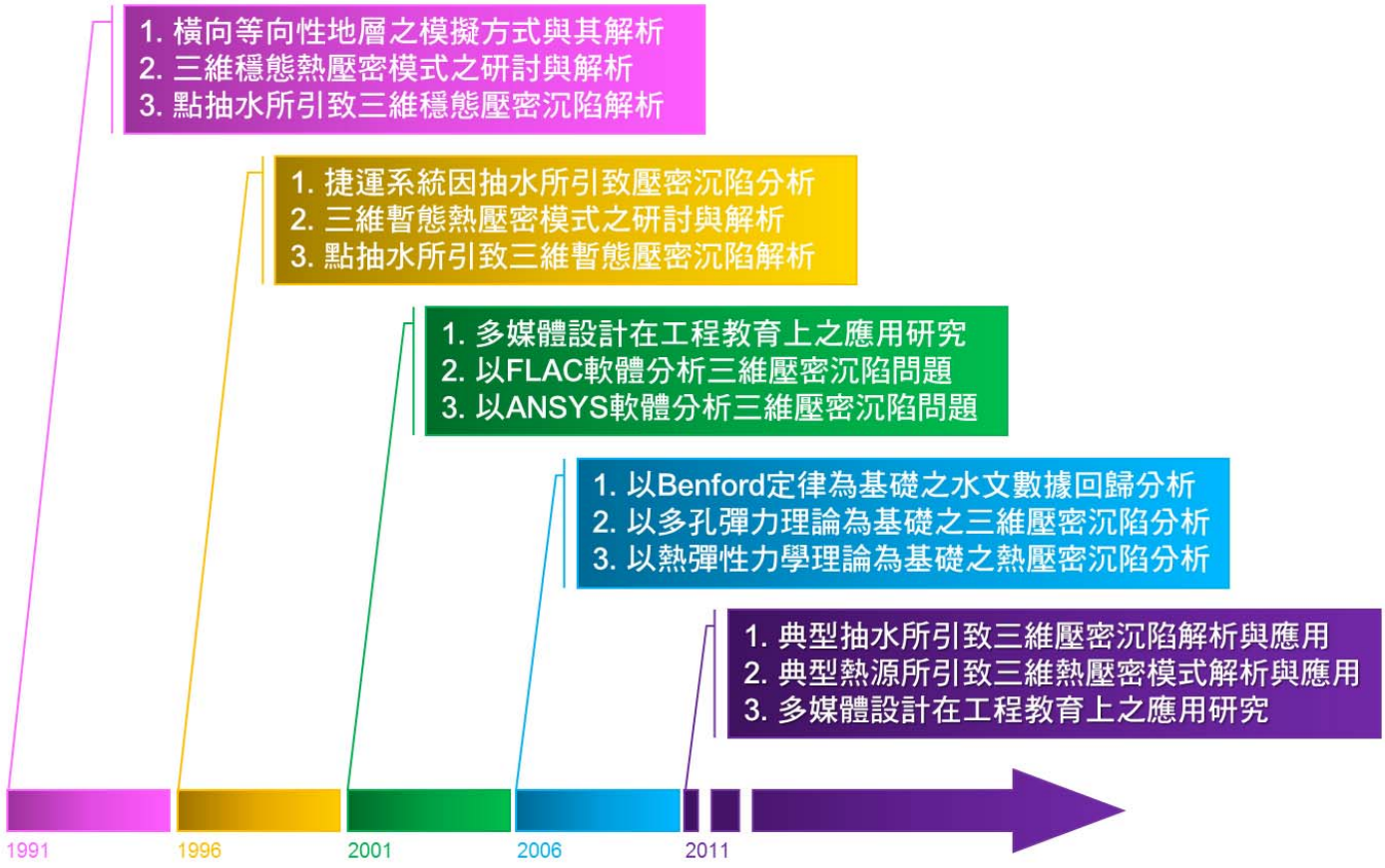

圖 1　計畫主持人歷年來之研究主題規劃說明

本計畫案之各項研究成果如附錄 1~9 所示，共計包括：

1. 已發表於 EI 等級期刊論文一篇[18]，如附件 1 所示。
2. 投稿後依審查意見修訂中之 EI/SCI 等級期刊論文一篇[19]，如附件 2 所示。
3. 已發表於 EI 等級之國際會議論文兩篇[20，21]，如附件 3 與附件 4 所示。
4. 研究成果經初步整理後擬繼續進行投稿之論文三篇[22-24]，如附件 6 至附件 8 所示。
5. 出席國際會議並擔任會議主持人，如附件 5 所示。
6. 人才培育：指導參與本計畫案之兼任研究助理謝適任同學完成其碩士論文「單井抽水所引致軸對稱

彈性沉陷之研究」[25]，如附件 9 所示。

本研究已研討出瞬時抽水[22]、週期性抽水[24]、點狀抽水[18，22，25]、圓形平面抽水[21]及線狀抽水[23，25]等所引致之地表沉陷、水平位移及地層超額孔隙水壓等。由於抽水問題與熱壓密問題具有類比關係，故亦將部分研究成果應用於熱作用源所引致的熱壓密問題之解析[18-20]。

二、研究目的

水為維繫所有生態體系運作之所需，地球上的水分布於各個角落，包括海洋、冰川、河川、湖泊、地層及大氣中。台灣雖然平均降雨量約為世界平均降雨量之 2.6 倍，但由於降雨多集中在 5~10 月之豐水期，故每人所分配之平均降雨量約只有世界平均值的 1/6，因此抽用地下水為解決用水問題的辦法之一，但由於大量使用並且管制成效不彰，導致地層下陷問題日益嚴重。當地下水因人為使用而被抽取出來時，原先由固體土壤與孔隙水共同承擔之荷重，會逐漸移轉至固體土壤上，故造成壓密(Consolidation)現象，所造成的地表下陷情況稱為壓密沉陷(Consolidation Settlement)。地層下陷的過程通常不易被發現，往往在排水設施功能降低、地下管線受損及土地淹水時才被發現，所以有人稱其為沉默的土地危機。台灣因工程上或是經濟上的因素過度抽取地下水且未考慮適當的補注機制，已造成不少縣市深「陷」危機，不只造成國土的流失，且對民生安全的影響亦甚鉅。

地層下陷為目前世界各國普遍遭遇的問題，其成因包括自然因素與人為因素兩方面，而過量抽取地下水乃是最嚴重的人為影響因素。地下水並非不可抽用，在台灣地下水也是解決部分季節缺水危機的辦法之一，但如何適量的取用，才不會造成無法挽回的後果是相當重要的。台灣西部沿海由於養殖業的發展，過量抽取地下水，已造成相當嚴重的地層下陷，致使地下水層的水位面下降、海水入侵地下水層、地下水層被汙染、土壤鹽化、排水不易等惡果。由於地層下陷為不可逆之現象，故應以嚴肅態度面對。

為解決抽水所引致的地層下陷問題，除依賴適當的教育宣導與法規的訂定，改變國人用水習慣與觀念外，亦應從工程上之學理分析層面切入，進行相關之學理分析，藉以瞭解抽水所引致的地層下陷機制與沉陷結果，其關鍵課題包括抽水所引致的地層位移變化量、及地層孔隙水壓變化量等的探討，本研究擬分別探討瞬時抽水[22]、週期性抽水[24]、點狀抽水[18，22，25]、圓形平面抽水[21]及線狀抽水[23，25]等所引致之三維壓密沉陷，並繪製相關之應用圖表，使有助於瞭解此一問題的關鍵影響因素及其影響結果，研究成果希冀能提供相關主管機關做為訂立相關規範之參考依據。

三、文獻探討

除本國外，抽水所引致的地層下陷亦是世界各國在經濟發展過程中常見的問題[26-35]，這些國家不僅包括中國大陸[26-28]、墨西哥[29，30]、泰國[31，32]、希臘[33，34]，連已開發國家如美國[35]、日本、義大利等等國家亦然，因這一類的問題，常是世界各國於經濟發展過程中，於面對水資源不足的課題時，必須使用地下水為替代性水資源所導致的問題。

探討地層因抽水所引致之力學與滲流行為變化問題時，常引用多孔介質壓密理論（Consolidation

Theory）建立問題之基本方程式。Terzaghi[36]首先提出單向度之壓密理論，其係以有效應力的觀念，說明土壤的單向度壓密過程。在陸續的研究中，Biot[37]所建立之耦合三維壓密模式，一般公認較為嚴謹合理，而廣受重視，此一理論模式，Biot[38]曾將其推廣至異向性介質情況。基於 Biot[37，38]壓密模式，Rice 與 Cleary[39]曾改寫 Biot 之耦合三維壓密模式，因其基本參數較易由試驗獲得，故所建立之基本方程式較常被引用。Booker 與 Carter[40-43]曾解析單點抽水所引致的半無限域壓密沉陷問題，數學模式中地層係模擬為均質等向性之線彈性飽和多孔介質，地下水的滲流則模擬為等向性[40]或橫斷面等向性[41-43]模式；Tarn 與 Lu[44]則進一步探討地層力學與滲流性質均模擬為橫斷面等向性情況下，抽水引致的半無限域地層下陷問題，其中地表面係模擬為透水暨不透水兩種情況；Barends[45]、Worsak 與 Chau[46]等人亦曾解析半無限域中之單點抽水所引致的地層下陷問題。直到如今，這一類問題仍廣受各界的重視[47-57]。

根據各界對抽水所引致地層下陷問題之學理分析發現，抽水時除會引起地層下陷外，亦會引起地層之水平位移，國內外亦已有許多相關之文獻[47-52]的監測結果印證此一結論。然而，地層水平位移常被忽略卻是事實，根據計畫主持人的研究發現[53-56]，當地表模擬為透水情況時，抽水所引致之最大地表水平位移，約為地表最大沉陷量之 30%，顯然這是地表水平位移不宜忽略的重要學理依據；以學理分析為基礎之相關研究成果，亦已有許多文獻[57-60]證明抽水所引致之地表水平位移相當顯著。本計畫之研究探討內容，亦包括抽水所引致之地表水平位移量之估算。

Tenney 等人[61]、Tenney 與 Lastoskie[62]曾探討地下水整治時，瞬時抽水問題之數學模式與其解析，但僅探討其滲流行為，並未進一步研討出所引致的壓密沉陷量。Renner 與 Messar[63]則研究週期性抽水試驗，對地下水位變化的影響；Propst[64]、Townley[65]、Gendelman 等人[66]、及 Zhao 等人[67]亦曾探討類似的問題。關於含水層的模擬方式，可包括自由含水層、限制含水層及半無限域含水層等模擬方式。有關線狀抽水的模擬方式，亦為近年來各界之研究重點。這一類問題，計畫主持人均已順利以 Biot 三維壓密沉陷理論為基礎，推導出問題的閉合解[17-25]。

一般而言，以數學模擬（Mathematical Modelling）方式探討抽水所引起的地層下陷問題前，基本而重要的課題是需能事先研討出地層受單點抽水影響時，其所引起的地層力學與滲流行為變化之解析解，因為這類的解相當關鍵，故亦稱為基本解（Fundamental Solution）。只要這類問題的解可以取得，則任意形態之抽水的影響，只要對所研討出之解作適當之積分，即可研討出各類相關問題之解。計畫主持人以往已研討出一系列問題之基本解，本計畫係將問題延伸至瞬時抽水[22]、線狀抽水[18，22，25]、週期性抽水[24]和圓形平面取水[21]等所引起的三維壓密沉陷問題之閉合解的解析，並已順利研討出各類問題的閉合解。本計畫於執行過程中，計畫主持人是將 65%左右的時間、人力與資源等投入於本計畫案中，其餘的時間、人力與資源等則專注於：(1)研究成果的投稿。(2)留意世界各國關於這一類問題的最新研究趨勢與成果。(3)人才的培育等。

四、研究方法

本研究係採用數學模擬(Mathematical Modelling)的方式進行相關之研究，並推導出問題之理論解析解(Theoretical Analytical Solution)，使用理論解析方式推估合理之壓密沉陷量。數學模式中乃將含水層模擬為一半無限域(Half Space)，含水層力學行為與滲流性質是考慮為均質(Homogeneous)等向性(Isotropy)或橫向等向性(Cross-anisotropy)，並考慮含水層為完全飽和狀態，且適於引用線彈性飽和多孔

介質彈性力學理論建立數學模式。基於此，研討出地層受抽水作用影響時之穩態(Steady State)或暫態(Transient)壓密沉陷解析解，其中抽水強度與抽水速率考慮為定值，此外地表邊界則模擬為完全透水與完全不透水兩種情況加以探討。

本研究基於 Biot 三維壓密理論，並根據以往所推導出之點抽水所導致地層下陷問題的基本解(Fundament Solution)，利用積分轉換方法(Integral Transform)與符號運算軟體 Mathematica 輔助積分之運算，用以討論因瞬時抽水[22]、線狀抽水[18，22，25]、週期性抽水[24]和圓形平面取水[21]等所引起的壓密沉陷問題，所研討出之解包括含水層的垂直位移、水平位移與超額孔隙水壓變化等，並繪製出相關之工程應用圖表。各項研究結果均可使用簡單之數學符號加以表達，故稱之為閉合解(Closed-form Solution)，此亦可為邊界元素法等數值模擬方法建立研究基礎。

本文之研究成果可應用於以下所述工程實務情況：(1)若能取得含水層的基本水文地質參數資料，即可進行簡易之沉陷量的估算，因本文是採用線彈性理論進行數學模擬，故通常沉陷量估算結果會較大，與工程上常希望進行保守評估相符。(2)若能確實考慮以下各種尺度因素的影響，包括含水層厚度、抽水深度、抽水量、抽水型態、抽水所引致之沉陷影響範圍等，則各項研究成果均可提供工程界於進行沉陷量估算時之參考。

五、結果與討論

本研究旨在引用數學模擬方式，探討抽水所引致的地表邊界沉陷量、水平位移量與超額孔隙水壓等，係採用 Biot 三維壓密理論建立基本方程式，將抽水行為模擬為點抽水、瞬時抽水[22]、線狀抽水[18，22，25]、週期性抽水[24]和圓形平面取水[21]等情況，並將地表邊界模擬為透水和不透水兩種滲流邊界條件。研討過程中有引用點抽水問題之基本解，再對其進行線積分或面積分的運算，推導出各類抽水所引致之壓密沉陷行為。經仔細研究與討論後，獲得以下結論：

1. 含水層柏松比對抽水所引致壓密行為有重要的影響：當含水層之柏松比變大時，地層較容易產生變形，因此會反映出較大之地表沉陷。
2. 模擬線狀抽水行為時，就取水長度與井深的比值之影響而言：當取水長度與井深的比值增加時，地表沉陷量也呈增加的現象，這是因為取水長度增加時，代表抽水量也會增加，故壓密沉陷量也跟著增加。
3. 各種抽水行為之模擬均呈地表滲流邊界條件有重要的影響：地表模擬為不透水情況下所引致的地表沉陷會較大，這是因為當地表面模擬為不透水邊界時，抽水所引起之負的超額孔隙水壓無法消散，含水層之有效應力因而升高，壓密沉陷之效應變大，故所導致的地表沉陷量會變大。
4. 抽水所引起的地表水平位移量會在水井邊逐漸升高後逐步降低：這是因為單井抽水所引起的地表水平位移是一軸對稱問題，故地表面在對稱點上之水平位移量應為零；另外，含水層遠處受抽水擾動的影響很小，故地表遠處之水平位移量亦很小，因此抽水所引起的地表水平位移量會在水井邊逐漸升高後逐步降低。另外，點抽水所引致的地表最大水平位移是落在$r = \sqrt{\phi}h \backsimeq 1.272h$位置上，其中符號 r 表徑向距離座標變數，h 是抽水深度，ϕ則是黃金數，$\phi \backsimeq 1.618$。

基於以上研究成果，擬對未來提供一些研究方向與建議：

1. 後續之研究可考慮進行視窗程式設計，讓使用者僅需輸入簡單之參數即可快速求得三維壓密沉陷之各項結果，以利研究成果之工程應用與推廣。

2. 可引用多孔介質彈力理論與熱彈力理論之類比關係，將相關研究成果推廣至熱彈性力學問題的應用與解析。

參考文獻

1. 葉弘德，2012/8/1~2013/7/31，「具不規則邊界且為非均質非等向水層的解析解」，國科會補助專題研究計畫，NSC99-2221-E009-062-MY3。

2. 譚義績，2012/8/1~2013/7/31，「地層下陷分析監測、防護管理與防治策略研擬-總計畫暨子計畫:利用類神經網路解析地下水位變化與地層下陷參數關聯性(I)」，國科會補助專題研究計畫，NSC101-2625-M002-008。

3. 羅偉誠，2012/8/1~2013/7/31，「地層下陷分析監測、防護管理與防治策略研擬-子計畫:地層下陷區域下陷量及海水入侵預測趨勢之研究(I)」，國科會補助專題研究計畫，NSC101-2625-M006-007。

4. 張誠信、陳世楷，2012/8/1~2013/7/31，「整合水質、水量及水文地質空間變異資訊評估地下水使用在水資源永續經營之角色」，國科會補助專題研究計畫，NSC100-2410-H424-017-MY2。

5. 張良正，2012/8/1~2013/7/31，「因應環境與社會變遷之穩定供水與減災總合政策研究-子計畫:區域地下水補注機制探討及管制與運用策略研究(I)」，國科會補助專題研究計畫，NSC101-2625-M009-003。

6. 徐國錦，2012/8/1~2013/7/31，「貝氏統計法於地下水文參數推估之研究」，國科會補助專題研究計畫，NSC101-2221-E006-194-MY3。

7. 黃志彬、袁如馨、楊磊，，2012/8/1~2013/7/31「台灣南部地區水產養殖業水資源永續發展對策 - 綠色水產養殖池及水循環回收系統之研發」，國科會補助專題研究計畫，NSC101-2119-M009-004。

8. 楊紹洋，2012/8/1~2013/7/31，「滲漏含水層考慮彎曲效應之地下水流半解析解」，國科會補助專題研究計畫，NSC101-2221-E238-009。

9. 黃安斌、馮道偉、張文忠、何彥德、馮正一、蔡東霖、張胤隆，2012/8/1~2013/7/31，「雲林地區地層下陷特性調查監測與模擬」，國科會補助專題研究計畫，NSC101-2119-M009-003。

10. 倪春發、張中白、董家鈞，2012/8/1~2013/7/31，「地層下陷多尺度時空觀測資訊整合、含水層沈陷參數推估及長期行為預測」，國科會補助專題研究計畫，NSC101-2116-M008-004。

11. 賴進松，2012/8/1~2013/7/31，「地層下陷分析監測、防護管理與防治策略研擬-子計畫:地層嚴重下陷地區防洪排水系統改善方案研擬(I)」，國科會補助專題研究計畫，NSC101-2625-M002-016。

12. 謝嘉聲，2012/8/1~2013/7/31，「整合多源衛星影像雷達干涉技術偵測屏東地區地表變形之研究」，國科會補助專題研究計畫，NSC101-2116-M151-001。

13. 蘇惠珍、連惠邦，2012/2/1~2012/12/31，「沿海低地環境改善之研究-以嘉義沿海魚塭區為例」，經濟部水利署補助專題研究計畫，MOEAWRA1010282。

14. 張良正、鄭蔚辰，2012/2/1~2012/12/31，「應用資料同化方法推估區域地下水利用之研究」，經濟部

水利署補助專題研究計畫，MOEAWRA1010209。

15. 李振誥、徐國錦、丁崇峯，2012/3/1~2012/12/31，「鳥嘴潭人工湖設置對彰化地區地層下陷防制之研究(1/2)」，經濟部水利署補助專題研究計畫，MOEAWRA1010216。

16. 許榮庭，2012/4/1~2012/12/31，「水產養殖經營管理研究-雲林沿海地區養殖產業現況及用水分析與養殖用水規劃」，行政院農業委員會補助專題研究計畫，101 農科-11.3.1-漁-F7。

17. **呂志宗**，2011/8/1~2012/10/31，「典型抽水所引致三維壓密沉陷解析」，國科會補助專題研究計畫，NSC100-2221-E-216-025。

18. **Lu, John C.-C.** and Feng-Tsai Lin, 2013, "Golden Ratio in the Green's Functions of Poromechanics and Thermomechanics," *International Journal of Modelling and Simulation, ISSN: 0228-6203*, **Accepted for Publication**. (This work is supported by the National Science Council through grant NSC81-0410-E-216-503 & NSC100-2221-E-216-025.) **(EI)**

19. **Lu, John C.-C.**, Meng-Qi Chen and Feng-Tsai Lin, 2013, "Point Heat Source Induced Thermoelastic Responses of the Cross-anisotropic Strata," Submitted on October 25, 2011 to *International Journal for Numerical and Analytical Methods in Geomechanics, ISSN: 0363-9061*, **Under Revision**. (This work is supported by the National Science Council through grant NSC100-2221-E-216-025.) **(EI, SCI)**

20. **Lu, John C.-C.** (Session Chair) and Feng-Tsai Lin, 2012/6/25~27, "Modelling of a Buried Deep Horizontal Line Heat Source in a Cross-Anisotropic Thermoelastic Medium," *Proceedings of the 20th IASTED International Conference on Applied Simulation and Modelling, CD ISBN: 978-0-88986-925-7*, Napoli, Italy, pp. 150-157. (This work is supported by the National Science Council through grants NSC100-2221-E-216-025.) **(EI)**

21. **Lu, John C.-C.** (Session Chair) and Feng-Tsai Lin, 2012/6/25~27, "Modelling of Consolidation Settlement Due to a Circularly Symmetric Fluid Sink," *Proceedings of the 20th IASTED International Conference on Applied Simulation and Modelling, CD ISBN: 978-0-88986-925-7*, Napoli, Italy, pp. 107-113. (This work is supported by the National Science Council through grants NSC100-2221-E-216-025.) **(EI)**

22. **Lu, John C.-C.** and Feng-Tsai Lin, 2013, "Closed-form Solutions of the Axisymmetric Elastic Consolidation Settlement Due to an Impulsive Point sink," Ready to Submit for Reviewing. (This work is supported by the National Science Council through grants NSC100-2221-E-216-025.)

23. **Lu, John C.-C.** and Feng-Tsai Lin, 2013, "Consolidation Settlement of a Poroelastic Half Space Subjected to a Line Sink," Ready to Submit for Reviewing. (This work is supported by the National Science Council through grants NSC100-2221-E-216-025.)

24. **Lu, John C.-C.** and Feng-Tsai Lin, 2013, "Elastic Subsidence Subjected to Periodic Pumping," Ready to Submit for Reviewing. (This work is supported by the National Science Council through grants NSC100-2221-E-216-025.)

25. 謝適任，2013，「單井抽水所引致軸對稱彈性沉陷之研究」，碩士論文，中華大學土木工程學系，共 104 頁。

26. Hu, R.L., Z.Q. Yue, L.C. Wang, and S.J. Wang, 2004, “Review on Current Status and Challenging Issues of Land Subsidence in China,” *Engineering Geology*, Vol. 76, pp. 65-77.

27. 馬志強，2007，「漳州某基坑抽水引起地面沉降的初探」，科技信息，第 24 卷，第 104-105 頁。

28. 潘國營、鐘福平、姜衍祥、林雲，2006，「應用灰色關聯分析法識別導致地面沉降的抽水層位」，河南理工大學學報，第 25 卷，第 1 期，第 18-21 頁。

29. Ovando-Shelley, E., A. Ossa, and M.P. Romo, 2007, “The Sinking of Mexico City: Its Effects on Soil Properties and Seismic Response,” *Soil Dynamics and Earthquake Engineering*, Vol. 27, pp. 333-343.

30. Gonzalez-Moran, T., R. Rodriguez, and S.A. Cortes, 1999, “The Basin of Mexico and its Metropolitan Area: Water Abstraction and Related Environmental Problems,” *Journal of South American Earth Sciences*, Vol. 12, pp. 607-613.

31. Phien-wej, N., P.H. Giao, and P. Nutalaya, 2006, “Land Subsidence in Bangkok, Thailand,” *Engineering Geology*, Vol. 82, pp. 187-201.

32. Phien-wej, N., P.H. Giao, and P. Nutalaya, 1998, “Field Experiment of Artificial Recharge Through a Well with Reference to Land Subsidence Control,” *Engineering Geology*, Vol. 50, pp. 187-201.

33. Stiros, S.C., 2001, “Subsidence of the Thessaloniki (Northern Greece) Coastal Plain, 1960-1999,” *Engineering Geology*, Vol. 61, pp. 243-256.

34. Psimoulis, P., M. Ghilardi, E. Fouache, and S. Stiros, 2007, “Subsidence and Evolution of the Thessaloniki Plain, Greece, Based on Historical Leveling and GPS Data,” *Engineering Geology*, Vol. 90, pp. 55-70.

35. Poland, J.F., 1984, *Guidebook to Studies of Land Subsidence Due to Ground-water Withdrawal*, The United Nations Educational Scientific and Cultural Organization, Unesco, Paris.

36. Terzaghi, K., 1943, *Theoretical Soil Mechanics*, John Wiley & Sons, New York, N.Y., pp. 256-296.

37. Biot, M.A., 1941, “General Theory of Three-Dimensional Consolidation,” *J. Appl. Phys.*, Vol. 12, No. 2, pp. 155-164.

38. Biot, M.A., 1955, “Theory of Elasticity and Consolidation for a Porous Anisotropic Solid,” *J. Appl. Phys.*, Vol. 26, No. 2, pp. 182-185.

39. Rice, J.R. and M.P. Cleary, 1976, “Some Basic Stress Diffusion Solutions for Fluid-Saturated Elastic Porous Media with Compressible Constituents,” *Review Geophys. Space Phys.*, Vol. 14, No. 2, pp. 227-241.

40. Booker, J.R. and J.P. Carter, 1986*a*, “Analysis of a Point Sink Embedded in a Porous Elastic Half Space,” *Int. J. Numer. Anal. Methods Geomech.*, Vol. 10, No. 2, pp. 137-150.

41. Booker, J.R. and J.P. Carter, 1986*b*, “Long Term Subsidence Due to Fluid Extraction from a Saturated, Anisotropic, Elastic Soil Mass,” *Q. J. Mech. Appl. Math.*, Vol. 39, Pt. 1, pp. 85-97.

42. Booker, J.R. and J.P. Carter, 1987*a*, “Elastic Consolidation Around a Point Sink Embedded in a

Half-Space with Anisotropic Permeability," *Int. J. Numer. Anal. Methods Geomech.*, Vol. 11, No. 1, pp. 61-77.

43. Booker, J.R. and J.P. Carter, 1987*b*, "Withdrawal of a Compressible Pore Fluid from a Point Sink in an Isotropic Elastic Half Space with Anisotropic Permeability," *Int. J. Solids Struct.*, Vol. 23, No. 3, pp. 369-385.

44. Tarn, J.-Q. and **C.-C. Lu**, 1991, "Analysis of Subsidence Due to a Point Sink in an Anisotropic Porous Elastic Half Space," *Int. J. Numer. Anal. Methods Geomech.*, Vol. 15, No. 8, pp. 573-592. **(EI, SCI)**

45. Barends, F.B.J., 1981, "Landsubsidence Due to a Well in an Elastic Saturated Subsoil," in A. Verruijt and F.B.J. Barends(ed.), *Flow and Transport in Porous Media*, Proceedings of Eurmech 143/Delft/2-4 September 1981, A.A. Balkema/Rotterdam, pp. 11-18.

46. Worsak, K.N. and K.T. Chau, 1990, "Point Sink Fundamental Solutions for Subsidence Prediction," *J. Engng. Mech.*, ASCE, Vol. 116, No. 5, pp. 1176-1182.

47. Burbey, T.J., S.M. Warner, G. Blewitt, J.W. Bell, and E. Hill, 2006, "Three-dimensional Deformation and Strain Induced by Municipal Pumping, Part 1: Analysis of Field Data," *Journal of Hydrology*, Vol. 319, No. 1-4, pp. 123-142.

48. Burbey, T.J., 2006, "Three-dimensional Deformation and Strain Induced by Municipal Pumping, Part 2: Numerical Analysis," *Journal of Hydrology*, Vol. 330, pp. 422-434.

49. Kim, J.M. and R.R. Parizek, 1999, "Three-dimensional Finite Element Modelling for Consolidation Due to Groundwater Withdrawal in a Desaturating Anisotropic Aquifer System," *Int. J. Numer. Anal. Methods Geomech.*, Vol. 23, No. 6, pp. 549-571.

50. Bawden, G.W., W. Thatcher, R.S. Stein, K.W. Hudnut, and G. Peltzer, 2001, "Tectonic Contraction Across Los Angeles After Removal of Groundwater Pumping Effects," *Nature*, Vol. 412, No. 6849, pp. 812-815.

51. Hou, C.S., J.C. Hu, L.C. Shen, J.S. Wang, C.L. Chen, T.C. Lai, C. Huang, Y.R. Yang, R.F. Chen, Y.G. Chen, and J. Angelier, 2005, "Estimation of *Subsidence* Using GPS Measurements, and Related Hazard: the Pingtung Plain, Southwestern Taiwan," *Comptes Rendus Geoscience*, Vol. 337, No. 13, pp. 1184-1193.

52. Gambolati, G., M. Putti, and P. Teatini, 1996, "Coupled and Uncoupled Poroelastic Solutions to Land Subsidence Due to Groundwater Withdrawal," *Proceedings of Engineering Mechanics, ASCE*, Vol. 1, pp. 483-486.

53. Lin, Feng-Tsai and **John C.-C. Lu**, 2010/4, "Golden Ratio in the Point Sink Induced Consolidation Settlement of a Poroelastic Half Space," *Modelling, Simulation and Optimization*, Shkelzen Cakaj (ed.), *ISBN: 978-953-307-056-8, I-Tech Education and Publishing*, Vienna, Austria, *www.intechweb.org*, pp. 25-40.

54. **Lu, John C.-C.** and Feng-Tsai Lin, 2011/7/4~6, "Elastic Consolidation Settlement Due to Periodic Pumping," *Proceedings of the 3rd IASTED International Conference on Environmental Management and Engineering, CD ISBN: 978-0-88986-886-1*, Calgary, Alberta, Canada, pp. 53-59. **(EI)**

55. **Lu, John C.-C.** and F.-T. Lin, 2006, "The Transient Ground Surface Displacements Due to a Point Sink/Heat Source in an Elastic Half-Space," *Geotechnical Special Publication No. 148, GeoShanghai International Conference 2006, ASCE,* Shanghai, China, pp. 210-218. **(EI)**

56. **Lu, John C.-C.** and Feng-Tsai Lin, 2011/7/4~6, "Consolidation Settlement Due to a Point Sink with Compressible Constituents," *Proceedings of the 22nd IASTED International Conference on Modelling and Simulation, CD ISBN: 978-0-88986-887-8,* Calgary, Alberta, Canada, pp. 275-281. **(EI)**

57. Yeh, H.-D., R.-H. Lu, and G.-T. Yeh, 1996, "Finite Element Modelling for Land Displacements Due to Pumping," *Int. J. Numer. Anal. Methods Geomech.*, Vol. 20, pp. 79-99.

58. Bear, J. and M.Y. Corapcioglu, 1981, "Mathematical Model for Regional Land Subsidence Due to Pumping, 2. Integrated Aquifer Subsidence Equations for Vertical and Horizontal Displacements," *Water Resour. Res.*, Vol. 17, pp. 947-958.

59. Bear, J. and M.Y. Corapcioglu, 1984, *Fundamentals of Transport Phenomena in Porous Media*, NATO ASI Series, Martinus Nijhoff Published.

60. 曾鈞敏，「地下水超抽引致地層下陷之三維解析研究」，博士論文，國立臺灣大學土木工程研究所 (2009) 。

61. Tenney, C.M., C.M. Lastoskie, and M.J. Dybas, 2004, "A Reactor Model for Pulsed Pumping Groundwater Remediation," *Water Research*, Vol. 38, pp. 3869-3880.

62. Tenney, C.M. and C.M. Lastoskie, 2007, "Pulsed Pumping Process Optimization Using a Potential Flow Model," *Journal of Contaminant Hydrology*, Vol. 93, pp. 111-121.

63. Renner, J. and M. Messar, 2006, "Periodic Pumping Tests," *Geophysical Journal International*, Vol. 167, No. 1, pp. 479-493.

64. Propst, G., 2006, "Pumping Effects in Models of Periodically Forced Flow Configurations," *Physica D*, Vol. 217, pp. 193-201.

65. Townley, L.R., 1995, "The Response of Aquifers to Periodic Forcing," *Advances in Water Resources*, Vol. 18, No. 3, pp. 125-146.

66. Gendelman, O.V., E. Gourdon, and C.H. Lamarque, 2006, "Quasiperiodic Energy Pumping in Coupled Oscillators under Periodic Forcing," *Journal of Sound and Vibration*, Vol. 294, pp. 651-662.

67. Zhao, C.-Y. and W.-H. Tan, 2009, "Einstein–Podolsky–Rosen Entanglement in Time-dependent Periodic Pumping Non-degenerate Optical Parametric Amplifier," *Chinese Phys. B*, Vol. 18, pp. 4143-4153.

附錄 1

研究成果投稿後已被接受之 EI 等級期刊論文一篇

Lu, John C.-C. and Feng-Tsai Lin, 2013, "Golden Ratio in the Green's Functions of Poromechanics and Thermomechanics," *International Journal of Modelling and Simulation, ISSN: 0228-6203*, **Accepted for Publication**. (This work is supported by the National Science Council through grant NSC81-0410-E-216-503 & NSC100-2221-E-216-025.) (EI)

論文接受函

John Lu

寄件者: journals@actapress.com
寄件日期: 2012年10月16日星期二 下午 8:41
收件者: cclu@chu.edu.tw
主旨: Paper Status - Paper 205-5645 (Accepted for Publication)

標幟狀態: 已標幟

Re: Paper Number 205-5645
Dear Dr. John Lu,

I am pleased to inform you that your paper, entitled GOLDEN RATIO IN THE GREEN?S FUNCTIONS OF POROMECHANICS AND THERMOMECHANICS, has been accepted for publication in the journal International Journal of Modelling and Simulation. This paper has passed peer-review and final approval by the Editor-in-Chief. Please access our online system to view the reviewers' comments; try to include these suggestions in the final paper.

In order to begin processing your paper, we require several items:
1. The final paper and accompanying files (email it to journals@actapress.com by Jan-16-2013)

A double-spaced MS Word document of your final paper. If your paper is in Latex (.tex) format, please also submit your final paper as a PDF file. Please visit http://www.actapress.com/submissioninfo.aspx for the final paper formatting guide.
An electronic copy of the figures (.eps, .ps, .jpg, etc.). Please ensure that the filenames of the figures are labelled according to the figure number (e.g., for Figure 1 it is "figure 1.eps").
A brief biography for each author, and if possible, a photo of each author. Photos must be of high resolution (300 dpi), black and white, and no less than 3.5 cm in width.

NOTE: For papers exceeding 8 (EIGHT) printed pages (single-spaced, 12-pt font size) inclusive of illustrations, there is a charge of $100.00 (US currency) per additional page.

To access the review assessments of your paper, please visit
http://www.actapress.com/review/UI/AuthorViewResults.aspx?pn=205-5645

Username: cclu@chu.edu.tw
Password: ilovejesus

Thank you very much, and we look forward to publishing your paper.

Sincerely,

ACTA Press / IASTED
Building B6, Suite #101, 2509 Dieppe Avenue SW, Calgary, AB T3E 7J9 Canada
phone: (403) 288-1195
fax: (403) 247-6851
e-mail: journals@actapress.com
Website: http://www.actapress.com/

Peer-review portal: http://www.actapress.com/review/

附 4

論文全文

GOLDEN RATIO IN THE GREEN'S FUNCTIONS OF POROMECHANICS AND THERMOMECHANICS

John C.-C. Lu* and Feng-Tsai Lin**

Abstract

This paper presents the transient responses of a point fluid sink or a point heat source in the strata. Green's functions of the elastic displacements and excess pore fluid pressure or temperature increment of strata are derived by using Laplace-Hankel integral transforms. The strata are modeled as a poroelastic or thermoelastic half space in the mathematical modelling. Poroelasticity and thermoelasticity are applied on the formulation of basic governing equations, and analogy is drawn between poroelasticity and thermoelasticity. Attention is focused on the golden ratio which appears in the magnitude of maximum ground surface horizontal displacement and corresponding vertical displacement of the half space Green's functions. The study concludes that golden ratio exists in these phenomena, and the horizontal displacement should be properly considered in the prediction of displacements induced by groundwater withdrawal or buried heat source.

Key Words

Golden ratio, Green's function, point fluid sink, point heat source, poromechanics, thermomechanics

1. Introduction

The golden ratio ϕ [1, 2] is an irrational algebraic number 1.6180339887498948482… which is well known in mathematics, science, biology, art, architecture, nature and beyond [3]. It is interesting to

* Department of Civil Engineering, Chung Hua University, Taiwan, R.O.C.; email: cclu@chu.edu.tw
** Department of Naval Architecture, National Kaohsiung Marine University, Taiwan, R.O.C.; email: ftlin@mail.nkmu.edu.tw

discover that the golden ratio exists in the point fluid sink and point heat source induced elastic displacements of a homogeneous isotropic half space. Examples of the golden ratio in engineering include the shear flow in porous half space [4], classical mechanics of coupled-oscillator problem [5], and magnetic compound [6], *etc*. This study is focused on the transient responses of a point fluid sink or a point heat source in the strata. The derived closed-form solutions are defined as Green's functions of poromechanics and thermomechanics.

The three-dimensional consolidation theory introduced by Biot [7, 8] is generally regarded as the fundamental theory for modelling land subsidence. The approach is followed by Rice and Cleary [9] who provided an elegant formulation of Biot's theory by using easily identifiable quantities and material constants. Bear and Corapcioglu [10, 11] presented the modified Biot's equations when the pore fluid is treated as compressible and the solid skeleton is assumed as incompressible. Based on Biot's theory modified by Bear and Corapcioglu [10, 11], Booker and Carter [12-15], Tarn and Lu [16] presented solutions of subsidence by a point fluid sink embedded in the saturated elastic half space at a constant rate. Chen [17, 18], Kanok-Nukulchai and Chau [19] presented analytic solutions for the steady-state responses of displacements and stresses in a half space subject to a fluid point sink. Lu and Lin [20, 21] displayed transient displacements of the pervious half space due to steady pumping rate [20] and impulsive pumping [21]. The results presented by Hou *et al.* [22] shown that ground horizontal displacement occurred during groundwater withdrawal from an aquifer.

Nuclear wastes are usually deposited at a great depth, such as 200 to 700 meters below ground surface to be isolated from the living environment of human beings. Hueckel and Peano [23] indicated that European guidelines require that temperature increments in the soil close to the heat source should not exceed 80°C while the temperature increments at the ground surface is limited to less than 1°C. It suggested that linear theory was adequate for a repository design based on technical conservatism [23].

Given these modest temperature increments, Hollister, Anderson and Health [24] observed that any significant non-linear behaviour and/or plastic deformation of the soil would be confined to a relatively small volume of soil around the waste canister itself. In this case, a linear model can provide reasonable approximation to the assessment of a proposed design [25]. The responses of the strata were satisfactorily modeled by assuming it as a thermoelastic continuum [26]. Booker and Savvidou [26, 27], Savvidou and Booker [28] derived an extended Biot's theory including the thermal effects and presented solutions of thermo-consolidation around the spherical and point heat sources. The analogy between thermoelasticity and poroelasticity was drawn by Lu and Lin [20], Norris [29], Manolis and Beskos [30], Cheng *et al.* [31], *etc*.

Based on the axially symmetric poromechanics and thermomechanics, the Green's functions of the transient elastic deformations in half spaces due to a point fluid sink and a point heat source are presented in this paper. The transient closed-form solutions are derived through Laplace-Hankel integral transforms. The homogeneous isotropic stratum is modeled as either poroelastic or thermoelastic half space in the mathematical model. The golden ratio, known as $\phi \approx 1.618$, appears in the maximum ground surface horizontal displacement and corresponding vertical displacement. The study concludes that golden ratio exists in these phenomena, and the horizontal displacement should be properly considered in the prediction of displacements induced by groundwater withdrawal or buried heat source.

2. The Golden Ratio

The golden ratio ϕ, approximately 1.6180339887498948482…, is an irrational mathematical constant. The symbol ϕ is also known as golden section, golden mean, divine proportion, divine section, golden proportion, golden cut, golden number, *etc*. The golden ratio ϕ can be derived from a geometrical line segment and ratio as shown in Figure 1, where the ratio of the full length 1 to the length of x is equal to the

ratio of longer section x to shorter section $1-x$:

$$\frac{1}{x}=\frac{x}{1-x} \tag{1}$$

Assuming $x=1/\phi$, hence, ϕ satisfies

$$\phi^2-\phi-1=0 \tag{2}$$

The golden ratio is the positive solution of equation (2) as shown below:

$$\phi=(1+\sqrt{5})/2 \tag{3}$$

Figure 1. Dividing a segment into the golden ratio.

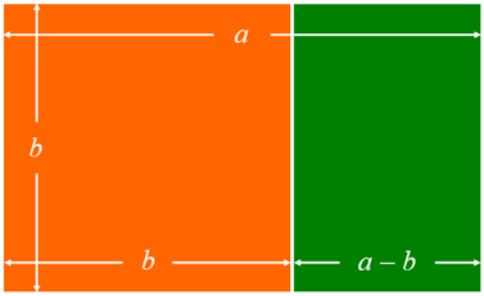

Figure 2. The golden rectangle.

Figure 2 displayed another geometric description of golden ratio through the golden rectangle. Giving a rectangle with sides' ratio *a*:*b*, the removing of square section leaves remaining rectangle with the same ratio as original rectangle, i.e.,

$$\frac{b}{a-b}=\frac{a}{b} \tag{4}$$

Thus, this solution is the golden ratio ϕ:

$$\phi=\frac{a}{b}=\frac{1+\sqrt{5}}{2} \tag{5}$$

The golden ratio is a remarkable number that arises in various areas of mathematics, nature, and arts,

etc. There are many interesting mathematical properties of ϕ. For example, ϕ can be expressed as a continuous fraction with the single number 1 [1]:

$$\phi = 1 + \cfrac{1}{1 + \cfrac{1}{1 + \cfrac{1}{1 + \cfrac{1}{1 + \cdots}}}} \tag{6}$$

Also, the golden ratio ϕ can be expressed as a continuous square root of the number 1:

$$\phi = \sqrt{1 + \sqrt{1 + \sqrt{1 + \sqrt{1 + \cdots}}}} \tag{7}$$

However, the most interesting is that ϕ is within Fibonacci series [1, 2]. The Fibonacci series is a set of numbers that begins with two 1s, and each following term is the sum of the prior two terms, i.e., 1, 1, 2, 3, 5, 8, 13, 21, 34, 55, 89, 144, 233, 377, 610, 987, 1597, ⋯ . The relationship between two successive numbers of Fibonacci series tends to approach ϕ.

Based on the theory of poromechanics and thermomechanics, the strata are modeled as homogeneous isotropic half spaces. This paper presents the Green's functions of the transient and long-term ground surface elastic deformations of the strata due to a point fluid sink or a point heat source. It is interesting to find that the golden ratio ϕ appears in this study for the maximum ground surface horizontal displacement and corresponding vertical displacement.

3. Poroelastic Modelling

3.1 Governing Equations

The formulation of Biot's equations follows that of Rice and Cleary [9] with easily identifiable quantities and material constants. Four basic material constants are selected in the constitutive equations including the shear modulus G, the drained Poisson's ratio ν, the undrained Poisson's ratio ν_u and Skempton's

pore pressure coefficient B [32]. The physical ranges of B and ν_u are obviously $0 \le B \le 1$ and $0 \le \nu \le \nu_u \le \frac{1}{2}$ [9], respectively. For the situation of incompressible constituents, the poroelastic coefficients $B = 1$ and $\nu_u = \frac{1}{2}$. According to Rice and Cleary [9], the reformulated constitutive relations can be expressed as [33]:

$$\sigma_{ij} = 2G\varepsilon_{ij} + \frac{2G\nu}{1-2\nu}\varepsilon\delta_{ij} - \frac{3(\nu_u - \nu)}{B(1-2\nu)(1+\nu_u)}p\delta_{ij} \tag{8}$$

$$p = -\frac{2GB(1+\nu_u)}{3(1-2\nu_u)}\varepsilon + \frac{2GB^2(1-2\nu)(1+\nu_u)^2}{9(\nu_u - \nu)(1-2\nu_u)}\varsigma \tag{9}$$

in which σ_{ij}, p and ε_{ij} are the total stress components, excess pore fluid pressure and solid strain components of the poroelastic media, respectively. The fluid pressure p is positive for compression. The parameter ς is the variation of fluid content per unit reference volume. The volumetric strain of the skeletal material is denoted by ε and $\varepsilon = \varepsilon_{11} + \varepsilon_{22} + \varepsilon_{33}$. The symbol δ_{ij} is the Kronecker delta. The inversions of equations (8) and (9) are shown as the form:

$$\varepsilon_{ij} = \frac{1}{2G}\left(\sigma_{ij} - \frac{\nu}{1+\nu}\sigma_{kk}\delta_{ij}\right) + \frac{3(\nu_u - \nu)}{2GB(1+\nu)(1+\nu_u)}p\delta_{ij} \tag{8*}$$

$$\varsigma = \frac{9(\nu_u - \nu)(1-2\nu_u)}{2GB^2(1-2\nu)(1+\nu_u)^2}p + \frac{3(\nu_u - \nu)}{B(1-2\nu)(1+\nu_u)}\varepsilon \tag{9*}$$

The solid strain components ε_{ij} and displacement components u_i are governed by the linear kinematic equation:

$$\varepsilon_{ij} = \frac{1}{2}\left(u_{i,j} + u_{j,i}\right) \tag{10}$$

The total stress components σ_{ij} must satisfy the equilibrium equation:

$$\sigma_{ij,j} + b_i = 0 \tag{11}$$

where b_i denotes the body force components. The mass balance for the fluid phase is denoted by:

$$\frac{\partial \varsigma}{\partial t} + v_{i,i} = \gamma \tag{12}$$

in which v_i is the specific discharge velocity components, and γ is the rate of injected fluid source into the saturated porous aquifer per unit volume. Assuming that the pore fluid flow is governed by Darcy's law, we have

$$v_i = -\frac{k}{\gamma_f} p_{,i} \tag{13}$$

in which k denotes the permeability of the porous media and γ_f is the unit weight of pore fluid.

The governing equations (8) to (13) are combined to yield the field equations for solutions of the boundary value problems. Substituting (8) and (10) into (11), (9*) and (13) into (12), then the equilibrium equation (11) and mass balance equation (12) are expressed in terms of displacement components u_i and excess pore fluid pressure p as below:

$$G\nabla^2 u_i + \frac{G\nu}{1-2\nu}\frac{\partial \varepsilon}{\partial x_i} - \alpha \frac{\partial p}{\partial x_i} + b_i = 0 \tag{14a}$$

$$-\frac{k}{\gamma_f}\nabla^2 p + \frac{9(\nu_u - \nu)(1-2\nu_u)}{2GB^2(1-2\nu)(1+\nu_u)^2}\frac{\partial p}{\partial t} + \alpha \frac{\partial \varepsilon}{\partial t} = \gamma \tag{14b}$$

where α is known as Biot's coefficient of effective stress which is defined as

$$\alpha = \frac{3(\nu_u - \nu)}{B(1-2\nu)(1+\nu_u)} \tag{15}$$

The above mathematical model is known as coupled model of poroelasticity where the flow field is dependent on the displacement field. The coupling term $\partial\varepsilon/\partial t$ in equation (14b) is neglected in this study.

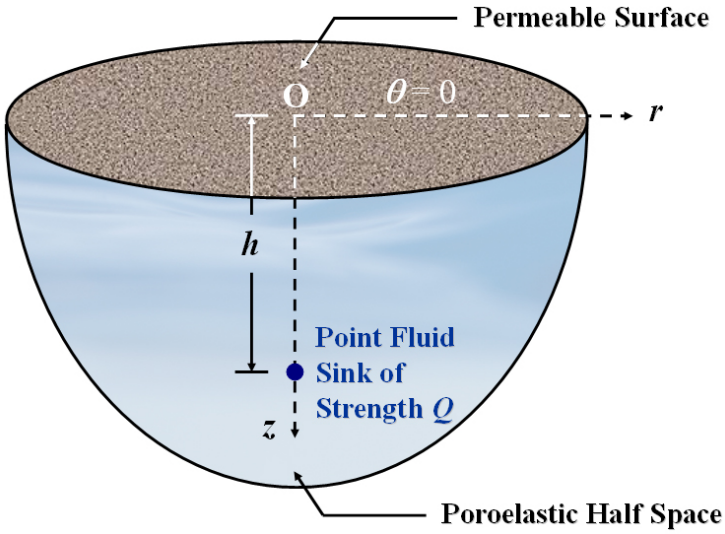

Figure 3. Mechanics of poroelastic point fluid sink problem.

Figure 3 presents a point fluid sink buried in a saturated porous half space at a depth *h*. The constant sink strength is denoted as Q at the location $(0,h)$. Applying the equilibrium equations to axisymmetric poromechanics problem with a vertical axis of symmetry and neglecting the effects of body forces b_i, then equation (14a) is transformed to equations (16a) and (16b). Moreover, assuming the flow field is independent of the displacement field, thus the mass balance equation (14b) is expressed as (16c). Therefore, the uncoupled governing equations in axially symmetric coordinates (r,z) are derived in terms of displacements $u_i\,(i=r,z)$ and excess pore fluid pressure *p* as following:

$$G\nabla^2 u_r+\frac{G}{1-2\nu}\frac{\partial\varepsilon}{\partial r}-G\frac{u_r}{r^2}-\alpha\frac{\partial p}{\partial r}=0 \tag{16a}$$

$$G\nabla^2 u_z+\frac{G}{1-2\nu}\frac{\partial\varepsilon}{\partial z}-\alpha\frac{\partial p}{\partial z}=0 \tag{16b}$$

$$-\frac{k}{\gamma_f}\nabla^2 p+\frac{9(\nu_u-\nu)(1-2\nu_u)}{2GB^2(1-2\nu)(1+\nu_u)^2}\frac{\partial p}{\partial t}+\frac{Q}{2\pi r}\delta(r)\delta(z-h)u(t)=0 \tag{16c}$$

where $\nabla^2=\frac{\partial^2}{\partial r^2}+\frac{1}{r}\frac{\partial}{\partial r}+\frac{\partial^2}{\partial z^2}$ and $\varepsilon=\frac{\partial u_r}{\partial r}+\frac{u_r}{r}+\frac{\partial u_z}{\partial z}$; $\delta(x)$ and $u(t)$ are the Dirac delta function and Heaviside unit step function, respectively. Equations (16a) to (16c) are the uncoupled basic field equations with a point fluid sink at constant rate, in which the fluid and solid are treated as compressible

constituents.

3.2 Boundary Conditions and Initial Conditions

The half space ground surface is treated as pervious traction-free boundary for all times $t \geq 0$. The mathematical statements of the ground surface boundary $z = 0$ in axisymmetric coordinates (r, z) are:

$$\sigma_{rz}(r,0,t) = 0,\ \sigma_{zz}(r,0,t) = 0, \text{ and } p(r,0,t) = 0 \tag{17a}$$

The displacements and excess pore fluid pressure at the remote boundary due to the effect of a point fluid sink must be nil at any time. These conditions are written as

$$\lim_{z\to\infty}\left\{u_r(r,z,t), u_z(r,z,t), p(r,z,t)\right\} = \{0,0,0\} \tag{17b}$$

Assuming no initial displacements and seepage of the strata, the initial conditions at time $t = 0^+$ of the mathematical model due to a point fluid sink are treated as

$$u_r(r,z,0^+) = 0,\ u_z(r,z,0^+) = 0 \text{ and } p(r,z,0^+) = 0 \tag{18}$$

The mathematical model in this study is based on the governing equations (16a)-(16c), the corresponding boundary conditions (17a)-(17b) and initial conditions (18).

4. Thermoelastic Modelling

4.1 Governing Equations

The constitutive behavior of the isotropic body with a point heat source buried in an isotropic thermoelastic half space at depth *h* as shown in Figure 4 is expressed as

$$\sigma_{ij} = 2G\varepsilon_{ij} + \frac{2G\nu}{1-2\nu}\varepsilon\delta_{ij} - \frac{2G(1+\nu)\alpha_s}{1-2\nu}\vartheta\delta_{ij} \tag{19}$$

$$s = \frac{2G(1+\nu)\alpha_s}{1-2\nu}\varepsilon + \frac{c_\varepsilon}{T_0}\vartheta \tag{20}$$

Here, σ_{ij} and ε_{ij} are the thermal stress components and strain components of the thermoelastic medium,

respectively. The symbol ε denotes the volumetric strain of the thermoelastic medium and $\varepsilon = \varepsilon_{11} + \varepsilon_{22} + \varepsilon_{33}$. The temperature increment ϑ is measured from the reference state. The entropy s is the function for internal state of the thermoelastic system. The average temperature in the natural state corresponding with $\varepsilon_{ij} = 0$ is denoted by T_0. The material constants ν, G, α_s and c_ε are the Poisson's ratio, shear modulus, linear thermal expansion coefficient and specific heat at constant strain of the thermoelastic medium, respectively. The coefficient $c_\varepsilon = \rho c$, where the constants ρ and c define the density and specific heat of the thermoelastic medium, respectively.

The conservation of energy in the form of the entropy flow is as:

$$T_0 \frac{\partial s}{\partial t} + q_{i,i} = W \tag{21}$$

where q_i is the heat flux, and W is the quantity of heat generated in a unit volume and unit time. The thermal flow is assumed to follow the Fourier law for heat conduction. In the case of an isotropic body, the Fourier heat conduction law has the form

$$q_i = -\lambda_t \vartheta_{,i} \tag{22}$$

in which λ_t is the coefficient of heat conduction.

The thermal stresses σ_{ij} should satisfy the equilibrium relations in equation (11). Substituting the linear kinematic equation (10) and constitutive equation (19) into the equilibrium equation (11), and the entropy equation (20) and Fourier heat conduction law (22) into the conservation of energy (21), respectively. Then the equations (11) and (21) are expressed in terms of thermal displacements u_i and temperature increment ϑ of the thermoelastic medium as follows:

$$G\nabla^2 u_i + \frac{G}{1-2\nu}\frac{\partial \varepsilon}{\partial x_i} - \frac{2G(1+\nu)\alpha_s}{1-2\nu}\frac{\partial \vartheta}{\partial x_i} = 0 \tag{23a}$$

$$-\lambda_t \nabla^2 \vartheta + c_\varepsilon \frac{\partial \vartheta}{\partial t} + \frac{2G(1+\nu)\alpha_s T_0}{1-2\nu} \frac{\partial \varepsilon}{\partial t} = W \tag{23b}$$

Figure 4 presents a point heat source buried in a thermoelastic half space at a depth h. The constant heat generating rate is denoted as H at the location $(0,h)$ in axisymmetric coordinates system (r,z). The equilibrium equations are applied to axisymmetric thermomechanics problem with a vertical axis of symmetry and neglecting the effects of body forces b_i. Moreover, assuming the thermal flow field is independent from the displacement field in the conservation of energy. Therefore, the uncoupled governing equations in axially symmetric coordinates (r,z) are derived in terms of thermal displacements $u_i\,(i=r,z)$ and temperature increment ϑ as following:

$$G\nabla^2 u_r + \frac{G}{1-2\nu}\frac{\partial \varepsilon}{\partial r} - G\frac{u_r}{r^2} - \frac{2G(1+\nu)\alpha_s}{1-2\nu}\frac{\partial \vartheta}{\partial r} = 0 \tag{24a}$$

$$G\nabla^2 u_z + \frac{G}{1-2\nu}\frac{\partial \varepsilon}{\partial z} - \frac{2G(1+\nu)\alpha_s}{1-2\nu}\frac{\partial \vartheta}{\partial z} = 0 \tag{24b}$$

$$-\lambda_t \nabla^2 \vartheta + c_\varepsilon \frac{\partial \vartheta}{\partial t} - \frac{H}{2\pi r}\delta(r)\delta(z-h)u(t) = 0 \tag{24c}$$

Equations (24a) to (24c) constitute the fundamental equations of transient responses for a thermoelastic medium subjected to a point heat source.

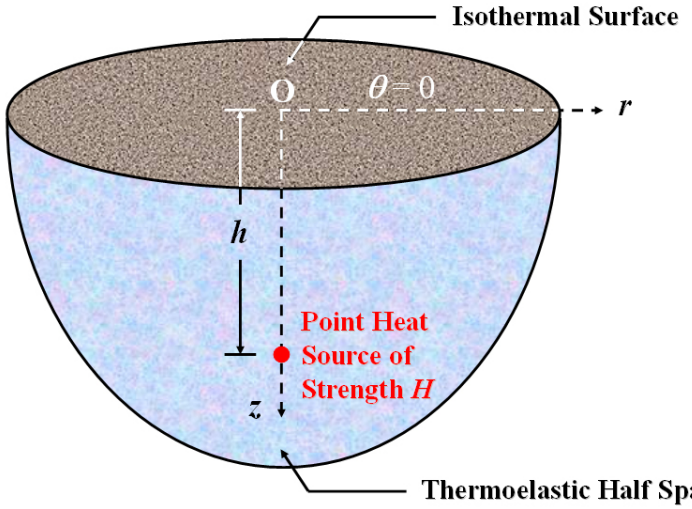

Figure 4. Mechanics of thermoelastic point heat source problem.

4.2 Boundary Conditions and Initial Conditions

The half space ground surface, $z = 0$, is considered as traction-free, and it remains the same temperature at all times $t \geq 0$. Therefore, the boundary conditions on surface $z = 0$ in axisymmetric coordinates (r, z) are given by

$$\sigma_{rz}(r,0,t) = 0,\ \sigma_{zz}(r,0,t) = 0, \text{ and } \vartheta(r,0,t) = 0 \tag{25a}$$

The remote boundary conditions due to the effect of a point heat source must be nil at any time as below:

$$\lim_{z\to\infty}\{u_r(r,z,t), u_z(r,z,t), \vartheta(r,z,t)\} = \{0,0,0\} \tag{25b}$$

Assuming there are no initial change of thermal displacements and temperature increment for the thermoelastic medium, the initial conditions at time $t = 0^+$ due to a point heat source are treated as

$$u_r(r,z,0^+) = 0,\ u_z(r,z,0^+) = 0, \text{ and } \vartheta(r,z,0^+) = 0 \tag{26}$$

From these basic governing equations, the corresponding quantities of poroelasticity and thermoelasticity are shown in Table 1.

Table 1
Analogy of Poroelastic and Thermoelastic Quantities

Poromechanics	Thermomechanics
p	ϑ
$u_i\,(i = r, z)$	$u_i\,(i = r, z)$
$\dfrac{3(\nu_u - \nu)}{B(1-2\nu)(1+\nu_u)}$	$\dfrac{2G(1+\nu)\alpha_s}{1-2\nu}$
$\dfrac{9(\nu_u - \nu)(1-2\nu_u)}{2GB^2(1-2\nu)(1+\nu_u)^2}$	$\dfrac{c_\varepsilon}{T_0}$
$\dfrac{k}{\gamma_w}$	$\dfrac{\lambda_t}{T_0}$
γ	$\dfrac{W}{T_0}$

5. Green's Functions

5.1 Green's Functions for a Poroelastic Half Space

Applying Laplace-Hankel integral transformations [34, 35], the transient ground surface horizontal displacement, ground surface vertical displacement and excess pore fluid pressure of the stratum due to a point fluid sink in axially symmetric coordinates (r,z) are obtained as follows:

$$u_r(r,0,t)=\frac{Q\gamma_f(1-2\nu)}{2\pi Gk}\left\{-\frac{ctr}{\left(h^2+r^2\right)^{3/2}}+\int_0^{ct}\frac{(ct-\tau)hr}{16\tau^3}e^{-\frac{r^2+2h^2}{8\tau}}\left[I_0\left(\frac{r^2}{8\tau}\right)-I_1\left(\frac{r^2}{8\tau}\right)\right]d\tau\right\} \quad (27a)$$

$$u_z(r,0,t)=\frac{Q\gamma_f(1-2\nu)}{4\pi Gk}\left\{\frac{2cth}{\left(h^2+r^2\right)^{3/2}}erf\left(\frac{\sqrt{h^2+r^2}}{2\sqrt{ct}}\right)\right.$$
$$\left.-\frac{2h}{h^2+r^2}\sqrt{\frac{ct}{\pi}}e^{-\frac{h^2+r^2}{4ct}}+\frac{h}{\sqrt{h^2+r^2}}erfc\left(\frac{\sqrt{h^2+r^2}}{2\sqrt{ct}}\right)\right\} \quad (27b)$$

$$p(r,z,t)=-\frac{Q\gamma_f}{4\pi k}\left\{\frac{1}{\sqrt{r^2+(z-h)^2}}erfc\left[\frac{\sqrt{r^2+(z-h)^2}}{2\sqrt{ct}}\right]\right.$$
$$\left.-\frac{1}{\sqrt{r^2+(z+h)^2}}erfc\left[\frac{\sqrt{r^2+(z+h)^2}}{2\sqrt{ct}}\right]\right\} \quad (27c)$$

where the parameter $c=\frac{9(\nu_u-\nu)(1-2\nu_u)}{2GB^2(1-2\nu)(1+\nu_u)^2}\frac{k}{\gamma_f}$; $erf(x)$ and $erfc(x)$ are error function and complementary error function, respectively; and $I_\alpha(x)$ is the modified Bessel function of the first kind of order α. The magnitude of long-term ground surface horizontal displacement and vertical displacement are obtained when $t\to\infty$:

$$u_r(r,0,\infty)=-\frac{Q\gamma_f(1-2\nu)}{4\pi Gk}\frac{hr}{\sqrt{h^2+r^2}(\sqrt{h^2+r^2}+h)} \quad (28a)$$

$$u_z(r,0,\infty)=\frac{Q\gamma_f(1-2\nu)}{4\pi Gk}\frac{h}{\sqrt{h^2+r^2}} \quad (28b)$$

Equations (27a)-(27c) and (28a)-(28b) are known as the Green's functions for a poroelastic half space.

5.2 Green's Functions for a Thermoelastic Half Space

Using the equivalence between thermomechanics and poromechanics as shown in Table 1, the transient ground surface horizontal displacement, ground surface vertical displacement, and temperature increment of the stratum due to a point heat source in axisymmetric coordinates (r,z) are obtained as below:

$$u_r(r,0,t)=-\frac{H\alpha_s(1+\nu)}{\pi\lambda_t}\left\{-\frac{ctr}{\left(h^2+r^2\right)^{3/2}}+\int_0^{ct}\frac{(ct-\tau)hr}{16\tau^3}e^{-\frac{r^2+2h^2}{8\tau}}\left[I_0\left(\frac{r^2}{8\tau}\right)-I_1\left(\frac{r^2}{8\tau}\right)\right]d\tau\right\} \quad (29a)$$

$$u_z(r,0,t)=-\frac{H\alpha_s(1+\nu)}{2\pi\lambda_t}\left\{\frac{2cth}{\left(h^2+r^2\right)^{3/2}}erf\left(\frac{\sqrt{h^2+r^2}}{2\sqrt{ct}}\right)\right.$$
$$\left.-\frac{2h}{h^2+r^2}\sqrt{\frac{ct}{\pi}}e^{-\frac{h^2+r^2}{4ct}}+\frac{h}{\sqrt{h^2+r^2}}erfc\left(\frac{\sqrt{h^2+r^2}}{2\sqrt{ct}}\right)\right\} \quad (29b)$$

$$\vartheta(r,z,t)=\frac{H}{4\pi\lambda_t}\left\{\frac{1}{\sqrt{r^2+(z-h)^2}}erfc\left[\frac{\sqrt{r^2+(z-h)^2}}{2\sqrt{ct}}\right]\right.$$
$$\left.-\frac{1}{\sqrt{r^2+(z+h)^2}}erfc\left[\frac{\sqrt{r^2+(z+h)^2}}{2\sqrt{ct}}\right]\right\} \quad (29c)$$

where the parameter c is defined as $c=\lambda_t/c_\varepsilon$.

Similarly, the magnitude of long-term ground surface horizontal displacement and vertical displacement are derived when $t\to\infty$:

$$u_r(r,0,\infty)=\frac{H\alpha_s(1+\nu)}{2\pi\lambda_t}\frac{hr}{\sqrt{h^2+r^2}(\sqrt{h^2+r^2}+h)} \quad (30a)$$

$$u_z(r,0,\infty)=-\frac{H\alpha_s(1+\nu)}{2\pi\lambda_t}\frac{h}{\sqrt{h^2+r^2}} \quad (30b)$$

Equations (29a)-(29c) and (30a)-(30b) are known as the Green's functions for a thermoelastic half space.

6. Golden Ratio in the Long-Term Ground Surface Displacements

The maximum long-term ground surface horizontal displacement and vertical displacement of the half space due to a point fluid sink and a point heat source are derived from equations (28a)-(28b) and (30a)-(30b) by letting $r=\sqrt{\phi}h\approx 1.272h$ and $r=0$, respectively.

For the point fluid sink problem, the maximum horizontal displacement $u_{r\max}^{(f)}$ and vertical displacement $u_{z\max}^{(f)}$ of the ground surface derived from equations (28a)-(28b) are

$$u_r\left(\sqrt{\phi}h,0,\infty\right)=u_{r\max}^{(f)}=-\frac{Q\gamma_w\left(1-2\nu\right)}{4\pi Gk}\frac{1}{\phi^{2.5}}\approx -0.3003\frac{Q\gamma_w\left(1-2\nu\right)}{4\pi Gk} \tag{31a}$$

$$u_z\left(0,0,\infty\right)=u_{z\max}^{(f)}=\frac{Q\gamma_w\left(1-2\nu\right)}{4\pi Gk} \tag{31b}$$

For the point heat source problem, the maximum horizontal displacement $u_{r\max}^{(h)}$ and vertical displacement $u_{z\max}^{(h)}$ of the ground surface derived from equations (30a)-(30b) are

$$u_r\left(\sqrt{\phi}h,0,\infty\right)=u_{r\max}^{(h)}=\frac{H\alpha_s\left(1+\nu\right)}{2\pi\lambda_t}\frac{1}{\phi^{2.5}}\approx 0.3003\frac{H\alpha_s\left(1+\nu\right)}{2\pi\lambda_t} \tag{32a}$$

$$u_z\left(0,0,\infty\right)=u_{z\max}^{(h)}=-\frac{H\alpha_s\left(1+\nu\right)}{2\pi\lambda_t} \tag{32b}$$

Here, $\phi=(1+\sqrt{5})/2\approx 1.618$ is known as the golden ratio. The exact solutions of maximum ground surface horizontal displacement and vertical displacement are derived as shown in equations (31a)-(31b) and (32a)-(32b), and the maximum ground surface horizontal displacement is approximately 30% of the maximum ground surface vertical displacement, i.e.,

$$\left|\frac{u_{r\max}^{(f)}}{u_{z\max}^{(f)}}\right|=\left|\frac{u_{r\max}^{(h)}}{u_{z\max}^{(h)}}\right|=\frac{1}{\phi^{2.5}}\approx 0.3003 \text{ at } r=\sqrt{\phi}h \tag{33}$$

The value $r=\sqrt{\phi}h$ is derived when $du_r\left(r,0,\infty\right)/dr$ is equal to zero. For the point fluid sink problem, the derivative is

$$\frac{du_r\left(r,0,\infty\right)}{dr}=-\frac{Q\gamma_w\left(1-2\nu\right)}{4\pi Gk}\frac{hR\left(h^2-r^2\right)+h^4}{R^3\left(R+h\right)^2}=0 \tag{34a}$$

For the point heat source problem, the similar derivative is

$$\frac{du_r\left(r,0,\infty\right)}{dr}=\frac{H\alpha_s\left(1+\nu\right)}{2\pi\lambda_t}\frac{hR\left(h^2-r^2\right)+h^4}{R^3\left(R+h\right)^2}=0 \tag{34b}$$

Here $R=\sqrt{h^2+r^2}$. Equations (34a)-(34b) leads to four possible solutions of $r=\pm\sqrt{(1+\sqrt{5})/2}h$ and $r=\pm\sqrt{(1-\sqrt{5})/2}h$. However, only $r=\sqrt{(1+\sqrt{5})/2}h$ is realistic for the radial variable $r\in\left[0,\infty\right)$.

It is interesting to discover that the golden ratio ϕ appears not only in the fluid sink and heat source induced maximum ground surface horizontal displacements, but also on the corresponding vertical displacements by letting $r=\sqrt{\phi}h$ in equations (28b) and (30b), respectively.

For the point fluid sink problem, the vertical displacement at $r=\sqrt{\phi}h$ is

$$u_z\left(\sqrt{\phi}h,0,\infty\right)=\frac{Q\gamma_w\left(1-2\nu\right)}{4\pi Gk}\frac{1}{\phi}=\frac{1}{\phi}\,u_{z\max}^{(f)}\approx 0.6180\,u_{z\max}^{(f)} \tag{35a}$$

For the point heat source problem, the vertical displacement at $r=\sqrt{\phi}h$ is

$$u_z\left(\sqrt{\phi}h,0,\infty\right)=-\frac{H\alpha_s\left(1+\nu\right)}{2\pi\lambda_t}\frac{1}{\phi}=\frac{1}{\phi}u_{z\max}^{(h)}\approx 0.6180\,u_{z\max}^{(h)} \tag{35b}$$

This shows that the ground surface vertical displacement is around 61.8% of the maximum ground surface vertical displacement at radial variable $r=\sqrt{\phi}h$, where the maximum ground surface horizontal displacement occurred. Besides, the equations (31a)-(31b) and (32a)-(32b) show that the maximum ground surface horizontal displacement and vertical displacement are not directly dependent on the depth h for both point fluid sink and point heat source induced poroelastic and thermoelastic problems.

The profiles of normalized vertical and horizontal displacements at the ground surface $z=0$ for

different dimensionless time factor $\sqrt{ct/h^2}$ are shown in Figures 5(a) and 5(b), respectively. Figure 5(a) shows the relationship between normalized radius $r/h=\sqrt{\phi}$ and normalized maximum horizontal displacement $\left|u_{r\max}/u_{z\max}\right|=1/\sqrt{\phi^5}$. Figure 5(b) shows the corresponding vertical displacement when horizontal displacement is at its maximum. The ground surface reveals significant horizontal displacement. For example, Figure 5(a) shows that the maximum ground surface horizontal displacement is around 30% of the maximum ground surface vertical displacement at $r/h=\sqrt{\phi}\approx 1.272$, which can also be found from equations (35a) and (35b).

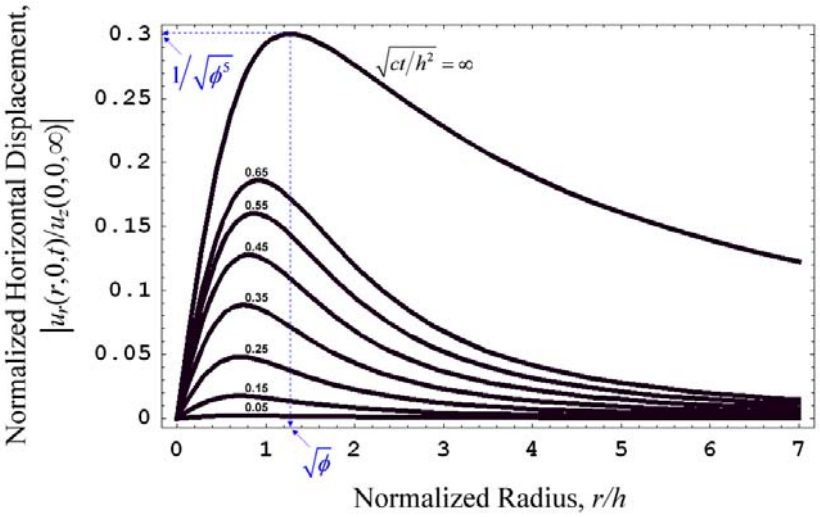

(a)

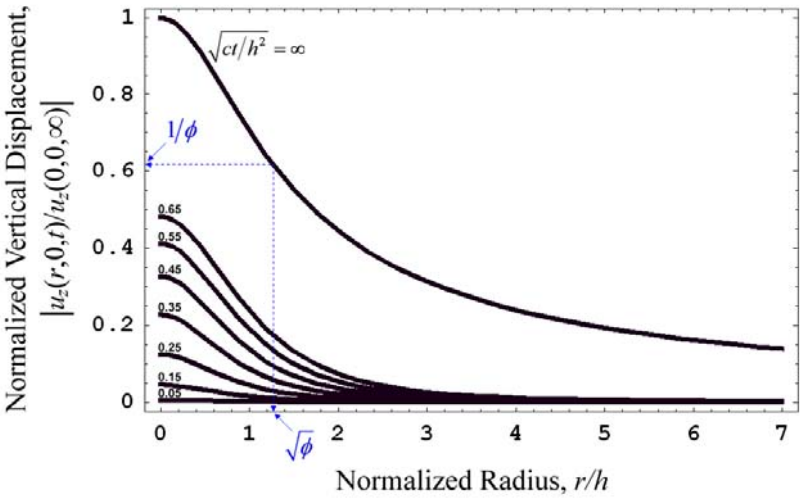

(b)

Figure 5. Normalized displacement profiles at the ground surface $z = 0$ for pervious poroelastic half space or isothermal thermoelastic half space.

The discovery of golden ratio exists in these mechanical phenomena reveals the originality and uniqueness of this study. The major practical contributions of this research also include the confirmation of mechanics display the science of art. The experimental verification related to the theoretical derivation is not supplied in the research for the purpose of the study is concentrate on the golden ratio in the Green's functions of poroelasticity and thermelasticity. The derived Green's functions can be applied to the numerical simulation of fluid sink or heat source buried in the strata induced mechanical problems by boundary element method.

7. Conclusions

The closed-form Green's functions of transient and long-term displacements due to a point fluid sink and a point heat source of an elastic half space were obtained by using Laplace-Hankel transformations. The results show:

1. The maximum ground surface horizontal displacement is approximately 30% of the maximum ground surface vertical displacement at $r = \sqrt{\phi} h \approx 1.272h$, where $\phi = (1+\sqrt{5})/2 \approx 1.618$ is known as the golden ratio. It indicates that the horizontal displacement should be properly considered in the prediction of displacements induced by fluid extraction or buried heat source.

2. The golden ratio ϕ also appears in the corresponding vertical displacement of the elastic half space caused by point fluid extraction or point heat source. The results reveal the ground surface vertical displacement at $r = \sqrt{\phi} h$ is around 61.8% of the maximum ground surface vertical displacement.

3. The maximum ground surface horizontal and vertical displacements are independent of the buried depth h for both point fluid sink and point heat source induced poroelastic and thermoelastic problems.

Acknowledgements

This work is supported by the National Science Council of Republic of China through grants NSC100-2221-E-216-025, NSC81-0410-E-216-503, and also by the Chung Hua University under grant CHU-99-A-03.

References

[1] M. Livio, *The golden ratio: The story of phi, the world's most astonishing number* (New York: Broadway Books, 2002).

[2] R.A. Dunlap, *The golden ratio and Fibonacci numbers* (Singapore: World Scientific Publishing, 1997).

[3] S.K. Sen & R.P. Agarwal, Golden ratio in science, as random sequence source, its computation and

beyond, *Computers and Mathematics with Applications*, 56(2), 2008, 469-498.

[4] P. Puri & P.M. Jordan, On the steady shear flow of a dipolar fluid in a porous half-space, *International Journal of Engineering Science*, 44(3-4), 2006, 227-240.

[5] C.M. Moorman & J.E. Goff, Golden ratio in a coupled-oscillator problem, *European Journal of Physics*, 28(5), 2007, 897-902.

[6] I. Affleck, Solid-state physics: Golden ratio seen in a magnet, *Nature*, 464, 2010, 362-363.

[7] M.A. Biot, General theory of three-dimensional consolidation, *Journal of Applied Physics*, 12(2), 1941, 155-164.

[8] M.A. Biot, Theory of elasticity and consolidation for a porous anisotropic solid, *Journal of Applied Physics*, 26(2), 1955, 182-185.

[9] J.R. Rice & M.P. Cleary, Some basic stress-diffusion solutions for fluid saturated elastic porous media with compressible constituents, *Reviews of Geophysics and Space Physics*, 14(2), 1976, 227-241.

[10] J. Bear & M.Y. Corapcioglu, Mathematical model for regional land subsidence due to pumping, 1. Integrated aquifer subsidence equations based on vertical displacement only, *Water Resources Research*, 17(4), 1981, 937-946.

[11] J. Bear & M.Y. Corapcioglu, Mathematical model for regional land subsidence due to pumping, 2. Integrated aquifer subsidence equations for vertical and horizontal displacements, *Water Resources Research*, 17(4), 1981, 947-958.

[12] J.R. Booker & J.P. Carter, Analysis of a point sink embedded in a porous elastic half space, *International Journal for Numerical and Analytical Methods in Geomechanics*, 10(2), 1986, 137-150.

[13] J.R. Booker & J.P. Carter, Long term subsidence due to fluid extraction from a saturated, anisotropic, elastic soil mass, *The Quarterly Journal of Mechanics and Applied Mathematics*, 39(1), 1986, 85-98.

[14] J.R. Booker & J.P. Carter, Elastic consolidation around a point sink embedded in a half-space with anisotropic permeability, *International Journal for Numerical and Analytical Methods in Geomechanics*, 11(1), 1987, 61-77.

[15] J.R. Booker & J.P. Carter, Withdrawal of a compressible pore fluid from a point sink in an isotropic elastic half space with anisotropic permeability, *International Journal of Solids and Structures*, 23(3), 1987, 369-385.

[16] J.-Q. Tarn & C.-C. Lu, Analysis of subsidence due to a point sink in an anisotropic porous elastic half space, *International Journal for Numerical and Analytical Methods in Geomechanics*, 15(8), 1991, 573-592.

[17] G.J. Chen, Analysis of pumping in multilayered and poroelastic half space, *Computers and Geotechnics*, 30(1), 2002, 1-26.

[18] G.J. Chen, Steady-state solutions of multilayered and cross-anisotropic poroelastic half-space due to a point sink, *International Journal of Geomechanics*, 5(1), 2005, 45-57.

[19] W. Kanok-Nukulchai & K.T. Chau, Point sink fundamental solutions for subsidence prediction, *Journal of Engineering Mechanics, ASCE*, 116(5), 1990, 1176-1182.

[20] J. C.-C. Lu & F.-T. Lin, The transient ground surface displacements due to a point sink/heat source in an elastic half-space, *Geotechnical Special Publication No. 148, ASCE*, 2006, 210-218.

[21] J. C.-C. Lu & F.-T. Lin, Analysis of transient ground surface displacements due to an impulsive point sink in an elastic half space, *Proceedings of the IASTED International Conference on Environmental Management and Engineering*, Banff, Alberta, Canada, 2009, 211-217.

[22] C.-S. Hou, J.-C. Hu, L.-C. Shen, J.-S. Wang, C.-L. Chen, T.-C. Lai, C. Huang, Y.-R. Yang, R.-F. Chen, Y.-G. Chen & J. Angelier, Estimation of Subsidence Using GPS Measurements, and Related Hazard: the Pingtung Plain, Southwestern Taiwan, *Comptes Rendus Geoscience*, 337(13), 2005,

1184-1193.

[23] T. Hueckel & A. Peano, Some geotechnical aspects of radioactive waste isolation in continental clays, *Computers and Geotechnics*, 3(2-3), 1987, 157-182.

[24] C.D. Hollister, D.R. Anderson & G.R. Health, Subseabed disposal of nuclear wastes, *Science*, 213(4514), 1981, 1321-1326.

[25] D.W. Smith & J.R. Booker, Boundary element analysis of linear thermoelastic consolidation, *International Journal for Numerical and Analytical Methods in Geomechanics*, 20(7), 1996, 457-488.

[26] J.R. Booker & C. Savvidou, Consolidation around a point heat source, *International Journal for Numerical and Analytical Methods in Geomechanics*, 9(2), 1985, 173-184.

[27] J.R. Booker & C. Savvidou, Consolidation around a spherical heat source, *International Journal of Solids and Structures*, 20(11/12), 1984, 1079-1090.

[28] C. Savvidou & J.R. Booker, Consolidation around a heat source buried deep in a porous thermoelastic medium with anisotropic flow properties, *International Journal for Numerical and Analytical Methods in Geomechanics*, 13(1), 1989, 75-90.

[29] A. Norris, On the correspondence between poroelasticity and thermoelasticity, *Journal of Applied Physics*, 71(3), 1992, 1138-1141.

[30] G.D. Manolis & D.E. Beskos, Integral formulation and fundamental solutions of dynamic poroelasticity and thermoelasticity, *Acta Mechanica*, 76(1-2), 1989, 89-104.

[31] A. H.-D. Cheng, T. Badmus & D.E. Beskos, Integral equation for dynamic poroelasticity in frequency domain with BEM solution, *Journal of Engineering Mechanics, ASCE*, 117(5), 1991, 1136-1157.

[32] A. Skempton, The pore pressure coefficients A and B, *Geotechnique*, 4, 1954, 143-147.

[33] E. Detournay & A. H.-D. Cheng, Poroelastic response of a borehole in a non-hydrostatic stress field, *International Journal of Rock Mechanics and Mining Sciences & Geomechanics Abstracts*, 25(3), 1988, 171-182.

[34] I.N. Sneddon, *Fourier transforms* (New York: McGraw-Hill, 1951, 48-70).

[35] A. Erdelyi, W. Magnus, F. Oberhettinger & F.G. Tricomi, *Tables of integral transforms* (New York: McGraw-Hill, 1954).

Symbols

b_i	Body forces (*Pa/m*)
B	Skempton's pore pressure coefficient (Dimensionless)
c	Parameter, $c=\frac{2GB^2(1-2\nu)(1+\nu_u)^2}{9(\nu_u-\nu)(1-2\nu_u)}\frac{k}{\gamma_f}$ (m^2/s) or $c=\lambda_t/c_\varepsilon$ (m^2/s); Specific heat of the thermoelastic medium (*J/kg°C*)
c_ε	Specific heat at constant strain of the thermoelastic medium, $c_\varepsilon=\rho c$ ($J/m^3°C$)
$erf(x)$	Error function (Dimensionless)
$erfc(x)$	Complementary error function (Dimensionless)
G	Shear modulus of the poroelastic/thermoelastic medium (*Pa*)
h	Depth of point fluid sink (*m*); Buried depth of point heat source (*m*)
H	Constant strength of the point heat source (*J/s*)
$I_\alpha(x)$	Modified Bessel function of the first kind of order α (Dimensionless)
k	Permeability of the isotropic poroelastic medium (*m/s*)
p	Excess pore fluid pressure (*Pa*)
q_i	Heat flux (J/sm^2)
Q	Constant strength of the point fluid sink rate (m^3/s)
(r,θ,z)	Cylindrical coordinates system (*m*, *radian*, *m*)
s	Entropy of the internal state function of the thermoelastic system ($J/°Cm^3$)
t	Time (*s*)
T_0	Average temperature in the natural state corresponding with $\varepsilon_{ij}=0$ (°*C*)
$u(t)$	Heaviside step function (Dimensionless)
u_i	Displacement components of the poroelastic/thermoelastic medium (*m*)
$u_{r\max}^{(f)}, u_{z\max}^{(f)}$	Maximum ground surface horizontal displacement and vertical displacement of the poroelastic medium (*m*)
$u_{r\max}^{(h)}, u_{z\max}^{(h)}$	Maximum ground surface horizontal displacement and vertical displacement of the thermoelastic medium (*m*)

v_i	Specific discharge velocity components (*m/s*)
W	Quantity of heat generated in a unit volume and unit time (J/sm^3)
α_s	Linear thermal expansion coefficient of the thermoelastic medium ($°C^{-1}$)
γ	Rate of injected fluid source into the saturated porous medium per unit volume (s^{-1})
γ_f	Unit weight of pore fluid (N/m^3)
$\delta(x)$	Dirac delta function (m^{-1})
δ_{ij}	Kronecker delta (Dimensionless)
ε	Volumetric strain of the poroelastic/thermoelastic medium (Dimensionless)
ε_{ij}	Strain components of the poroelastic/thermoelastic medium (Dimensionless)
ς	Variation of fluid content per unit reference volume (Dimensionless)
ϑ	Temperature increment of the thermoelastic medium ($°C$)
λ_t	Thermal conductivity of the thermoelastic medium ($J/sm°C$)
ν	Poisson's ratio of the poroelastic/thermoelastic medium (Dimensionless)
ν_u	Undrained Poisson's ratio of the poroelastic medium (Dimensionless)
ρ	Density of the thermoelastic medium (kg/m^3)
σ_{ij}	Total stress components of the poroelastic medium (*Pa*); Thermal stress components of the thermoelastic medium (*Pa*)
ϕ	Golden ratio, $\phi \approx 1.6180339887498948482...$ (Dimensionless)
∇^2	Laplacian operator, $\nabla^2 = \partial^2/\partial r^2 + 1/r\,\partial/\partial r + \partial^2/\partial z^2$ (m^{-2})

Biographies

John C.-C. Lu received his Ph.D. degree in Civil Engineering from the National Cheng Kung University and started his academic career in the Department of Civil Engineering at Chung Hua University in 1991. His fields of interest are poromechanics, thermomechanics, geomechanics, environmental engineering, mathematical modelling, and numerical simulation.

Feng-Tsai Lin obtained her M.S. degree in Department of Applied Mathematics from the National Cheng Kung University in 1991. She is currently an Assistant Professor in Department of Naval Architecture of National Kaohsiung Marine University. Her research work is focused on applied mathematics and statistics.

附錄 2

研究成果投稿後依審查意見修訂中之EI/SCI等級期刊論文一篇

Lu, John C.-C., Meng-Qi Chen and Feng-Tsai Lin, 2013, "Point Heat Source Induced Thermoelastic Responses of the Cross-anisotropic Strata," *International Journal for Numerical and Analytical Methods in Geomechanics, ISSN: 0363-9061*, **Under Revision**. (This work is supported by the National Science Council through grant NSC100-2221-E-216-025.) (EI, SCI)

論文審査意見通知函

主要識別身分

寄件者: <ajwhittl@mit.edu>
收件者: <cclu@chu.edu.tw>; <m8804505@chu.edu.tw>; <ftlin@mail.nkmu.edu.tw>
傳送日期: 2012年5月23日 下午 08:58
主旨: NAG-11-0223 - Decision

Dear Dr Lu,

Manuscript ID NAG-11-0223 entitled "Point heat source induced thermoelastic responses of the cross-anisotropic strata" which you submitted to International Journal for Numerical and Analytical Methods in Geomechanics, has been reviewed. The comments of the referee(s) are included at the bottom of this letter. If the referee supplied an attachment this will be viewable in your Author Center - not attached to this message.

A revised version of your manuscript that takes into account the comments of the referee(s) will be reconsidered for publication. The revised version must address the comments of reviewer #2 and demonstrate the originality and contribution of their solutions.

Please note that submitting a revision of your manuscript does not guarantee eventual acceptance, and that your revision may be subject to re-review by the referee(s) before a decision is rendered.

You can upload your revised manuscript and submit it through your Author Center. Log into http://mc.manuscriptcentral.com/nag and enter your Author Center, where you will find your manuscript title listed under "Manuscripts with Decisions".

When submitting your revised manuscript, you will be able to respond to the comments made by the referee (s) in the space provided. You can use this space to document any changes you make to the original manuscript.

IMPORTANT: Please make sure you closely follow the instructions for acceptable files.

Please remember that the publishers will not accept a manuscript unless accompanied by the Copyright Transfer Agreement. Please go to: http://media.wiley.com/assets/1540/86/ctaaglobal.pdf

The Copyright Transfer Form and the Permissions Form should be scanned and uploaded with your submission to Manuscript Central, designated as "Supplementary Material Not for Review". If you do not have access to a scanner, further instructions will be provided upon the acceptance of your paper. Forms should not be sent to the editorial office.

Once again, thank you for submitting your manuscript to International Journal for Numerical and Analytical Methods in Geomechanics and I look forward to receiving your revision.

Sincerely,

Prof. Andrew Whittle
Editor, International Journal for Numerical and Analytical Methods in Geomechanics
ajwhittl@mit.edu

Referee(s)' Comments to Author:

Reviewing: 1
Comments to the Author
This is a worthwhile paper, which apart from a few very minor issues (e.g. 'gave advices') is nicely written and cleanly presented.

However, the solutions presented are long term solutions, and authors should point out to readers of the paper potential limitations of their solutions. For example, transient states may present stress states and fluid and

mass transport that are more problematic from a design perspective, that steady state stress states and steady state fluid and mass transport. Another potentially important limitation in practice is the absence of a free surface (as the point source is assumed infinitely deep). Perhaps these issues warrant some discussion in the paper.

The relationship to previous solutions (e.g. greens functions and the authors previous work) could also be made more clear.

It would be useful for the authors to point out where their work is going, and so what is planned in the future. For example, their current solution could be employed in boundary element formulation to obtain solutions when there is a free surface, or for more complicated geometries and source distributions.

Reviewing: 2
Comments to the Author
The review are included in teh file attached

Comments on “point heat source induced thermoelastic responses of the cross-anisotropic strata” by John C.C. Lu, Meng-Qi Chen and Feng-Tsai Lin (25-Oct-2011)

In this manuscript, a fundamental analytical solution for the steady state of uncoupled thermo-elasticity of a transversely isotropic infinite space due to an embedded heat source is developed and presented. For this purpose, the integral transform techniques are employed to solve the related governing equations of the classical theory of thermo-elasticity. The generated solution is next reduced to the cases which fit in the special cases of mechanical and/or thermal properties isotropy. Lastly, some numerical examples are provided to discuss the influence of the anisotropy of mechanical or thermo-mechanical properties on the generated displacement and stress.

The presented formulation is straightforward which can be easily followed. However, the particular problem addressed within the manuscript seems to be dramatically over-simplified compared to currently published solutions to more generalized cases of the same problem. More specifically, further support for the authors’ statement in the introduction as “The present investigation is focused on the closed-form solutions of a cross-anisotropic thermo-elastic medium due to a deep point heat source which still have not been derived in previous studies” should have been provided.

The transient thermo-elasticity of a transversely isotropic half-space is considered in publications as early as 1958, i.e. “Sharma B, et al. thermal stresses in transversely isotropic semi-infinite elastic solids, Journal of applied mechanics”. More relevantly, the dual potential solution of “singh B. 1960 the axisymmetrical thermal stresses in transversely isotropic bodies, Archives of Mechanics, 287-304” has formulated the axisymmetric thermal stress problem in a transversely isotropic half-space. The authors are also encouraged to read “Noda et al. 1985 on a general treatise of three-dimensional thermo-elastic problems in transversely isotropic Bodies, Math. Mech. 65(10), 509-512” which consider the 3D alternative of the same problem. More generalized cases which encounter the free boundary of a half-space together with layered inhomogeneity are considered in the following highly cited papers by Ernian Pan:
1. E. Pan, 1990, Thermo-elastic deformation of a transversely isotropic and layered half-space by surface loads and internal sources, Physics of the Earth and Planetary Interiors, 60, 254-264.
2. E. Pan, 1997, Static Green’s functions in multilayered half spaces, Applied Mathematical Modeling, 21, 509-521.

Recent publications on this subject mostly elaborate on more sophisticated physical phenomena e.g. poro-thermo-elasticity of transversely isotropic materials, see “Abousleiman Y. and Ekbote S. 2002 Porothermoelasticity in Transversely Isotropic Porous Materials, IUTAM symposium on theoretical and numerical methods in continuum mechanics of porous materials; Solid mechanics and Its Applications, 2002, 87, 145-152” or magneto-electro-thermo-elastic coupling effects in transversely isotropic bodies “Hu PF., 2009, Three-dimensional Green’s function for a point heat source in two-phase transversely isotropic magneto-electro-thermo-elastic material, Mechanics of Materials, 41, 329-338”.

For this reason, the reviewer suggests that the paper not be accepted for publication in the International Journal of Numerical and Analytical methods in Geomechanics because neither the employed mathematical technique nor its generated solution is novel.

Important note:
The reviewer may have returned thier comments to me as a separate file. This file is not necessarily attached to the decision letter. You can view reviewer's attachment by visiting your Author Centre at http://mc.manuscriptcentral.com/nag .
Click on the "Manuscripts with Decisions" queue. In the list appearing at the bottom of the screen click on "View Decision Letter".
In the new window the files can be seen in the section "Files attached" at the bottom. Please do not hesitate to contact Alice Wood, awood@wiley.com if you experience any problems.

==========

==========

論文全文

Preview

From: awood@wiley.com

To: cclu@chu.edu.tw, m8804505@chu.edu.tw, ftlin@mail.nkmu.edu.tw

CC:

Subject: NAG-11-0223 successfully submitted

Body:

Dear Dr Lu,

Your manuscript entitled "Point heat source induced thermoelastic responses of the cross-anisotropic strata" has been successfully submitted online and is presently being given full consideration for publication in International Journal for Numerical and Analytical Methods in Geomechanics.

Your manuscript number is NAG-11-0223. Please mention this number in all future correspondence regarding this submission.

You can view the status of your manuscript at any time by checking your Author Center after logging into http://mc.manuscriptcentral.com/nag . If you have difficulty using this site, please click the 'Get Help Now' link at the top right corner of the site.

Thank you for submitting your manuscript to International Journal for Numerical and Analytical Methods in Geomechanics.

Sincerely,

International Journal for Numerical and Analytical Methods in Geomechanics Editorial Office

==========

Don't miss a thing- sign up to Wiley Online Library content alerts so you can be notified when new articles are published in your research area.

http://olabout.wiley.com/WileyCDA/Section/id-404508.html

Now available online, all articles from the International Journal for Numerical and Analytical Methods in Geomechanics since 1977, Volume 1, Issue 1. More information at http://onlinelibrary.wiley.com/

Also available online, the Encyclopedia of Computational Mechanics: http://onlinelibrary.wiley.com/book/10.1002/0470091355

This encyclopedia also exists in print: http://www.wiley.com/WileyCDA/WileyTitle/productCd-0470846992.html

==========

Date Sent: 25-Oct-2011

Close Window

Point heat source induced thermoelastic responses of the cross-anisotropic strata

Journal:	*International Journal for Numerical and Analytical Methods in Geomechanics*
Manuscript ID:	NAG-11-0223
Wiley - Manuscript type:	Research Article
Date Submitted by the Author:	25-Oct-2011
Complete List of Authors:	Lu, John C.-C.; Chung Hua University, Department of Civil Engineering Chen, Meng-Qi; Chung Hua University, Department of Civil Engineering Lin, Feng-Tsai; National Kaohsiung Marine University, Department of Naval Architecture
Keywords:	closed-form solution, point heat source, cross-anisotropic strata, full space, integral transform

Point heat source induced thermoelastic responses of the cross-anisotropic strata

John C.-C. Lu[1,*,†], Meng-Qi Chen[1] and Feng-Tsai Lin[2]

[1]*Department of Civil Engineering, Chung Hua University, No. 707, Sec. 2, WuFu Rd., Hsinchu, Taiwan 30012, R.O.C.*
[2]*Department of Naval Architecture, National Kaohsiung Marine University, No. 142, Haijhuan Rd., Kaohsiung 81157, R.O.C.*

SUMMARY

This work presents the closed-form solutions of the long-term thermal stresses, displacements and temperature increment of the cross-anisotropic strata subjected to a point heat source at great depth. The medium is initially modeled with cross-anisotropic mechanical and thermal properties. Under this assumption, the properties of the materials are different between the planes on and normal to the isotropic plane. Using Hankel and Fourier transforms, this paper presents the analytic solutions to soils or rocks affected by the point heat source, such as the repositories of nuclear wastes. The general solutions are further simplified to cases of materials with isotropic mechanical properties, and they are finally extended to fully isotropic in each property of the strata. Based on numerical results, the thermal stresses, displacements and temperature change of the thermoelastic half space are significantly affected by the anisotropy of mechanical and thermal properties of the strata.

KEY WORDS: closed-form solution; point heat source; cross-anisotropic strata; full space; integral transform

[*]Correspondence to: John C.-C. Lu, Department of Civil Engineering, Chung Hua University, No. 707, Sec. 2, WuFu Rd., Hsinchu, Taiwan 30012, R.O.C.
[†]E-mail: cclu@chu.edu.tw

1. INTRODUCTION

The thermal mechanical responses of strata due to heat generated by the radioactive waste in deep underground are important environmental engineering issues. For their impact on environment and human safety, many studies were conducted to understand the mechanical, thermal and hydraulic behaviour of deep repository radioactive waste. Nuclear wastes are usually deposited at a great depth, such as 200 to 700 meters below ground; therefore, they can be isolated from the living environment of human beings. Excessive thermal difference usually results in a volume change of water and solid skeleton. This change can increase excess pore water pressure and lead to decrease in effective stress, which can result in a thermal failure in the strata due to loss of shear resistance of solid skeleton. The simulation of these physical features is a complex task, and its validation is a major concern for the safety improvement of the repository.

The disposal in stable deep geological formations has been proven as a technically viable solution in disposing the high level radioactive wastes [1]. Based on the theory of mixtures applied to the multiphysics of porous media, Tong *et al.* [2] presented a numerical method for modeling coupled thermo-hydro-mechanical processes of geomaterials with multiphase fluid flow. Analytical solutions of the thermal consolidation for a saturated elastic porous media around a point heat source were presented by Booker and Savvidou [3,4], Savvidou and Booker [5]. In their solutions, the flow was considered isotropic [3,4] or cross-anisotropic [5], whereas the mechanical and thermal properties of the strata were only treated as isotropic. However, it was identified that the anisotropic property in the permeability of the strata has significant effects on the excess pore water pressure generated by a heat source [5]. Lu and Lin [6] displayed transient ground surface displacements produced by a point heat source or fluid sink through analog quantities between thermoelasticity and poroelasticity. Based on three-dimensional thermoelastic theory of homogeneous isotropic media, the golden ratio appears in the maximum ground surface horizontal displacement and corresponding vertical displacement of a half space were presented by Lin and Lu [7]. Wang and Sudak [8] derived the three-dimensional temperature field induced by a steady point heat source interacting with a homogeneous imperfect interface by using the image method. Hudson *et al.* [9] gave advices on how to incorporate thermo-hydro-mechanical coupled processes into performance, safety assessments and design studies for disposal of radioactive waste in geological formations. Within the framework of linear theory of thermoelasticity, Chao, Chen and Shen [10] discussed the situation of circularly cylindrical layered media subjected to an arbitrary point heat source.

In general, soils are deposited through a geologic process of sedimentation over a long period of time. Under the accumulative overburden pressure, strata display significant anisotropy on mechanical, seepage and thermal properties. Both stratified soil and rock masses show the phenomenon of anisotropy. For this reason, theoretical and numerical models should be able to simulate the layered soils and rocks as cross-anisotropic media [11-15].

The present investigation is focused on the closed-form solutions of a cross-anisotropic thermoelastic medium due to a deep point heat source which still have not been derived in previous studies. In this paper, the soil or rock mass is modelled as a linearly elastic medium with cross-anisotropic properties. Both thermal flow and mechanical properties are assumed to be cross-anisotropic. By using the Hankel and Fourier transforms, closed-form solutions of the long-term displacements, temperature changes and thermal stresses of the strata due to a point heat source at large depth are obtained. The results are reduced to an isotropic case to provide better understanding of the thermal induced responses of the strata.

2. MATHEMATICAL MODEL

2.1. Basic Equations

Figure 1 shows a point heat source buried in the strata at a great depth. The property of soil or rock is considered as cross-anisotropic homogeneous layer. To simplify the model, the plane of symmetry of the strata is set in the horizontal direction. The cylindrical coordinate system (r,θ,z) is applied to the layer of solid where the plane of isotropy coincides with the horizontal ($r-\theta$) plane. The symbols u_r and u_z are the displacements in radial and vertical directions, respectively. The constitutive law for an elastic medium with linear axisymmetric deformation can thus be expressed as

$$\sigma_{rr} = A\frac{\partial u_r}{\partial r} + (A-2N)\frac{u_r}{r} + F\frac{\partial u_z}{\partial z} - \beta_r \vartheta, \tag{1a}$$

$$\sigma_{\theta\theta} = (A-2N)\frac{\partial u_r}{\partial r} + A\frac{u_r}{r} + F\frac{\partial u_z}{\partial z} - \beta_r \vartheta, \tag{1b}$$

$$\sigma_{zz} = F\frac{\partial u_r}{\partial r} + F\frac{u_r}{r} + C\frac{\partial u_z}{\partial z} - \beta_z \vartheta, \tag{1c}$$

$$\sigma_{rz} = L\left(\frac{\partial u_r}{\partial z} + \frac{\partial u_z}{\partial r}\right), \tag{1d}$$

where σ_{ij} are the thermal stress components, and ϑ is the temperature change of the strata. The coefficients A, C, F, L, N are the material constants of a cross-anisotropic medium defined by Love [16]. For axially symmetric problem, the shear stresses $\sigma_{r\theta}$, $\sigma_{\theta z}$, and circumferential displacement u_θ can vanish as the vertical z-axis positioned through the point heat source. In these equations, β_r and β_z represent the thermal expansion factors along and normal to the symmetric plane, respectively. The expression for the thermal expansion factors are:

$$\beta_r = 2(A-N)\alpha_{sr} + F\alpha_{sz}, \tag{2a}$$

$$\beta_z = 2F\alpha_{sr} + C\alpha_{sz}, \tag{2b}$$

where α_{sr} and α_{sz} are the linear thermal expansion coefficients of the strata in horizontal and vertical directions, respectively.

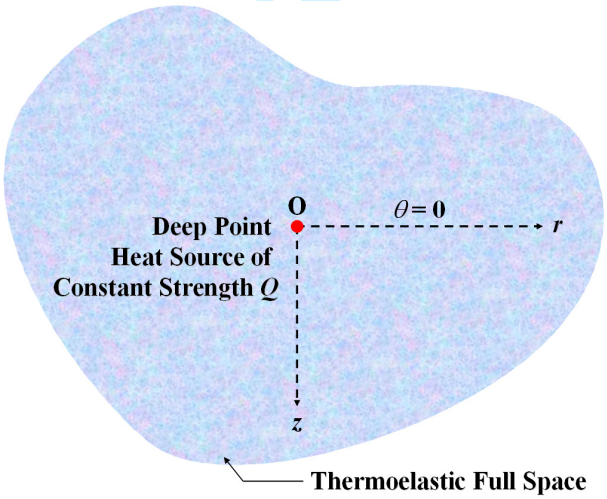

Figure 1. Point heat source buried deep in the cross-anisotropic strata.

Equations (1a) to (1d) can be converted to

$$\begin{Bmatrix} \frac{\partial u_r}{\partial r}-\alpha_{sr}\vartheta \\ \frac{u_r}{r}-\alpha_{sr}\vartheta \\ \frac{\partial u_z}{\partial z}-\alpha_{sz}\vartheta \\ \frac{\partial u_r}{\partial z}+\frac{\partial u_z}{\partial r} \end{Bmatrix} = \begin{bmatrix} \frac{1}{E_r} & -\frac{\nu_{r\theta}}{E_r} & -\frac{\nu_{rz}}{E_r} & 0 \\ -\frac{\nu_{r\theta}}{E_r} & \frac{1}{E_r} & -\frac{\nu_{rz}}{E_r} & 0 \\ -\frac{\nu_{zr}}{E_z} & -\frac{\nu_{zr}}{E_z} & \frac{1}{E_z} & 0 \\ 0 & 0 & 0 & \frac{1}{G_{rz}} \end{bmatrix} \begin{Bmatrix} \sigma_{rr} \\ \sigma_{\theta\theta} \\ \sigma_{zz} \\ \sigma_{rz} \end{Bmatrix}. \tag{3}$$

Here, the Young's moduli E_r and E_z are defined as directions lying in and perpendicular to the plane of isotropy, respectively; $\nu_{r\theta}$ is the Poisson's ratio for strain in the horizontal direction due to horizontal direct stress; ν_{rz} is the Poisson's ratio for strain in the vertical direction due to horizontal direct stress; ν_{zr} is the Poisson's ratio for strain in the horizontal direction due to a vertical direct stress; and G_{rz} is shear modulus for planes normal to the plane of isotropy. The mechanical constants A, C, F, L, N are employed in equations (1a) to (1d) and (3) through the following equations:

$$A=\frac{E_r\left(1-\nu_{rz}\nu_{zr}\right)}{\left(1+\nu_{r\theta}\right)\left(1-\nu_{r\theta}-2\nu_{rz}\nu_{zr}\right)}, \tag{4a}$$

$$C=\frac{E_z\left(1-\nu_{r\theta}\right)}{1-\nu_{r\theta}-2\nu_{rz}\nu_{zr}}, \tag{4b}$$

$$F=\frac{E_z\nu_{rz}}{1-\nu_{r\theta}-2\nu_{rz}\nu_{zr}}=\frac{E_r\nu_{zr}}{1-\nu_{r\theta}-2\nu_{rz}\nu_{zr}}, \tag{4c}$$

$$L=G_{rz}, \tag{4d}$$

$$N=\frac{E_r}{2\left(1+\nu_{r\theta}\right)}. \tag{4e}$$

For the cases of isotropic thermoelastic medium, the mechanical and thermal elastic constants A, C, F, L, N, β_r and β_z can be simplified as

$$A=C=\lambda+2G, \tag{5a}$$

$$F=\lambda, \tag{5b}$$

$$L=N=G, \tag{5c}$$

$$\beta_r=\beta_z=\left(2G+3\lambda\right)\alpha_s. \tag{5d}$$

The constants λ and G are the Lame moduli of the isotropic thermoelastic medium, and α_s is the linear thermal expansion coefficient of the isotropic solid skeleton.

These axially symmetric thermal stresses in equations (1a) to (1d) must satisfy the equilibrium equations:

$$\frac{\partial\sigma_{rr}}{\partial r}+\frac{\sigma_{rr}-\sigma_{\theta\theta}}{r}+\frac{\partial\sigma_{rz}}{\partial z}+f_r=0, \tag{6a}$$

$$\frac{\partial\sigma_{rz}}{\partial r}+\frac{\sigma_{rz}}{r}+\frac{\partial\sigma_{zz}}{\partial z}+f_z=0, \tag{6b}$$

where $f_i\left(i=r,z\right)$ denotes the body force components. A straightforward substitution of constitutive law (1a) to

(1d) into the equilibrium equations with body forces neglected, the equilibrium equations are expressed in terms of displacements $u_i\,(i=r,z)$ and temperature change of the strata ϑ as follows:

$$A\left(\frac{\partial^2 u_r}{\partial r^2}+\frac{1}{r}\frac{\partial u_r}{\partial r}-\frac{u_r}{r^2}\right)+L\frac{\partial^2 u_r}{\partial z^2}+(F+L)\frac{\partial^2 u_z}{\partial r\partial z}-\beta_r\frac{\partial \vartheta}{\partial r}=0, \tag{7a}$$

$$(F+L)\left(\frac{\partial^2 u_r}{\partial r\partial z}+\frac{1}{r}\frac{\partial u_r}{\partial z}\right)+L\left(\frac{\partial^2 u_z}{\partial r^2}+\frac{1}{r}\frac{\partial u_z}{\partial r}\right)+C\frac{\partial^2 u_z}{\partial z^2}-\beta_z\frac{\partial \vartheta}{\partial z}=0. \tag{7b}$$

Let $\boldsymbol{h}$ be the heat flux vector and q_h be the heat sources, the law of conservation of energy is then listed as:

$$-\nabla\cdot\boldsymbol{h}+q_h=0. \tag{8}$$

The constants λ_{tr} and λ_{tz} are used to describe the behavior of the heat flow in a cross-anisotropic medium, in which λ_{tr} denotes the horizontal thermal conductivity of heat flow in the planes of isotropy and λ_{tz} is the corresponding vertical thermal conductivity in the plane perpendicular to isotropic plane. Assuming that the heat flow follows Fourier's law, then

$$\boldsymbol{h}=-\lambda_{tr}\frac{\partial \vartheta}{\partial r}\boldsymbol{i}_r-\lambda_{tz}\frac{\partial \vartheta}{\partial z}\boldsymbol{i}_z, \tag{9}$$

in which $\boldsymbol{i}_r$ and $\boldsymbol{i}_z$ are unit vectors parallel to the radial and vertical directions, respectively. The point heat source of constant strength Q is considered at great depth of point $(0,0)$. Substituting (9) into (8) yields the third governing equation of temperature change ϑ as below:

$$\lambda_{tr}\left(\frac{\partial^2 \vartheta}{\partial r^2}+\frac{1}{r}\frac{\partial \vartheta}{\partial r}\right)+\lambda_{tz}\frac{\partial^2 \vartheta}{\partial z^2}+\frac{Q}{2\pi r}\delta(r)\delta(z)=0, \tag{10}$$

where $\delta(r)$ and $\delta(z)$ are the Dirac delta functions.

For a linearly elastic medium with cross-anisotropic properties, the differential equations (7a), (7b) and (10) govern the steady state responses of the medium subjected to axisymmetric and thermoelastic disturbance.

2.2. Boundary Conditions

The point heat source at great depth is assumed no impact on the ground surface. This implies that the ground surface can be treated as a remote boundary, and the strata can be modeled as an infinite space as shown in Figure 1. Thus, the effect of the deep thermally disturbance vanishes at the remote boundaries, $z\to\pm\infty$. In other words, the displacements and the temperature change of the strata at remote boundaries should be vanished. Therefore, the remote boundary conditions are expressed as

$$u_r(r,z)\to 0,\ u_z(r,z)\to 0, \text{ and } \vartheta(r,z)\to 0 \text{ as } z\to\pm\infty. \tag{11}$$

The thermoelastic responses are derived in this study by Hankel and Fourier transforms from the differential equations (7a), (7b) and (10) corresponding with the remote boundary conditions at $z\to\pm\infty$.

3. ANALYTIC SOLUTIONS

3.1. Hankel-Fourier Transform Solutions

The governing partial differential equations (7a), (7b) and (10) are simplified to ordinary differential equations by

performing appropriate Hankel transforms [17] with respect to the radial coordinate r of first, zeroth and zeroth orders in each equation, respectively. These equations then become:

$$-\xi^2 A U_r + L\frac{d^2U_r}{dz^2} - \xi(F+L)\frac{dU_z}{dz} + \xi\beta_r\Theta = 0\,, \tag{12a}$$

$$\xi(F+L)\frac{dU_r}{dz} - \xi^2 L U_z + C\frac{d^2U_z}{dz^2} - \beta_z\frac{d\Theta}{dz} = 0\,, \tag{12b}$$

$$-\xi^2\lambda_{tr}\Theta + \lambda_{tz}\frac{d^2\Theta}{dz^2} = -\frac{Q}{2\pi}\delta(z)\,, \tag{12c}$$

where

$$U_r(z;\xi) = \int_0^\infty r\,u_r(r,z)\,J_1(\xi r)\,dr\,, \tag{13a}$$

$$U_z(z;\xi) = \int_0^\infty r\,u_z(r,z)\,J_0(\xi r)\,dr\,, \tag{13b}$$

$$\Theta(z;\xi) = \int_0^\infty r\,\vartheta(r,z)\,J_0(\xi r)\,dr\,. \tag{13c}$$

In these equations, $J_\nu(x)$ represents the Bessel's function of the first kind of order ν. The displacements and the temperature change of the strata are obtained by inverting the equations (13a) to (13c) as shown below:

$$u_r(r,z) = \int_0^\infty \xi U_r(z;\xi)\,J_1(\xi r)\,d\xi\,, \tag{14a}$$

$$u_z(r,z) = \int_0^\infty \xi U_z(z;\xi)\,J_0(\xi r)\,d\xi\,, \tag{14b}$$

$$\vartheta(r,z) = \int_0^\infty \xi\Theta(z;\xi)\,J_0(\xi r)\,d\xi\,. \tag{14c}$$

The Fourier transformations [17] are performed with respect to the axial coordinate z on equations (12a) to (12c). The results are expressed as

$$-\left(\xi^2 A + \omega^2 L\right)\tilde{U}_r + i\omega\xi(F+L)\,\tilde{U}_z + \xi\beta_r\tilde{\Theta} = 0\,, \tag{15a}$$

$$-i\omega\xi(F+L)\,\tilde{U}_r - \left(\xi^2 L + \omega^2 C\right)\tilde{U}_z + i\omega\beta_z\tilde{\Theta} = 0\,, \tag{15b}$$

$$\left(\xi^2\lambda_{tr} + \omega^2\lambda_{tz}\right)\tilde{\Theta} = \frac{Q}{2\pi}\,, \tag{15c}$$

where

$$\tilde{U}_r(\xi,\omega) = \int_{-\infty}^\infty U_r(z;\xi)\,e^{i\omega z}\,dz\,, \tag{16a}$$

$$\tilde{U}_z(\xi,\omega) = \int_{-\infty}^\infty U_z(z;\xi)\,e^{i\omega z}\,dz\,, \tag{16b}$$

$$\tilde{\Theta}(\xi,\omega) = \int_{-\infty}^\infty \Theta(z;\xi)\,e^{i\omega z}\,dz\,. \tag{16c}$$

The closed-form solutions of the long-term thermoelastic deformations and temperature change of the cross-anisotropic medium subjected to a deep point heat source are easily obtained in the Hankel-Fourier integral

transformed domain (ξ,ω) by solving the simultaneous algebraic equations of (15a) to (15c). The results are shown as follows:

$$\tilde{U}_r(\xi,\omega)=\frac{Q}{2\pi}\frac{\xi\left\{\xi^2 L\beta_r-\left[(F+L)\beta_z-C\beta_r\right]\omega^2\right\}}{\left(\xi^2\lambda_{tr}+\omega^2\lambda_{tz}\right)\Omega(\xi,\omega)}, \tag{17a}$$

$$\tilde{U}_z(\xi,\omega)=\frac{Q}{2\pi}\frac{i\omega\left\{\omega^2 L\beta_z-\left[(F+L)\beta_r-A\beta_z\right]\xi^2\right\}}{\left(\xi^2\lambda_{tr}+\omega^2\lambda_{tz}\right)\Omega(\xi,\omega)}, \tag{17b}$$

$$\tilde{\Theta}(\xi,\omega)=\frac{Q}{2\pi}\frac{1}{\xi^2\lambda_{tr}+\omega^2\lambda_{tz}}, \tag{17c}$$

where $\Omega(\xi,\omega)$ is defined as

$$\Omega(\xi,\omega)=CL\omega^4+\left[AC-F(F+2L)\right]\xi^2\omega^2+AL\xi^4. \tag{18}$$

These solutions are also expressed in the domain $(z;\xi)$ by applying the following inverse Fourier transforms to equations (17a) to (17c):

$$U_r(z;\xi)=\frac{1}{2\pi}\int_{-\infty}^{\infty}\tilde{U}_r(\xi,\omega)\,e^{-i\omega z}d\omega, \tag{19a}$$

$$U_z(z;\xi)=\frac{1}{2\pi}\int_{-\infty}^{\infty}\tilde{U}_z(\xi,\omega)\,e^{-i\omega z}d\omega, \tag{19b}$$

$$\Theta(z;\xi)=\frac{1}{2\pi}\int_{-\infty}^{\infty}\tilde{\Theta}(\xi,\omega)\,e^{-i\omega z}d\omega. \tag{19c}$$

Then, we have

$$U_r(z;\xi)=\frac{Q}{4\pi\lambda_{tz}}\left(\frac{a_1}{\xi^2}e^{-\mu_1\xi|z|}+\frac{a_2}{\xi^2}e^{-\mu_2\xi|z|}+\frac{a_3}{\xi^2}e^{-\mu_3\xi|z|}\right), \tag{20a}$$

$$U_z(z;\xi)=\mp\frac{Q}{4\pi\lambda_{tz}}\left(\frac{b_1}{\xi^2}e^{-\mu_1\xi|z|}+\frac{b_2}{\xi^2}e^{-\mu_2\xi|z|}+\frac{b_3}{\xi^2}e^{-\mu_3\xi|z|}\right), \tag{20b}$$

$$\Theta(z;\xi)=\frac{Q}{4\pi\lambda_{tz}\mu_3}\frac{1}{\xi}e^{-\mu_3\xi|z|}. \tag{20c}$$

The upper and lower signs in equation (20b) are for the conditions of $z\geq 0$ and $z<0$, respectively. Here, the constants $a_i\ (i=1,2,3)$ and $b_i\ (i=1,2,3)$ are defined as

$$a_1=\frac{L\beta_r+\left[(F+L)\beta_z-C\beta_r\right]\mu_1^2}{CL\mu_1\left(\mu_1^2-\mu_2^2\right)\left(\mu_1^2-\mu_3^2\right)}, \tag{21a}$$

$$a_2=\frac{L\beta_r+\left[(F+L)\beta_z-C\beta_r\right]\mu_2^2}{CL\mu_2\left(\mu_2^2-\mu_1^2\right)\left(\mu_2^2-\mu_3^2\right)}, \tag{21b}$$

$$a_3=\frac{L\beta_r+\left[(F+L)\beta_z-C\beta_r\right]\mu_3^2}{CL\mu_3\left(\mu_3^2-\mu_1^2\right)\left(\mu_3^2-\mu_2^2\right)}, \tag{21c}$$

$$b_1 = \frac{L\beta_z\mu_1^2 + (F+L)\beta_r - A\beta_z}{CL(\mu_1^2-\mu_2^2)(\mu_1^2-\mu_3^2)}, \tag{21d}$$

$$b_2 = \frac{L\beta_z\mu_2^2 + (F+L)\beta_r - A\beta_z}{CL(\mu_2^2-\mu_1^2)(\mu_2^2-\mu_3^2)}, \tag{21e}$$

$$b_3 = \frac{L\beta_z\mu_3^2 + (F+L)\beta_r - A\beta_z}{CL(\mu_3^2-\mu_1^2)(\mu_3^2-\mu_2^2)}. \tag{21f}$$

In addition, the characteristic roots μ_1 and μ_2 must satisfy the following characteristic equation

$$CL\mu^4 - [AC - F(F+2L)]\mu^2 + AL = 0, \tag{22}$$

and $\mu_3 = \sqrt{\lambda_{tr}/\lambda_{tz}}$.

Furthermore, using the inversions of Hankel transform formula [17-19] and the constitutive equations (1a) to (1d), the closed-form solutions of thermoelastic deformation, temperature increment and thermal stresses of the strata in real domain (r,z) are obtained from the solutions of (20a) to (20c) in Hankel transformed domain $(\xi;z)$ as below:

$$u_r = \frac{Q}{4\pi\lambda_{tz}}\left(a_1\frac{r}{R_1^*} + a_2\frac{r}{R_2^*} + a_3\frac{r}{R_3^*}\right), \tag{23a}$$

$$u_z = \frac{Q}{4\pi\lambda_{tz}}\left(b_1\sinh^{-1}\frac{\mu_1 z}{r} + b_2\sinh^{-1}\frac{\mu_2 z}{r} + b_3\sinh^{-1}\frac{\mu_3 z}{r}\right), \tag{23b}$$

$$\vartheta = \frac{Q}{4\pi\lambda_{tz}}\frac{1}{\mu_3 R_3}, \tag{23c}$$

$$\sigma_{rr} = \frac{Q}{4\pi\lambda_{tz}}\left[A\left(a_1\frac{1}{R_1} + a_2\frac{1}{R_2} + a_3\frac{1}{R_3}\right) - 2N\left(a_1\frac{1}{R_1^*} + a_2\frac{1}{R_2^*} + a_3\frac{1}{R_3^*}\right) + F\left(b_1\frac{\mu_1}{R_1} + b_2\frac{\mu_2}{R_2} + b_3\frac{\mu_3}{R_3}\right) - \beta_r\frac{1}{\mu_3 R_3}\right], \tag{23d}$$

$$\sigma_{\theta\theta} = \frac{Q}{4\pi\lambda_{tz}}\left[A\left(a_1\frac{1}{R_1} + a_2\frac{1}{R_2} + a_3\frac{1}{R_3}\right) - 2N\left(a_1\frac{\mu_1|z|}{R_1R_1^*} + a_2\frac{\mu_2|z|}{R_2R_2^*} + a_3\frac{\mu_3|z|}{R_3R_3^*}\right) + F\left(b_1\frac{\mu_1}{R_1} + b_2\frac{\mu_2}{R_2} + b_3\frac{\mu_3}{R_3}\right) - \beta_r\frac{1}{\mu_3 R_3}\right], \tag{23e}$$

$$\sigma_{zz} = \frac{Q}{4\pi\lambda_{tz}}\left[F\left(a_1\frac{1}{R_1} + a_2\frac{1}{R_2} + a_3\frac{1}{R_3}\right) + C\left(b_1\frac{\mu_1}{R_1} + b_2\frac{\mu_2}{R_2} + b_3\frac{\mu_3}{R_3}\right) - \beta_z\frac{1}{\mu_3 R_3}\right], \tag{23f}$$

$$\sigma_{rz} = \mp\frac{Q}{4\pi\lambda_{tz}}\left[L\left(a_1\frac{\mu_1 r}{R_1R_1^*} + a_2\frac{\mu_2 r}{R_2R_2^*} + a_3\frac{\mu_3 r}{R_3R_3^*}b_1\frac{\mu_1|z|}{rR_1} + b_2\frac{\mu_2|z|}{rR_2} + b_3\frac{\mu_3|z|}{rR_3}\right)\right]. \tag{23g}$$

The upper and lower signs in equation (23g) are for conditions of $z \geq 0$ and $z < 0$, respectively. In equations (23a) to (23g), $R_i = \sqrt{r^2 + \mu_i^2 z^2}$ and $R_i^* = R_i + \mu_i|z|$ $(i = 1, 2, 3)$.

3.2. Cases of Isotropic Mechanical Behaviour and Cross-anisotropic Thermal Properties

The displacements, temperature change and thermal stresses for the strata with cross-anisotropic properties in mechanical and heat flows are analytically solved and expressed in equations (23a) to (23g) for the disturbance of a deep point heat source. For the special case of medium with isotropic mechanical properties, the associated

closed-form solutions are obtained by the conditions of $\mu_1 = \mu_2 = 1$ for equations (23a) to (23g). This is carried out by using L'Hospital's rule with careful calculations. The results are given as follows:

$$u_r = \frac{Q\alpha_{sz}}{4\pi\eta\lambda_{tz}}\left\{\beta_r^*\phi_1(r,z)+\left[2\eta\beta_r^*-(2\eta-1)\beta_z^*\right]\phi_2(r,z)\right\}, \tag{24a}$$

$$u_z = \frac{Q\alpha_{sz}}{4\pi\eta\lambda_{tz}}\left\{\beta_z^*\phi_3(r,z)+\left[2\eta\beta_z^*-(2\eta-1)\beta_r^*\right]\phi_4(r,z)\right\}, \tag{24b}$$

$$\vartheta = \frac{Q}{4\pi\lambda_{tz}}\phi_5(r,z), \tag{24c}$$

$$\sigma_{rr} = \frac{QG\alpha_{sz}}{4\pi\eta\lambda_{tz}}\left\{(2\eta-1)\beta_r^*\phi_6(r,z)+2(\eta-1)\beta_z^*\phi_7(r,z)+\left[2(2\eta-1)\beta_r^*-\beta_z^*\right]\phi_8(r,z)+\eta\beta_r^*\phi_9(r,z)\right.$$
$$\left.+\beta_r^*\phi_{10}(r,z)+\left[2\eta\beta_r^*-(2\eta-1)\beta_z^*\right]\phi_{11}(r,z)\right\}, \tag{24d}$$

$$\sigma_{\theta\theta} = \frac{QG\alpha_{sz}}{4\pi\eta\lambda_{tz}}\left\{(2\eta-1)\beta_r^*\phi_6(r,z)+2(\eta-1)\beta_z^*\phi_7(r,z)+\left[2(2\eta-1)\beta_r^*-\beta_z^*\right]\phi_8(r,z)+\eta\beta_r^*\phi_9(r,z)\right.$$
$$\left.-\beta_r^*\phi_{10}(r,z)-\left[2\eta\beta_r^*-(2\eta-1)\beta_z^*\right]\phi_{11}(r,z)\right\}, \tag{24e}$$

$$\sigma_{zz} = \frac{QG\alpha_{sz}}{4\pi\eta\lambda_{tz}}\left\{2(\eta-1)\beta_r^*\phi_6(r,z)+2\eta\beta_z^*\phi_7(r,z)+\left[-2\eta\beta_r^*+2(3\eta-1)\beta_z^*\right]\phi_8(r,z)+\eta\beta_z^*\phi_9(r,z)\right\}, \tag{24f}$$

$$\sigma_{rz} = \frac{QG\alpha_{sz}}{4\pi\eta\lambda_{tz}}\left\{\left[2\eta\beta_r^*-2(\eta-1)\beta_z^*\right]\phi_{12}(r,z)+\left[2\eta\beta_z^*-2(\eta-1)\beta_r^*\right]\phi_{13}(r,z)\right\}, \tag{24g}$$

where $\eta = (1-\nu)/(1-2\nu)$. The parameters β_r^* and β_z^* are defined as follows:

$$\beta_r^* = 2(\nu+\alpha_{sr}/\alpha_{sz})/(1-2\nu), \tag{25a}$$

$$\beta_z^* = 2\left[(1-\nu)+2\nu\,\alpha_{sr}/\alpha_{sz}\right]/(1-2\nu). \tag{25b}$$

The definitions of functions $\phi_i\,(i=1,\cdots,13)$ in equations (24a) to (24g) are listed below:

$$\phi_1(r,z) = \frac{1}{4(\mu^2-1)}\frac{r}{R}-\frac{1}{2(\mu^2-1)^2}\frac{r}{R^*}+\frac{1}{2\mu(\mu^2-1)^2}\frac{r}{R_\mu^*}, \tag{26a}$$

$$\phi_2(r,z) = \frac{1}{4(\mu^2-1)}\left(-\frac{r|z|}{RR^*}+\frac{r}{R^*}\right)+\frac{1}{2(\mu^2-1)^2}\frac{r}{R^*}-\frac{\mu}{2(\mu^2-1)^2}\frac{r}{R_\mu^*}, \tag{26b}$$

$$\phi_3(r,z) = -\frac{1}{4(\mu^2-1)}\frac{z}{R}-\frac{\mu^2}{2(\mu^2-1)^2}\sinh^{-1}\frac{z}{r}+\frac{\mu^2}{2(\mu^2-1)^2}\sinh^{-1}\frac{\mu z}{r}, \tag{26c}$$

$$\phi_4(r,z) = \frac{1}{4(\mu^2-1)}\frac{z}{R}+\frac{1}{2(\mu^2-1)^2}\sinh^{-1}\frac{z}{r}-\frac{1}{2(\mu^2-1)^2}\sinh^{-1}\frac{\mu z}{r}, \tag{26d}$$

$$\phi_5(r,z) = \frac{1}{\mu R_\mu}, \tag{26e}$$

$$\phi_6(r,z) = \frac{1}{4(\mu^2-1)}\left(\frac{1}{R}+\frac{z^2}{R^3}\right)-\frac{1}{2(\mu^2-1)^2}\frac{1}{R}+\frac{1}{2\mu(\mu^2-1)^2}\frac{1}{R_\mu}, \tag{26f}$$

$$\phi_7(r,z)=\frac{1}{4(\mu^2-1)}\left(-\frac{3}{R}+\frac{z^2}{R^3}\right)-\frac{1}{2(\mu^2-1)^2}\frac{1}{R}+\frac{\mu^3}{2(\mu^2-1)^2}\frac{1}{R_\mu}, \tag{26g}$$

$$\phi_8(r,z)=\frac{1}{4(\mu^2-1)}\frac{r^2}{R^3}+\frac{1}{2(\mu^2-1)^2}\frac{1}{R}-\frac{\mu}{2(\mu^2-1)^2}\frac{1}{R_\mu}, \tag{26h}$$

$$\phi_9(r,z)=-\frac{1}{\mu R_\mu}, \tag{26i}$$

$$\phi_{10}(r,z)=-\frac{1}{4(\mu^2-1)}\frac{r^2}{R^3}+\frac{1}{2(\mu^2-1)^2}\frac{r^2}{RR^{*2}}-\frac{1}{2\mu(\mu^2-1)^2}\frac{r^2}{R_\mu R_\mu^{*2}}, \tag{26j}$$

$$\phi_{11}(r,z)=\frac{1}{4(\mu^2-1)}\frac{r^2}{R^3}-\frac{\mu^2}{2(\mu^2-1)^2}\frac{r^2}{RR^{*2}}+\frac{\mu}{2(\mu^2-1)^2}\frac{r^2}{R_\mu R_\mu^{*2}}, \tag{26k}$$

$$\phi_{12}(r,z)=\frac{1}{4(\mu^2-1)}\frac{rz}{R^3}-\frac{\mu^2}{2(\mu^2-1)^2}\frac{r}{RR^{*}}+\frac{\mu^2}{2(\mu^2-1)^2}\frac{r}{R_\mu R_\mu^{*}}, \tag{26l}$$

$$\phi_{13}(r,z)=-\frac{1}{4(\mu^2-1)}\frac{rz}{R^3}+\frac{1}{2(\mu^2-1)^2}\frac{r}{RR^{*}}-\frac{1}{2(\mu^2-1)^2}\frac{r}{R_\mu R_\mu^{*}}, \tag{26m}$$

where the parameters $\mu=\sqrt{\lambda_{tr}/\lambda_{tz}}$, $R=\sqrt{r^2+z^2}$, $R^*=R+|z|$, $R_\mu=\sqrt{r^2+\mu^2z^2}$ and $R_\mu^*=R_\mu+\mu|z|$.

3.3. Cases of Isotropic Mechanical and Thermal Properties

Furthermore, the closed-form solutions for the special case of medium with isotropic mechanics and heat flows properties are acquired through the conditions of $\mu=1$ for equations (24a) to (24g). Applying the L'Hospital's rule and careful calculations, the results are given as below:

$$u_r=\frac{Q\alpha_s(1+\nu)}{8\pi\lambda_t(1-\nu)}\frac{r}{R}, \tag{27a}$$

$$u_z=\frac{Q\alpha_s(1+\nu)}{8\pi\lambda_t(1-\nu)}\frac{z}{R}, \tag{27b}$$

$$\vartheta=\frac{Q}{4\pi\lambda_t}\frac{1}{R}, \tag{27c}$$

$$\sigma_{rr}=-\frac{QG\alpha_s(1+\nu)}{4\pi\lambda_t(1-\nu)}\left(\frac{1}{R}+\frac{r^2}{R^3}\right), \tag{27d}$$

$$\sigma_{\theta\theta}=-\frac{QG\alpha_s(1+\nu)}{4\pi\lambda_t(1-\nu)}\frac{1}{R}, \tag{27e}$$

$$\sigma_{zz}=-\frac{QG\alpha_s(1+\nu)}{4\pi\lambda_t(1-\nu)}\left(\frac{1}{R}+\frac{z^2}{R^3}\right), \tag{27f}$$

$$\sigma_{rz}=-\frac{QG\alpha_s(1+\nu)}{4\pi\lambda_t(1-\nu)}\frac{rz}{R^3}, \tag{27g}$$

where λ_t denotes thermal conductivity of the isotropic soils or rocks.

The derived closed-form solutions, equations (27a) to (27g), illustrated that all field quantities are functions of the distance from the heat source and they are inversely proportional to the thermal conductivity. Besides, the shear modulus does not have influence on displacements and temperature increment of the homogeneous isotropic strata.

4. ILLUSTRATIVE EXAMPLE

To study the effect of anisotropy on displacements, temperature increment and thermal stresses of the strata due to a point heat source, numerical results were obtained for different appropriate sets of soil thermoelastic constants. These thermoelastic constants are summarized in Table 1. The degrees of anisotropic linear thermal expansion coefficient $\alpha_{sr}/\alpha_{sz}=10.0$ and thermal conductivity $\lambda_{tr}/\lambda_{tz}=10.0$ are assumed in cases 2 to 5. For the heavily over-consolidated London clay, the range of the ratio E_r/E_z is 1.35 to 2.37 and the ratio G_{rz}/E_z is 1.35 to 2.37 [22,23]. The average values of E_r/E_z and G_{rz}/E_z are 1.84 and 0.38, respectively. In these numerical studies, the Young's modulus in vertical direction E_z, linear thermal expansion coefficient in vertical direction α_{sz}, and thermal conductivity in vertical direction λ_{tz} are treated as constants in cases 1 to 5.

Table 1. Material properties of isotropic and cross-anisotropic soils (*assumed values).

Case	$\nu_{r\theta}$	ν_{rz}	G_{rz}/E_z	E_r/E_z	α_{sr}/α_{sz}	$\lambda_{tr}/\lambda_{tz}$	Reference
Case 1: Isotropy	0.25	0.25	0.4	1.0	1.0	1.0	Booker & Carter [20]
Case 2: Cross-anisotropy	0.125	0.75	0.445	2.0	10.0*	10.0*	Poulos & Davis [21]
Case 3: Cross-anisotropy	0.125	0.75	0.64	3.0	10.0*	10.0*	Poulos & Davis [21]
Case 4: Cross-anisotropy	0.125	0.75	0.64	4.0	10.0*	10.0*	Poulos & Davis [21]
Case 5: Cross-anisotropy	0	0.38	0.38	1.84	10.0*	10.0*	Tarn & Lu [12], Lee & Rowe [22], Wang *et al.* [23]

The influence of anisotropy on long-term thermoelastic responses are given in Figures 2 to 4. In these figures, the thermoelastic responses have been normalized. It is observed from Figures 2 to 4 that the anisotropy of the soils has significant effect on long-term thermally elastic responses compared with the results obtained for an isotropic soil of case 1. For example, the long-term horizontal displacement of case 4 is reduced to around 75% of the corresponding value for the isotropic soil of case 1, while the long-term vertical displacement of case 4 increases to 150% of case 1 for $z/r > 3$ as shown in Figure 2. For the assumed ratios of $\lambda_{tr}/\lambda_{tz}$ at 10.0 in cases 2 to 5, the long-term temperature increments of the strata of cases 2 to 5 are reduced to around 10% of the corresponding value for the isotropic soil of case 1 as illustrated in Figure 3.

Figures 5 to 7 illustrate the long-term horizontal and vertical displacements effected by the anisotropy of the strata. As shown in Figure 5(a), the ratio E_r/E_z ranges from 0.5 to 10.0, and the effect of E_r/E_z on horizontal displacement of the strata is secondary. However, the ratio of E_r/E_z has an apparent effect on long-term vertical displacement of the strata as shown in Figure 5(b). Based on the available data of $\nu_{r\theta}=0.00$, $\nu_{rz}=0.38$, $G_{rz}/E_z=0.38$, $\alpha_{sr}/\alpha_{sz}=10.0$ and $\lambda_{tr}/\lambda_{tz}=10.0$, Figures 6(a) and 6(b) use the ratio of α_{sr}/α_{sz} to display its influence on long-term horizontal and vertical displacements of the strata. It is shown from Figure 7 that the degree of anisotropic thermal conductivity $\lambda_{tr}/\lambda_{tz}$ has the most significant effect on long-term horizontal and vertical displacements of the strata due to a point heat source.

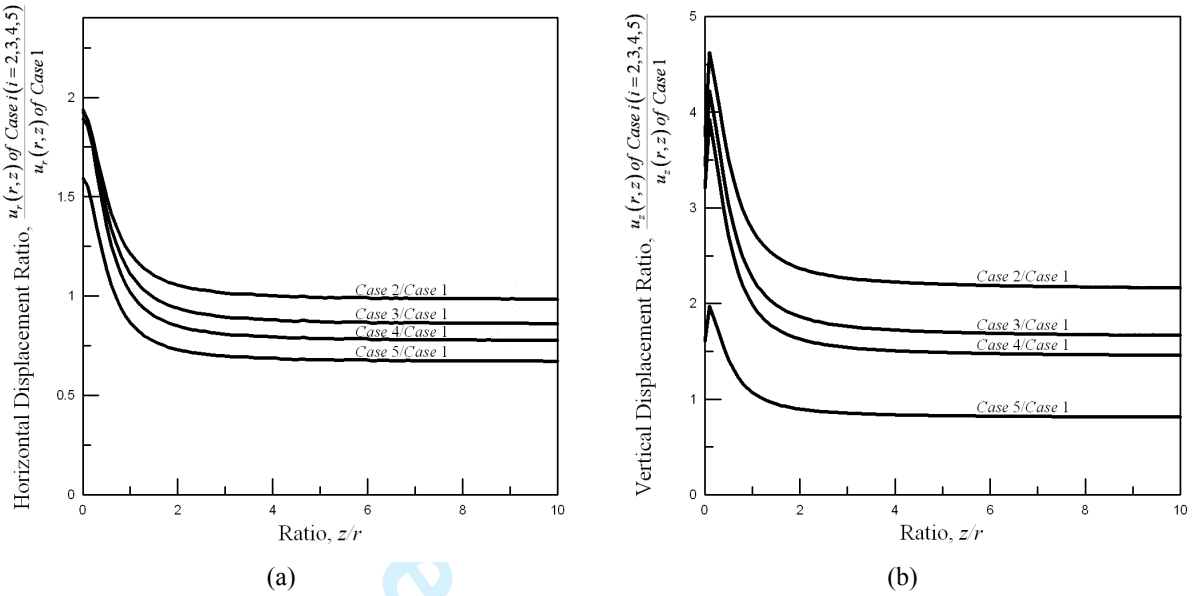

Figure 2. Influence of anisotropy on long-term (a) horizontal displacements u_r and (b) vertical displacement u_z of the strata.

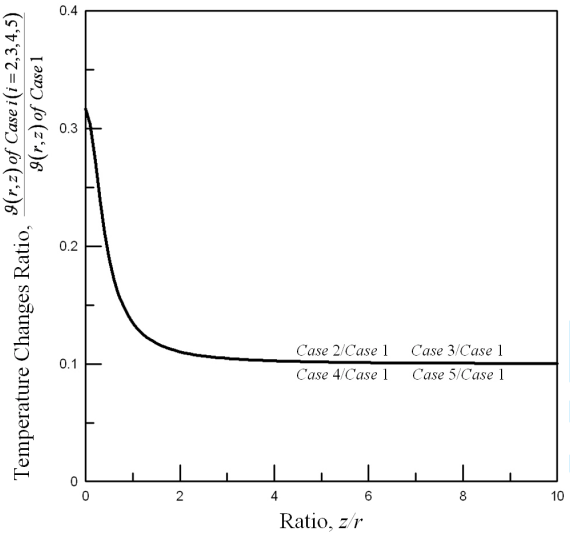

Figure 3. Influence of anisotropy on long-term temperature changes of the strata.

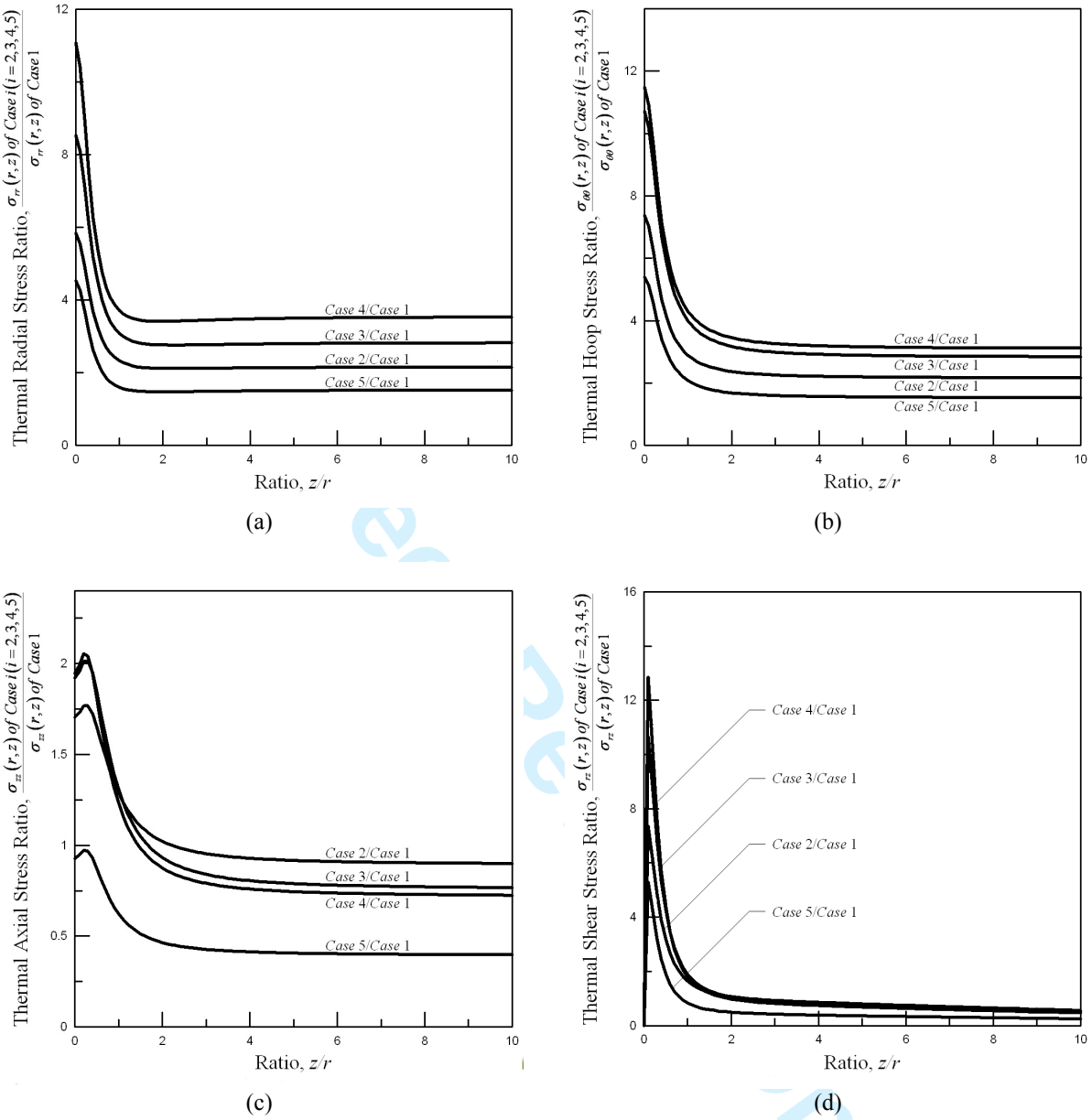

Figure 4. Influence of anisotropy on long-term (a) thermal radial stress σ_{rr}, (b) thermal hoop stress $\sigma_{\theta\theta}$, (c) thermal axial stress σ_{zz} and (d) thermal shear stress σ_{rz} of the strata.

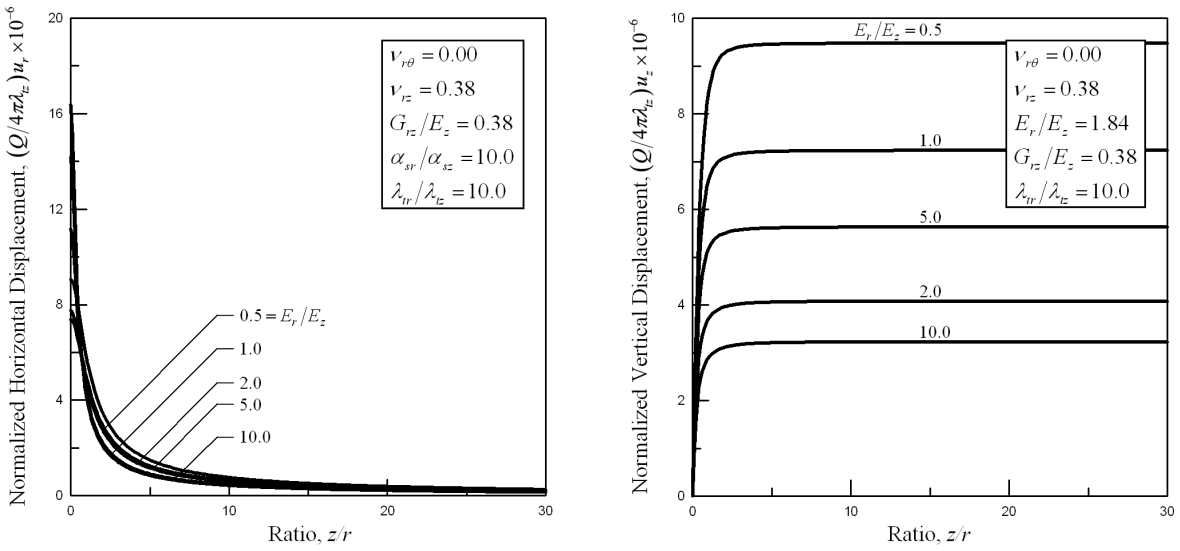

Figure 5. Influence of the degree of anisotropy E_r/E_z on long-term (a) horizontal displacements u_r and (b) vertical displacement u_z of the strata.

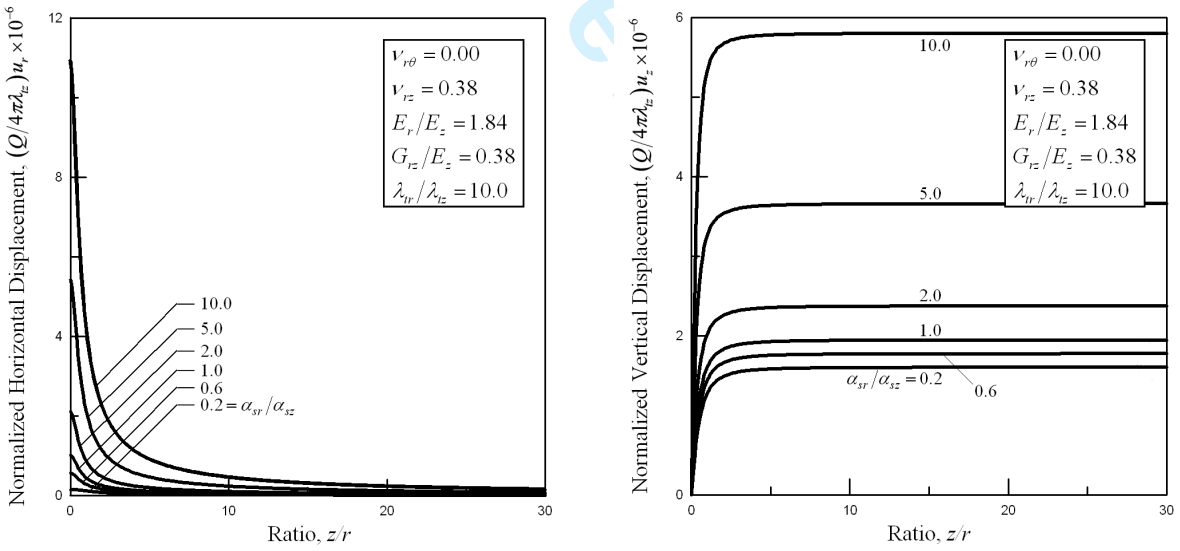

Figure 6. Influence of the degree of anisotropy α_{sr}/α_{sz} on long-term (a) horizontal displacements u_r and (b) vertical displacement u_z of the strata.

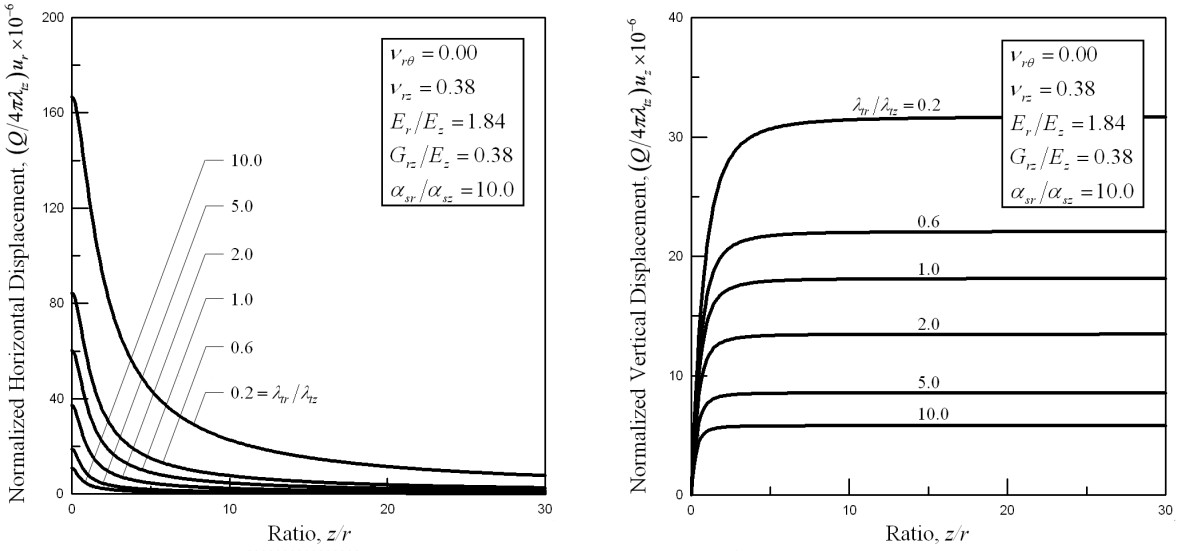

Figure 7. Influence of the degree of anisotropy $\lambda_{tr}/\lambda_{tz}$ on long-term (a) horizontal displacements u_r and (b) vertical displacement u_z of the strata.

Figures 8 to 10 illustrate the thermal stresses affected by the anisotropy of the strata. Based on the available data of $\nu_{r\theta} = 0.00$, $\nu_{rz} = 0.38$, $G_{rz}/E_z = 0.38$, $\alpha_{sr}/\alpha_{sz} = 10.0$ and $\lambda_{tr}/\lambda_{tz} = 10.0$, Figures 8(a) to 8(d) use the ratio of E_r/E_z to display the influence on thermal stresses of the strata. As shown in Figures 9(a) to 9(d), the ratio α_{sr}/α_{sz} ranges from 0.2 to 10.0, and the effect of α_{sr}/α_{sz} on long-term thermal stresses of the strata is important. It is shown from Figures 10(a) to 10(d) that the degree of anisotropic thermal conductivity $\lambda_{tr}/\lambda_{tz}$ has the most significant effect on long-term thermal stresses of the strata due to a deep point heat source.

As illustrated in Figures 5 to 10, the higher ratio of linear thermal expansion coefficients α_{sr}/α_{sz} leads to corresponding higher displacements and thermal stress components of the strata with varying degrees of anisotropy. However, the displacements and thermal stress components decrease with higher ratio of the thermal conductivities $\lambda_{tr}/\lambda_{tz}$. Based on the numerical results obtained from this anisotropic thermoelastic research, all of the thermal stresses of strata subjected to a point heat source are compressive and significantly affected by the ratio of mechanical property E_r/E_z and thermal properties α_{sr}/α_{sz} and $\lambda_{tr}/\lambda_{tz}$.

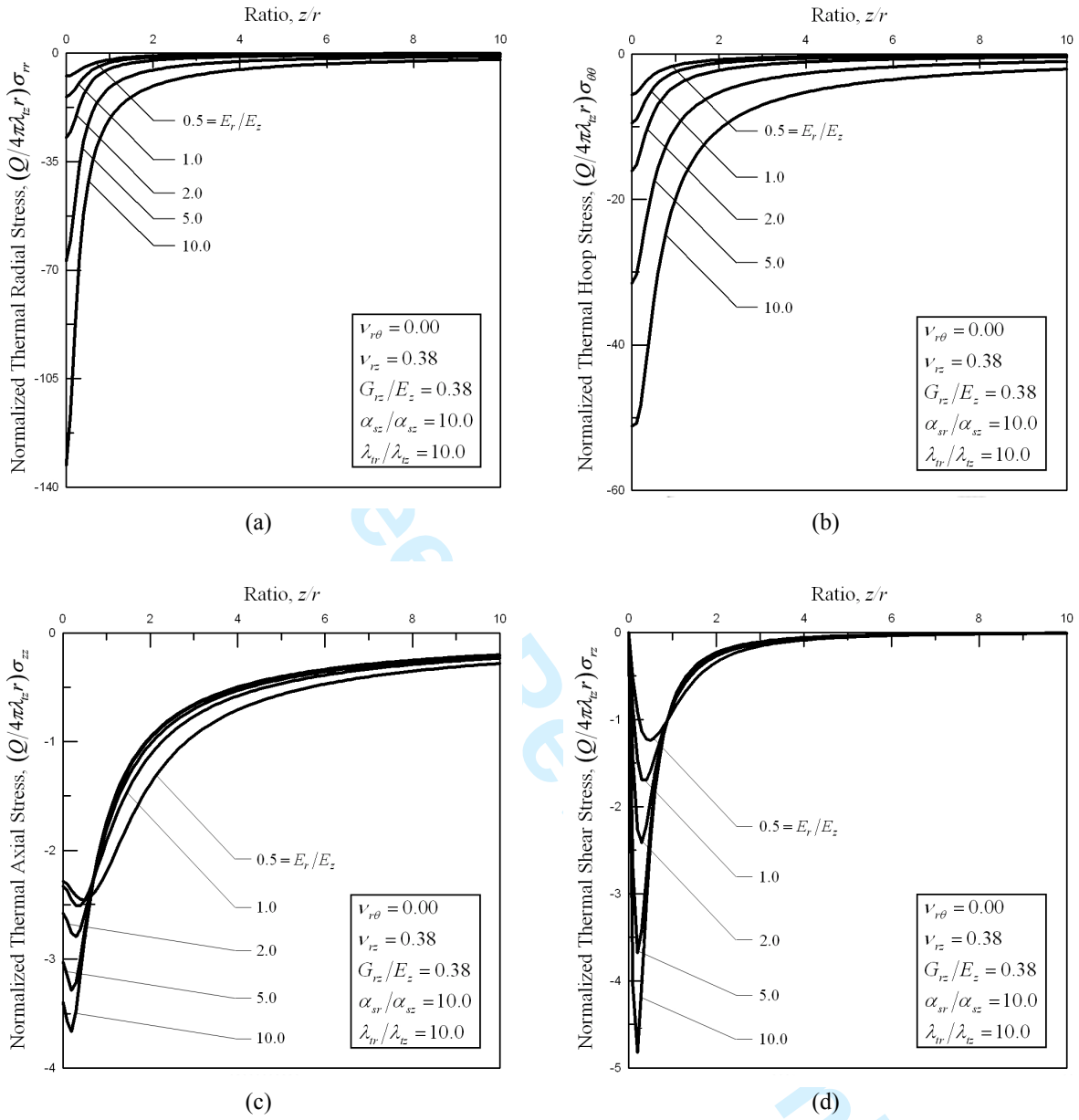

Figure 8. Influence of the degree of anisotropy E_r/E_z on long-term (a) thermal radial stress σ_{rr}, (b) thermal hoop stress $\sigma_{\theta\theta}$, (c) thermal axial stress σ_{zz} and (d) thermal shear stress σ_{rz} of the strata.

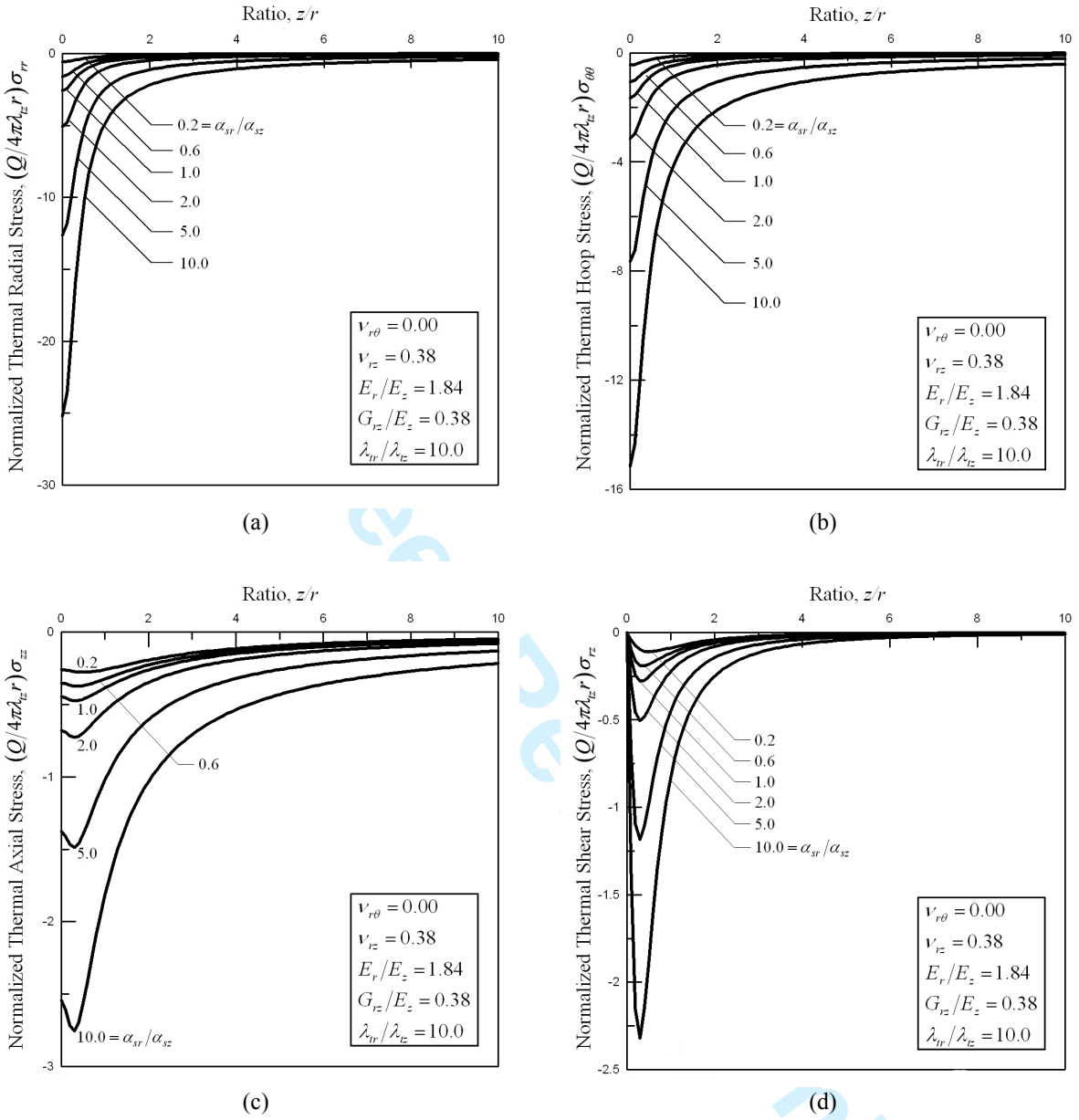

Figure 9. Influence of the degree of anisotropy α_{sr}/α_{sz} on long-term (a) thermal radial stress σ_{rr}, (b) thermal hoop stress $\sigma_{\theta\theta}$, (c) thermal axial stress σ_{zz} and (d) thermal shear stress σ_{rz} of the strata.

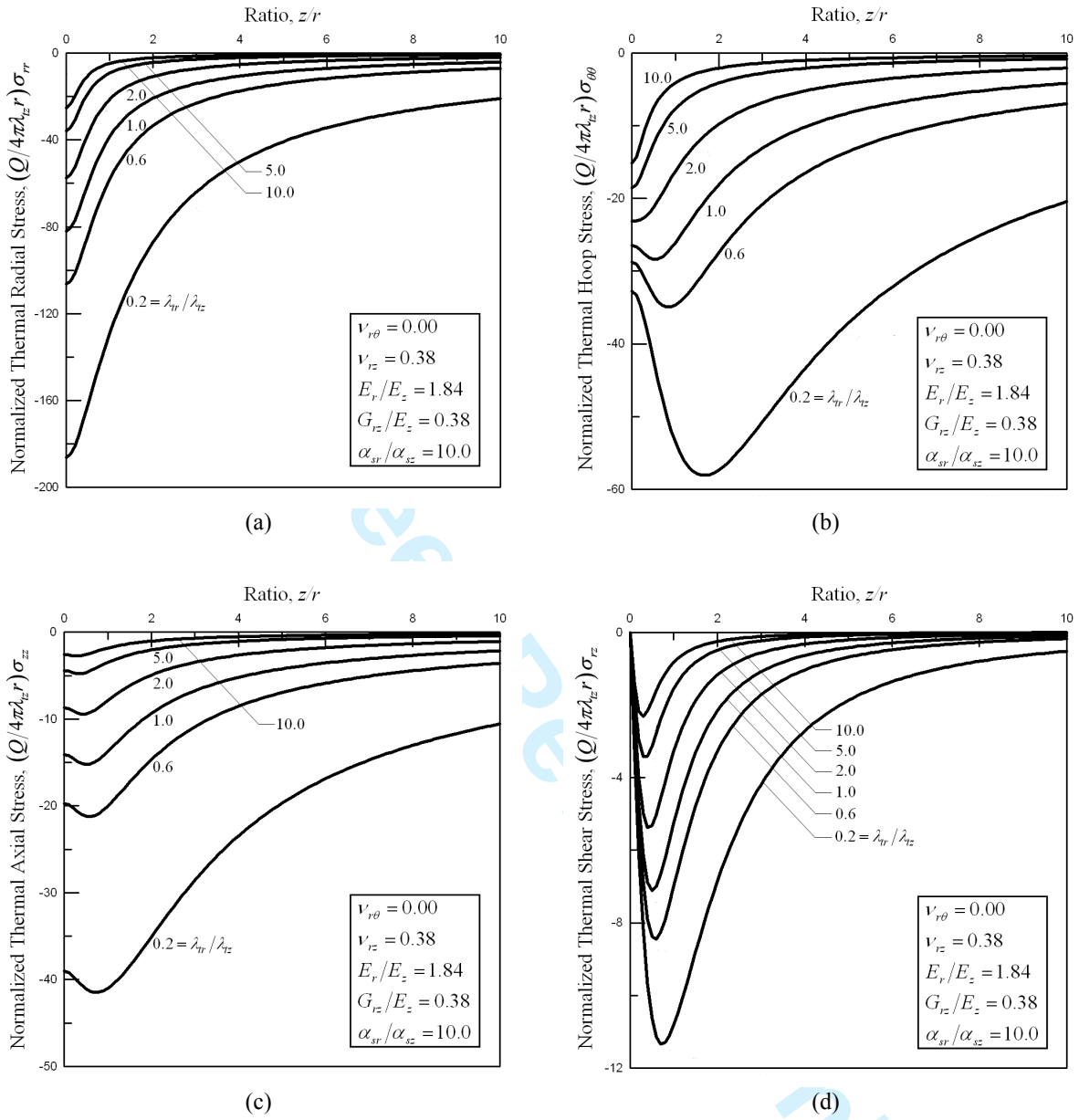

Figure 10. Influence of the degree of anisotropy $\lambda_{tr}/\lambda_{tz}$ on long-term (a) thermal radial stress σ_{rr}, (b) thermal hoop stress $\sigma_{\theta\theta}$, (c) thermal axial stress σ_{zz} and (d) thermal shear stress σ_{rz} of the strata.

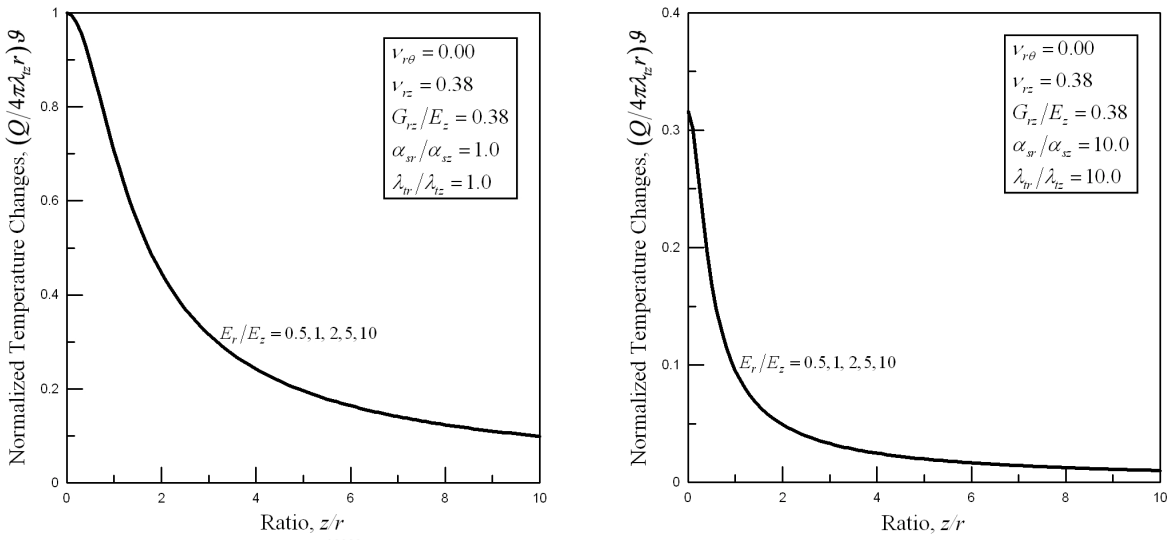

(a) (b)

Figure 11. Influence of the degree of anisotropy E_r/E_z on long-term temperature changes of the strata with (a) $\alpha_{sr}/\alpha_{sz}=1.0$, $\lambda_{tr}/\lambda_{tz}=1.0$ and (b) $\alpha_{sr}/\alpha_{sz}=10.0$, $\lambda_{tr}/\lambda_{tz}=10.0$.

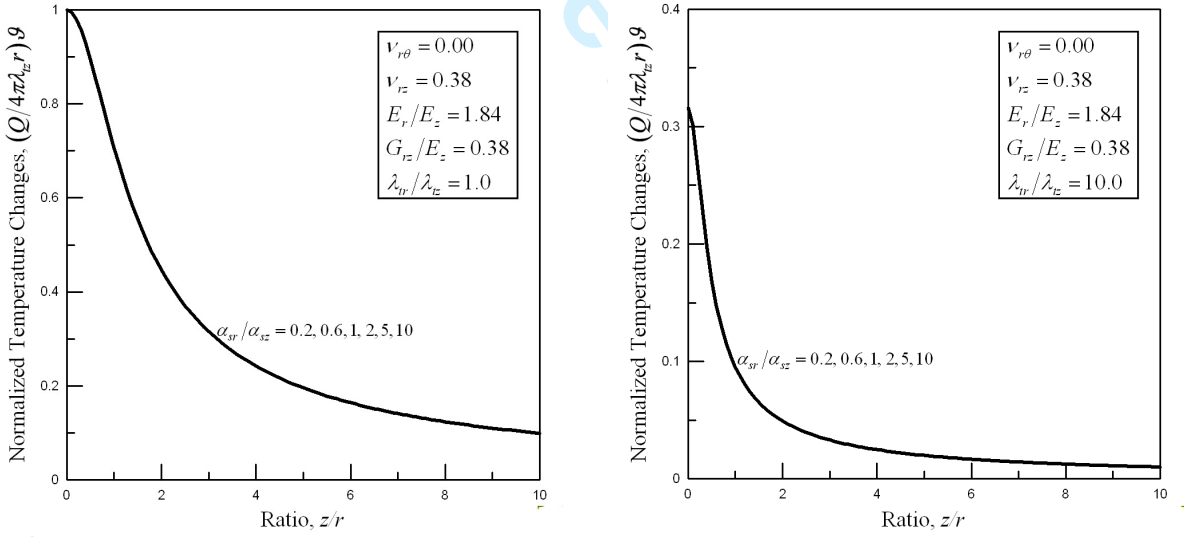

(a) (b)

Figure 12. Influence of the degree of anisotropy α_{sr}/α_{sz} on long-term temperature changes of the strata with (a) $\lambda_{tr}/\lambda_{tz}=1.0$ and (b) $\lambda_{tr}/\lambda_{tz}=10.0$.

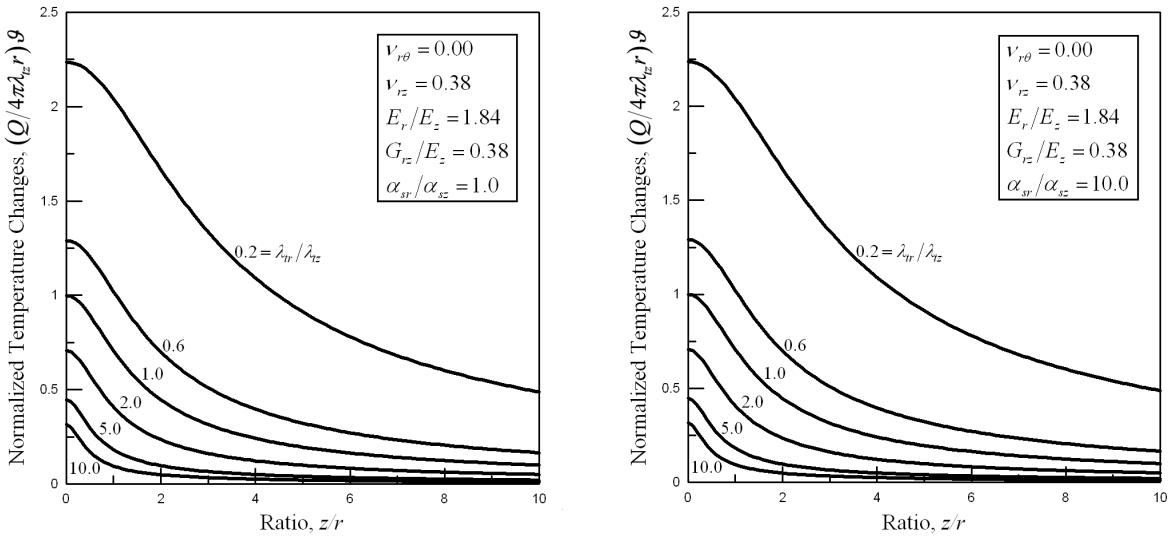

Figure 13. Influence of the degree of anisotropy $\lambda_{tr}/\lambda_{tz}$ on long-term temperature changes of the strata with (a) $\alpha_{sr}/\alpha_{sz}=1.0$ and (b) $\alpha_{sr}/\alpha_{sz}=10.0$.

The long-term normalized temperature increment of the strata were calculated from equation (23c) for values of various anisotropic ratio E_r/E_z, α_{sr}/α_{sz}, $\lambda_{tr}/\lambda_{tz}$, and the results are shown in Figures 11 to 13. Figures 11 and 12 display the anisotropic ratio E_r/E_z and α_{sr}/α_{sz}, and they have no effect on the long-term temperature increment of the strata due to a point heat source. However, Figure 13 illustrates that the ratio of anisotropic thermal conductivity $\lambda_{tr}/\lambda_{tz}$ has the most significant effect on temperature increment of the strata. In all cases, the temperature increment of the strata is larger when the location is closer to the point heat source.

5. CONCLUSIONS

The closed-form solutions of thermoelastic responses due to a point heat source buried in a cross-anisotropic thermoelastic full space were obtained by using Hankel and Fourier integral transforms. The results were examined by simplifying the solutions of cross-anisotropic thermoelastic responses into the case of isotropic strata. The investigations show that:

1. The derived solutions illustrated that all field quantities are functions of the distance from the heat source, and they are inversely proportional to the thermal conductivity. Besides, the shear modulus does not have influence on long-term displacements and temperature increment of the strata for the totally isotropic properties case.
2. Based on the numerical results, the thermal stresses of strata are compressive, and they are significantly affected by the ratio of mechanical and thermal properties E_r/E_z, α_{sr}/α_{sz} and $\lambda_{tr}/\lambda_{tz}$. For example, the higher ratio of linear thermal expansion coefficients α_{sr}/α_{sz} leads to corresponding higher thermal stress components of the strata with varying degrees of anisotropy. However, the thermal stress components decrease with higher ratio of the thermal conductivities $\lambda_{tr}/\lambda_{tz}$.
3. The influence of the ratio of anisotropy E_r/E_z on long-term horizontal displacement due to a point heat source is secondary while the effects of thermoelastic anisotropy α_{sr}/α_{sz} or $\lambda_{tr}/\lambda_{tz}$ has an appreciable effect on the long-term horizontal displacement.

ACKNOWLEDGEMENTS

The authors are grateful for the funds provided by National Science Council of Taiwan, R.O.C., Grant No. NSC100-2221-E-216-025, and Chung Hua University, Grant No. CHU-99-A-03.

REFERENCES

1. Gonzalez-Romero EM. Impact of partitioning and transmutation on the high level waste management. *Nuclear Engineering and Design* 2011; **241**:3436-3444.
2. Tong F, Jing L, Zimmerman RB. A fully coupled thermo-hydro-mechanical model for simulating multiphase flow, deformation and heat transfer in buffer material and rock masses. *International Journal of Rock Mechanics and Mining Sciences* 2010; **47**:205-217.
3. Booker JR, Savvidou C. Consolidation around a spherical heat source. *International Journal of Solids and Structures* 1984; **20**(11-12):1079-1090.
4. Booker JR, Savvidou C. Consolidation around a point heat source. *International Journal for Numerical and Analytical Methods in Geomechanics* 1985; **9**(2):173-184.
5. Savvidou C, Booker JR. Consolidation around a heat source buried deep in a porous thermoelastic medium with anisotropic flow properties. *International Journal for Numerical and Analytical Methods in Geomechanics* 1989; **13**(1):75-90.
6. Lu J CC, Lin FT. The transient ground surface displacements due to a point sink/heat source in an elastic half-space. *Geotechnical Special Publication No. 148* (ASCE) 2006; 210-218.
7. Lin FT, Lu J CC. Golden ratio in the point heat source induced horizontal and vertical displacements of an isotropic elastic half space. *Geotechnical Special Publication No. 204* (ASCE) 2010; 87-94.
8. Wang X, Sudak LJ. 3D Green's functions for a steady point heat source interacting with a homogeneous imperfect interface. *Journal of Mechanics of Materials and Structures* 2006; **1**(7):1269-1280.
9. Hudson JA, Stephansson O, Andersson J. Guidance on numerical modelling of thermo-hydro-mechanical coupled processes for performance assessment of radioactive waste repositories. *International Journal of Rock Mechanics and Mining Sciences* 2005; **42**(5-6):850-870.
10. Chao CK, Chen FM, Shen MH. Green's functions for a point heat source in circularly cylindrical layered media. *Journal of Thermal Stresses* 2006; **29**(9):809-847.
11. Amadei B, Swolfs HS, Savage WZ. Gravity-induced stresses in stratified rock masses. *Rock Mechanics and Rock Engineering* 1988; **21**(1):1-20.
12. Tarn JQ, Lu CC. Analysis of subsidence due to a point sink in an anisotropic porous elastic half space. *International Journal for Numerical and Analytical Methods in Geomechanics* 1991; **15**(8):573-592.
13. Sheorey PR. A theory for in situ stresses in isotropic and transversely isotropic rock. *International Journal of Rock Mechanics and Mining Sciences and Geomechanics Abstracts* 1994; **31**(1):23-34.
14. Lee SL, Yang JH. Modeling of effective thermal conductivity for a nonhomogeneous anisotropic porous medium. *International Journal of Heat and Mass Transfer* 1998; **41**(6-7):931-937.
15. Wang CD, Tzeng CS. Displacements and stresses due to nonuniform circular loadings in an inhomogeneous cross-anisotropic material. *Mechanics Research Communications* 2009; **36**:921-932.
16. Love AEH. *A Treatise on the Mathematical Theory of Elasticity*. Dover Publications: New York, 1944; 643.
17. Sneddon IN. *Fourier Transforms*. McGraw-Hill: New York, 1951; 48-70.
18. Erdelyi A, Magnus W, Oberhettinger F, Tricomi FG. *Tables of Integral Transforms*, vol. 1 & 2. McGraw-Hill: New York, 1954.
19. Gradshteyn IS, Ryzhik IM. *Table of Integrals, Series, and Products* (7th edn). Academic Press: New York, 2007; 1171.
20. Booker JR, Carter JP. Analysis of a point sink embedded in a porous elastic half space. *International Journal for Numerical and Analytical Methods in Geomechanics* 1986; **10**(2):137-150.
21. Poulos HG, Davis EH. *Elastic Solutions for Soil and Rock Mechanics*. John Wiley & Sons: New York, 1974; 183-192.
22. Lee KM, Rowe RK. Deformations caused by surface loading and tunnelling: The role of elastic anisotropy. *Geotechnique* 1989; **39**(1):125-140.
23. Wang CD, Pan E, Tzeng CS, Han F, Liao JJ. Displacements and stresses due to a uniform vertical circular load in an inhomogeneous cross-anisotropic half-space. *International Journal of Geomechanics* (ASCE) 2006;

6(1):1-10.

NOMENCLATURE

$a_i\,(i=1,2,3)$	Constants defined in equations (21a) to (21c) ($^oC^{-1}$)
A, C, F, L, N	Material constants defined by Love (*Pa*)
$b_i\,(i=1,2,3)$	Constants defined in equations (21d) to (21f) ($^oC^{-1}$)
E_r, E_z	Young's modulus in horizontal/vertical direction (*Pa*)
$f_i\,(i=r,z)$	Body forces of the strata (N/m^3)
G	Shear modulus of the isotropic strata (*Pa*)
G_{rz}	Modulus of shear deformation in vertical plane (*Pa*)
$\boldsymbol{h}$	Heat flux vector (J/sm^2)
$\boldsymbol{i}_r$, $\boldsymbol{i}_z$	Unit vector parallel to the radial/vertical direction(Dimensionless)
$J_\alpha(x)$	First kind of the Bessel function of order α (Dimensionless)
q_h	Internal (or external) heat sources (J/sm^3)
Q	Strength of the point heat source (J/s)
(r,θ,z)	Cylindrical coordinates system (*m*, *radian*, *m*)
R	Parameter, $R=\sqrt{r^2+z^2}$ (*m*)
$R_i\,(i=1,2,3)$	Parameter, $R_i=\sqrt{r^2+\mu_i^2 z^2}$ (*m*)
R^*	Parameter, $R^*=\sqrt{r^2+z^2}+\lvert z\rvert$ (*m*)
$R_i^*\,(i=1,2,3)$	Parameter, $R_i^*=R_i+\mu_i\lvert z\rvert$ (*m*)
$u_i\,(i=r,z)$	Displacement components of the strata (*m*)
U_r, U_z	Hankel transforms of u_r and u_z, equations (13a) and (13b) (m^3)
$\tilde{U}_r$, $\tilde{U}_z$	Fourier transforms of U_r and U_z, equations (16a) and (16b) (m^4)
Greek letters	
α_s	Linear thermal expansion coefficient of the isotropic strata ($^oC^{-1}$)
α_{sr}, α_{sz}	Linear thermal expansion coefficient of the cross-anisotropic strata in horizontal/vertical direction ($^oC^{-1}$)
β_r, β_z	Thermal expansion factors of the cross-anisotropic strata (*Pa*/^{o}*C*)
β_r^*, β_z^*	Thermal expansion factors of the isotropic strata (*Pa*/^{o}*C*)
$\delta(x)$	Dirac delta function (m^{-1})
η	Parameter, $\eta=(1-\nu)/(1-2\nu)$ (Dimensionless)
ϑ	Temperature change of the strata (^{o}*C*)
Θ	Hankel transform of ϑ, equation (13c) ($^oCm^2$)
$\tilde{\Theta}$	Fourier transform of Θ, equation (16c) ($^oCm^3$)

λ	Lame constant of the isotropic strata (Pa)
λ_t	Thermal conductivity of the isotropic thermoelastic medium ($J/sm°C$)
λ_{tr}, λ_{tz}	Thermal conductivity of the cross-anisotropic thermoelastic medium in the horizontal/ vertical direction ($J/sm°C$)
μ	Characteristic root, $\mu = \sqrt{\lambda_{tr}/\lambda_{tz}}$ (Dimensionless)
μ_1, μ_2	Characteristic roots of characteristic equation (22) (Dimensionless)
μ_3	Characteristic root, $\mu_3 = \sqrt{\lambda_{tr}/\lambda_{tz}}$ (Dimensionless)
ν	Poisson's ratio of the isotropic strata (Dimensionless)
ν_{rz}	Poisson's ratio for strain in the vertical direction due to a horizontal direct stress (Dimensionless)
$\nu_{r\theta}$	Poisson's ratio for strain in the horizontal direction due to a horizontal direct stress (Dimensionless)
ν_{zr}	Poisson's ratio for strain in the horizontal direction due to a vertical direct stress (Dimensionless)
ξ	Hankel transform parameter (m^{-1})
$\sigma_{ij}\left(i,j=r,\theta,z\right)$	Thermal stress components of the strata (Pa)
$\phi_i\left(i=1,2,3,4\right)$	Functions defined in equations (26a) to (26d) (Dimensionless)
$\phi_i\left(i=5,\cdots,13\right)$	Functions defined in equations (26e) to (26m) (m^{-1})
ω	Fourier transform parameter (m^{-1})

附錄 3

研究成果投稿後已發表於 EI 等級之國際會議論文(第一篇)

Lu, John C.-C. **(Session Chair)** and Feng-Tsai Lin, 2012/6/25~27, "Modelling of a Buried Deep Horizontal Line Heat Source in a Cross-Anisotropic Thermoelastic Medium," *Proceedings of the 20th IASTED International Conference on Applied Simulation and Modelling*, *CD ISBN: 978-0-88986-925-7*, Napoli, Italy, pp. 150-157. (This work is supported by the National Science Council through grants NSC100-2221-E-216-025.) **(EI)**

論文收錄於 EI 資料庫之證明文件

Abstract | Detailed

Highlight search terms

Record 1 from Compendex & Inspec for: ((Modelling of a Buried Deep Horizontal Line Heat Source in a Cross-Anisotropic Thermoelastic Medium) WN TI), 1969-2013

Check record to add to Selected Records

1.

Accession number: 20124115537529

Title: Modelling of a buried deep horizontal line heat source in a cross-anisotropic thermoelastic medium

Authors: Lu, John C.-C.[1]; Lin, Feng-Tsai[2]

Author affiliation: [1] Department of Civil Engineering, Chung Hua University, No. 707, WuFu Rd., Hsinchu 30012, Taiwan

[2] Department of Naval Architecture, National Kaohsiung Marine University, No. 142, Haijhuan Rd., Kaohsiung 81157, Taiwan

Corresponding author: Lu, J.C.-C. (cclu@chu.edu.tw)

Source title: Proceedings of the IASTED International Conference on Applied Simulation and Modelling, ASM 2012

Abbreviated source title: Proc. IASTED Int. Conf. Appl. Simul. Model., ASM

Monograph title: Proceedings of the IASTED International Conference on Applied Simulation and Modelling, ASM 2012

Issue date: 2012

Publication year: 2012

Pages: 150-157

Language: English

ISBN-13: 9780889869257

Document type: Conference article (CA)

Conference name: 20th IASTED International Conference on Applied Simulation and Modelling, ASM 2012

Conference date: June 25, 2012 - June 27, 2012

Conference location: Napoli, Italy

Conference code: 92890

Publisher: Acta Press, Building B6, Suite 101, 2509 Dieppe Avenue S.W., Calgary, AB, T3E 7J9, Canada

Abstract: In this paper, the deep buried line heat source of constant strength affects the thermally mechanical responses of the stratum are presented. To simulate the stratified earth medium, the soil mass is modeled as cross-anisotropic with different properties in the horizontal and vertical directions. On the basis of fundamental solutions caused by a deep point heat source, the analytic solutions of ground deformation, thermal stresses and temperature changes of the thermoelastic medium due to deep line heat source are presented by using appropriate line integral techniques. The anisotropic soil shows significant effect on long-term thermally elastic responses compared with the results from isotropic soil. Besides, the derived solutions illustrated that shear modulus does not have influence on long-term displacements and temperature increment of the strata for the case of isotropic properties.

Number of references: 19

Main heading: Anisotropic media

Controlled terms: Anisotropy - Modal analysis - Soils - Thermoelasticity

Uncontrolled terms: Analytic solution - Closed form solutions - Elastic response - Fundamental solutions - Ground deformations - Isotropic property - Line heat sources - Line integrals - Mechanical response - Point heat source - Soil mass - Temperature changes - Temperature increment - Thermoelastics - Vertical direction

Classification code: 483.1 Soils and Soil Mechanics - 921 Mathematics - 931.2 Physical Properties of Gases, Liquids and Solids - 951 Materials Science

DOI: 10.2316/P.2012.776-040

Database: Compendex

論文全文


IASTED
776, 777
A Publication of the International Association
of Science and Technology for Development
Proceedings of the
20th IASTED International Conference on
Applied Simulation and Modelling
Editor: A. Bruzzone
June 25 - 27, 2012
Napoli, Italy
Proceedings of the
15th IASTED International Conference on
Artificial Intelligence and
Soft Computing
Editor: M.H. Hamza
ISBN: 978-0-88986-925-7

Proceedings of the IASTED International Conference
Applied Simulation and Modelling (ASM 2012)
June 25 - 27, 2012 Napoli, Italy

MODELLING OF A BURIED DEEP HORIZONTAL LINE HEAT SOURCE IN A CROSS-ANISOTROPIC THERMOELASTIC MEDIUM

John C.-C. Lu[1] and Feng-Tsai Lin[2]
[1]Department of Civil Engineering, Chung Hua University
No. 707, Sec. 2, WuFu Rd., Hsinchu 30012, Taiwan, R.O.C.
cclu@chu.edu.tw
[2]Department of Naval Architecture, National Kaohsiung Marine University
No. 142, Haijhuan Rd., Kaohsiung 81157, Taiwan, R.O.C.
ftlin@mail.nkmu.edu.tw

ABSTRACT
In this paper, the deep buried line heat source of constant strength affects the thermally mechanical responses of the stratum are presented. To simulate the stratified earth medium, the soil mass is modeled as cross-anisotropic with different properties in the horizontal and vertical directions. On the basis of fundamental solutions caused by a deep point heat source, the analytic solutions of ground deformation, thermal stresses and temperature changes of the thermoelastic medium due to deep line heat source are presented by using appropriate line integral techniques. The anisotropic soil shows significant effect on long-term thermally elastic responses compared with the results from isotropic soil. Besides, the derived solutions illustrated that shear modulus does not have influence on long-term displacements and temperature increment of the strata for the case of isotropic properties.

KEY WORDS
Point Heat Source, Line Heat Source, Fundamental Solution, Closed-form Solution.

1. Introduction

The deep buried line heat source of constant strength affects the thermally mechanical responses of the stratum. The heat source such as a canister of radioactive waste can cause temperature rise in the soil, and thus the solid skeleton and pore fluid can expand. This leads to increase in pore water pressure and reduction in effective stress, because the volume increment of the pore water is greater than that of the voids of solid matrix. Therefore, thermal failure of soil can occur as a result of losing shear resistance due to reduction in effective stress.

Booker and Savvidou [1,2], Savvidou and Booker [3] presented the solutions of thermo-consolidation around spherical and point heat sources. In their solutions, the thermal properties were considered as isotropic [1,2] or cross-anisotropic [3] whereas the elastic properties of the soil were treated as isotropic [1-3]. Moreover, the stratum was modeled in full space to simulate the deep buried heat sources. Georgiadis *et al.* [4] analyzed the transient dynamic coupled thermoelasticity paradigm of a half-space under the action of a buried thermal/mechanical source. Shendeleva [5] theoretically presented a model comprising an instantaneous line heat source situated parallel to the interface between two semi-infinite heat-conductive media in perfect thermal contact. Three-dimensional Green's functions for a steady point heat source were derived by Wang *et al.* [6]. Lu and Lin [7] displayed the transient ground surface displacement produced by a point heat source or fluid sink through analog quantities between thermoelasticity and poroelasticity. Lu *et al.* [8] presented the closed-form solutions of a homogeneous isotropic elastic half space subjected to circular plane heat source on the basis of the fundamental solutions of half space due to a point heat source. Analytical solutions of the transient and long-term horizontal and vertical displacements due to a point heat source were presented by Lin and Lu [9].

Soils in general are deposited through process of sedimentation over a long period of time. Under the accumulative overburden pressure, soils display significant anisotropic mechanical and thermal properties. In order to describe the anisotropic nature of soils, it can be modeled as cross-anisotropic medium whose properties are symmetric about the vertical axis. For the heat source buried at a great depth, the effects of half space boundary on thermally response can be neglected.

In general, soils or rocks are deposited through a geologic process of sedimentation over a long period of time. Under the accumulative overburden pressure, strata display significant anisotropic mechanical, seepage and thermal properties. Both stratified soil and rock masses can show the phenomenon of anisotropy. For this reason, theoretical and numerical models should be able to simulate the layered soils and rocks as cross-anisotropic media [10-14].

The investigation is focused on long-term thermally elastic mechanical behaviors of the stratum. On the basis of the derived deep point heat source induced fundamental solutions, the closed-form solutions of long-term ground deformation, thermal stresses, and temperature changes of the soil mass due to a deep line heat source are obtained by using appropriate line integral techniques. Results are simplified to isotropic case to

DOI: 10.2316/P.2012.776-040

provide better understanding of the thermally induced mechanical responses of the stratum. The solutions can be used to test numerical models and evaluate numerical simulations of the thermoelastic responses near the line heat source.

2. Fundamental Solutions Caused by a Deep Point Heat Source

2.1 Basic Governing Equations

Theoretical and numerical models usually simulate the layered strata as cross-anisotropic media [10-14]. Figure 1 shows a point heat source buried deep in the cross-anisotropic thermoelastic strata. The stratum is considered as a homogeneous cross-anisotropic medium with vertical axis of symmetry. The constitutive behavior of the elastic soil or rock skeleton for linear axially symmetric deformation in the cylindrical coordinates (r, θ, z) can be expressed by

$$\sigma_{rr} = A\varepsilon_{rr} + (A-2N)\varepsilon_{\theta\theta} + F\varepsilon_{zz} - \beta_r\vartheta, \tag{1a}$$

$$\sigma_{\theta\theta} = (A-2N)\varepsilon_{rr} + A\varepsilon_{\theta\theta} + F\varepsilon_{zz} - \beta_r\vartheta, \tag{1b}$$

$$\sigma_{zz} = F\varepsilon_{rr} + F\varepsilon_{\theta\theta} + C\varepsilon_{zz} - \beta_z\vartheta, \tag{1c}$$

$$\sigma_{rz} = 2L\varepsilon_{rz}, \tag{1d}$$

where σ_{ij} is the thermal stress tensor. The temperature change of the stratum is denoted by ϑ. The material constants of A, C, F, L, N for the cross-anisotropic strata are defined by Love [15]. The symbols $\beta_r = 2(A-N)\alpha_{sr} + F\alpha_{sz}$ and $\beta_z = 2F\alpha_{sr} + C\alpha_{sz}$ are the thermal expansion factors in the horizontal and vertical directions, respectively. The linear thermal expansion coefficients of the strata in the horizontal and vertical directions are denoted by α_{sr} and α_{sz}, respectively. The strain components ε_{ij} and displacement components u_i are governed by the linear kinematic equation:

$$\varepsilon_{rr} = \frac{\partial u_r}{\partial r}, \tag{2a}$$

$$\varepsilon_{\theta\theta} = \frac{u_r}{r}, \tag{2b}$$

$$\varepsilon_{zz} = \frac{\partial u_z}{\partial z}, \tag{2c}$$

$$\varepsilon_{rz} = \frac{1}{2}\left(\frac{\partial u_r}{\partial z} + \frac{\partial u_z}{\partial r}\right). \tag{2d}$$

Note that u_r and u_z are displacements of the stratum in the radial and axial directions, respectively. The shear stress components $\sigma_{r\theta}$ and $\sigma_{\theta z}$ vanish by locating the vertical z-axis through the point heat source. For an isotropic stratum, $A = C = \lambda + 2G$, $F = \lambda$, $L = N = G$, $\beta_r = \beta_z = (2G + 3\lambda)\alpha_s$, where λ, G, α_s are the Lame constant, shear modulus and linear thermal expansion coefficient of the isotropic stratum, respectively.

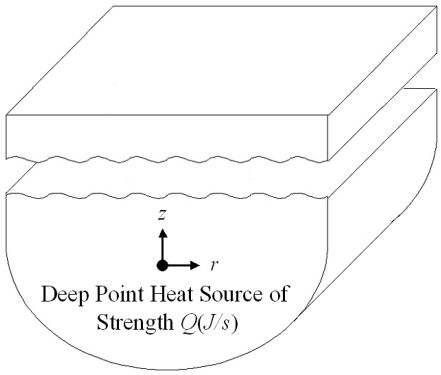

Figure 1. Point heating problem.

The thermal stresses must satisfy the equilibrium relations of axial symmetry in cylindrical coordinates as below:

$$\frac{\partial\sigma_{rr}}{\partial r} + \frac{\sigma_{rr} - \sigma_{\theta\theta}}{r} + \frac{\partial\sigma_{rz}}{\partial z} + b_r = 0, \tag{3a}$$

$$\frac{\partial\sigma_{rz}}{\partial r} + \frac{\partial\sigma_{zz}}{\partial z} + \frac{\sigma_{rz}}{r} + b_z = 0, \tag{3b}$$

where $b_i\,(i = r, z)$ denotes the body force tensor.

Using equations (1a)-(1d) and the linear kinematic equations (2a)-(2d), the equilibrium equations (3a)-(3b) for axially symmetric problem without body forces b_i are expressed in terms of displacements u_i and temperature change of the stratum ϑ as follows:

$$A\left(\frac{\partial^2 u_r}{\partial r^2} + \frac{1}{r}\frac{\partial u_r}{\partial r} - \frac{u_r}{r^2}\right) + L\frac{\partial^2 u_r}{\partial z^2} + (F+L)\frac{\partial^2 u_z}{\partial r\partial z} - \beta_r\frac{\partial\vartheta}{\partial r} = 0, \tag{4a}$$

$$(F+L)\left(\frac{\partial^2 u_r}{\partial r\partial z} + \frac{1}{r}\frac{\partial u_r}{\partial z}\right) + L\left(\frac{\partial^2 u_z}{\partial r^2} + \frac{1}{r}\frac{\partial u_z}{\partial r}\right) + C\frac{\partial^2 u_z}{\partial z^2} - \beta_z\frac{\partial\vartheta}{\partial z} = 0. \tag{4b}$$

The third relation among u_r, u_z and ϑ can be obtained from the conservation of energy:

$$-\nabla\cdot\boldsymbol{h} + q_h = 0, \tag{5}$$

where $\boldsymbol{h}$ is the heat flux vector; q_h is the internal or external heat sources.

Assuming that the cross-anisotropic thermal flow is governed by Fourier's heat conduction law, we have

$$\boldsymbol{h} = -\lambda_{tr}\frac{\partial\vartheta}{\partial r}\boldsymbol{i}_r - \lambda_{tz}\frac{\partial\vartheta}{\partial z}\boldsymbol{i}_z, \tag{6}$$

where λ_{tr} and λ_{tz} are the thermal conductivities in the horizontal and vertical direction, respectively; $\boldsymbol{i}_r$ and $\boldsymbol{i}_z$ are the unit vector parallel to the radial and vertical direction, respectively.

Considering a point heat source of constant heat generation rate Q located at point $(0,0)$. Equation (6) is substituted into (5) to yield

$$\lambda_{tr}\left(\frac{\partial^2\vartheta}{\partial r^2}+\frac{1}{r}\frac{\partial\vartheta}{\partial r}\right)+\lambda_{tz}\frac{\partial^2\vartheta}{\partial z^2}+\frac{Q}{2\pi r}\delta(r)\delta(z)=0, \tag{7}$$

in which $\delta(x)$ is the Dirac delta function.

Equations (4a), (4b) and (7) constitute the basic governing equations of the steady state axially symmetric thermoelastic responses of a homogeneous cross-anisotropic stratum due to a deep point heat source.

2.2 Boundary Conditions

The point heat source is buried at a great depth, and the effect of the point heat source must vanish at the infinity depth ($z\to\pm\infty$). Therefore, the boundary conditions of the mathematical model are as below:

$$\lim_{z\to\pm\infty}\left\{u_r(r,z),u_z(r,z),\vartheta(r,z)\right\}=\{0,0,0\}. \tag{8}$$

This mathematical model is based on the governing equations (4a), (4b), (7) and the corresponding boundary conditions (8).

2.3 Analytic Fundamental Solutions

The closed-form analytic solutions of the long-term thermally elastic responses of ground deformations, thermal stresses, and temperature change of the stratum due to a point heat source buried deep in a cross-anisotropic full space are obtained by using Hankel transform as follows:

$$u_r(r,z)=\frac{Q}{4\pi\lambda_{tz}}\left(a_1\frac{r}{R_1^*}+a_2\frac{r}{R_2^*}+a_3\frac{r}{R_3^*}\right), \tag{9a}$$

$$u_z(r,z)=\frac{Q}{4\pi\lambda_{tz}}\left(b_1\sinh^{-1}\frac{\mu_1 z}{r}+b_2\sinh^{-1}\frac{\mu_2 z}{r}+b_3\sinh^{-1}\frac{\mu_3 z}{r}\right), \tag{9b}$$

$$\vartheta(r,z)=\frac{Q}{4\pi\lambda_{tz}}\frac{1}{\mu_3 R_3}, \tag{9c}$$

$$\sigma_{rr}(r,z)=\frac{Q}{4\pi\lambda_{tz}}\left[A\left(a_1\frac{1}{R_1}+a_2\frac{1}{R_2}+a_3\frac{1}{R_3}\right)-2N\left(a_1\frac{1}{R_1^*}+a_2\frac{1}{R_2^*}+a_3\frac{1}{R_3^*}\right)+F\left(b_1\frac{\mu_1}{R_1}+b_2\frac{\mu_2}{R_2}+b_3\frac{\mu_3}{R_3}\right)-\beta_r\frac{1}{\mu_3 R_3}\right], \tag{9d}$$

$$\sigma_{\theta\theta}(r,z)=\frac{Q}{4\pi\lambda_{tz}}\left[A\left(a_1\frac{1}{R_1}+a_2\frac{1}{R_2}+a_3\frac{1}{R_3}\right)-2N\left(a_1\frac{\mu_1|z|}{R_1R_1^*}+a_2\frac{\mu_2|z|}{R_2R_2^*}+a_3\frac{\mu_3|z|}{R_3R_3^*}\right)+F\left(b_1\frac{\mu_1}{R_1}+b_2\frac{\mu_2}{R_2}+b_3\frac{\mu_3}{R_3}\right)-\beta_r\frac{1}{\mu_3 R_3}\right], \tag{9e}$$

$$\sigma_{zz}(r,z)=\frac{Q}{4\pi\lambda_{tz}}\left[F\left(a_1\frac{1}{R_1}+a_2\frac{1}{R_2}+a_3\frac{1}{R_3}\right)+C\left(b_1\frac{\mu_1}{R_1}+b_2\frac{\mu_2}{R_2}+b_3\frac{\mu_3}{R_3}\right)-\beta_z\frac{1}{\mu_3 R_3}\right], \tag{9f}$$

$$\sigma_{rz}(r,z)=\mp\frac{Q}{4\pi\lambda_{tz}}\left[L\left(a_1\frac{\mu_1 r}{R_1R_1^*}+a_2\frac{\mu_2 r}{R_2R_2^*}+a_3\frac{\mu_3 r}{R_3R_3^*}+b_1\frac{\mu_1|z|}{rR_1}+b_2\frac{\mu_2|z|}{rR_2}+b_3\frac{\mu_3|z|}{rR_3}\right)\right], \tag{9g}$$

in which the upper and lower signs of $\sigma_{rz}(r,z)$ are for the conditions of $z\ge 0$ and $z<0$, respectively. The symbols $R_i^*=R_i+\mu_i|z|$ and $R_i=\sqrt{r^2+\mu_i^2 z^2}$ $(i=1,\ 2,\ 3)$. The coefficients a_i and b_i are defined as following:

$$a_1=\frac{L\beta_r+\left[(F+L)\beta_z-C\beta_r\right]\mu_1^2}{CL\mu_1\left(\mu_1^2-\mu_2^2\right)\left(\mu_1^2-\mu_3^2\right)}, \tag{10a}$$

$$a_2=\frac{L\beta_r+\left[(F+L)\beta_z-C\beta_r\right]\mu_2^2}{CL\mu_2\left(\mu_2^2-\mu_1^2\right)\left(\mu_2^2-\mu_3^2\right)}, \tag{10b}$$

$$a_3=\frac{L\beta_r+\left[(F+L)\beta_z-C\beta_r\right]\mu_3^2}{CL\mu_3\left(\mu_3^2-\mu_1^2\right)\left(\mu_3^2-\mu_2^2\right)}, \tag{10c}$$

$$b_1=\frac{L\beta_z\mu_1^2+(F+L)\beta_r-A\beta_z}{CL\left(\mu_1^2-\mu_2^2\right)\left(\mu_1^2-\mu_3^2\right)}, \tag{10d}$$

$$b_2=\frac{L\beta_z\mu_2^2+(F+L)\beta_r-A\beta_z}{CL\left(\mu_2^2-\mu_1^2\right)\left(\mu_2^2-\mu_3^2\right)}, \tag{10e}$$

$$b_3=\frac{L\beta_z\mu_3^2+(F+L)\beta_r-A\beta_z}{CL\left(\mu_3^2-\mu_1^2\right)\left(\mu_3^2-\mu_2^2\right)}, \tag{10f}$$

in which the characteristic roots μ_1 and μ_2 must satisfy the characteristic equation

$$CL\mu^4-\left[AC-F(F+2L)\right]\mu^2+AL=0, \tag{11}$$

and the characteristic root $\mu_3 = \sqrt{\lambda_{tr}/\lambda_{tz}}$. Using the computational software Mathematica, the fundamental solutions of an isotropic stratum are obtained from (9a)-(9g) by taking appropriate limit of $\mu_1 = \mu_2 = \mu_3 = 1$ and using L'Hospital's rule. Carrying out the tedious procedure, the solutions are obtained as below:

$$u_r = \frac{Q\alpha_s(1+\nu)}{8\pi\lambda_t(1-\nu)}\frac{r}{R}, \tag{12a}$$

$$u_z = \frac{Q\alpha_s(1+\nu)}{8\pi\lambda_t(1-\nu)}\frac{z}{R}, \tag{12b}$$

$$\vartheta = \frac{Q}{4\pi\lambda_t}\frac{1}{R}, \tag{12c}$$

$$\sigma_{rr} = -\frac{QG\alpha_s(1+\nu)}{4\pi\lambda_t(1-\nu)}\left(\frac{1}{R}+\frac{r^2}{R^3}\right), \tag{12d}$$

$$\sigma_{\theta\theta} = -\frac{QG\alpha_s(1+\nu)}{4\pi\lambda_t(1-\nu)}\frac{1}{R}, \tag{12e}$$

$$\sigma_{zz} = -\frac{QG\alpha_s(1+\nu)}{4\pi\lambda_t(1-\nu)}\left(\frac{1}{R}+\frac{z^2}{R^3}\right), \tag{12f}$$

$$\sigma_{rz} = -\frac{QG\alpha_s(1+\nu)}{4\pi\lambda_t(1-\nu)}\frac{rz}{R^3}, \tag{12g}$$

where λ_t , G, ν , and α_s are the thermal conductivity, shear modulus, Poisson's ratio, and linear thermal expansion coefficient of the stratum, respectively. The symbol $R = \sqrt{r^2+z^2}$ denotes the distance from the point heat source located at the origin $(0,0)$ to the arbitrary observation point (r,z) of the stratum. The negative signs in equations (12d)-(12f) represent that the thermal stresses due to a point heat source are compressive normal stresses.

3. Closed-form Solutions Caused by a Deep Horizontal Line Heat Source

The deep horizontal line heat source, shown in Figure 2, can also introduce thermoelastic responses, and the responses are derived from the fundamental solutions caused by a deep point heat source. In the Cartesian coordinates system (x, y, z), the fundamental solutions in (9a)-(9g) or (12a)-(12g) are expressed as:

$$u_x(x,y,z) = u_r(r,\theta,z)\cos\theta - u_\theta(r,\theta,z)\sin\theta, \tag{13a}$$

$$u_y(x,y,z) = u_r(r,\theta,z)\sin\theta + u_\theta(r,\theta,z)\cos\theta, \tag{13b}$$

$$u_z(x,y,z) = u_z(r,\theta,z), \tag{13c}$$

$$\vartheta(x,y,z) = \vartheta(r,\theta,z), \tag{13d}$$

$$\sigma_{xx}(x,y,z) = \sigma_{rr}(r,\theta,z)\cos^2\theta + \sigma_{\theta\theta}(r,\theta,z)\sin^2\theta + \sigma_{r\theta}(r,\theta,z)\sin 2\theta, \tag{13e}$$

$$\sigma_{yy}(x,y,z) = \sigma_{rr}(r,\theta,z)\sin^2\theta + \sigma_{\theta\theta}(r,\theta,z)\cos^2\theta - \sigma_{r\theta}(r,\theta,z)\sin 2\theta, \tag{13f}$$

$$\sigma_{zz}(x,y,z) = \sigma_{zz}(r,\theta,z), \tag{13g}$$

$$\sigma_{xy}(x,y,z) = \left[\sigma_{rr}(r,\theta,z) - \sigma_{\theta\theta}(r,\theta,z)\right]\cos\theta\sin\theta + \sigma_{r\theta}(r,\theta,z)\cos 2\theta, \tag{13h}$$

$$\sigma_{xz}(x,y,z) = \sigma_{yz}(x,y,z) = \sigma_{rz}(r,\theta,z), \tag{13i}$$

in which $u_\theta = 0$ and $\sigma_{r\theta} = 0$ for the case of axially symmetric thermoelastic medium.

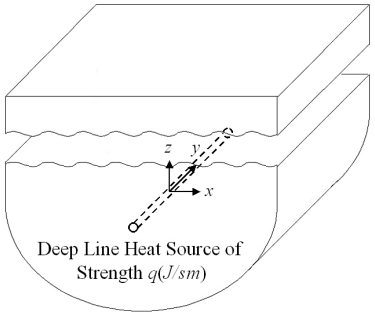

Figure 2. Horizontal line heating problem.

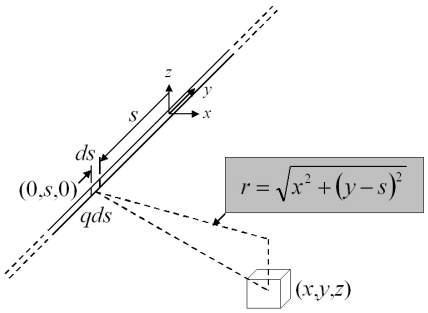

Figure 3. The horizontal component of the distance from an elementary heat source at point (0, *s*, 0).

Figure 3 presents the horizontal component of the distance from an elementary heat source at point (0, *s*, 0), and the strength of the line heat source is treated as *q*. Considering the elementary length *ds* of the line heat source, the thermal strength of the length *ds* is equal to *qds*. The quantity *qds* can be treated as a point heat source. To determine the thermally mechanical responses due to the elementary heat source at a point (*x*, *y*, *z*), the quantity *qds* is substituted for *Q*, and $r = \sqrt{x^2 + (y-s)^2}$ for $r = \sqrt{x^2+y^2}$. Using Mathematica, the thermo-mechanical behaviors at a point (*x*, *y*, *z*) on the *xz*-plane due to the entire line heating source can be obtained by integration with the symbol *s* from –∞ to ∞ as below:

$$u_x = \frac{q}{4\pi\lambda_{tz}}(h_1 + h_2 + h_3), \tag{14a}$$

$$u_y = 0\,, \tag{14b}$$

$$u_z = \frac{q}{4\pi\lambda_{tz}}\left(h_4 + h_5 + h_6\right), \tag{14c}$$

$$\vartheta = \frac{q}{4\pi\lambda_{tz}} h_7\,, \tag{14d}$$

$$\sigma_{xx} = \frac{q}{4\pi\lambda_{tz}}\left(Ah_8 + Fh_9 - \beta_r h_7\right), \tag{14e}$$

$$\sigma_{yy} = \frac{q}{4\pi\lambda_{tz}}\left[\left(A-2N\right)h_8 + Fh_9 - \beta_r h_7\right], \tag{14f}$$

$$\sigma_{zz} = \frac{q}{4\pi\lambda_{tz}}\left(Fh_8 + Ch_9 - \beta_z h_7\right), \tag{14g}$$

$$\sigma_{xy} = 0\,, \tag{14h}$$

$$\sigma_{xz} = \frac{q}{4\pi\lambda_{tz}} Lh_{10}\,, \tag{14i}$$

$$\sigma_{yz} = 0\,, \tag{14j}$$

where $h_i\left(i = 1, 2, \cdots, 10\right)$ are expressed as following:

$$h_1 = -a_1\left[x\ln\left(x^2 + \mu_1^2 z^2\right) + \mu_1 z\tan^{-1}\frac{2\mu_1 xz}{\mu_1^2 z^2 - x^2} + \pi\mu_1\left|z\right|\right], \tag{15a}$$

$$h_2 = -a_2\left[x\ln\left(x^2 + \mu_2^2 z^2\right) + \mu_2 z\tan^{-1}\frac{2\mu_2 xz}{\mu_2^2 z^2 - x^2} + \pi\mu_2\left|z\right|\right], \tag{15b}$$

$$h_3 = -a_3\left[x\ln\left(x^2 + \mu_3^2 z^2\right) + \mu_3 z\tan^{-1}\frac{2\mu_3 xz}{\mu_3^2 z^2 - x^2} + \pi\mu_3\left|z\right|\right], \tag{15c}$$

$$h_4 = -b_1\left[x\tan^{-1}\frac{2\mu_1 xz}{x^2 - \mu_1^2 z^2} + \mu_1 z\ln\left(x^2 + \mu_1^2 z^2\right)\right], \tag{15d}$$

$$h_5 = -b_2\left[x\tan^{-1}\frac{2\mu_2 xz}{x^2 - \mu_2^2 z^2} + \mu_2 z\ln\left(x^2 + \mu_2^2 z^2\right)\right], \tag{15e}$$

$$h_6 = -b_3\left[x\tan^{-1}\frac{2\mu_3 xz}{x^2 - \mu_3^2 z^2} + \mu_3 z\ln\left(x^2 + \mu_3^2 z^2\right)\right], \tag{15f}$$

$$h_7 = -\frac{1}{\mu_3}\ln\left(x^2 + \mu_3^2 z^2\right), \tag{15g}$$

$$h_8 = -a_1\ln\left(x^2 + \mu_1^2 z^2\right) - a_2\ln\left(x^2 + \mu_2^2 z^2\right) - a_3\ln\left(x^2 + \mu_3^2 z^2\right), \tag{15h}$$

$$h_9 = -b_1\mu_1\ln\left(x^2 + \mu_1^2 z^2\right) - b_2\mu_2\ln\left(x^2 + \mu_2^2 z^2\right) - b_3\mu_3\ln\left(x^2 + \mu_3^2 z^2\right), \tag{15i}$$

$$h_{10} = a_1\mu_1\tan^{-1}\frac{2\mu_1 xz}{\mu_1^2 z^2 - x^2} + a_2\mu_2\tan^{-1}\frac{2\mu_2 xz}{\mu_2^2 z^2 - x^2} + a_3\mu_3\tan^{-1}\frac{2\mu_3 x\left|z\right|}{\mu_3^2 z^2 - x^2} + \frac{b_1\mu_1 z}{x}\ln\left(x^2 + \mu_1^2 z^2\right) + \frac{b_2\mu_2 z}{x}\ln\left(x^2 + \mu_2^2 z^2\right) + \frac{b_3\mu_3 z}{x}\ln\left(x^2 + \mu_3^2 z^2\right). \tag{15j}$$

Proceeding with similar manner, the solutions of an isotropic stratum due to the deep horizontal line heat source are determined as below:

$$u_x = -\frac{q\left(1+\nu\right)\alpha_s}{4\pi\lambda_t\left(1-\nu\right)} x\ln\sqrt{x^2 + z^2}\,, \tag{16a}$$

$$u_y = 0\,, \tag{16b}$$

$$u_z = -\frac{q\left(1+\nu\right)\alpha_s}{4\pi\lambda_t\left(1-\nu\right)} z\ln\sqrt{x^2 + z^2}\,, \tag{16c}$$

$$\vartheta = -\frac{q}{2\pi\lambda_t}\ln\sqrt{x^2 + z^2}\,, \tag{16d}$$

$$\sigma_{xx} = \frac{q\left(1+\nu\right)G\alpha_s}{2\pi\lambda_t\left(1-\nu\right)}\left(\ln\sqrt{x^2 + z^2} - \frac{x^2}{x^2 + z^2}\right), \tag{16e}$$

$$\sigma_{yy} = \frac{q\left(1+\nu\right)G\alpha_s}{\pi\lambda_t\left(1-\nu\right)}\ln\left(x^2 + z^2\right), \tag{16f}$$

$$\sigma_{zz} = \frac{q\left(1+\nu\right)G\alpha_s}{2\pi\lambda_t\left(1-\nu\right)}\left(\ln\sqrt{x^2 + z^2} - \frac{z^2}{x^2 + z^2}\right), \tag{16g}$$

$$\sigma_{xy} = 0\,, \tag{16h}$$

$$\sigma_{xz} = -\frac{q\left(1+\nu\right)G\alpha_s}{2\pi\lambda_t\left(1-\nu\right)}\frac{xz}{x^2 + z^2}\,, \tag{16i}$$

$$\sigma_{yz} = 0\,, \tag{16j}$$

in which the displacement component u_y and shear stress components, σ_{xy} and σ_{yz}, vanish by locating the *y*-axis through the deep line heat source as shown in Figure 3.

The results of (14a)-(14j) are confirmed by simplifying the solutions of cross-anisotropic thermoelastic behaviors to isotropic case of (16a)-(16j). All field quantities are functions of the distance from heat source and are proportional to the linear thermal expansion coefficient, but they are inversely proportional to the thermal conductivity. For isotropic cases, the shear modulus does not have influence on the displacements and temperature change of the stratum as shown in (16a)-(16d).

4. Numerical Results

The numerical results were obtained for different appropriate sets of soil thermoelastic constants to investigate the effect of anisotropy on displacements, temperature increment and thermal stresses of the strata due to a deep point heat source. The related thermoelastic constants are summarized in Table 1.

Table 1. Material properties of isotropic and cross-anisotropic soils (*assumed values).

Case	$\nu_{r\theta}$	ν_{rz}	G_{rz}/E_z	E_r/E_z	α_{sr}/α_{sz}	$\lambda_{tr}/\lambda_{tz}$
Case 1: Isotropy [16]	0.25	0.25	0.4	1.0	1.0	1.0
Case 2: Cross-anisotropy [17]	0.125	0.75	0.445	2.0	10.0*	10.0*
Case 3: Cross-anisotropy [17]	0.125	0.75	0.64	3.0	10.0*	10.0*
Case 4: Cross-anisotropy [17]	0.125	0.75	0.64	4.0	10.0*	10.0*
Case 5: Cross-anisotropy [11,18,19]	0	0.38	0.38	1.84	10.0*	10.0*

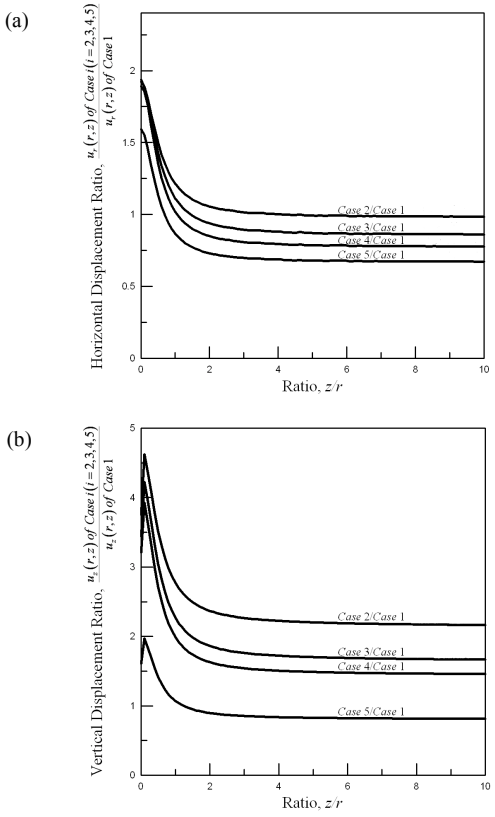

Figure 4. Influence of anisotropy on long-term (a) horizontal displacements u_r and (b) vertical displacement u_z of the strata.

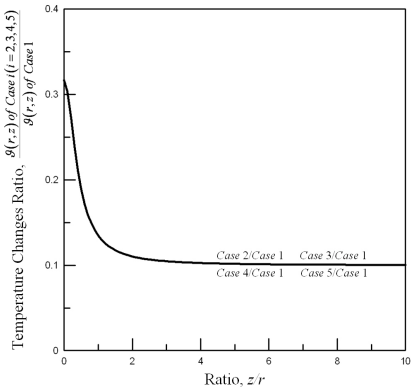

Figure 5. Influence of anisotropy on long-term temperature changes of the strata.

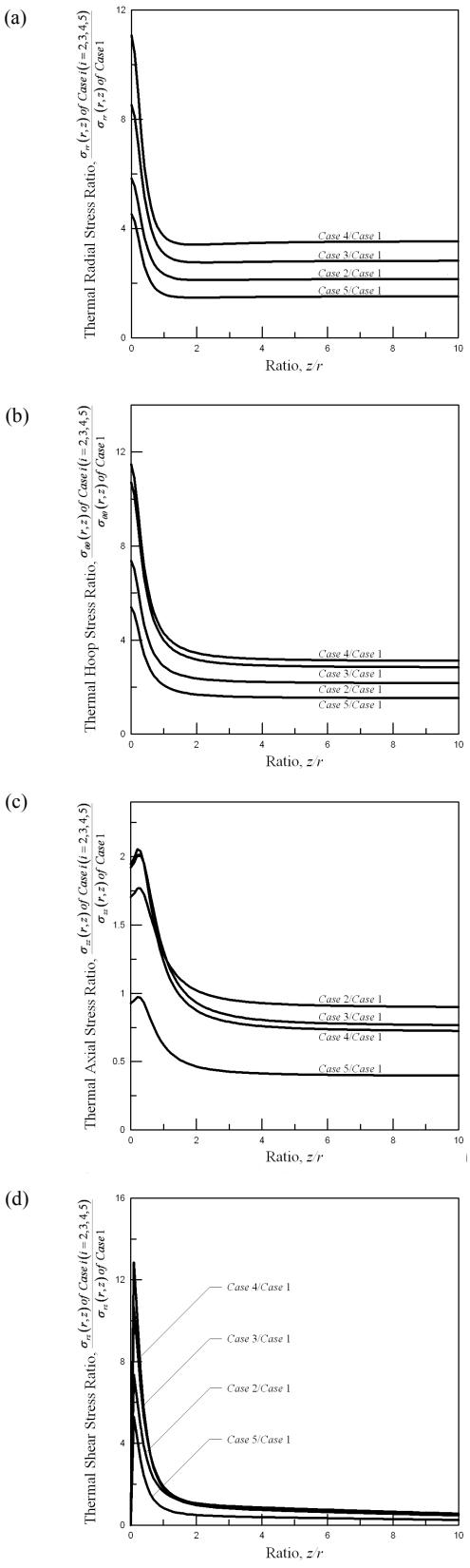

Figure 6. Influence of anisotropy on long-term (a) thermal radial stress σ_{rr}, (b) thermal hoop stress $\sigma_{\theta\theta}$, (c) thermal axial stress σ_{zz} and (d) thermal shear stress σ_{rz} of the strata.

The values of anisotropic linear thermal expansion coefficient $\alpha_{sr}/\alpha_{sz}=10.0$ and thermal conductivity $\lambda_{tr}/\lambda_{tz}=10.0$ are assumed in cases 2 to 5. For the heavily over-consolidated London clay, the range of the ratio E_r/E_z is between 1.35 and 2.37, and the ratio G_{rz}/E_z is between 1.35 and 2.37 [18,19]. The average values of E_r/E_z and G_{rz}/E_z are 1.84 and 0.38, respectively. In these numerical studies, the Young's modulus in vertical direction E_z, linear thermal expansion coefficient in vertical direction α_{sz}, and thermal conductivity in vertical direction λ_{tz} are treated as constants in cases 2 to 5.

The influence of anisotropy on long-term thermoelastic responses are given in Figures 4 to 6. In these figures, the thermoelastic responses are normalized. From Figures 4 to 6,the anisotropy properties of the soils show significant effect on long-term thermally elastic responses compared with the results obtained for an isotropic soil of case 1. For example, the long-term horizontal displacement of case 4 is reduced to around 75% of the corresponding value for the isotropic soil of case 1, while the long-term vertical displacement of case 4 increases to 150% of case 1 for ratio $z/r > 3$ as shown in Figure 4. For ratio of $\lambda_{tr}/\lambda_{tz}$ at 10.0 in cases 2 to 5, the long-term temperature increments of the strata in cases 2 to 5 are reduced to around 10% of the corresponding value for the isotropic soil of case 1 as illustrated in Figure 5.

5. Conclusion

Using the computational software Mathematica, this investigation obtains closed-form solutions of the long-term thermoelastic responses due to an infinite horizontal line heat source of constant heat generation rate buried deep in a cross-anisotropic elastic full space. Results for solutions of cross-anisotropic thermoelastic behaviors are obtained by simplifying closed-form solutions to the isotropic case of thermoelastic full space. The solutions are used to evaluate detail numerical simulations of thermoelastic responses near the heat source. The results show:

1. The derived solutions illustrate that all field quantities are inversely proportional to the thermal conductivity. However, the shear modulus does not have influence on long-term displacements and temperature increment of the strata for the case of isotropic properties.
2. The anisotropy of the soils has significant effect on long-term thermally elastic responses compared with the results obtained for an isotropic soil. For example, the long-term horizontal displacement for anisotropic soil of case 4 is reduced to around 75% of the corresponding value for the isotropic soil of case 1, while the long-term vertical displacement of case 4 increases to 150% of case 1 for ratio $z/r > 3$ as shown in Figure 4.

Acknowledgements

This work is supported by the National Science Council of Republic of China through grant NSC100-2221-E-216-025.

References

[1] J.R. Booker & C. Savvidou, Consolidation around a spherical heat source, *International Journal of Solids and Structures*, 20(11/12), 1984, 1079-1090.

[2] J.R. Booker & C. Savvidou, Consolidation around a point heat source, *International Journal for Numerical and Analytical Methods in Geomechanics*, 9(2), 1985, 173-184.

[3] C. Savvidou & J.R. Booker, Consolidation around a heat source buried deep in a porous thermoelastic medium with anisotropic flow properties, *International Journal for Numerical and Analytical Methods in Geomechanics*, 13(1), 1989, 75-90.

[4] H.G. Georgiadis, A.P. Rigatos & L.M. Brock, Thermoelastodynamic disturbances in a half-space under the action of a buried thermal/mechanical line source, *International Journal of Solids and Structures*, 36(24), 1999, 3639-3660.

[5] M.L. Shendeleva, Instantaneous line heat source near a plane interface, *Journal of Applied Physics*, 95(5), 2004, 2839-2845.

[6] X. Wang, E. Pan & A.K. Roy, Three-dimensional Green's functions for a steady point heat source in a functionally graded half-space and some related problems, *International Journal of Engineering Science*, 45(11), 2007, 939-950.

[7] J. C.-C. Lu & F.-T. Lin, The transient ground surface displacements due to a point sink/heat source in an elastic half-space, *Geotechnical Special Publication No. 148*, *ASCE*, 2006, 210-218.

[8] J. C.-C. Lu, W.-C. Lin & F.-T. Lin, Closed-form solutions of the homogeneous isotropic elastic half space subjected to a circular plane heat source, *Geotechnical Special Publication No. 204*, *ASCE*, 2010, 79-86.

[9] F.-T. Lin & J. C.-C. Lu, Golden ratio in the point heat source induced horizontal and vertical displacements of an isotropic elastic half space, *Geotechnical Special Publication No. 204*, *ASCE*, 2010, 87-94.

[10] B. Amadei, H.S. Swolfs, W.Z. Savage, Gravity-induced stresses in stratified rock masses, *Rock Mechanics and Rock Engineering*, 21(1), 1988, 1-20.

[11] J.Q. Tarn & C.-C. Lu, Analysis of subsidence due to a point sink in an anisotropic porous elastic half space, *International Journal for Numerical and Analytical Methods in Geomechanics*, 15(8), 1991, 573-592.

[12] P.R. Sheorey, A theory for in situ stresses in isotropic and transversely isotropic rock, *International Journal of Rock Mechanics and Mining Sciences and Geomechanics Abstracts*, 31(1), 1994, 23-34.

[13] S.L. Lee & J.H. Yang, Modeling of effective thermal conductivity for a nonhomogeneous anisotropic porous medium, *International Journal of Heat and Mass Transfer*, 41(6-7), 1998, 931-937.

[14] C.D. Wang & C.S. Tzeng, Displacements and stresses due to nonuniform circular loadings in an inhomogeneous cross-anisotropic material, *Mechanics Research Communications*; 36, 2009, 921-932.

[15] A.E.H. Love, *A Treatise on the mathematical theory of elasticity* (New York: Dover Press, 1944, 636p).

[16] J.R. Booker & J.P. Carter, Analysis of a point sink embedded in a porous elastic half space, *International Journal for Numerical and Analytical Methods in Geomechanics*, 10(2), 1986, 137-150.

[17] H.G. Poulos & E.H. Davis, *Elastic solutions for soil and rock mechanics* (New York: John Wiley & Sons, 1974, 183-192).

[18] K.M. Lee & R.K. Rowe, Deformations caused by surface loading and tunnelling: The role of elastic anisotropy, *Geotechnique*, 39(1), 1989, 125-140.

[19] C.D. Wang, E. Pan, C.S. Tzeng, F. Han & J.J. Liao, Displacements and stresses due to a uniform vertical circular load in an inhomogeneous cross-anisotropic half-space, *International Journal of Geomechanics*, ASCE, 6(1), 2006, 1-10.

Nomenclature

a_1, a_2, a_3	Parameters defined in equations (10a)-(10c)
A, C, F, L, N	Elastic constants of the cross-anisotropic stratum defined by Love [15]
b_1, b_2, b_3	Parameters defined in equations (10d)-(10f)
$b_i\ (i = r, z)$	Body forces in cylindrical coordinates
G	Shear modulus of the isotropic stratum
$\boldsymbol{h}$	Heat flux vector
$h_1, \cdots, h_{10}$	Functions defined in equations (15a)-(15j)
$\boldsymbol{i}_r, \boldsymbol{i}_z$	Unit vector parallel to the radial/vertical direction
q	Heat generation rate of the line heat source
q_h	Internal/external heat sources
Q	Heat generation rate of the point heat source
(r, θ, z)	Cylindrical coordinates system
R	Distance parameter defined as $R = \sqrt{r^2 + z^2}$
R_1, R_2, R_3	Distance parameters defined as $R_i = \sqrt{r^2 + \mu_i^2 z^2}$, $(i = 1, 2, 3)$
R_1^*, R_2^*, R_3^*	Distance parameters defined as $R_i^* = R_i + \mu_i \lvert z \rvert$, $(i = 1, 2, 3)$
u_r, u_θ, u_z	Radial/tangential/axial displacement of the thermoelastic stratum
u_x, u_y, u_z	Displacements of the medium expressed in Cartesian coordinates system
(x, y, z)	Cartesian coordinates system
α_s	Linear thermal expansion coefficient for the isotropic thermoelastic stratum
α_{sr}, α_{sz}	Linear thermal expansion coefficient of the cross-anisotropic thermoelastic stratum in the horizontal/vertical direction
β_r, β_z	Linear thermal expansion factor of the cross-anisotropic thermoelastic stratum in the horizontal/vertical direction
$\delta(x)$	Dirac delta function
δ_{ij}	Kronecker delta
ε_{ij}	Strain components of the stratum
ϑ	Temperature change of the thermoelastic stratum
λ	Lame constant of the thermoelastic stratum
λ_t	Thermal conductivity of the thermoelastic stratum
$\lambda_{tr}, \lambda_{tz}$	Horizontal/vertical thermal conductivity of the cross-anisotropic stratum
μ_1, μ_2	Characteristic roots defined in equation (11)
μ_3	Characteristic root, $\mu_3 = \sqrt{\lambda_{tr} / \lambda_{tz}}$
ν	Poisson's ratio for the isotropic thermoelastic stratum
σ_{ij}	Thermal stress components of the thermoelastic stratum

附錄 4

研究成果投稿後已發表於 EI 等級之國際會議論文(第二篇)

Lu, John C.-C. **(Session Chair)** and Feng-Tsai Lin, 2012/6/25~27, "Modelling of Consolidation Settlement Due to a Circularly Symmetric Fluid Sink," *Proceedings of the 20th IASTED International Conference on Applied Simulation and Modelling, CD ISBN: 978-0-88986-925-7*, Napoli, Italy, pp. 107-113. (This work is supported by the National Science Council through grants NSC100-2221-E-216-025.) (EI)

論文收錄於 EI 資料庫之證明文件

Blog This | Email | Print | Download | Save to Folder

Abstract | Detailed Highlight search terms

Record 2 from Compendex & Inspec for: (({Lin, Feng-Tsai}) WN AU), 1969-2013

Check record to add to Selected Records

2.

Accession number: 20124115537526

Title: Modelling of consolidation settlement due to a circularly symmetric fluid sink

Authors: Lu, John C.-C.[1]; Lin, Feng-Tsai[2]

Author affiliation: [1] Department of Civil Engineering, Chung Hua University, No. 707, WuFu Rd., Hsinchu 30012, Taiwan

[2] Department of Naval Architecture, National Kaohsiung Marine University, No. 142, Haijhuan Rd., Kaohsiung 81157, Taiwan

Corresponding author: Lu, J.C.-C. (cclu@chu.edu.tw)

Source title: Proceedings of the IASTED International Conference on Applied Simulation and Modelling, ASM 2012

Abbreviated source title: Proc. IASTED Int. Conf. Appl. Simul. Model., ASM

Monograph title: Proceedings of the IASTED International Conference on Applied Simulation and Modelling, ASM 2012

Issue date: 2012

Publication year: 2012

Pages: 107-113

Language: English

ISBN-13: 9780889869257

Document type: Conference article (CA)

Conference name: 20th IASTED International Conference on Applied Simulation and Modelling, ASM 2012

Conference date: June 25, 2012 - June 27, 2012

Conference location: Napoli, Italy

Conference code: 92890

Publisher: Acta Press, Building B6, Suite 101, 2509 Dieppe Avenue S.W., Calgary, AB, T3E 7J9, Canada

Abstract: On the basis of a point sink induced half space fundamental solutions, the investigation presents analytical solutions of the long-term consolidation settlement and excess pore fluid pressure of a saturated elastic aquifer subjected to a circularly symmetric fluid sink. The governing equations of the mathematical model are based on the theory of poroelasticity. The aquifer is modeled as a homogeneous isotropic poroelastic half space, and the total stresses of the aquifer obey Newton's second law and Hooke's law. Besides, the mass conservation and Darcy's law are introduced to formulate the governing equations of pore fluid flow. The software Mathematica is used to complete the symbolic calculations, and the closed-form solutions are derived.

Number of references: 21

Main heading: Aquifers

Controlled terms: Fluid dynamics - Geometry - Mathematical models - Modal analysis - Porous materials - Settlement of structures

Uncontrolled terms: Closed form solutions - Consolidation settlement - Darcy's law - Fundamental solutions - Governing equations - Half spaces - Hooke's Law - Mass conservation - Mathematica - Newton's second law - Pore fluid flow - Pore fluid pressure - Poro-elasticity - Poroelastic half spaces - Porous medium - Symbolic calculation

Classification code: 402 Buildings and Towers - 444.2 Groundwater - 921 Mathematics - 931.1 Mechanics - 951 Materials Science

DOI: 10.2316/P.2012.776-044

Database: Compendex

Full-text and Local Holdings Links

SDOS | STIC Union Catalog | CHU | 館藏查詢

論文全文


IASTED
776, 777
A Publication of the International Association
of Science and Technology for Development
Proceedings of the
20th IASTED International Conference on
Applied Simulation and Modelling
Editor: A. Bruzzone
June 25 - 27, 2012
Napoli, Italy
Proceedings of the
15th IASTED International Conference on
Artificial Intelligence and
Soft Computing
Editor: M.H. Hamza
ISBN: 978-0-88986-925-7

Proceedings of the IASTED International Conference
Applied Simulation and Modelling (ASM 2012)
June 25 - 27, 2012 Napoli, Italy

MODELLING OF CONSOLIDATION SETTLEMENT DUE TO A CIRCULARLY SYMMETRIC FLUID SINK

John C.-C. Lu[1] and Feng-Tsai Lin[2]
[1]Department of Civil Engineering, Chung Hua University
No. 707, Sec. 2, WuFu Rd., Hsinchu 30012, Taiwan, R.O.C.
cclu@chu.edu.tw
[2]Department of Naval Architecture, National Kaohsiung Marine University
No. 142, Haijhuan Rd., Kaohsiung 81157, Taiwan, R.O.C.
ftlin@mail.nkmu.edu.tw

ABSTRACT
On the basis of a point sink induced half space fundamental solutions, the investigation presents analytical solutions of the long-term consolidation settlement and excess pore fluid pressure of a saturated elastic aquifer subjected to a circularly symmetric fluid sink. The governing equations of the mathematical model are based on the theory of poroelasticity. The aquifer is modeled as a homogeneous isotropic poroelastic half space, and the total stresses of the aquifer obey Newton's second law and Hooke's law. Besides, the mass conservation and Darcy's law are introduced to formulate the governing equations of pore fluid flow. The software Mathematica is used to complete the symbolic calculations, and the closed-form solutions are derived.

KEY WORDS
Fluid Sink, Half Space, Closed-form Solution, Porous Medium.

1. Introduction

Large amounts of groundwater withdrawal can induce land subsidence [1]. The stratum compact on itself when the groundwater is withdrawn from the saturated aquifer of the strata. As water pumped from an aquifer, the pore water pressure is reduced in the withdrawal region. It leads to increase in effective stress between the solid skeleton and the subsidence of ground surface.

The coupled three-dimensional consolidation theory introduced by Biot [2,3] is generally regarded as the fundamental theory for modelling consolidation settlement. The approach followed Rice and Cleary [4] who provided an elegant formulation of Biot's theory in terms of easily identifiable quantities and material constants. Bear and Corapcioglu [5,6] presented the modified Biot's equations where the pore fluid was treated as compressible and the solid skeleton was assumed incompressible. Based on Biot's theory modified by Bear and Corapcioglu [5,6], Booker and Carter [7-10], Tarn and Lu [11] presented solutions of subsidence by a point sink embedded in the saturated elastic half space at a constant rate. Chen [12,13], Kanok-Nukulchai and Chau [14] presented analytic solutions for the steady-state responses of displacements and stresses in a porous half space subject to a fluid point sink. Lu and Lin [15,16] displayed transient displacements of the pervious half space due to steady pumping rate [15] and impulsive pumping [16]. Hou *et al.* [17] presented that the ground horizontal displacement occurred as groundwater withdrawn from an aquifer.

The present investigation is focused on the closed-form solutions of an isotropic poroelastic half space due to a circularly symmetric fluid sink which still have not been derived in previous studies. In this study, the aquifer is modelled as a linearly elastic medium with homogeneous isotropic properties. The half space fundamental solutions of the long-term displacements and excess pore fluid pressure of the saturated aquifer due to a point sink are obtained by using Hankel and Fourier transforms.

Based on the derived fundamental solutions, the software Mathematica is used to complete the symbolic calculations and obtain the closed-form solutions for the aquifer subjected to a circularly symmetric fluid sink. The solutions can be used to develop numerical models and the detailed numerical simulations of the consolidation settlement near the circularly symmetric fluid sink.

2. Modelling of Poroelastic Point Sink Problem

2.1 Basic Governing Equations

The formulation of Biot's equations follows that of Rice and Cleary [4] who provided an easily identifiable quantities and material constants. Four basic material constants are selected in the constitutive equations including the shear modulus G, the drained Poisson's ratio ν, the undrained Poisson's ratio ν_u and Skempton's pore pressure coefficient B [18]. The physical ranges of material constants B and ν_u are $0 \le B \le 1$ and

DOI: 10.2316/P.2012.776-044

$0 \le \nu \le \nu_u \le \frac{1}{2}$ [4], respectively. For the situation of incompressible constituents, the poroelastic coefficients $B = 1$ and $\nu_u = \frac{1}{2}$. According to Rice and Cleary [4], the reformulated constitutive relations are expressed as [19]:

$$\sigma_{ij} = 2G\varepsilon_{ij} + \frac{2G\nu}{1-2\nu}\varepsilon\delta_{ij} - \frac{3(\nu_u - \nu)}{B(1-2\nu)(1+\nu_u)}p\delta_{ij}, \quad (1a)$$

$$p = -\frac{2GB(1+\nu_u)}{3(1-2\nu_u)}\varepsilon + \frac{2GB^2(1-2\nu)(1+\nu_u)^2}{9(\nu_u - \nu)(1-2\nu_u)}\varsigma, \quad (1b)$$

in which σ_{ij}, p and ε_{ij} are the total stress components, excess pore fluid pressure and solid strain components of the poroelastic media, respectively. Note that positive σ_{ij} and p represent tension. The parameter ς is variation of fluid content per unit reference volume of the aquifer. The volumetric strain of the skeletal material is denoted by ε and $\varepsilon = \varepsilon_{11} + \varepsilon_{22} + \varepsilon_{33}$; δ_{ij} is the Kronecker delta. The inversions of equations (1a) and (1b) are shown as the form:

$$\varepsilon_{ij} = \frac{1}{2G}\left(\sigma_{ij} - \frac{\nu}{1+\nu}\sigma_{kk}\delta_{ij}\right) + \frac{3(\nu_u - \nu)}{2GB(1+\nu)(1+\nu_u)}p\delta_{ij}, \quad (1a^*)$$

$$\varsigma = \frac{9(\nu_u - \nu)(1-2\nu_u)}{2GB^2(1-2\nu)(1+\nu_u)^2}p + \frac{3(\nu_u - \nu)}{B(1-2\nu)(1+\nu_u)}\varepsilon. \quad (1b^*)$$

The solid strain components ε_{ij} and displacement components u_i are governed by the linear kinematic equation:

$$\varepsilon_{ij} = \tfrac{1}{2}\left(u_{i,j} + u_{j,i}\right). \quad (2)$$

The total stress components σ_{ij} must satisfy the equilibrium equations:

$$\sigma_{ij,j} + b_i = 0, \quad (3)$$

where b_i denote the body force components. The mass balance for the fluid phase is denoted by:

$$\frac{\partial \varsigma}{\partial t} + v_{i,i} + q = 0, \quad (4)$$

in which v_i is the specific discharge velocity components; the quantity q is the rate of fluid extracted from the saturated porous aquifer per unit volume by the sink. The pore fluid flow is governed by Darcy's law as below:

$$v_i = -\frac{k}{\gamma_f}p_{,i}, \quad (5)$$

in which k and γ_f denotes the permeability of the porous aquifer and the unit weight of pore fluid, respectively.

The governing equations (1) to (5) are combined to derive various field equations for their corresponding solutions of boundary value problems. The equilibrium equation (3) and mass balance equation (4) are expressed in terms of displacement components u_i and excess pore fluid pressure p by substituting (1a) into (3), (1b*) and (5) into (4) as below [20]:

$$G\nabla^2 u_i + \frac{G}{1-2\nu}\frac{\partial \varepsilon}{\partial x_i} - \alpha\frac{\partial p}{\partial x_i} + b_i = 0, \quad (6a)$$

$$-\frac{k}{\gamma_f}\nabla^2 p + \frac{9(\nu_u - \nu)(1-2\nu_u)}{2GB^2(1-2\nu)(1+\nu_u)^2}\frac{\partial p}{\partial t} + \alpha\frac{\partial \varepsilon}{\partial t} + q = 0, \quad (6b)$$

where α is known as Biot's coefficient of effective stress which can be defined as

$$\alpha = \frac{3(\nu_u - \nu)}{B(1-2\nu)(1+\nu_u)}. \quad (7)$$

The above mathematical model is known as coupled model of poroelasticity where the flow field is dependent on the displacement field. The long-term consolidation settlement model is preferred in this investigation, and the time dependent differentiation terms in equation (6b) are neglected.

Figure 1 presents a fluid point sink buried in a saturated porous elastic half space at a depth h. The constant pumping strength is denoted as Q at the location $(0,h)$. Introducing the equilibrium equations for axisymmetric poroelasticity model with a vertical axis of symmetry and neglect the effects of body forces b_i, the equation (6a) are transformed to equations (8a) and (8b). Moreover, the mass balance equation (6b) are expressed as (8c) by assuming the long-term consolidation settlement. After doing so, the governing equations in axially symmetric coordinates (r,z) are derived in terms of displacements $u_i\,(i = r,z)$ and excess pore fluid pressure p as following:

$$G\nabla^2 u_r + \frac{G}{1-2\nu}\frac{\partial \varepsilon}{\partial r} - G\frac{u_r}{r^2} - \alpha\frac{\partial p}{\partial r} = 0, \quad (8a)$$

$$G\nabla^2 u_z + \frac{G}{1-2\nu}\frac{\partial \varepsilon}{\partial z} - \alpha\frac{\partial p}{\partial z} = 0, \quad (8b)$$

$$-\frac{k}{\gamma_f}\nabla^2 p + \frac{Q}{2\pi r}\delta(r)\delta(z-h) = 0, \quad (8c)$$

where the differential operator $\nabla^2 = \frac{\partial^2}{\partial r^2} + \frac{1}{r}\frac{\partial}{\partial r} + \frac{\partial^2}{\partial z^2}$ and solid strain components $\varepsilon = \frac{\partial u_r}{\partial r} + \frac{u_r}{r} + \frac{\partial u_z}{\partial z}$; $\delta(x)$ is the Dirac delta function. Equations (8a) to (8c) are the basic field equations of long-term consolidation settlement with a point sink at a constant pumping rate, in which the fluid and solid are treated as compressible constituents.

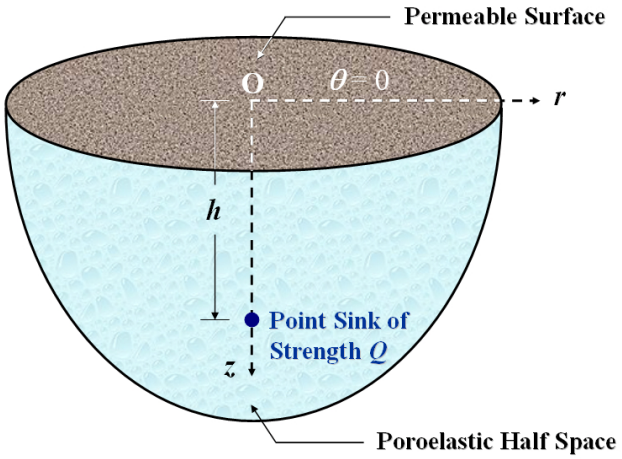

Figure 1. Poroelastic point sink problem.

2.2 Boundary Conditions

The ground surface of the half space is treated as a pervious and traction-free boundary for all times $t \geq 0$. Therefore, the mathematical statements of the ground surface boundary $z = 0$ in axisymmetric coordinates (r, z) are:

$$\sigma_{rz}(r,0) = 0,\ \sigma_{zz}(r,0) = 0, \text{ and } p(r,0) = 0. \tag{9a}$$

The displacements and excess pore fluid pressure at the remote boundary $z \to \infty$ due to the effect of a point sink must be nil at any time. These conditions are written as

$$\lim_{z\to\infty}\{u_r(r,z), u_z(r,z), p(r,z)\} = \{0,0,0\}. \tag{9b}$$

This mathematical model is based on the governing equations (8a)-(8c) and the corresponding boundary conditions (9a)-(9b).

2.3 Fundamental Solutions

Applying Hankel integral transformation [21] with respect to the variable *r*, the closed-form analytic fundamental solutions of the long-term responses of ground deformations and excess pore water pressure of the elastic aquifer due to a point sink in an isotropic half space are obtained as follows [11]:

$$u_r(r,z) = \frac{(1-2\nu)\alpha Q\gamma_f}{16\pi(1-\nu)Gk}\left[-\frac{r}{\tilde{R}_1} + \frac{r}{\tilde{R}_2^*} - (3-4\nu)\frac{rh}{\tilde{R}_2\tilde{R}_2^*} + \frac{rz}{\tilde{R}_2\tilde{R}_2^*} + \frac{2hrz}{\tilde{R}_2^3}\right], \tag{10a}$$

$$u_z(r,z) = \frac{(1-2\nu)\alpha Q\gamma_f}{16\pi(1-\nu)Gk}\left[-\frac{z-h}{\tilde{R}_1} + (3-4\nu)\frac{h}{\tilde{R}_2} + \frac{z}{\tilde{R}_2} + \frac{2hz(z+h)}{\tilde{R}_2^3}\right], \tag{10b}$$

$$p(r,z) = -\frac{Q\gamma_f}{4\pi k}\left(\frac{1}{\tilde{R}_1} - \frac{1}{\tilde{R}_2}\right), \tag{10c}$$

where $\tilde{R}_1 = \sqrt{r^2 + (z-h)^2}$, $\tilde{R}_2 = \sqrt{r^2 + (z+h)^2}$ and $\tilde{R}_2^* = \sqrt{r^2 + (z+h)^2} + z + h$. The equations (10a)-(10c) are the fundamental solutions of the poroelastic half space due to a fluid point sink.

3. Closed-form Solution Due to a Circularly Symmetric Fluid Sink

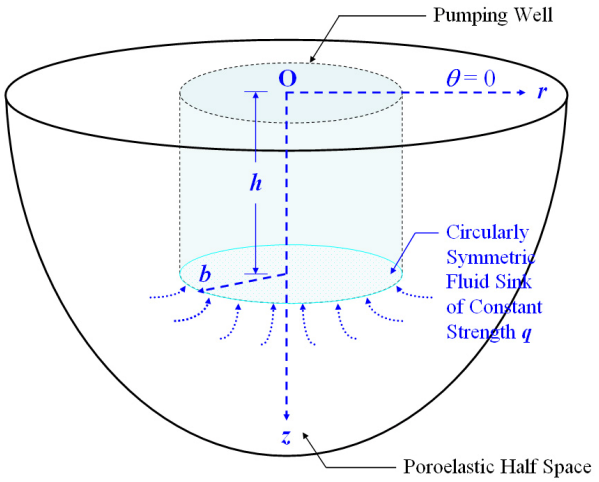

Figure 2. Circularly symmetric fluid sink problem.

Figure 2 displays the circularly symmetric fluid sink model. The closed-form solutions of the horizontal displacement $u_r(r,z)$, vertical displacement $u_z(r,z)$ and excess pore fluid pressure $p(r,z)$ due to a circularly symmetric fluid sink with radius *b* at a depth *h* are derived from equations (10a)-(10c).

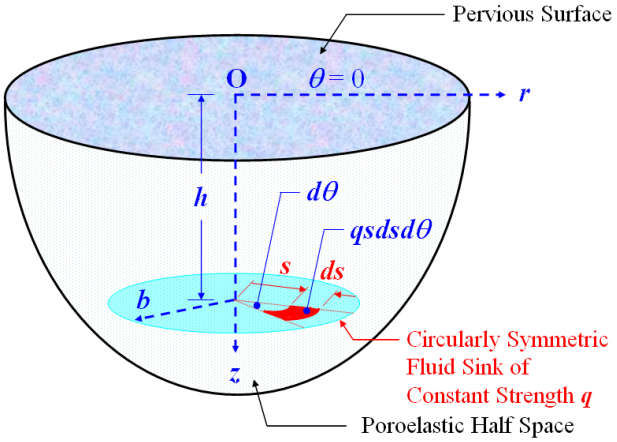

Figure 3. Analysis of the circularly symmetric fluid sink problem.

Figure 3 shows a unit area dA located at a distance s from the center of circularly symmetric fluid sink. The pumping strength of this unit area is qdA, and it is approximated as a fluid point sink. The increment of displacements u_r, u_z and excess pore fluid pressure p due to the elementary circularly symmetric fluid sink are obtained by substituting $r-s$ for r and $qsdsd\theta$ for Q in equations (10a)-(10c). Thus, the induced total increment of displacements and excess pore fluid pressure of the aquifer are determined by the integration with radial limits of $s=0$ to $s=b$ and circumferential limits of $\theta=0$ to $\theta=2\pi$. Using Mathematica to complete the symbolic calculations, the closed-form solutions are given as below:

$$u_r(r,z)=\frac{(1-2\nu)\alpha q\gamma_f}{16(1-\nu)Gk}\left\{-rR_{r,z-h}+(r+b)R_{r-b,z-h}\right.$$
$$-(z-h)^2\ln\frac{R^*_{r,z-h}}{R^*_{r-b,z-h}}+\left[-(z+h)^2\ln\frac{R^*_{r,z+h}}{R^*_{r-b,z+h}}\right.$$
$$+2b(z+h)+rR_{r,z+h}-(r+b)R_{r-b,z+h}$$
$$\left.-2r(z+h)\ln\frac{R_{z+h,r}}{R_{z+h,r-b}}\right]$$
$$-2(3-4\nu)h\left[-b+(z+h)\ln\frac{R^*_{r,z+h}}{R^*_{r-b,z+h}}+r\ln\frac{R_{z+h,r}}{R_{z+h,r-b}}\right]$$
$$+2z\left[-b+(z+h)\ln\frac{R^*_{r,z+h}}{R^*_{r-b,z+h}}+r\ln\frac{R_{z+h,r}}{R_{z+h,r-b}}\right]$$
$$\left.+4hz\left(\frac{b}{R_{r-b,z+h}}-\ln\frac{R^*_{r,z+h}}{R^*_{r-b,z+h}}\right)\right\}, \tag{11a}$$

$$u_z(r,z)=\frac{(1-2\nu)\alpha q\gamma_f}{8(1-\nu)Gk}\left\{\right.$$
$$-(z-h)\left(R_{r-b,z-h}-R_{r,z-h}+r\ln\frac{R^*_{r,z-h}}{R^*_{r-b,z-h}}\right)$$
$$+\left[(3-4\nu)h+z\right]\left(R_{r-b,z+h}-R_{r,z+h}+r\ln\frac{R^*_{r,z+h}}{R^*_{r-b,z+h}}\right)$$
$$\left.+\frac{2hz}{z+h}\left[R_{r,z+h}-\frac{r(r-b)+(z+h)^2}{R_{r-b,z+h}}\right]\right\}, \tag{11b}$$

$$p(r,z)=\frac{q\gamma_f}{2k}\left[-R_{r,z+h}+R_{r,z-h}-R_{r-b,z-h}+R_{r-b,z+h}\right.$$
$$\left.-r\ln\frac{R^*_{r,z-h}R^*_{r-b,z+h}}{R^*_{r,z+h}R^*_{r-b,z-h}}\right], \tag{11c}$$

in which $R_{i,j}=\sqrt{i^2+j^2}$, $R^*_{i,j}=i+\sqrt{i^2+j^2}$, and $i,j=r,\ r-b,\ z-h,\ z+h$.

The ground surface horizontal and vertical displacements are found when $z=0$:

$$u_r(r,0)=\frac{(1-2\nu)\alpha q\gamma_f h^2}{2Gk}\left[\bar{b}-\bar{r}\ln\frac{\sqrt{\bar{r}^2+1}+1}{\sqrt{(\bar{r}-\bar{b})^2+1}+1}\right.$$
$$\left.+\ln\frac{\sqrt{\bar{r}^2+1}+1}{\sqrt{(\bar{r}-\bar{b})^2+1}+\bar{r}-\bar{b}}\right], \tag{12a}$$

$$u_z(r,0)=\frac{(1-2\nu)\alpha q\gamma_f h^2}{2Gk}\left[-\sqrt{\bar{r}^2+1}+\sqrt{(\bar{r}-\bar{b})^2+1}\right.$$
$$\left.-\bar{r}\ln\frac{\sqrt{(\bar{r}-\bar{b})^2+1}+\bar{r}-\bar{b}}{\sqrt{\bar{r}^2+1}+\bar{r}}\right], \tag{12b}$$

where $\bar{r}=r/h$ and $\bar{b}=b/h$. The solutions can be used to test numerical models and the detailed numerical simulations of the consolidation processes near the circularly symmetric fluid sink.

4. Numerical Results

The normalized parameter of circularly symmetric fluid sink with radius b to depth h ratio (b/h) is used to verify the proposed solutions. The profiles of vertical and horizontal displacements at the ground surface $z=0$ are normalized by $(1-2\nu)\alpha q\gamma_f h^2/2Gk$ as shown in Figures 4 and 5, respectively. The results shown in Figures 4 and 5 indicate that the higher normalized parameter b/h can induce larger displacements on the ground surface. The values in Figure 4 are the ground surface horizontal

displacement pointed outward from the axial symmetric center near the circularly symmetric fluid sink, and the negative value indicates that ground surface horizontal displacement is directed toward the axial symmetric center. Figures 4 and 5 also concluded that the elastic ground surface deformations due to a circularly symmetric fluid sink reached their extreme values near the edge of circularly symmetric fluid sink, i.e., *r* equals *b*. At distance away from the sink, the displacements reduced at remote ground surface boundary.

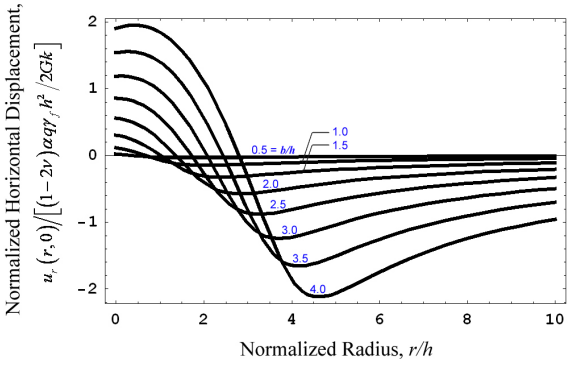

Figure 4. Normalized horizontal displacement profile at the ground surface $z = 0$ due to circularly symmetric fluid sink.

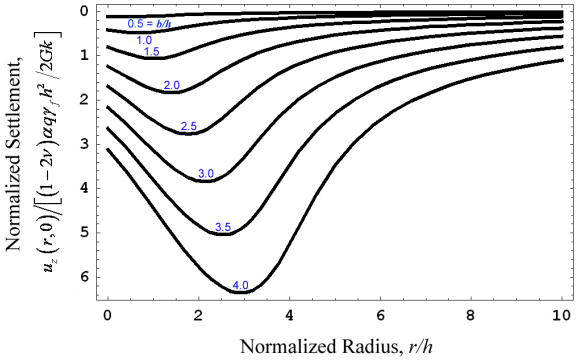

Figure 5. Normalized settlement profile at the ground surface $z = 0$ due to circularly symmetric fluid sink.

5. Conclusion

Based on the fundamental solutions due to a fluid point sink, the analytical solutions of long-term horizontal displacement, vertical displacement and excess pore fluid pressure of a poroelastic half space subject to a circularly symmetric fluid sink were obtained. The closed-form solutions are derived by using Mathematica to complete the symbolic calculations. The solutions provide valuable information to test numerical models and simulations of the groundwater withdrawal processes near the circularly symmetric fluid sink. The results show:

1. The numerical results indicate that the larger normalized circularly symmetric fluid sink radius *b/h* can induce larger displacements of the ground surface.
2. The long-term poroelastic ground surface deformations due to a circularly symmetric fluid sink reached their extreme values near the edge of fluid sink, and the values reduced at remote ground surface boundary.

Acknowledgements

This work is supported by the National Science Council of Republic of China through grant NSC100-2221-E-216-025.

References

[1] J.F. Poland, *Guidebook to studies of land subsidence due to ground-water withdrawal* (Paris: Unesco, 1984).

[2] M.A. Biot, General theory of three-dimensional consolidation, *Journal of Applied Physics*, 12(2), 1941, 155-164.

[3] M.A. Biot, Theory of elasticity and consolidation for a porous anisotropic solid, *Journal of Applied Physics*, 26(2), 1955, 182-185.

[4] J.R. Rice & M.P. Cleary, Some basic stress-diffusion solutions for fluid saturated elastic porous media with compressible constituents, *Reviews of Geophysics and Space Physics,* 14(2), 1976, 227-241.

[5] J. Bear & M.Y. Corapcioglu, Mathematical model for regional land subsidence due to pumping, 1. Integrated aquifer subsidence equations based on vertical displacement only, *Water Resources Research*, 17(4), 1981, 937-946.

[6] J. Bear & M.Y. Corapcioglu, Mathematical model for regional land subsidence due to pumping, 2. Integrated aquifer subsidence equations for vertical and horizontal displacements, *Water Resources Research*, 17(4), 1981, 947-958.

[7] J.R. Booker & J.P. Carter, Analysis of a point sink embedded in a porous elastic half space, *International Journal for Numerical and Analytical Methods in Geomechanics*, 10(2), 1986, 137-150.

[8] J.R. Booker & J.P. Carter, Long term subsidence due to fluid extraction from a saturated, anisotropic, elastic soil mass, *The Quarterly Journal of Mechanics and Applied Mathematics*, 39(1), 1986, 85-98.

[9] J.R. Booker & J.P. Carter, Elastic consolidation around a point sink embedded in a half-space with anisotropic permeability, *International Journal for Numerical and Analytical Methods in Geomechanics*, 11(1), 1987, 61-77.

[10] J.R. Booker & J.P. Carter, Withdrawal of a compressible pore fluid from a point sink in an isotropic elastic half space with anisotropic permeability, *International Journal of Solids and Structures*, 23(3), 1987, 369-385.

[11] J.-Q. Tarn & C.-C. Lu, Analysis of subsidence due to a point sink in an anisotropic porous elastic half space, *International Journal for Numerical and Analytical Methods in Geomechanics*, 15(8), 1991, 573-592.

[12] G.J. Chen, Analysis of pumping in multilayered and poroelastic half space, *Computers and Geotechnics*, 30(1), 2002, 1-26.

[13] G.J. Chen, Steady-state solutions of multilayered and cross-anisotropic poroelastic half-space due to a point sink, *International Journal of Geomechanics*, 5(1), 2005, 45-57.

[14] W. Kanok-Nukulchai & K.T. Chau, Point sink fundamental solutions for subsidence prediction, *Journal of Engineering Mechanics*, *ASCE*, 116(5), 1990, 1176-1182.

[15] J. C.-C. Lu & F.-T. Lin, The transient ground surface displacements due to a point sink/heat source in an elastic half-space, *Geotechnical Special Publication No. 148*, *ASCE*, 2006, 210-218.

[16] J. C.-C. Lu & F.-T. Lin, Analysis of transient ground surface displacements due to an impulsive point sink in an elastic half space, *Proceedings of the IASTED International Conference on Environmental Management and Engineering*, Banff, Alberta, Canada, 2009, 211-217.

[17] C.-S. Hou, J.-C. Hu, L.-C. Shen, J.-S. Wang, C.-L. Chen, T.-C. Lai, C. Huang, Y.-R. Yang, R.-F. Chen, Y.-G. Chen & J. Angelier, Estimation of Subsidence Using GPS Measurements, and Related Hazard: the Pingtung Plain, Southwestern Taiwan, *Comptes Rendus Geoscience*, 337(13), 2005, 1184-1193.

[18] A. Skempton, The pore pressure coefficients A and B, *Geotechnique*, 4, 1954, 143-147.

[19] E. Detournay & A. H.-D. Cheng, Poroelastic response of a borehole in a non-hydrostatic stress field, *International Journal of Rock Mechanics and Mining Sciences & Geomechanics Abstracts*, 25(3), 1988, 171-182.

[20] A. H.-D. Cheng & E. Detournay, A direct boundary element method for plane strain poroelasticity, *International Journal for Numerical and Analytical Methods in Geomechanics*, 12(5), 1988, 551-572.

[21] I.N. Sneddon, *Fourier transforms* (New York: McGraw-Hill, 1951, 48-70).

Nomenclature

b_i	Body forces (*Pa/m*)
$\overline{b}$	Normalized radius of the circularly symmetric fluid sink, $\overline{b} = b/h$ (Dimensionless)
B	Skempton's pore pressure coefficient (Dimensionless)
dA	Elementary area of the circularly symmetric fluid sink (m^2)
ds	Elementary distance of the distance from the center of circularly symmetric fluid sink (*m*)
$d\theta$	Elementary circumferential angle (radian)
G	Shear modulus of the isotropic porous aquifer (N/m^2)
h	Pumping depth of the sink point (*m*)
k	Permeability of the isotropic porous aquifer (*m/s*)
p	Excess pore water pressure (N/m^2)
q	Rate of fluid extracted from the saturated porous aquifer per unit volume (s^1)
Q	Pumping strength of the point sink (m^3/s)
(r,θ,z)	Cylindrical coordinates system (*m*, *radian*, *m*)
$\overline{r}$	Normalized radial variable, $\overline{r} = r/h$ (Dimensionless)
$R_{i,j}$	Distance parameter, $R_{i,j} = \sqrt{i^2 + j^2}$ (*m*)
$\tilde{R}_1$	Distance parameter, $\tilde{R}_1 = \sqrt{r^2 + (z-h)^2}$ (*m*)
$\tilde{R}_2$	Distance parameter, $\tilde{R}_2 = \sqrt{r^2 + (z+h)^2}$ (*m*)
$R^*_{i,j}$	Distance parameter, $R^*_{i,j} = i + \sqrt{i^2 + j^2}$ (*m*)
$\tilde{R}^*_2$	Distance parameter, $\tilde{R}^*_2 = \sqrt{r^2 + (z+h)^2} + z + h$ (*m*)
s	Distance from the center of circularly symmetric fluid sink (*m*)
t	Time variable (*s*)
u_i	Displacement components of the poroelastic aquifer (*m*)
u_r, u_z	Radial/axial displacement of the porous aquifer (*m*)
v_i	Specific discharge velocity components (*m/s*)
α	Biot's coefficient of effective stress (Dimensionless)

γ_f	Unit weight of pore fluid (N/m^3)
$\delta(x)$	Dirac delta function (m^{-1})
δ_{ij}	Kronecker delta (Dimensionless)
ε	Volume strain of the porous aquifer (Dimensionless)
ε_{ij}	Strain components of the poroelastic medium (Dimensionless)
ς	Variation of fluid content per unit reference volume (Dimensionless)
ν	Poisson's ratio of the isotropic porous strata (Dimensionless)
ν_u	Undrained Poisson's ratio of the poroelastic medium (Dimensionless)
σ_{ij}	Stress components of the porous strata (N/m^2)
∇^2	Differential operator, $\nabla^2 = \frac{\partial^2}{\partial r^2} + \frac{1}{r}\frac{\partial}{\partial r} + \frac{\partial^2}{\partial z^2}$ ($1/m^2$)

附錄 5

出席國際會議並擔任會議主持人之心得報告

會議名稱：The 20th IASTED International Conference on Applied Simulation and Modelling

會議時間：2012/6/25~27

會議地點：Napoli, Italy

發表論文：如附錄 3 與附錄 4 所示

行政院國家科學委員會補助國內專家學者出席國際學術會議報告

2012 年 7 月 18 日

附件三

報告人姓名	呂　志　宗	服務機構及職稱	中華大學土木工程學系副教授
時間 會議 地點	2012 年 6 月 25~27 日 義大利／那不勒斯／拿坡里	本會核定 補助文號	101-2914-I-216-003-A1
會議名稱	（中文）第 20 屆 IASTED 應用模擬與模式化國際學術會議 （英文）The 20th IASTED International Conference on Applied Simulation and Modelling		
發表論文題目	（中文）1. 橫向等向性的熱彈性介質受深層水平線熱源作用之模擬 2. 圓形對稱抽水所引致的壓密沉陷模擬 （英文）1. Modelling of a Buried Deep Horizontal Line Heat Source in a Cross-Anisotropic Thermoelastic Medium 2. Modelling of Consolidation Settlement Due to a Circularly Symmetric Fluid Sink		

一、參加會議經過

本次申請人所參加的國際學術會議為「The 20th IASTED International Conference on Applied Simulation and Modelling」，其係與「The 15th IASTED International Conference on Computers and Advanced Technology in Education」、「The 11th IASTED European Conference on Power and Energy Systems」及「The 15th IASTED International Conference on Artificial Intelligence and Soft Computing」在同一時間暨同一地點舉辦。申請人共計發表兩篇 EI 等級的論文，並擔任分組會議之主持人，所投稿的論文已順利完成論文簡報。

本國際學術會議是由「國際科學與技術發展協會（International Association of Science and Technology for Development）」所主辦，本會議之重點為模擬與模式化在各個領域的應用，此次會議為第 20 次舉辦，可見其已具有甚佳的傳統、能見度與國際化，故廣受世界各國相關領域之學者專家的高度重視。例如會議籌備委員會的委員分別來自 21 個國家，包括：英國、日本、美國、巴西、加拿大、比利時、法國、紐西蘭、匈牙利、希臘、印度、德國、葡萄牙、拉脫維亞、義大利、芬蘭、波蘭、墨西哥、馬其頓、澳大地亞、羅馬尼亞等，可見此一國際會議已受到歐洲、亞洲、美洲、澳洲等各個國家的高度重視。

大會在各個領域中，均有安排多場的專題演講，分別為：(1)義大利的 Fabio De Felice 博士之演講：「AHP and Simulation: Two winning Methodologies Combined Together」；(2)西班牙的 Javier Contreras 博士之演講：「Integration of Renewable Energies into the Iberian Electricity Market」；(3)義大利的 Enzo Bergamini 博士和 Dayana Pesando 博士之演講：「High-Fidelity Physical System Modeling in Maplesim」；(4)德國的 Thomas Alexander 博士之演講：「Advances Towards a Comprehensive Simulation: Combining Live, Virtual and Constructive」。相關之不同領域的學術交流，尚有許多，對本人均有極大的幫助。

因實施夏令時間，義大利的時間比台灣晚 6 個小時，世界各國的遊客絡繹不絕。會議地點鄰近歐洲大陸唯一的活火山維蘇威火山，其海拔高度是 1,281 公尺；此外，義大利擁有許多的人類文化遺產，是歐洲文化的搖籃，故很值得親身前往體驗。本

次行程先從台灣飛到泰國曼谷的蘇汪納蓬國際機場，轉機後飛往羅馬的費米齊諾國際機場，再從費米齊諾國際機場搭兩班火車前往拿坡里開會，很感謝國科會的經費支持！

二、與會心得

由「國際科學與技術發展協會」主辦之本次會議所發表的論文，均已納入 EI、Scopus 檢索資料庫等。本國際學術會議是在義大利的拿坡里舉辦，主辦單位希能提供一個交流平臺，讓世界各國的研究人員及學者專家等，在模擬與模式化於各個領域的應用上，能有彼此交流與相互學習的機會，並祈使各國能在相關領域之應用上有長足的進步。

會議之研討主題包括五大類，如以下說明所示：

(1) Modelling and Simulation Methods：共計 15 個子題
(2) Simulation Tools and Techniques：共計 21 個子題
(3) Environmental Modelling and Simulation：共計 32 個子題
(4) Applied Simulation in the Energy Sector：共計 14 個子題
(5) Biomechanics Modelling：共計 29 個子題

會議之性質、重要性及學術地位等可用以下五點加以說明：

(1) 這個研討會的舉辦已來到第 20 年，會議主旨是提供各界模擬與模式化(Simulation and Modelling)領域之應用、研究、分享與探索的平台，目前已逐步形成一卓越且重要的全球性研討會。

(2) 本次會議共獲得約 30 餘個國家的專家學者投稿參與，本人有兩篇投稿論文被接受，已於會中發表。藉由論文發表，本人確信已得到與會學者專家寶貴的建議與評論，可藉此使研究論文更紮實，對後續投稿到 SCI 等級的期刊會很有幫助。

(3) 「國際科學與技術發展協會」希望能藉先導型國際學術會議之舉辦，將各個領域的模擬與模式化之議題納入討論，並藉由各國之相關研究成果的交流，提出可行的方案，以供各界參考。

(4) 藉由觀摩與請益來自 30 餘國的與會學者專家之研究心得與經驗分享，參加本次會議確實有助於提昇個人的研究能力與視野。會議論文亦已被收錄於 EI、Scopus 等資料庫。

(5) 申請人之參與除有助於瞭解並掌握國際間關於相關領域的模擬與模式化之研究現況外，亦可與世界各國之相關領域學者專家相互切磋交流，此應有利於提昇本國相關領域在模擬與模式化等方面之應用與推廣。

三、考察參觀活動

會議主辦單位雖未安排參觀或考察活動，但申請人有自行安排相關的參觀與考察，主要重點為與土木和文化相關之參訪活動。

四、建議

參與國際性之學術會議，極有助於開拓學術研究領域之視野，也可以在會議期間，多認識一些來自世界各地的學者專家，此應有助於建立友誼，並瞭解世界各國相關科技領域之發展現況，對以後提出國際性之學術合作應極有幫助。另外，瞭解

不同國家間之民俗文化，並與其有深入之對話，對增進人類各國家民族間彼此關懷與照顧的情誼，亦有極大的幫助。建議國科會可鼓勵大專院校之教師們，多參與類似之重要國際學術會議。

五、攜回資料名稱及內容

所攜回資料包括以下兩大類，說明如下：

(1) 攜回「第 20 屆 IASTED 應用模擬與模式化國際學術會議論文集（Proceedings of the 20th IASTED International Conference on Applied Simulation and Modelling）」，資料主要內容為會議中的各個研討主題之論文電子檔。

(2) 相關領域之其他學術會議資料的蒐集。

六、其他（用照片說明會議經過）

照片 1　會議舉辦地點拿坡里位於義大利南部，摘自 Google 地圖，http://maps.google.com.tw/maps?hl=zh-TW&tab=wl

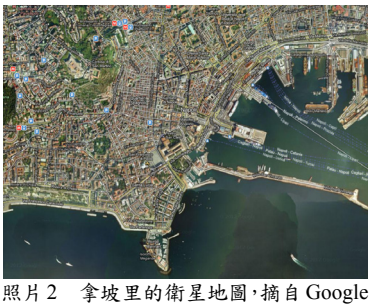

照片 2　拿坡里的衛星地圖，摘自 Google 地圖，http://maps.google.com.tw/maps?hl=zh-TW&tab=wl

照片 3　於桃園國際機場準備搭乘 TG635 班機前往曼谷的蘇汪納蓬國際機場轉機

照片 4　於曼谷的蘇汪納蓬國際機場準備搭乘 TG944 班機前往羅馬的費米齊諾國際機場

照片 5　於羅馬的費米齊諾國際機場準備搭乘 Leonardo 高速火車前往羅馬的 Termini 火車站再轉搭火車前往拿坡里

照片 6　於羅馬的 Termini 中央火車站準備轉搭火車前往會議地點拿坡里

照片 7　終於抵達拿坡里的中央火車站

照片 8　會議地點在鄰近地中海的 Royal Continental Hotel

照片 9　會議地點的對面是 Dell'ovo 城堡

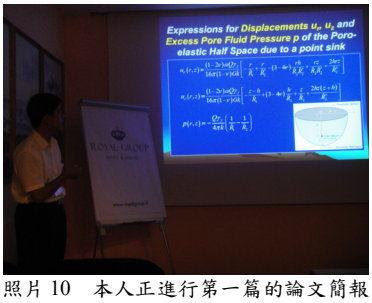

照片 10　本人正進行第一篇的論文簡報 (6 月 25 日)

照片 11　本人正進行第二篇的論文簡報 (6 月 26 日)

照片 12　來自斯洛維尼亞(Slovenia)的 Primož Potočnik 博士正進行論文簡報

表 Y04

照片 13　來自伊朗的 Mohammadsaleh Malekinejad 博士正進行論文簡報

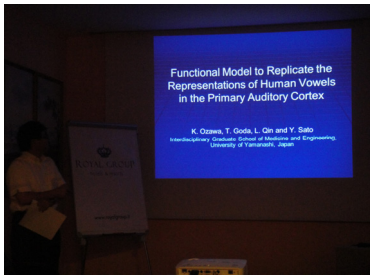

照片 14　來自日本的 Kenji Ozawa 博士正進行論文簡報

照片 15　來自法國的 Kalyana Chakravarthy Veluvolu 博士正進行論文簡報

照片 16　來自俄羅斯的 Ilya A. Gudkov 先生正進行論文簡報

照片 17　來自哈薩克(Kazakhstan)的 Nikolay Y. Borovskiy 博士正進行論文簡報

照片 18　來自韓國的 Hongrae Kim 博士正進行論文簡報

照片 19　來自希臘的 Foteini Grivokostopoulou 博士生正進行論文簡報

照片 20　來自義大利的 Fabio De Felice 博士正進行專題演講

照片 21　來自加拿大的 Adif 先生正進行論文簡報

照片 22　來自瑞典的 Asif Rahman 博士生正進行論文簡報

照片 23　來自日本的 Nobuyuki Ohmori 博士生正進行論文簡報

照片 24　來自義大利的 Enzo Bergamini 博士正進行專題演講

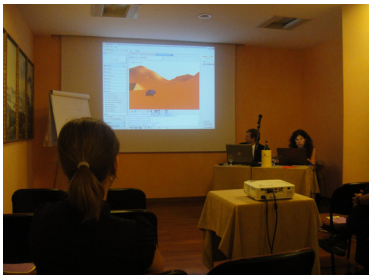

照片 25　來自義大利的 Dayana Pesando 博士正進行專題演講

照片 26　本人與來自西班牙的 Jose Gonzalez Monteagudo 博士合影

照片 27　拿坡里的 Nuovo 城堡

表 Y04

照片 28　拿坡里的保羅聖方濟各教堂 (Chiesa di San Francesco di Paola)

照片 29　拿坡里的 Galleria Umerto

照片 30　Galleria Umerto 內正在拍攝婚紗照的花童

照片 31　本人在羅馬的圓形競技場前留影

照片 32　本人在羅馬的威尼斯廣場前留影

照片 33　羅馬的君士坦丁凱旋門

照片 34　羅馬的西班牙廣場

照片 35　羅馬的許願池

照片 36　梵蒂岡的聖天使城堡

照片 37　梵蒂岡的聖彼得大教堂

照片 38　台灣的大使館國旗飄揚於梵蒂岡

照片 39　於羅馬的 Termini 中央火車站準備搭乘火車前往費米齊諾國際機場後搭機返國

照片 40　於羅馬的費米齊諾國際機場準備搭乘 TG945 班機至曼谷的蘇汪納蓬國際機場轉機

照片 41　於曼谷的蘇汪納蓬國際機場準備搭乘 TG634 班機返國

照片 42　順利完成任務返抵國門

表 Y04

CERTIFICATE OF PARTICIPATION
AS
SESSION CHAIR

This is to certify **John** *C.-C. Lu chaired the following session:*

MODELLING AND SIMULATION II

at the 20th IASTED International Conference on
Applied Simulation and Modelling
which was held in Napoli, Italy
June 25, 2012 – June 27, 2012

IASTED Secretariat

June 27, 2012
Date

圖 1　擔任分組會議之主持人的證明文件

表 Y04

ASM 2012

Certificate of Participation

This is to certify that ***J.C. Lu*** attended the
20th IASTED International Conference on
Applied Simulation and Modelling
held June 25 - June 27, 2012,
in *Napoli, Italy*
and presented the following paper:

Paper Number: 776-040

Entitled: Modelling of a Buried Deep Horizontal Line Heat Source in a Cross-Anisotropic Thermoelastic Medium

IASTED

IASTED Secretariat

June 27, 2012
Date

圖 2　親自簡報已接受論文「Modelling of a Buried Deep Horizontal Line Heat Source in a Cross-Anisotropic Thermoelastic Medium」之證明文件

表 Y04

ASM 2012

Certificate of Participation

This is to certify that ***J.C. Lu*** attended the
20th IASTED International Conference on
Applied Simulation and Modelling
held June 25 - June 27, 2012,
in *Napoli, Italy*
and presented the following paper:

Paper Number: 776-044

Entitled: Modelling of Consolidation Settlement
Due to a Circularly Symmetric Fluid Sink

IASTED

IASTED Secretariat

June 27, 2012
Date

圖 3　親自簡報已接受論文「Modelling of Consolidation Settlement Due to a Circularly Symmetric Fluid Sink」之證明文件

表 Y04

附錄 6

初步整理後擬進行投稿之其他相關研究成果(1)

Lu, John C.-C. and Feng-Tsai Lin, 2013, "Closed-form Solutions of the Axisymmetric Elastic Consolidation Settlement Due to an Impulsive Point sink," **Ready to Submit for Reviewing**. (This work is supported by the National Science Council through grants NSC100-2221-E-216-025.)

CLOSED-FORM SOLUTIONS OF THE AXISYMMETRIC ELASTIC CONSOLIDATION SETTLEMENT DUE TO AN IMPULSIVE POINT SINK

John C.-C. Lu[1] and Feng-Tsai Lin[2]
[1]Department of Civil Engineering, Chung Hua University
No. 707, Sec. 2, WuFu Rd., Hsinchu 30012, Taiwan, R.O.C.
cclu@chu.edu.tw
[2]Department of Naval Architecture, National Kaohsiung Marine University
No. 142, Haijhuan Rd., Kaohsiung 81157, Taiwan, R.O.C.
ftlin@mail.nkmu.edu.tw

ABSTRACT
This paper presents the axisymmetric ground surface displacements and excess pore water pressure caused by impulsive point sink in a saturated isotropic poroelastic half space. The formulations of the mathematical model are based on Biot's three-dimensional consolidation theory of porous media. Closed-form solutions of the transient consolidation deformation and excess pore water pressure are derived by using the Laplace and Hankel integral transforms. The consolidation affected by the consolidation parameters are illustrated and discussed. Results show that the maximum ground surface horizontal displacement is around 38.5% of the maximum vertical displacement for the pervious ground surface. The study concludes that horizontal displacement is significant and should be considered in prediction of the transient consolidation deformations induced by impulsive groundwater withdrawal.

KEY WORDS
Impulsive Point Sink, Consolidation Settlement, Closed-form Solution, Half Space

1. Introduction

Large amounts of groundwater withdrawal can induce land subsidence [1]. The stratum compact on itself when the groundwater is withdrawn from the saturated aquifer of the strata. As water pumps from an aquifer, the pore water pressure is reduced in the withdrawal region. It leads to increase in effective stress between the solid skeleton and thus the subsidence of ground surface.

The coupled three-dimensional consolidation theory introduced by Biot [2,3] is generally regarded as the fundamental theory for modelling consolidation settlement. The approach followed here is that of Rice and Cleary [4] who have provided an elegant formulation of Biot's theory which is in terms of easily identifiable quantities and material constants. Bear and Corapcioglu [5,6] presented the modified Biot's equations where the pore fluid is treated as compressible while the solid skeleton is assumed as incompressible. Based on Biot's theory modified by Bear and Corapcioglu [5,6], Booker and Carter [7-10], Tarn and Lu [11] presented solutions of subsidence by a point sink embedded in the saturated elastic half space at a constant rate. Chen [12,13], Kanok-Nukulchai and Chau [14] presented analytic solutions for the steady-state responses of displacements and stresses in a porous half space subject to a fluid point sink. Lu and Lin [15,16] displayed transient displacements of the pervious half space due to steady pumping rate [15] and impulsive pumping [16]. The results presented by Hou *et al.* [17] shown that ground horizontal displacement occurred when groundwater withdrawal from an aquifer.

The present investigation is focused on the closed-form solutions of an isotropic poroelastic half space due to an impulsive point sink with compressible constituents which still have not been derived in previous studies. In this paper, the aquifer is modelled as a linearly elastic medium with homogeneous isotropic properties. By using Laplace and Hankel transforms, the half space closed-form solutions of the transient displacements and excess pore fluid pressure of the saturated aquifer due to an impulsive point sink are obtained. The solutions can be used to test numerical models and the detailed numerical simulations of the consolidation settlement near the impulsive point sink.

2. Mathematical Models

2.1 Basic Equations

The formulation of Biot's equations is following that of Rice and Cleary [4] who have provided an easily identifiable quantities and material constants. Four basic material constants are selected in the constitutive equations: the shear modulus G, the drained Poisson's ratio ν, the undrained Poisson's ratio ν_u and Skempton's pore pressure coefficient B [18]. The physical ranges of material constants B and ν_u are obviously $0 \le B \le 1$ and $0 \le \nu \le \nu_u \le \frac{1}{2}$ [4], respectively. For the situation of incompressible constituents, the poroelastic coefficients $B = 1$ and $\nu_u = \frac{1}{2}$. According to Rice and Cleary [4], the reformulated constitutive relations can be expressed as [19]:

$$\sigma_{ij} = 2G\varepsilon_{ij} + \frac{2G\nu}{1-2\nu}\varepsilon\delta_{ij} - \frac{3(\nu_u-\nu)}{B(1-2\nu)(1+\nu_u)}p\delta_{ij}, \quad (1a)$$

$$p = -\frac{2GB(1+\nu_u)}{3(1-2\nu_u)}\varepsilon + \frac{2GB^2(1-2\nu)(1+\nu_u)^2}{9(\nu_u-\nu)(1-2\nu_u)}\varsigma, \quad (1b)$$

in which σ_{ij}, p and ε_{ij} are the total stress components, excess pore fluid pressure and solid strain components of the poroelastic media. Note that σ_{ij} and p are here taken as positive for tension. The parameter ς is the variation of fluid content per unit reference volume of the aquifer. The volumetric strain of the skeletal material is denoted by ε and $\varepsilon = \varepsilon_{11} + \varepsilon_{22} + \varepsilon_{33}$; δ_{ij} is the Kronecker delta. The inversions of equations (1a) and (1b) can be shown to take the form:

$$\varepsilon_{ij} = \frac{1}{2G}\left(\sigma_{ij} - \frac{\nu}{1+\nu}\sigma_{kk}\delta_{ij}\right) + \frac{3(\nu_u-\nu)}{2GB(1+\nu)(1+\nu_u)}p\delta_{ij}, \quad (1a^*)$$

$$\varsigma = \frac{9(\nu_u-\nu)(1-2\nu_u)}{2GB^2(1-2\nu)(1+\nu_u)^2}p + \frac{3(\nu_u-\nu)}{B(1-2\nu)(1+\nu_u)}\varepsilon. \quad (1b^*)$$

The solid strain components ε_{ij} and displacement components u_i are governed by the linear kinematic equation:

$$\varepsilon_{ij} = \tfrac{1}{2}(u_{i,j} + u_{j,i}). \quad (2)$$

The total stress components σ_{ij} must satisfy the equilibrium equations:

$$\sigma_{ij,j} + b_i = 0, \quad (3)$$

where b_i denote the body force components. The mass balance for the fluid phase is denoted by:

$$\frac{\partial\varsigma}{\partial t} + v_{i,i} + q = 0, \quad (4)$$

in which v_i is the specific discharge velocity components; and q is the rate of fluid extracted from the saturated porous aquifer per unit volume by the sink. Assuming that the pore fluid flow is governed by Darcy's law, we have

$$v_i = -\frac{k}{\gamma_f}p_{,i}, \quad (5)$$

in which k denotes the permeability of the porous aquifer and γ_f is the unit weight of pore fluid.

The governing equations (1) to (5) can be combined to yield various field equations for the solutions of boundary value problems. Substituting (1a) into (3), (1b*) and (5) into (4), respectively, then the equilibrium equation (3) and mass balance equation (4) can be expressed in terms of displacement components u_i and excess pore fluid pressure p as below:

$$G\nabla^2 u_i + \frac{G}{1-2\nu}\frac{\partial\varepsilon}{\partial x_i} - \alpha\frac{\partial p}{\partial x_i} + b_i = 0, \quad (6a)$$

$$-\frac{k}{\gamma_f}\nabla^2 p + \frac{9(\nu_u-\nu)(1-2\nu_u)}{2GB^2(1-2\nu)(1+\nu_u)^2}\frac{\partial p}{\partial t} + \alpha\frac{\partial\varepsilon}{\partial t} + q = 0, \quad (6b)$$

where α is known as Biot's coefficient of effective stress which can be defined as

$$\alpha = \frac{3(\nu_u-\nu)}{B(1-2\nu)(1+\nu_u)}. \quad (7)$$

The above mathematical model is known as coupled model of poroelasticity where the flow field is dependent on the displacement field. The coupling term $\partial\varepsilon/\partial t$ in equation (6b) is neglected in this paper.

Figure 1 presents a fluid point sink buried in a saturated porous half space at a depth *h*. The impulsive pumping strength at $t = 0$ is denoted as Q at the location $(0,h)$. Introducing the equilibrium equations for axisymmetric poroelasticity problem with a vertical axis of symmetry and neglect the effects of body forces b_i, then equation (6a) is transformed to equations (8a) and (8b). Moreover, assuming the flow field is independent from the displacement field, then the mass balance equation (6b) can be expressed as (8c). After doing so, the uncoupled governing equations in axisymmetric coordinates (r,z) are derived in terms of displacements $u_i\,(i = r,z)$ and excess pore fluid pressure *p* as following:

$$G\nabla^2 u_r + \frac{G}{1-2\nu}\frac{\partial\varepsilon}{\partial r} - G\frac{u_r}{r^2} - \alpha\frac{\partial p}{\partial r} = 0, \quad (8a)$$

$$G\nabla^2 u_z + \frac{G}{1-2\nu}\frac{\partial\varepsilon}{\partial z} - \alpha\frac{\partial p}{\partial z} = 0, \quad (8b)$$

$$-\frac{k}{\gamma_f}\nabla^2 p + \frac{9(\nu_u-\nu)(1-2\nu_u)}{2GB^2(1-2\nu)(1+\nu_u)^2}\frac{\partial p}{\partial t} + \frac{Q}{2\pi r}\delta(r)\delta(z-h)\delta(t) = 0, \quad (8c)$$

where $\nabla^2 = \frac{\partial^2}{\partial r^2} + \frac{1}{r}\frac{\partial}{\partial r} + \frac{\partial^2}{\partial z^2}$ is the Laplacian operator and $\varepsilon = \frac{\partial u_r}{\partial r} + \frac{u_r}{r} + \frac{\partial u_z}{\partial z}$ is the volumetric strain of the

poroelastic aquifer; $\delta(x)$ is the Dirac delta function. Equations (8a) to (8c) are the uncoupled basic field equations with an impulsive point sink at a pumping strength Q in which the fluid and solid are treated as compressible constituents.

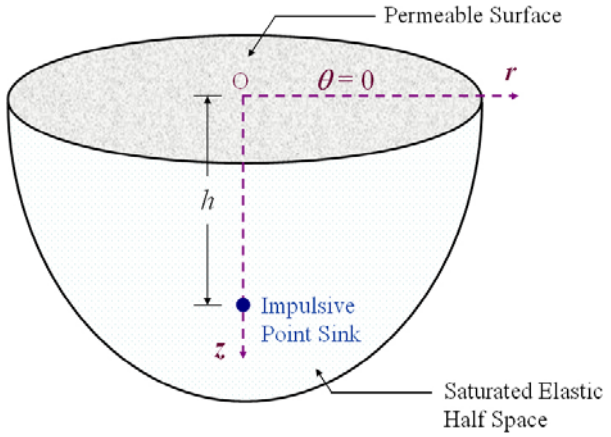

Figure 1. Impulsive point sink induced consolidation deformation problem.

2.2 Boundary Conditions and Initial Conditions

Consider the half space surface as a traction-free boundary for all times $t \geq 0$. Hence, the mechanical boundary conditions at $z = 0$ are expressed as

$$\tau_{rz}(r,0,t) = 0 \text{ and } \tau_{zz}(r,0,t) = 0 . \quad (9a)$$

An additional condition is provided by considering the half space as pervious. The mathematical statement of the hydraulic boundary condition at $z = 0$ is given by

$$p(r,0,t) = 0 . \quad (9b)$$

The boundary conditions at the far boundary $z \to \infty$ due to the effect of an impulsive point sink must vanish at any time. This can be written as

$$\lim_{z\to\infty}\{u_r(r,z,t), u_z(r,z,t), p(r,z,t)\} = \{0,0,0\} . \quad (9c)$$

Assuming no initial changes in displacements and seepage of the aquifer, then the initial conditions at time $t = 0^+$ of the mathematical model are:

$$u_r(r,z,0^+) = 0 , \; u_z(r,z,0^+) = 0 \text{ and } p(r,z,0^+) = 0 . \quad (10)$$

The mathematical model in this study is based on the governing equations (8a) to (8c), the corresponding boundary conditions (9a) to (9c) and initial conditions (10).

3. Analytic Solutions

3.1 Laplace and Hankel Transforms Solutions

Applying initial conditions in equation (10), the governing partial differential equations (8a) to (8c) are reduced to ordinary differential equations by performing Laplace-Hankel transforms [20] with respect to the time variable t and the radial coordinate r, respectively:

$$\left(\frac{d^2}{dz^2} - 2\eta\xi^2\right)\tilde{u}_r - (2\eta - 1)\xi\frac{d\tilde{u}_z}{dz} + \frac{\alpha}{G}\xi\tilde{p} = 0 , \quad (11a)$$

$$(2\eta - 1)\xi\frac{d\tilde{u}_r}{dz} + \left(2\eta\frac{d^2}{dz^2} - \xi^2\right)\tilde{u}_z - \frac{\alpha}{G}\frac{d\tilde{p}}{dz} = 0 , \quad (11b)$$

$$-\frac{k}{\gamma_f}\left(\frac{d^2}{dz^2} - \xi^2\right)\tilde{p} + \frac{9(\nu_u - \nu)(1-2\nu_u)}{2GB^2(1-2\nu)(1+\nu_u)^2}s\tilde{p} + \frac{Q}{2\pi}\delta(z-h) = 0 , \quad (11c)$$

where ξ and s are Hankel and Laplace transform parameters. The symbols $\eta = (1-\nu)/(1-2\nu)$ and $\tilde{u}_r$, $\tilde{u}_z$, $\tilde{p}$ are defined as

$$\tilde{u}_r(z;\xi,s) = \int_0^\infty\int_0^\infty r u_r(r,z,t)\exp(-st)J_1(\xi r)\,dt\,dr, \quad (12a)$$

$$\tilde{u}_z(z;\xi,s) = \int_0^\infty\int_0^\infty r u_z(r,z,t)\exp(-st)J_0(\xi r)\,dt\,dr, \quad (12b)$$

$$\tilde{p}(z;\xi,s) = \int_0^\infty\int_0^\infty r p(r,z,t)\exp(-st)J_0(\xi r)\,dt\,dr, \quad (12c)$$

in which $J_a(x)$ represents the first kind of Bessel function of order a. The Laplace-Hankel inversions of equations (12a) to (12c) are:

$$u_r(r,z,t) = \frac{1}{2\pi i}\int_0^\infty\int_{\alpha-i\infty}^{\alpha+i\infty}\xi\tilde{u}_r(z;\xi,s)e^{st}J_1(\xi r)\,ds\,d\xi, \quad (13a)$$

$$u_z(r,z,t) = \frac{1}{2\pi i}\int_0^\infty\int_{\alpha-i\infty}^{\alpha+i\infty}\xi\tilde{u}_z(z;\xi,s)e^{st}J_0(\xi r)\,ds\,d\xi, \quad (13b)$$

$$p(r,z,t) = \frac{1}{2\pi i}\int_0^\infty\int_{\alpha-i\infty}^{\alpha+i\infty}\xi\tilde{p}(z;\xi,s)e^{st}J_0(\xi r)\,ds\,d\xi. \quad (13c)$$

The general solutions of equations (11a) to (11c) are obtained as

$$\tilde{u}_r(z;\xi,s) = C_1\exp(\xi z) + C_2 z\exp(\xi z) + C_3\exp(-\xi z) + C_4 z\exp(-\xi z) + C_5\exp\left(\sqrt{\xi^2 + \frac{s}{c}}z\right) + C_6\exp\left(-\sqrt{\xi^2 + \frac{s}{c}}z\right)$$

$$+\frac{Q\alpha\gamma_f}{8\pi\eta Gk}\left[-\frac{c}{s}exp\left(-\xi|z-h|\right)\right.$$
$$\left.+\frac{c}{s}\xi\sqrt{\xi^2+\frac{s}{c}}^{-1}exp\left(-\sqrt{\xi^2+\frac{s}{c}}|z-h|\right)\right], \quad (14a)$$

$$\tilde{u}_z\left(z;\xi,s\right)=\left(-C_1+\frac{2\eta+1}{2\eta-1}\frac{1}{\xi}C_2\right)exp\left(\xi z\right)-C_2 z\,exp\left(\xi z\right)$$
$$+\left(C_3+\frac{2\eta+1}{2\eta-1}\frac{1}{\xi}C_4\right)exp\left(-\xi z\right)+C_4 z\,exp\left(-\xi z\right)$$
$$-\frac{1}{\xi}\sqrt{\xi^2+\frac{s}{c}}C_5\,exp\left(\sqrt{\xi^2+\frac{s}{c}}z\right)$$
$$+\frac{1}{\xi}\sqrt{\xi^2+\frac{s}{c}}C_6\,exp\left(-\sqrt{\xi^2+\frac{s}{c}}z\right)$$
$$\mp\frac{Q\alpha\gamma_f}{8\pi\eta Gk}\left[\frac{c}{s}exp\left(-\xi|z-h|\right)\right.$$
$$\left.-\frac{c}{s}exp\left(-\sqrt{\xi^2+\frac{s}{c}}|z-h|\right)\right], \quad (14b)$$

$$\tilde{p}\left(z;\xi,s\right)=-2\eta G\frac{1}{\xi}\frac{s}{c}C_5\,exp\left(\sqrt{\xi^2+\frac{s}{c}}z\right)$$
$$-2\eta G\frac{1}{\xi}\frac{s}{c}C_6\,exp\left(-\sqrt{\xi^2+\frac{s}{c}}z\right)$$
$$-\frac{Q\gamma_f}{4\pi k}\sqrt{\xi^2+\frac{s}{c}}^{-1}exp\left(-\sqrt{\xi^2+\frac{s}{c}}|z-h|\right), \quad (14c)$$

where the parameter $c=\frac{2GB^2\left(1-2\nu\right)\left(1+\nu_u\right)^2}{9\left(\nu_u-\nu\right)\left(1-2\nu_u\right)}\frac{k}{\gamma_f}$ and the constants $C_i\left(i=1,2,\cdots,6\right)$ are functions of the transformed variables ξ and s. These variables are determined from the transformed boundary conditions. The upper and lower signs in equation (14b) are for the conditions of $\left(z-h\right)\ge 0$ and $\left(z-h\right)<0$, respectively.

The constitutive relations (1) and linear kinematic equation (2) for axisymmetric deformation, i.e., $\varepsilon_{rr}=\frac{\partial u_r}{\partial r}$, $\varepsilon_{\theta\theta}=\frac{u_r}{r}$ and $\varepsilon_{zz}=\frac{\partial u_z}{\partial z}$, are used to reformulate the half space boundary conditions in equation (9a). After doing so, the Laplace-Hankel transforms are applied to (9a) to (9c) with respect to the time variable t and radial coordinate r, respectively. The mechanical and hydraulic boundary conditions at $z=0$ and $z\to\infty$ of the transformed domains $\left(z;\xi,s\right)$ are derived as follows:

$$\eta\frac{d\tilde{u}_z\left(0;\xi,s\right)}{dz}+\left(\eta-1\right)\xi\tilde{u}_r\left(0;\xi,s\right)=0, \quad (15a)$$

$$\frac{d\tilde{u}_r\left(0;\xi,s\right)}{dz}-\xi\tilde{u}_z\left(0;\xi,s\right)=0, \quad (15b)$$

$$\tilde{p}\left(0;\xi,s\right)=0, \quad (15c)$$

$$\lim_{z\to\infty}\left\{\tilde{u}_r\left(z;\xi,s\right),\tilde{u}_z\left(z;\xi,s\right),\tilde{p}\left(z;\xi,s\right)\right\}=\left\{0,0,0\right\}, \quad (15d)$$

where $\tilde{u}_r$, $\tilde{u}_z$ and $\tilde{p}$ follow the definitions shown in equations (12a) to (12c). The symbol $\eta=\left(1-\nu\right)/\left(1-2\nu\right)$.

The constants $C_i\left(i=1,2,\cdots,6\right)$ of the general solutions are determined by the transformed half space boundary conditions at $z=0$ and $z\to\infty$ as shown in equations (15a) to (15d). Finally, the desired quantities u_r, u_z and p are obtained by applying appropriate inverse Laplace-Hankel transformations [21,22].

The focus of the study is on the ground surface horizontal displacement $u_r\left(r,0,t\right)$, settlement $u_z\left(r,0,t\right)$ and excess pore fluid pressure $p\left(r,z,t\right)$ of the strata due to a point sink. The transformed ground surface displacements and excess pore fluid pressure of the strata are derived from equations (14a) to (14c) with the transformed boundary conditions (15a) to (15d), and they are obtained as follows:

$$\tilde{u}_r\left(0;\xi,s\right)=\frac{Q\alpha\gamma_f\left(1-2\nu\right)}{2\pi Gk}\left[-\frac{c}{s}exp\left(-\xi h\right)\right.$$
$$\left.+\frac{c}{s}exp\left(-\sqrt{\xi^2+\frac{s}{c}}h\right)\right], \quad (16a)$$

$$\tilde{u}_z\left(0;\xi,s\right)=\frac{Q\alpha\gamma_f\left(1-2\nu\right)}{2\pi Gk}\left[\frac{c}{s}exp\left(-\xi h\right)\right.$$
$$\left.-\frac{c}{s}exp\left(-\sqrt{\xi^2+\frac{s}{c}}h\right)\right], \quad (16b)$$

$$\tilde{p}\left(z;\xi,s\right)=-\frac{Q\gamma_f}{4\pi k}\left[\sqrt{\xi^2+\frac{s}{c}}^{-1}exp\left(-\sqrt{\xi^2+\frac{s}{c}}|z-h|\right)\right.$$
$$\left.-\sqrt{\xi^2+\frac{s}{c}}^{-1}exp\left(-\sqrt{\xi^2+\frac{s}{c}}\left(z+h\right)\right)\right]. \quad (16c)$$

Applying the Laplace-Hankel inversion formulae (13a) to (13c), equations (16a) to (16c) lead to the following transient ground surface displacements by letting z = 0 and the excess pore fluid pressure of strata as below:

$$u_r\left(r,0,t\right)=\frac{Q\alpha\gamma_f\left(1-2\nu\right)}{2\pi Gk}\left\{-\frac{cr}{\left(h^2+r^2\right)^{3/2}}\right.$$
$$\left.+\int_0^{ct}\frac{chr}{16\tau^3}e^{-\frac{r^2+2h^2}{8\tau}}\left[I_0\left(\frac{r^2}{8\tau}\right)-I_1\left(\frac{r^2}{8\tau}\right)\right]d\tau\right\}, \quad (17a)$$

$$u_z(r,0,t)=\frac{Q\alpha\gamma_f(1-2\nu)}{2\pi Gk}\left\{\frac{ch}{\left(h^2+r^2\right)^{3/2}}erf\left(\frac{\sqrt{h^2+r^2}}{2\sqrt{ct}}\right)\right.$$

$$\left.-\frac{ch}{h^2+r^2}\frac{1}{\sqrt{\pi ct}}e^{-\frac{h^2+r^2}{4ct}}\right\}, \quad (17b)$$

$$p(r,z,t)=\frac{Q\gamma_f}{8\pi k}\frac{1}{\sqrt{\pi ct^3}}\left[e^{-\frac{r^2+(z+h)^2}{4ct}}-e^{-\frac{r^2+(z-h)^2}{4ct}}\right]. \quad (17c)$$

where $I_\alpha(x)$ is known as the modified Bessel function of the first kind of order α ; and $erf(x)$ denotes error function. The instantaneous ground surface horizontal and vertical displacements of the pervious half space at $t\to 0^+$ are obtained from equations (17a) and (17b) as following:

$$u_r(r,0,0^+)=-\frac{cQ\alpha\gamma_f(1-2\nu)}{2\pi Gk}\frac{r}{\left(h^2+r^2\right)^{3/2}}, \quad (18a)$$

$$u_z(r,0,0^+)=\frac{cQ\alpha\gamma_f(1-2\nu)}{2\pi Gk}\frac{h}{\left(h^2+r^2\right)^{3/2}}. \quad (18b)$$

The maximum ground surface horizontal displacement $u_{r\,max}$ and vertical displacement $u_{z\,max}$ of the half space due to an impulsive point sink are derived from equations (18a) and (18b) by letting $r=h/\sqrt{2}\approx 0.707h$ and $r=0$, respectively, as below:

$$u_{r\,max}=u_r\left(h/\sqrt{2},0,0^+\right)=-\frac{\sqrt{3}cQ\alpha\gamma_f(1-2\nu)}{9\pi Gkh^2}, \quad (19a)$$

$$u_{z\,max}=u_z(0,0,0^+)=\frac{cQ\alpha\gamma_f(1-2\nu)}{2\pi Gkh^2}, \quad (19b)$$

in which the critical value $r=h/\sqrt{2}$ is derived when $du_r(r,0,0^+)/dr$ is set equal to zero. Hence, the absolute value of the displacement ratio $u_{r\,max}/u_{z\,max}$ can be derived from equations (19a) and (19b) as below:

$$\left|\frac{u_{r\,max}}{u_{z\,max}}\right|\times 100\%=\frac{2\sqrt{3}}{9}\times 100\%\cong 38.5\%. \quad (20)$$

The above result shows the maximum ground surface horizontal displacement is around 38.5% of the maximum vertical displacement for the pervious ground surface due to an impulsive point sink. Hou *et al.* [16] shown that ground horizontal displacement occurred when pumping from an aquifer.

4. Numerical results

The particular interest is the vertical displacement of stratum at each stage of the consolidation process, and the average consolidation ratio U is defined as:

$$U=\frac{\text{Ground surface vertical displacement at time } t}{\text{Maximum vertical displacement, } u_{z\,max}}. \quad (21)$$

For pervious half space, U can be derived as below:

$$U=\frac{h^3}{\left(h^2+r^2\right)^{3/2}}\left[erf\left(\frac{\sqrt{h^2+r^2}}{2\sqrt{ct}}\right)-\frac{\sqrt{h^2+r^2}}{\sqrt{\pi ct}}e^{-\frac{h^2+r^2}{4ct}}\right]. \quad (22)$$

Figure 2 shows the average consolidation ratio U at $r/h=0$, 1, 2 and 5 for the impulsive pumping. Note that U initially decreases rapidly, and then the rate of vertical displacement reduces gradually. Each final value of U vanished for the saturated aquifer is treated as linear elastic porous medium in this mathematical model.

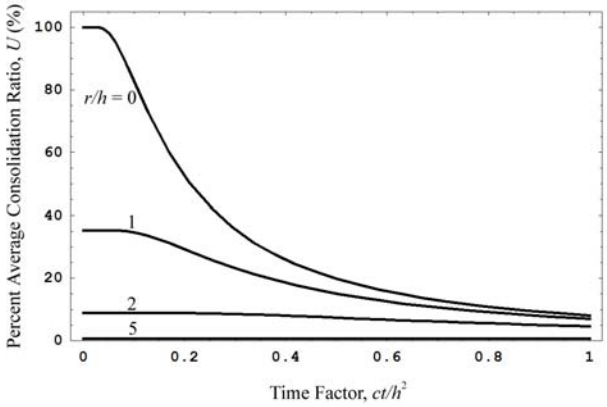

Figure 2. Average consolidation ratio U at r/h = 0, 1, 2 and 5 for impulsive pumping.

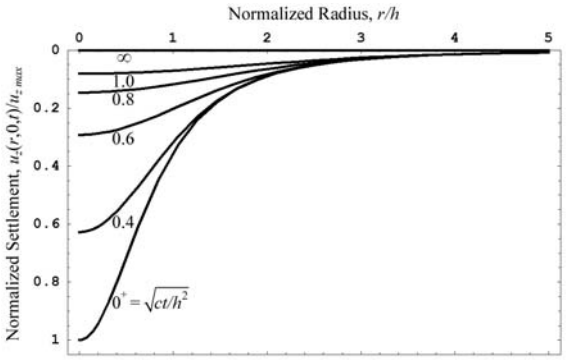

Figure 3. Normalized vertical displacement profile at the ground surface $z=0$ for impulsive pumping.

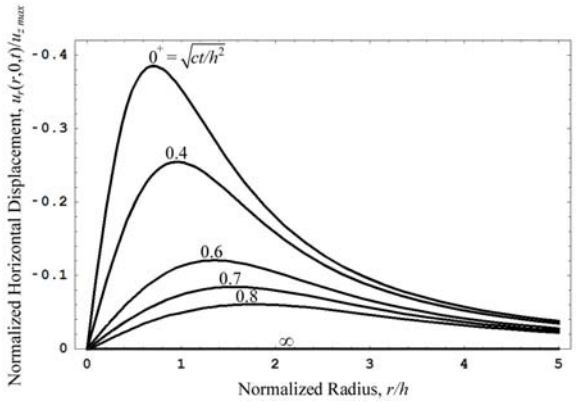

Figure 4. Normalized horizontal displacement profile at the ground surface $z = 0$ for impulsive pumping.

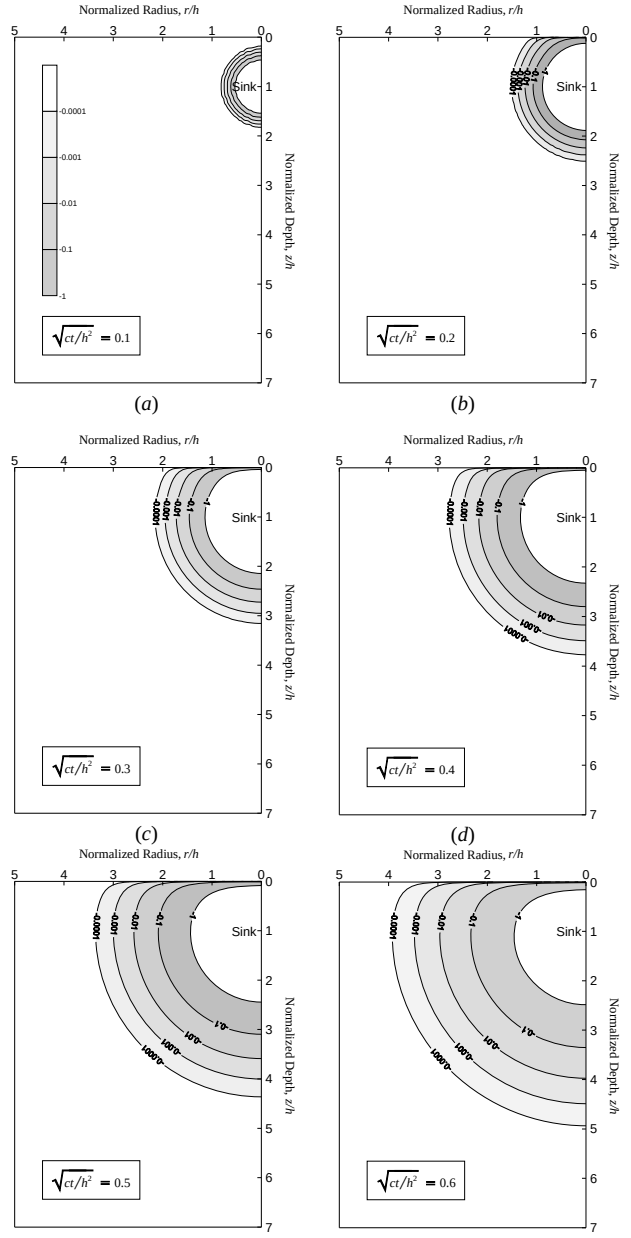

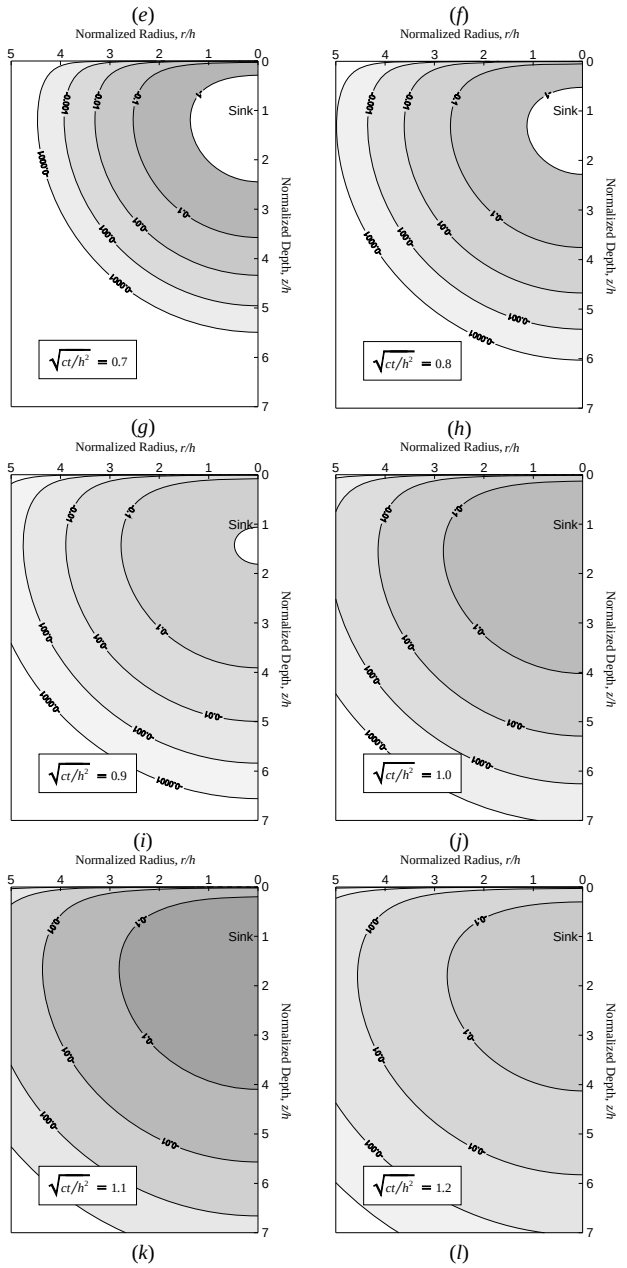

Figure 5. Distribution of normalized excess pore water pressures $p(r,z,t)/\left[cQ\gamma_f/8\pi^{1.5}kh^3\right]$.

The profiles of normalized vertical and horizontal displacements at the ground surface $z = 0$ are shown in Figures 3 and 4, respectively. The results shown in Figures 3 and 4 indicate that the ground surface displacements due to impulsive pumping can reach its extreme values initially, and then the displacements decreases gradually. Figure 4 shows that the ground surface has significant horizontal displacement, and the maximum ground surface horizontal displacement is around 38.5% of the maximum vertical displacement at $r/h \approx 0.707$ for the impulsive pumping.

From equation (17c), the profiles of normalized excess pore water pressure $p(r,z,t)/\left[cQ\gamma_f/8\pi^{1.5}kh^3\right]$ of the pervious half space at four different dimensionless time factors $\sqrt{ct/h^2}$ = 0.1, 0.2, 0.3, 0.4, 0.5, 0.6, 0.7, 0.8, 0.9, 1.0, 1.1 and 1.2 are illustrated in Figures 5(*a*)-(*l*), respectively. The changes in excess pore water pressure have negative value p which is caused by suction of groundwater withdrawal. It's observed that the negative excess pore water pressure increases to a wider region of the aquifer initially and then gradually decreased. The impulsive pumping induced negative excess pore water pressure finally full dissipated. The elastic deformations of the stratum due to groundwater extraction will fully recover after the excess pore water pressure dissipated.

5. Conclusions

Closed-form solutions of the axisymmetric elastic consolidation due to impulsive pumping from pervious saturated elastic half space were obtained by using Laplace and Hankel transformations. Ground surface displacements and excess pore water pressure of the aquifer were investigated. The results show:

1. The ground surface displacements due to impulsive pumping reach its extreme values initially, and then the displacements decrease gradually in this model. Each final value of displacements vanished for the saturated aquifer is treated as linear elastic porous medium.
2. It is observed that the negative excess pore water pressure increases to a wider region of the aquifer initially and then gradually decreased. The impulsive pumping induced negative excess pore water pressure finally full dissipated.
3. The maximum ground surface horizontal displacement is around 38.5% of the maximum vertical displacement of the pervious half space at $r = h/\sqrt{2} \approx 0.707h$. It concludes that horizontal displacement must be properly considered for better prediction of the transient consolidation deformations induced by groundwater withdrawal.

Acknowledgements

This work is supported by the National Science Council of Republic of China through grant NSC100-2221-E-216-025.

References

[1] J.F. Poland, *Guidebook to studies of land subsidence due to ground-water withdrawal* (Paris: Unesco, 1984).

[2] M.A. Biot, General theory of three-dimensional consolidation, *Journal of Applied Physics*, 12(2), 1941, 155-164.

[3] M.A. Biot, Theory of elasticity and consolidation for a porous anisotropic solid, *Journal of Applied Physics*, 26(2), 1955, 182-185.

[4] J.R. Rice & M.P. Cleary, Some basic stress-diffusion solutions for fluid saturated elastic porous media with compressible constituents, *Reviews of Geophysics and Space Physics*, 14(2), 1976, 227-241.

[5] J. Bear & M.Y. Corapcioglu, Mathematical model for regional land subsidence due to pumping, 1. Integrated aquifer subsidence equations based on vertical displacement only, *Water Resources Research*, 17(4), 1981, 937-946.

[6] J. Bear & M.Y. Corapcioglu, Mathematical model for regional land subsidence due to pumping, 2. Integrated aquifer subsidence equations for vertical and horizontal displacements, *Water Resources Research*, 17(4), 1981, 947-958.

[7] J.R. Booker & J.P. Carter, Analysis of a point sink embedded in a porous elastic half space, *International Journal for Numerical and Analytical Methods in Geomechanics*, 10(2), 1986, 137-150.

[8] J.R. Booker & J.P. Carter, Long term subsidence due to fluid extraction from a saturated, anisotropic, elastic soil mass, *The Quarterly Journal of Mechanics and Applied Mathematics*, 39(1), 1986, 85-98.

[9] J.R. Booker & J.P. Carter, Elastic consolidation around a point sink embedded in a half-space with anisotropic permeability, *International Journal for Numerical and Analytical Methods in Geomechanics*, 11(1), 1987, 61-77.

[10] J.R. Booker & J.P. Carter, Withdrawal of a compressible pore fluid from a point sink in an isotropic elastic half space with anisotropic permeability, *International Journal of Solids and Structures*, 23(3), 1987, 369-385.

[11] J.-Q. Tarn & C.-C. Lu, Analysis of subsidence due to a point sink in an anisotropic porous elastic half space, *International Journal for Numerical and Analytical Methods in Geomechanics*, 15(8), 1991, 573-592.

[12] G.J. Chen, Analysis of pumping in multilayered and poroelastic half space, *Computers and Geotechnics*, 30(1), 2002, 1-26.

[13] G.J. Chen, Steady-state solutions of multilayered and cross-anisotropic poroelastic half-space due to a point

sink, *International Journal of Geomechanics*, 5(1), 2005, 45-57.

[14] W. Kanok-Nukulchai & K.T. Chau, Point sink fundamental solutions for subsidence prediction, *Journal of Engineering Mechanics, ASCE*, 116(5), 1990, 1176-1182.

[15] J. C.-C. Lu & F.-T. Lin, The transient ground surface displacements due to a point sink/heat source in an elastic half-space, *Geotechnical Special Publication No. 148, ASCE*, 2006, 210-218.

[16] J. C.-C. Lu & F.-T. Lin, Consolidation settlement due to a point sink with compressible constituents, *Proceedings of the 22nd IASTED International Conference on Modelling and Simulation*, Calgary, Alberta, Canada, 2011, 275-281.

[17] C.-S. Hou, J.-C. Hu, L.-C. Shen, J.-S. Wang, C.-L. Chen, T.-C. Lai, C. Huang, Y.-R. Yang, R.-F. Chen, Y.-G. Chen & J. Angelier, Estimation of Subsidence Using GPS Measurements, and Related Hazard: the Pingtung Plain, Southwestern Taiwan, *Comptes Rendus Geoscience*, 337(13), 2005, 1184-1193.

[18] A. Skempton, The pore pressure coefficients A and B, *Geotechnique*, 4, 1954, 143-147.

[19] E. Detournay & A. H.-D. Cheng, Poroelastic response of a borehole in a non-hydrostatic stress field, *International Journal of Rock Mechanics and Mining Sciences & Geomechanics Abstracts*, 25(3), 1988, 171-182.

[20] I.N. Sneddon, *Fourier transforms* (New York: McGraw-Hill, 1951, 48-70).

[21] A. Erdelyi, W. Magnus, F. Oberhettinger & F.G. Tricomi, *Tables of integral transforms* (New York: McGraw-Hill, 1954).

[22] I.S. Gradshteyn & I.M. Ryzhik, *Table of integrals, series, and products* (London: Elsevier Academic Press, 707-720, 1980).

Nomenclature

b_i	Body forces (*Pa/m*)
B	Skempton's pore pressure coefficient (Dimensionless)
c	Parameter, $c=\frac{2GB^2(1-2\nu)(1+\nu_u)^2}{9(\nu_u-\nu)(1-2\nu_u)}\frac{k}{\gamma_f}$ (m^2/s)
$erf(x)$	Error function (Dimensionless)
G	Shear modulus of the isotropic porous aquifer (N/m^2)
h	Impulsive pumping depth of the sink point (m)
$I_a(x)$	Modified Bessel function of the first kind of order a (Dimensionless)
$J_a(x)$	Bessel function of the first kind of order a (Dimensionless)
k	Permeability of the isotropic porous aquifer (m/s)
p	Excess pore water pressure (N/m^2)
$\tilde{p}$	Laplace-Hankel transforms of p (Ns)
q	Rate of fluid extracted from the saturated porous aquifer per unit volume (s^{-1})
Q	Impulsive pumping strength of the point sink (m^3)
(r,θ,z)	Cylindrical coordinates system (m, *radian*, m)
s	Laplace transform parameter (s^{-1})
t	Time variable (s)
u_i	Displacement components of the poroelastic aquifer (m)
u_r, u_z	Radial/axial displacement of the porous aquifer (m)
$\tilde{u}_r, \tilde{u}_z$	Laplace-Hankel transforms of u_r/u_z (m^3s)
$u_{r\max}$	Maximum ground surface horizontal displacement (m)
$u_{z\max}$	Maximum ground surface settlement (m)
v_i	Specific discharge velocity components (m/s)
α	Biot's coefficient of effective stress (Dimensionless)
γ_f	Unit weight of pore fluid (N/m^3)
$\delta(x)$	Dirac delta function (m^{-1})
δ_{ij}	Kronecker delta (Dimensionless)
ε	Volume strain of the porous aquifer (Dimensionless)
ε_{ij}	Strain components of the poroelastic medium (Dimensionless)
ς	Variation of fluid content per unit reference volume (Dimensionless)
η	Mechanical parameter, $\eta=(1-\nu)/(1-2\nu)$ (Dimensionless)
ν	Poisson's ratio of the isotropic porous strata (Dimensionless)
ν_u	Undrained Poisson's ratio of the poroelastic medium (Dimensionless)
ξ	Hankel transform parameter (m^{-1})
σ_{ij}	Stress components of the porous strata (N/m^2)

附錄 7

初步整理後擬進行投稿之其他相關研究成果(2)

Lu, John C.-C. and Feng-Tsai Lin, 2013, "Consolidation Settlement of a Poroelastic Half Space Subjected to a Line Sink," **Ready to Submit for Reviewing**. (This work is supported by the National Science Council through grants NSC100-2221-E-216-025.)

CONSOLIDATION SETTLEMENT OF A POROELASTIC HALF SPACE SUBJECTED TO A LINE SINK

John C.-C. Lu[1] and Feng-Tsai Lin[2]
[1]Department of Civil Engineering, Chung Hua University
No. 707, Sec. 2, WuFu Rd., Hsinchu 30012, Taiwan, R.O.C.
cclu@chu.edu.tw
[2]Department of Naval Architecture, National Kaohsiung Marine University
No. 142, Haijhuan Rd., Kaohsiung 81157, Taiwan, R.O.C.
ftlin@mail.nkmu.edu.tw

ABSTRACT
The investigation presents closed-form solutions of the long-term consolidation settlement and excess pore fluid pressure of a saturated elastic aquifer subjected to a fluid line sink. The governing equations of the mathematical model are based on the Biot's theory of poroelasticity. The aquifer is modeled as a homogeneous elastic half space of porous medium, and the total stresses of the aquifer obey Newton's second law and Hooke's law. Besides, the mass conservation and Darcy's law are introduced to formulate the governing equations of pore fluid flow. The software Mathematica is used to complete the symbolic calculations, and the closed-form solutions are derived.

KEY WORDS
Fluid Line Sink, Closed-form Solution, Half Space, Porous Medium.

1. Introduction

Groundwater withdrawal can induce land subsidence [1]. The stratum compact on itself when groundwater is withdrawn from the saturated aquifer of the strata. The pore water pressure is reduced in the withdrawal region as water pumped from an aquifer. It leads to increase in effective stress between the solid skeleton and thus the subsidence of ground surface occurred.

Biot's coupled three-dimensional consolidation theory [2,3] is generally regarded as the fundamental theory for modelling consolidation settlement. The approach followed Rice and Cleary [4] who provided an elegant formulation of Biot's theory in terms of easily identifiable quantities and material constants. Bear and Corapcioglu [5,6] presented the modified Biot's equations where the pore fluid was treated as compressible and the solid skeleton was assumed incompressible. Based on Biot's theory modified by Bear and Corapcioglu [5,6], Booker and Carter [7-10], Tarn and Lu [11] presented solutions of subsidence by a point sink embedded in the saturated elastic half space at a constant rate. Chen [12,13], Kanok-Nukulchai and Chau [14] presented analytic solutions for the steady-state responses of displacements and stresses in a porous half space subject to a fluid point sink. Lu and Lin [15,16] displayed transient displacements of the pervious half space due to steady pumping rate [15] and impulsive pumping [16]. Hou *et al.* [17] presented that the ground horizontal displacement occurred as groundwater withdrawn from an aquifer.

The present investigation is focused on the closed-form solutions of an isotropic poroelastic half space due to a fluid line sink which still have not been derived in previous studies. In this study, the aquifer is modelled as a linearly elastic medium with homogeneous isotropic properties.

Based on the derived fundamental solutions, the software Mathematica is used to complete the symbolic calculations and obtain the closed-form solutions for the aquifer subjected to a fluid line sink. The solutions can be used to develop numerical models and the detailed numerical simulations of the consolidation settlement near the fluid line sink.

2. Modelling of Poroelastic Point Sink Problem

2.1 Basic Governing Equations

The formulation of Biot's equations follows that of Rice and Cleary [4] who provided an easily identifiable quantities and material constants. According to Rice and Cleary [4], the reformulated constitutive relations are expressed as [19]:

$$\sigma_{ij} = 2G\varepsilon_{ij} + \frac{2G\nu}{1-2\nu}\varepsilon\delta_{ij} - \frac{3(\nu_u-\nu)}{B(1-2\nu)(1+\nu_u)}p\delta_{ij}, \qquad (1a)$$

$$p = -\frac{2GB(1+\nu_u)}{3(1-2\nu_u)}\varepsilon + \frac{2GB^2(1-2\nu)(1+\nu_u)^2}{9(\nu_u-\nu)(1-2\nu_u)}\varsigma, \qquad (1b)$$

in which σ_{ij}, p and ε_{ij} are the total stress components, excess pore fluid pressure and solid strain components of the poroelastic media, respectively. Note that positive σ_{ij}

and p represent tension. The parameter ς is variation of fluid content per unit reference volume of the aquifer. The volumetric strain of the skeletal material is denoted by ε and $\varepsilon = \varepsilon_{11} + \varepsilon_{22} + \varepsilon_{33}$; δ_{ij} is the Kronecker delta. Four basic material constants are selected in the constitutive equations (1a) and (1b) including the shear modulus G, the drained Poisson's ratio ν, the undrained Poisson's ratio ν_u and Skempton's pore pressure coefficient B [18]. The physical ranges of material constants B and ν_u are $0 \le B \le 1$ and $0 \le \nu \le \nu_u \le \frac{1}{2}$ [4], respectively. For the situation of incompressible constituents, the poroelastic coefficients $B = 1$ and $\nu_u = \frac{1}{2}$.

The inversions of equations (1a) and (1b) are shown as the form:

$$\varepsilon_{ij} = \frac{1}{2G}\left(\sigma_{ij} - \frac{\nu}{1+\nu}\sigma_{kk}\delta_{ij}\right) + \frac{3(\nu_u - \nu)}{2GB(1+\nu)(1+\nu_u)} p\delta_{ij}, \quad (1a^*)$$

$$\varsigma = \frac{9(\nu_u - \nu)(1-2\nu_u)}{2GB^2(1-2\nu)(1+\nu_u)^2} p + \frac{3(\nu_u - \nu)}{B(1-2\nu)(1+\nu_u)}\varepsilon. \quad (1b^*)$$

The solid strain components ε_{ij} and displacement components u_i are governed by the linear kinematic equation:

$$\varepsilon_{ij} = \tfrac{1}{2}\left(u_{i,j} + u_{j,i}\right). \quad (2)$$

The total stress components σ_{ij} must satisfy the equilibrium equations:

$$\sigma_{ij,j} + b_i = 0, \quad (3)$$

where b_i denote the body force components. The mass balance for the fluid phase is denoted by:

$$\frac{\partial \varsigma}{\partial t} + v_{i,i} + q = 0, \quad (4)$$

in which v_i is the specific discharge velocity components; the quantity q is the rate of fluid extracted from the saturated porous aquifer per unit volume by the sink. The pore fluid flow is governed by Darcy's law as below:

$$v_i = -\frac{k}{\gamma_f} p_{,i}, \quad (5)$$

in which k and γ_f denotes the permeability of the porous aquifer and the unit weight of pore fluid, respectively.

The governing equations (1) to (5) are combined to derive various field equations for their corresponding solutions of boundary value problems. The equilibrium equation (3) and mass balance equation (4) are expressed in terms of displacement components u_i and excess pore fluid pressure p by substituting (1a) into (3), (1b*) and (5) into (4) as below [20]:

$$G\nabla^2 u_i + \frac{G}{1-2\nu}\frac{\partial \varepsilon}{\partial x_i} - \alpha\frac{\partial p}{\partial x_i} + b_i = 0, \quad (6a)$$

$$-\frac{k}{\gamma_f}\nabla^2 p + \frac{9(\nu_u - \nu)(1-2\nu_u)}{2GB^2(1-2\nu)(1+\nu_u)^2}\frac{\partial p}{\partial t} + \alpha\frac{\partial \varepsilon}{\partial t} + q = 0, \quad (6b)$$

where α is known as Biot's coefficient of effective stress which can be defined as

$$\alpha = \frac{3(\nu_u - \nu)}{B(1-2\nu)(1+\nu_u)}. \quad (7)$$

The above mathematical model is known as coupled model of poroelasticity where the flow field is dependent on the displacement field. The long-term consolidation settlement model is preferred in this investigation, and the time dependent differentiation terms in equation (6b) are neglected.

Figure 1 presents a fluid point sink buried in a saturated porous elastic half space at a depth d. The constant pumping strength is denoted as Q at the location $(0, d)$. Introducing the equilibrium equations for axisymmetric poroelasticity model with a vertical axis of symmetry and neglect the effects of body forces b_i, the equation (6a) are transformed to equations (8a) and (8b). Moreover, the mass balance equation (6b) are expressed as (8c) by assuming the long-term consolidation settlement. After doing so, the governing equations in axially symmetric coordinates (r, z) are derived in terms of displacements $u_i\,(i = r, z)$ and excess pore fluid pressure p as following:

$$G\nabla^2 u_r + \frac{G}{1-2\nu}\frac{\partial \varepsilon}{\partial r} - G\frac{u_r}{r^2} - \alpha\frac{\partial p}{\partial r} = 0, \quad (8a)$$

$$G\nabla^2 u_z + \frac{G}{1-2\nu}\frac{\partial \varepsilon}{\partial z} - \alpha\frac{\partial p}{\partial z} = 0, \quad (8b)$$

$$-\frac{k}{\gamma_f}\nabla^2 p + \frac{Q}{2\pi r}\delta(r)\delta(z-d) = 0, \quad (8c)$$

where the differential operator $\nabla^2 = \frac{\partial^2}{\partial r^2} + \frac{1}{r}\frac{\partial}{\partial r} + \frac{\partial^2}{\partial z^2}$ and solid strain components $\varepsilon = \frac{\partial u_r}{\partial r} + \frac{u_r}{r} + \frac{\partial u_z}{\partial z}$; $\delta(x)$ is the Dirac delta function. Equations (8a) to (8c) are the basic field equations of long-term consolidation settlement with a point sink at a constant pumping rate, in which the fluid and solid are treated as compressible constituents.

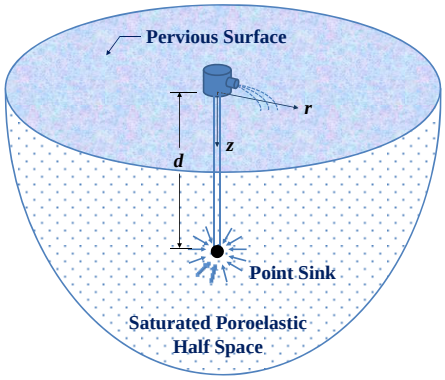

Figure 1. Fluid point sink problem.

2.2 Boundary Conditions

The ground surface of the half space is treated as a pervious and traction-free boundary for all times $t \geq 0$. Therefore, the mathematical statements of the ground surface boundary $z = 0$ in axisymmetric coordinates (r, z) are:

$$\sigma_{rz}(r,0) = 0,\ \sigma_{zz}(r,0) = 0, \text{ and } p(r,0) = 0. \tag{9a}$$

The displacements and excess pore fluid pressure at the remote boundary $z \to \infty$ due to the effect of a point sink must be nil at any time. These conditions are written as

$$\lim_{z\to\infty}\left\{u_r(r,z), u_z(r,z), p(r,z)\right\} = \{0,0,0\}. \tag{9b}$$

This mathematical model is based on the governing equations (8a)-(8c) and the corresponding boundary conditions (9a)-(9b).

2.3 Fundamental Solutions

Applying Hankel integral transformation [21] with respect to the variable *r*, the closed-form analytic fundamental solutions of the long-term responses of ground deformations and excess pore water pressure of the elastic aquifer due to a point sink in an isotropic half space are obtained as follows [11]:

$$u_r(r,z) = \frac{(1-2\nu)\alpha Q\gamma_f}{16\pi(1-\nu)Gk}\left[-\frac{r}{\tilde{R}_1} + \frac{r}{\tilde{R}_2^*} - (3-4\nu)\frac{rd}{\tilde{R}_2\tilde{R}_2^*} + \frac{rz}{\tilde{R}_2\tilde{R}_2^*} + \frac{2rzd}{\tilde{R}_2^3}\right], \tag{10a}$$

$$u_z(r,z) = \frac{(1-2\nu)\alpha Q\gamma_f}{16\pi(1-\nu)Gk}\left[-\frac{z-d}{\tilde{R}_1} + \frac{z}{\tilde{R}_2} + (3-4\nu)\frac{d}{\tilde{R}_2} + \frac{2zd(z+d)}{\tilde{R}_2^3}\right], \tag{10b}$$

$$p(r,z) = -\frac{Q\gamma_f}{4\pi k}\left(\frac{1}{\tilde{R}_1} - \frac{1}{\tilde{R}_2}\right), \tag{10c}$$

where $\tilde{R}_1 = \sqrt{r^2 + (z-d)^2}$, $\tilde{R}_2 = \sqrt{r^2 + (z+d)^2}$ and $\tilde{R}_2^* = \sqrt{r^2 + (z+d)^2} + z + d$. The equations (10a)-(10c) are the fundamental solutions of the poroelastic half space due to a fluid point sink.

3. Closed-form Solution Due to a Fluid Line Sink

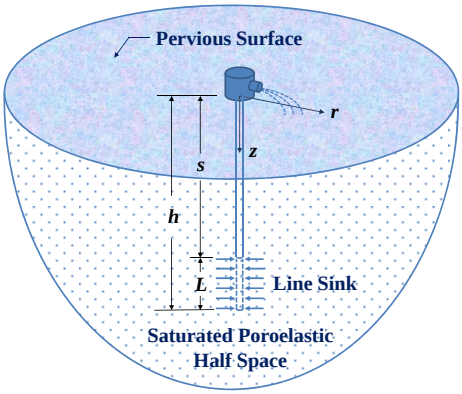

Figure 2. Fluid line sink problem.

Figure 2 displays the fluid line sink model. The closed-form solutions of the horizontal displacement $u_r(r,z)$, vertical displacement $u_z(r,z)$ and excess pore fluid pressure $p(r,z)$ due to a fluid line sink are derived from equations (10a)-(10c).

Let the length *ds* located at a depth *s* from the ground surface and considering *q* is the pumping strength per unit length. The pumping strength of this unit length is *qds* and it is approximated as a fluid point sink. The increment of displacements u_r, u_z and excess pore fluid pressure p due to the elementary fluid line sink are obtained by substituting *s* for *d* and *qds* for *Q* in equations (10a)-(10c). Thus, the induced total increment of displacements and excess pore fluid pressure of the aquifer are determined by the integration with depth limits of $s = h - L$ to $s = h$. Using Mathematica to complete the symbolic calculations, the closed-form solutions are given as below:

$$u_r(r,z) = \frac{q\gamma_f}{8\pi G\eta k}\left\{\frac{h^3+zh^2+(r^2-2z^2)h-2z(r^2+z^2)}{rR_{z+h}} - \frac{2[(h-L)^3+z(h-L)^2+(r^2-2z^2)(h-L)-2z(r^2+z^2)]}{rR_{z+h-L}} + \frac{r}{2}\left[ln\frac{\sqrt{r^2+(z-h+L)^2}-(z-h+L)}{\sqrt{r^2+(z-h)^2}-(z-h)} + (1-2\nu)ln\frac{R^*_{z+h-L}}{R^*_{z+h}}\right] + \frac{3(R_Z^2+h^2)+4hz}{R_{z+h}} - \frac{3[R_Z^2+(h-L)^2]+4(h-L)z}{R_{z+h-L}}\right\} \quad (11a)$$

$$u_z(r,z) = \frac{q\gamma_f}{16\pi G\eta k}\left\{R_{z-h} - R_{z-h+L} + 4\nu\left(R_{z+h-L} - R_{z+h} + zln\frac{R^*_{z+h}}{R^*_{z+h-L}}\right) + \frac{3(R_Z^2+h^2)+4hz}{R_{z+h}} - \frac{3[R_Z^2+(h-L)^2]+4(h-L)z}{R_{z+h-L}}\right\} \quad (11b)$$

$$p(r,z) = \frac{q\gamma_f}{4\pi k}\{\ln(R^*_{z+h}+R^*_{z-h}) + ln\frac{R^*_{z+h-L}}{R^*_{z-h-L}}\} \quad (11c)$$

in which $\eta = (1-\nu)/(1-2\nu)$; $R_i = \sqrt{r^2+i^2}$, $R_i^* = R_i + i$, and $i = z,\ z-h,\ z+h,\ z-h+L,\ z+h-L$. The maximum settlement can be found from equation (11b) by letting $L = h$:

$$u_{z\,max} = \frac{q\gamma_f L(1-2\nu)}{4\pi Gk}. \quad (12)$$

4. Numerical Results

The normalized parameter of fluid line sink is used to verify the proposed solutions. The profile of settlement at the ground surface $z = 0$ is normalized by the maximum settlement $\frac{q\gamma_f L(1-2\nu)}{4\pi Gk}$ as shown in Figure 3. The results shown in Figure 3 indicate that the higher normalized parameter *L/h* can induce larger settlement on the ground surface. Figure 3 also concluded that the elastic ground surface deformations due to a fluid line sink reached their extreme values near *r* equals 0. At distance away from the line sink, the displacements reduced at remote ground surface boundary.

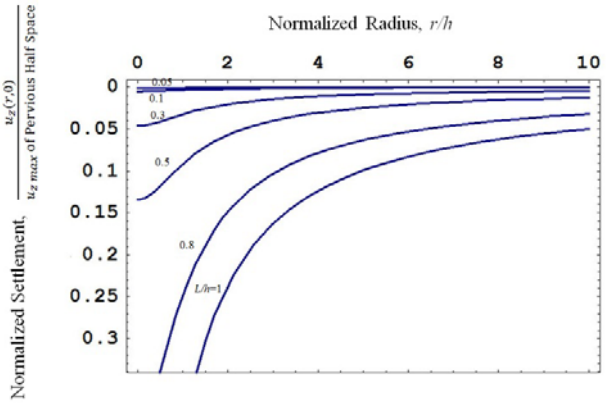

Figure 3. Normalized settlement profile at the ground surface *z* = 0 due to fluid line sink.

CONCLUSION

Based on the fundamental solutions due to a fluid point sink, the closed-form solutions of long-term horizontal displacement, vertical displacement and excess pore fluid pressure of a poroelastic half space subject to a fluid line sink were obtained. The solutions are derived by using Mathematica to complete the symbolic calculations. The solutions provide valuable information to test numerical models and simulations of the groundwater withdrawal processes near the fluid line sink. The results show:

1. The numerical results indicate that the larger normalized fluid line sink *L/h* can induce larger displacements of the ground surface.
2. The long-term poroelastic ground surface deformations due to a fluid line sink reached their extreme values near the fluid line sink, and the values reduced at remote ground surface boundary.

Acknowledgements

This work is supported by the National Science Council of Republic of China through grant NSC100-2221-E-216-025.

References

[1] J.F. Poland, *Guidebook to studies of land subsidence due to ground-water withdrawal* (Paris: Unesco, 1984).

[2] M.A. Biot, General theory of three-dimensional consolidation, *Journal of Applied Physics*, 12(2), 1941, 155-164.

[3] M.A. Biot, Theory of elasticity and consolidation for a porous anisotropic solid, *Journal of Applied Physics*, 26(2), 1955, 182-185.

[4] J.R. Rice & M.P. Cleary, Some basic stress-diffusion solutions for fluid saturated elastic porous media with compressible constituents, *Reviews of Geophysics and Space Physics*, 14(2), 1976, 227-241.

[5] J. Bear & M.Y. Corapcioglu, Mathematical model for regional land subsidence due to pumping, 1. Integrated aquifer subsidence equations based on vertical displacement only, *Water Resources Research*, 17(4), 1981, 937-946.

[6] J. Bear & M.Y. Corapcioglu, Mathematical model for regional land subsidence due to pumping, 2. Integrated aquifer subsidence equations for vertical and horizontal displacements, *Water Resources Research*, 17(4), 1981, 947-958.

[7] J.R. Booker & J.P. Carter, Analysis of a point sink embedded in a porous elastic half space, *International Journal for Numerical and Analytical Methods in Geomechanics*, 10(2), 1986, 137-150.

[8] J.R. Booker & J.P. Carter, Long term subsidence due to fluid extraction from a saturated, anisotropic, elastic soil mass, *The Quarterly Journal of Mechanics and Applied Mathematics*, 39(1), 1986, 85-98.

[9] J.R. Booker & J.P. Carter, Elastic consolidation around a point sink embedded in a half-space with anisotropic permeability, *International Journal for Numerical and Analytical Methods in Geomechanics*, 11(1), 1987, 61-77.

[10] J.R. Booker & J.P. Carter, Withdrawal of a compressible pore fluid from a point sink in an isotropic elastic half space with anisotropic permeability, *International Journal of Solids and Structures*, 23(3), 1987, 369-385.

[11] J.-Q. Tarn & C.-C. Lu, Analysis of subsidence due to a point sink in an anisotropic porous elastic half space, *International Journal for Numerical and Analytical Methods in Geomechanics*, 15(8), 1991, 573-592.

[12] G.J. Chen, Analysis of pumping in multilayered and poroelastic half space, *Computers and Geotechnics*, 30(1), 2002, 1-26.

[13] G.J. Chen, Steady-state solutions of multilayered and cross-anisotropic poroelastic half-space due to a point sink, *International Journal of Geomechanics*, 5(1), 2005, 45-57.

[14] W. Kanok-Nukulchai & K.T. Chau, Point sink fundamental solutions for subsidence prediction, *Journal of Engineering Mechanics, ASCE*, 116(5), 1990, 1176-1182.

[15] J. C.-C. Lu & F.-T. Lin, The transient ground surface displacements due to a point sink/heat source in an elastic half-space, *Geotechnical Special Publication No. 148, ASCE*, 2006, 210-218.

[16] J. C.-C. Lu & F.-T. Lin, Analysis of transient ground surface displacements due to an impulsive point sink in an elastic half space, *Proceedings of the IASTED International Conference on Environmental Management and Engineering*, Banff, Alberta, Canada, 2009, 211-217.

[17] C.-S. Hou, J.-C. Hu, L.-C. Shen, J.-S. Wang, C.-L. Chen, T.-C. Lai, C. Huang, Y.-R. Yang, R.-F. Chen, Y.-G. Chen & J. Angelier, Estimation of Subsidence Using GPS Measurements, and Related Hazard: the Pingtung Plain, Southwestern Taiwan, *Comptes Rendus Geoscience*, 337(13), 2005, 1184-1193.

[18] A. Skempton, The pore pressure coefficients A and B, *Geotechnique*, 4, 1954, 143-147.

[19] E. Detournay & A. H.-D. Cheng, Poroelastic response of a borehole in a non-hydrostatic stress field, *International Journal of Rock Mechanics and Mining Sciences & Geomechanics Abstracts*, 25(3), 1988, 171-182.

[20] A. H.-D. Cheng & E. Detournay, A direct boundary element method for plane strain poroelasticity, *International Journal for Numerical and Analytical Methods in Geomechanics*, 12(5), 1988, 551-572.

[21] I.N. Sneddon, *Fourier transforms* (New York: McGraw-Hill, 1951, 48-70).

Nomenclature

b_i	Body forces (*Pa/m*)
B	Skempton's pore pressure coefficient (Dimensionless)
d	Pumping depth of the sink point (*m*)
ds	Elementary legth of the fluid line sink (*m*)
G	Shear modulus of the isotropic porous aquifer (N/m^2)
h	Pumping depth of the line sink (*m*)
k	Permeability of the isotropic porous aquifer (*m/s*)
p	Excess pore water pressure (N/m^2)
q	Rate of fluid extracted from the saturated porous aquifer per unit length (m^2/s)
Q	Pumping strength of the point sink (m^3/s)
(r,θ,z)	Cylindrical coordinates system (*m, radian, m*)
R_i	Distance parameter, $R_i = \sqrt{r^2 + i^2}$ (*m*)
$\tilde{R}_1$	Distance parameter, $\tilde{R}_1 = \sqrt{r^2 + (z-d)^2}$ (*m*)

$\tilde{R}_2$	Distance parameter, $\tilde{R}_2 = \sqrt{r^2 + (z+d)^2}$ (m)
R_i^*	Distance parameter, $R_i^* = R_i + i$ (m)
$\tilde{R}_2^*$	Distance parameter, $\tilde{R}_2^* = \sqrt{r^2 + (z+d)^2} + z + d$ (m)
s	Depth of the fluid line sink (m)
t	Time variable (s)
u_i	Displacement components of the poroelastic aquifer (m)
u_r, u_z	Radial/axial displacement of the porous aquifer (m)
v_i	Specific discharge velocity components (m/s)
α	Biot's coefficient of effective stress (Dimensionless)
γ_f	Unit weight of pore fluid (N/m^3)
$\delta(x)$	Dirac delta function (m^{-1})
δ_{ij}	Kronecker delta (Dimensionless)
ε	Volume strain of the porous aquifer (Dimensionless)
ε_{ij}	Strain components of the poroelastic medium (Dimensionless)
ς	Variation of fluid content per unit reference volume (Dimensionless)
ν	Poisson's ratio of the isotropic porous strata (Dimensionless)
ν_u	Undrained Poisson's ratio of the poroelastic medium (Dimensionless)
σ_{ij}	Stress components of the porous strata (N/m^2)
∇^2	Differential operator, $\nabla^2 = \frac{\partial^2}{\partial r^2} + \frac{1}{r}\frac{\partial}{\partial r} + \frac{\partial^2}{\partial z^2}$ $(1/m^2)$

附錄 8

初步整理後擬進行投稿之其他相關研究成果(3)

Lu, John C.-C. and Feng-Tsai Lin, 2013, "Elastic Subsidence Subjected to Periodic Pumping," **Ready to Submit for Reviewing**. (This work is supported by the National Science Council through grants NSC100-2221-E-216-025.)

ELASTIC SUBSIDENCE SUBJECTED TO PERIODIC PUMPING

John C.-C. Lu[1] and Feng-Tsai Lin[2]
[1]Department of Civil Engineering
Chung Hua University
Hsinchu 30012, Taiwan, R.O.C.
cclu@chu.edu.tw
[2]Department of Naval Architecture
National Kaohsiung Marine University
Kaohsiung 81157, Taiwan, R.O.C.
ftlin@mail.nkmu.edu.tw

ABSTRACT
This paper presents the ground surface displacements induced by periodic groundwater withdrawal in a homogeneous isotropic poroelastic half space. The formulation of the mathematical model is based on Biot's consolidation theory of porous media. Using Laplace-Hankel integral transforms, the closed-form solutions of the transient consolidation deformations are derived. The solutions can be used to evaluate numerical models and numerical simulations of the poroelastic consolidation of a saturated porous aquifer due to periodic groundwater withdrawal.

KEY WORDS
Periodic Pumping, Point Sink, Closed-form Solution, Half Space

1. Introduction

Land subsidence due to groundwater withdrawal is a well-known phenomenon in environmental engineering [1]. The pore water pressure is reduced in the withdrawal region as groundwater pumped from an aquifer. It leads to increase in the effective stress between the soil particles and consolidation settlement of ground surface.

The three-dimensional consolidation theory presented by Biot [2,3] is generally regarded as the fundamental theory for modelling land subsidence. Based on Biot's theory, Booker and Carter [4-7], Chen [8,9], Kanok-Nukulchai and Chau [10] presented analytical solutions for the transient or steady-state responses of displacements and stresses in a half space subjected to a point sink of constant pumping rate. Tarn and Lu [11] presented solutions of subsidence by a point sink embedded in a saturated poroelastic half space. The pumping rate is treated as constant in the studies of Booker and Carter [4-7], Chen [8,9], Kanok-Nukulchai and Chau [10], Tarn and Lu [11], *etc*. Tarn and Lu [11] found that groundwater withdrawal from an impervious half space can induce a larger amount of consolidation settlement than a pervious one. The anisotropic permeability was proved to have significant effects on the land subsidence due to fluid extraction. Lu and Lin [12-14] displayed transient displacements of the pervious half space due to steady pumping rate [12,13] and impulsive pumping [14]. Nevertheless, both transient closed-form solutions of the consolidation settlement due to periodic pumping and the consolidation effects due to periodic pumping were not obtained in the above studies.

In this paper, the aquifer is modeled as an isotropic saturated pervious elastic half space. Transient ground surface displacements due to a periodic point sink are obtained by using Laplace-Hankel transforms. Results are useful to evaluate numerical models and numerical simulations of the poroelastic consolidation of a saturated porous aquifer due to periodic groundwater withdrawal.

2. Mathematical Model

2.1 Basic Equations

Figure 1 presents a saturated aquifer due to a periodic point sink at a depth h. The aquifer is considered as a homogeneous isotropic porous medium with a vertical axis of symmetry. The constitutive behaviours of the saturated elastic aquifer for linear axisymmetric deformation in the cylindrical coordinates (r,θ,z) are expressed as

$$\tau_{ij} = 2G\varepsilon_{ij} + \frac{2G\nu}{1-2\nu}\varepsilon\delta_{ij} - p\delta_{ij}, \tag{1}$$

where τ_{ij}, ε_{ij} and ε denote the incremental total stress components, strain components and volumetric strain of the porous aquifer, respectively. The symbol δ_{ij} is known as Kronecker delta. The excess pore water pressure p is positive for compression. The elastic constants ν and G are Poisson's ratio and shear modulus

of the skeletal materials, respectively. The strains ε_{ij} and displacement components u_i are given by the linear law $\varepsilon_{ij} = \frac{1}{2}\left(u_{i,j} + u_{j,i}\right)$.

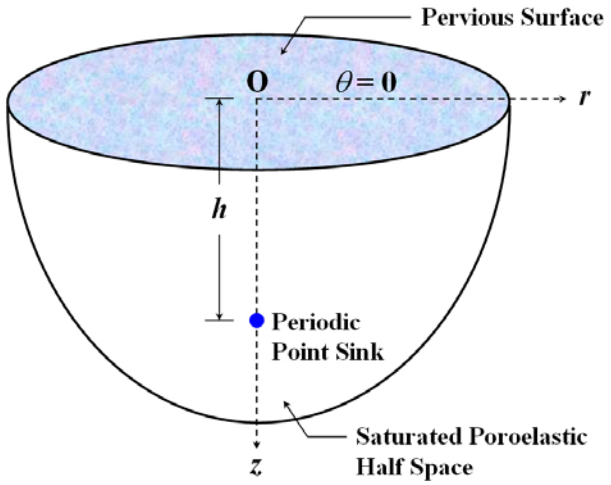

Figure 1. Periodic point sink induced consolidation deformation problem.

The total stress components τ_{ij} satisfy the equilibrium equations:

$$\tau_{ij,j} + b_i = 0\,, \tag{2}$$

where b_i denote the components of body force vector. From equation (1) and strain-displacement relationships $\varepsilon_{ij} = \frac{1}{2}\left(u_{i,j} + u_{j,i}\right)$, the equilibrium equation (2) for axially symmetric problem without body forces b_i can be expressed in terms of displacements u_i and excess pore water pressure p in cylindrical coordinates (r,θ,z) as follows:

$$G\nabla^2 u_r + \frac{G}{1-2\nu}\frac{\partial \varepsilon}{\partial r} - G\frac{u_r}{r^2} - \frac{\partial p}{\partial r} = 0\,, \tag{3a}$$

$$G\nabla^2 u_z + \frac{G}{1-2\nu}\frac{\partial \varepsilon}{\partial z} - \frac{\partial p}{\partial z} = 0\,, \tag{3b}$$

where $\nabla^2 = \partial^2/\partial r^2 + 1/r\,\partial/\partial r + \partial^2/\partial z^2$ is known as the Laplacian operator.

The model is decoupled with the flow field sought independently from the displacement field. The third relation between u_r, u_z and p is obtained from the conservation of mass as:

$$\nabla\cdot\left[n\left(\boldsymbol{v}_w - \boldsymbol{v}_s\right)\right] + n\beta\frac{\partial p}{\partial t} + q = 0\,, \tag{4}$$

where n is the porosity of the porous aquifer. The variables $\boldsymbol{v}_w$ and $\boldsymbol{v}_s$ are velocities of pore water and solid matrix, respectively. The symbol β denotes the compressibility of pore water, and q is the rate of water extracted from the saturated porous aquifer per unit volume. Assuming that Darcy's law governs the pore water flow, we have

$$n\left(\boldsymbol{v}_w - \boldsymbol{v}_s\right) = -\frac{k}{\gamma_w}\left(\frac{\partial p}{\partial r}\boldsymbol{i}_r + \frac{\partial p}{\partial z}\boldsymbol{i}_z\right), \tag{5}$$

in which k denotes the permeability of the saturated aquifer and γ_w is the unit weight of pore water.

Let us consider a periodic point sink of constant strength Q_0 as $t \ge 0$ located at point $(0,h)$. Substituting (5) into (4) yields

$$-\frac{k}{\gamma_w}\nabla^2 p + n\beta\frac{\partial p}{\partial t} + \frac{Q_0}{2\pi r}\delta(r)\delta(z-h)\,f(t) = 0\,, \tag{6}$$

in which the symbol $\delta(x)$ denotes the Dirac delta function. The pumping rate is represented by a periodic function $f(t)$ as shown in Figure 2, and $f(t)$ is expressed as below:

$$f(t) = \begin{cases} 1, & 0 \le t < T_d \\ 0, & T_d \le t < T \end{cases} \text{ and } f(t+T) = f(t)\,,\ t \ge 0\,, \tag{7}$$

where the pumping period T is reasonable to be assumed as 24 hours for daily agricultural irrigation. The symbol T_d is the duration of groundwater withdrawal in one period T.

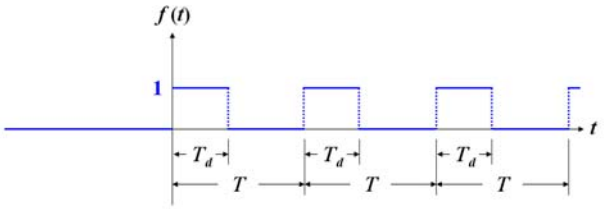

Figure 2. The pumping rate is represented by a periodic function $f(t)$ with pumping period T.

Equations (3a), (3b) and (6) constitute the basic governing equations of the axially symmetric time-dependent linear elastic responses of a saturated porous aquifer subjected to periodic pumping.

2.2 Boundary Conditions and Initial Conditions

Considering the half space surface as a traction-free boundary for all times $t \ge 0$, the mechanical boundary conditions at $z = 0$ are expressed as

$\tau_{rz}(r,0,t)=0$ and $\tau_{zz}(r,0,t)=0$. (8a)

An additional condition is provided by considering the half space as permeable. The mathematical statement of the hydraulic boundary condition at $z=0$ is given as

$$p(r,0,t)=0. \tag{8b}$$

The boundary conditions at the remote boundary $z\to\infty$ due to the effect of a periodic point sink must vanish at any time. These boundary conditions are written as

$$\lim_{z\to\infty}\{u_r(r,z,t),u_z(r,z,t),p(r,z,t)\}=\{0,0,0\}. \tag{8c}$$

Assuming no initial changes in displacements and seepage of the aquifer, the initial conditions at time $t=0^+$ of the mathematical model are:

$$u_r(r,z,0^+)=0,\ u_z(r,z,0^+)=0 \text{ and } p(r,z,0^+)=0. \tag{9}$$

3. Analytic Solutions

3.1 Laplace-Hankel Transforms Solutions

The initial conditions of equation (9), the governing equations (3a), (3b) and (6) are reduced to a set of ordinary differential equations by performing appropriate Laplace-Hankel transforms [15] with respect to the time variable *t* and the radial coordinate *r* as below:

$$\left(\frac{d^2}{dz^2}-2\eta\xi^2\right)\tilde{u}_r-(2\eta-1)\xi\frac{d\tilde{u}_z}{dz}+\frac{1}{G}\xi\tilde{p}=0, \tag{10a}$$

$$(2\eta-1)\xi\frac{d\tilde{u}_r}{dz}+\left(2\eta\frac{d^2}{dz^2}-\xi^2\right)\tilde{u}_z-\frac{1}{G}\frac{d\tilde{p}}{dz}=0, \tag{10b}$$

$$-\frac{k}{\gamma_w}\left(\frac{d^2}{dz^2}-\xi^2\right)\tilde{p}+n\beta s\tilde{p}+\frac{Q_0}{2\pi}\delta(z-h)F(s)=0, \tag{10c}$$

where ξ and s are the Hankel and Laplace transform parameters, respectively. The symbol η is defined as $\eta=(1-\nu)/(1-2\nu)$. Expressions for $\tilde{u}_r$, $\tilde{u}_z$, $\tilde{p}$ and $F(s)$ are denoted as:

$$\tilde{u}_r(z;\xi,s)=\int_0^\infty\int_0^\infty ru_r(r,z,t)e^{-st}J_1(\xi r)dtdr, \tag{11a}$$

$$\tilde{u}_z(z;\xi,s)=\int_0^\infty\int_0^\infty ru_z(r,z,t)e^{-st}J_0(\xi r)dtdr, \tag{11b}$$

$$\tilde{p}(z;\xi,s)=\int_0^\infty\int_0^\infty rp(r,z,t)e^{-st}J_0(\xi r)dtdr, \tag{11c}$$

$$F(s)=\int_0^\infty\int_0^\infty rf(t)e^{-st}J_0(\xi r)dtdr=\frac{1-e^{-sT_d}}{s\left(1-e^{-sT}\right)}, \tag{11d}$$

in which $J_\nu(x)$ represents the first kind of Bessel function of order ν.

The general solutions of equations (10a) to (10c) are obtained as below:

$$\begin{aligned}\tilde{u}_r=&(A_1+A_2z)exp(\xi z)+(A_3+A_4z)exp(-\xi z)\\&+A_5\,exp\left(\sqrt{\xi^2+\frac{s}{c}}z\right)+A_6\,exp\left(-\sqrt{\xi^2+\frac{s}{c}}z\right)\\&+\frac{Q_0\gamma_w}{8\pi\eta Gk}\frac{c}{s}F(s)\Big[-exp\left(-\xi|z-h|\right)\\&+\xi\sqrt{\xi^2+\frac{s}{c}}^{-1}exp\left(-\sqrt{\xi^2+\frac{s}{c}}|z-h|\right)\Big],\end{aligned} \tag{12a}$$

$$\begin{aligned}\tilde{u}_z=&\left(-A_1+\frac{2\eta+1}{2\eta-1}\frac{1}{\xi}A_2-A_2z\right)exp(\xi z)\\&-\frac{1}{\xi}\sqrt{\xi^2+\frac{s}{c}}\,A_5\,exp\left(\sqrt{\xi^2+\frac{s}{c}}z\right)\\&+\left(A_3+\frac{2\eta+1}{2\eta-1}\frac{1}{\xi}A_4+A_4z\right)exp(-\xi z)\\&+\frac{1}{\xi}\sqrt{\xi^2+\frac{s}{c}}A_6\,exp\left(-\sqrt{\xi^2+\frac{s}{c}}z\right)\\&\mp\frac{Q_0\gamma_w}{8\pi\eta Gk}\frac{c}{s}F(s)\Big[exp\left(-\xi|z-h|\right)\\&-exp\left(-\sqrt{\xi^2+\frac{s}{c}}|z-h|\right)\Big],\end{aligned} \tag{12b}$$

$$\begin{aligned}\tilde{p}=&-2\eta G\frac{1}{\xi}\frac{s}{c}\left[A_5\,exp\left(\sqrt{\xi^2+\frac{s}{c}}z\right)\right.\\&\left.+A_6\,exp\left(-\sqrt{\xi^2+\frac{s}{c}}z\right)\right]\\&-\frac{Q_0\gamma_w}{4\pi k}F(s)\sqrt{\xi^2+\frac{s}{c}}^{-1}exp\left(-\sqrt{\xi^2+\frac{s}{c}}|z-h|\right),\end{aligned} \tag{12c}$$

where the symbol c is defined as $c=k/n\beta\gamma_w$. The constants $A_i\,(i=1,2,\cdots,6)$ are functions of the transformed variables ξ and s which are determined from the transformed mechanical and hydraulic boundary conditions. The upper and lower signs in equation (12b) are for the conditions of $(z-h)\ge 0$ and $(z-h)<0$, respectively.

3.2 Transformed Boundary Conditions

The Laplace-Hankel transforms are applied to equations (8a)-(8c), and the transformed mechanical and hydraulic boundary conditions at $z=0$ and $z\to\infty$ are listed below:

$$\frac{d\tilde{u}_r\left(0;\xi,s\right)}{dz}-\xi\tilde{u}_z\left(0;\xi,s\right)=0\,, \tag{13a}$$

$$v\xi\tilde{u}_r\left(0;\xi,s\right)+\left(1-v\right)\frac{d\tilde{u}_z\left(0;\xi,s\right)}{dz}=0\,, \tag{13b}$$

$$\tilde{p}\left(0;\xi,s\right)=0\,, \tag{13c}$$

$$\lim_{z\to\infty}\left\{\tilde{u}_r\left(z;\xi,s\right),\tilde{u}_z\left(z;\xi,s\right),\tilde{p}\left(z;\xi,s\right)\right\}=\left\{0,0,0\right\}, \tag{13d}$$

where $\tilde{u}_r$, $\tilde{u}_z$ and $\tilde{p}$ follow the definitions of equations (11a) to (11c).

The constants $A_i\left(i=1,2,\cdots,6\right)$ of the general solutions are determined by the transformed half space boundary conditions at $z=0$ and the remote boundary conditions at $z\to\infty$. Finally, the desired quantities u_r, u_z and p are obtained by applying appropriate inverse Laplace-Hankel transformations with the help of a mathematical handbook [16].

3.3 Expressions for Ground Surface Displacements

The focus of this study is on the horizontal and vertical displacements of the ground surface, $z=0$, due to a periodic point sink. The transformed ground surface displacements $\tilde{u}_r\left(0;\xi,s\right)$ and $\tilde{u}_z\left(0;\xi,s\right)$ of the pervious half space are derived from equations (12a) and (12b) as follows:

$$\tilde{u}_r\left(0;\xi,s\right)=\frac{Q_0\left(1-2v\right)\gamma_w}{2\pi Gk}\frac{cF\left(s\right)}{s}\left[-exp\left(-\xi h\right)+exp\left(-\sqrt{\xi^2+\frac{s}{c}}h\right)\right], \tag{14a}$$

$$\tilde{u}_z\left(0;\xi,s\right)=\frac{Q_0\left(1-2v\right)\gamma_w}{2\pi Gk}\frac{cF\left(s\right)}{s}\left[exp\left(-\xi h\right)-exp\left(-\sqrt{\xi^2+\frac{s}{c}}h\right)\right]. \tag{14b}$$

Applying the Laplace-Hankel inversion formulae lead to the following displacements:

$$u_r\left(r,z,t\right)=\frac{1}{2\pi i}\int_{\alpha-i\infty}^{\alpha+i\infty}\int_0^\infty\xi\tilde{u}_r\left(z;\xi,s\right)J_1\left(\xi r\right)e^{st}d\xi ds, \tag{15a}$$

$$u_z\left(r,z,t\right)=\frac{1}{2\pi i}\int_{\alpha-i\infty}^{\alpha+i\infty}\int_0^\infty\xi\tilde{u}_z\left(z;\xi,s\right)J_0\left(\xi r\right)e^{st}d\xi ds. \tag{15b}$$

Using equations (15a)-(15b), the desired transient horizontal displacement $u_r\left(r,0,t\right)$ and vertical displacement $u_z\left(r,0,t\right)$ of the pervious ground surface due to a periodic point sink can be derived from equations (14a)-(14b) as follows:

$$u_r\left(r,0,t\right)=\frac{Q_0\gamma_w}{2\left(2\eta-1\right)\pi Gk}\left\{-\frac{r\Phi\left(ct\right)}{\left(r^2+h^2\right)^{3/2}}+\int_0^{ct}\frac{hr\Phi\left(ct-\tau\right)}{16\tau^3}exp\left(-\frac{r^2+2h^2}{8\tau}\right)\times\left[I_0\left(\frac{r^2}{8\tau}\right)-I_1\left(\frac{r^2}{8\tau}\right)\right]d\tau\right\}, \tag{16a}$$

$$u_z\left(r,0,t\right)=\frac{Q_0\gamma_w}{2\left(2\eta-1\right)\pi Gk}\left\{\frac{h\Phi\left(ct\right)}{\left(r^2+h^2\right)^{3/2}}-\int_0^{ct}\Psi\left(ct-\tau\right)\left[\frac{h}{\left(r^2+h^2\right)^{3/2}}erfc\left(\frac{\sqrt{r^2+h^2}}{2\sqrt{\tau}}\right)+\frac{h}{r^2+h^2}\frac{1}{\sqrt{\pi\tau}}exp\left(-\frac{r^2+h^2}{4\tau}\right)\right]d\tau\right\}, \tag{16b}$$

where $I_\alpha\left(x\right)$ is known as the modified Bessel function of the first kind of order α. The complementary error function is denoted as $erfc\left(x\right)$. The functions $\Phi\left(ct\right)$ and $\Psi\left(ct\right)$ in equations (16a) and (16b) are defined as below:

$$\Phi\left(ct\right)=\frac{cT_d}{cT}\left(ct\right)+\sum_{n=1}^{\infty}\frac{cT}{2n^2\pi^2}\left\{\sin\frac{2n\pi\left(cT_d\right)}{cT}\sin\frac{2n\pi\left(ct\right)}{cT}+\left[1-\cos\frac{2n\pi\left(cT_d\right)}{cT}\right]\left[1-\cos\frac{2n\pi\left(ct\right)}{cT}\right]\right\}, \tag{17a}$$

$$\Psi\left(ct\right)=\frac{cT_d}{cT}+\sum_{n=1}^{\infty}\frac{1}{n\pi}\left\{\sin\frac{2n\pi\left(cT_d\right)}{cT}\cos\frac{2n\pi\left(ct\right)}{cT}+\left[1-\cos\frac{2n\pi\left(cT_d\right)}{cT}\right]\sin\frac{2n\pi\left(ct\right)}{cT}\right\}, \tag{17b}$$

in which $d\Phi\left(t\right)/dt=\Psi\left(t\right)$. Solutions of consolidation deformations due to groundwater withdrawal at a constant strength are derived from equations (16a) and (16b) by taking an appropriate limit $T_d=T$ and using L'Hospital's rule. Carrying out the procedure, we obtain

$$u_r\left(r,0,t\right)=\frac{Q_0\gamma_w}{2\left(2\eta-1\right)\pi Gk}\left\{-\frac{ctr}{\left(r^2+h^2\right)^{3/2}}+\int_0^{ct}\frac{\left(ct-\tau\right)hr}{16\tau^3}exp\left(-\frac{r^2+2h^2}{8\tau}\right)\right.$$

$$\times\left[I_0\left(\frac{r^2}{8\tau}\right)-I_1\left(\frac{r^2}{8\tau}\right)\right]d\tau\Bigg\}, \tag{18a}$$

$$u_z(r,0,t)=\frac{Q_0\gamma_w}{2(2\eta-1)\pi Gk}\left\{-\frac{h}{r^2+h^2}\sqrt{\frac{ct}{\pi}}\,exp\left(-\frac{r^2+h^2}{4ct}\right)+\frac{cth}{\left(r^2+h^2\right)^{3/2}}erf\left(\frac{\sqrt{r^2+h^2}}{2\sqrt{ct}}\right)+\frac{h}{2\sqrt{r^2+h^2}}erfc\left(\frac{\sqrt{r^2+h^2}}{2\sqrt{ct}}\right)\right\}, \tag{18b}$$

where $erf(x)$ is known as the error function and $erf(x)=1-erfc(x)$.

The long-term ground surface horizontal and vertical displacements are found when $t\to\infty$. Let $u_r^\infty=\lim_{t\to\infty}u_r(r,0,t)$ and $u_z^\infty=\lim_{t\to\infty}u_z(r,0,t)$, then we have the closed-form solutions of long-term ground surface displacements.

For periodic pumping:

$$u_r^\infty=-\lim_{t\to\infty}\frac{Q_0\gamma_w}{4(2\eta-1)\pi Gk}\frac{hrf(t)}{\sqrt{r^2+h^2}\left(\sqrt{r^2+h^2}+h\right)}, \tag{19a}$$

$$u_z^\infty=\lim_{t\to\infty}\frac{Q_0\gamma_w}{4(2\eta-1)\pi Gk}\frac{hf(t)}{\sqrt{r^2+h^2}}. \tag{19b}$$

For pumping at a constant strength:

$$u_r^\infty=-\frac{Q_0\gamma_w}{4(2\eta-1)\pi Gk}\frac{hr}{\sqrt{r^2+h^2}\left(\sqrt{r^2+h^2}+h\right)}, \tag{20a}$$

$$u_z^\infty=\frac{Q_0\gamma_w}{4(2\eta-1)\pi Gk}\frac{h}{\sqrt{r^2+h^2}}. \tag{20b}$$

The maximum long-term ground surface horizontal displacement and vertical displacement of the half space due to a point fluid sink at a constant strength are derived from equations (20a) and (20b) by letting $r=\sqrt{\phi}h\approx1.272h$ and $r=0$, respectively. Here, $\phi=(1+\sqrt{5})/2\approx1.618$ is known as the golden ratio [17,18]. For the point fluid sink at a constant strength problem, the maximum horizontal displacement $u_{r\max}$ and vertical displacement $u_{z\max}$ of the ground surface derived from equations (20a) and (20b) are

$$u_{r\max}=u_r\left(\sqrt{\phi}h,0,\infty\right)=-\frac{Q_0\gamma_w(1-2\nu)}{4\pi Gk}\frac{1}{\phi^{2.5}}, \tag{21a}$$

$$u_{z\max}=u_z(0,0,\infty)=\frac{Q_0\gamma_w(1-2\nu)}{4\pi Gk}. \tag{21b}$$

The maximum ground surface horizontal displacement is approximately 30% of the maximum ground surface vertical displacement, i.e.,

$$\left|\frac{u_{r\max}}{u_{z\max}}\right|=\frac{1}{\phi^{2.5}}\approx0.3003 \text{ at } r=\sqrt{\phi}h. \tag{22}$$

The value $r=\sqrt{\phi}h$ is derived when $du_r(r,0,\infty)/dr$ is equal to zero. It is noticed from equations (21a) and (21b) that the maximum long-term ground surface horizontal displacement and settlement for pumping at a constant strength is not directly dependent on the pumping depth *h* of the point sink.

4. Numerical Results

The long-term elastic consolidation subjected to pumping at a constant strength is numerically analyzed. The profiles of normalized horizontal and vertical displacements at the ground surface $z=0$ for isotropic saturated half space are shown in Figures 3 and 4, respectively. The ground surface reveals significant horizontal displacement. The example in Figure 3 shows that the maximum ground surface horizontal displacement is about 30% of the maximum ground settlement at $r=\sqrt{\phi}h\approx1.272h$.

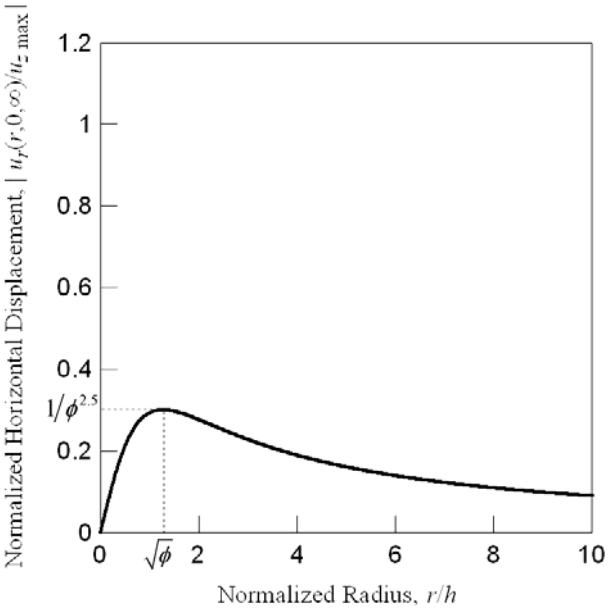

Figure 3. Normalized horizontal displacement profile at the ground surface *z* = 0 for pumping at a constant strength.

Figure 4 shows that the ground surface vertical displacement is around 61.8% of the maximum ground surface vertical displacement at radial variable $r = \sqrt{\phi}h$, where the maximum ground surface horizontal displacement occurred.

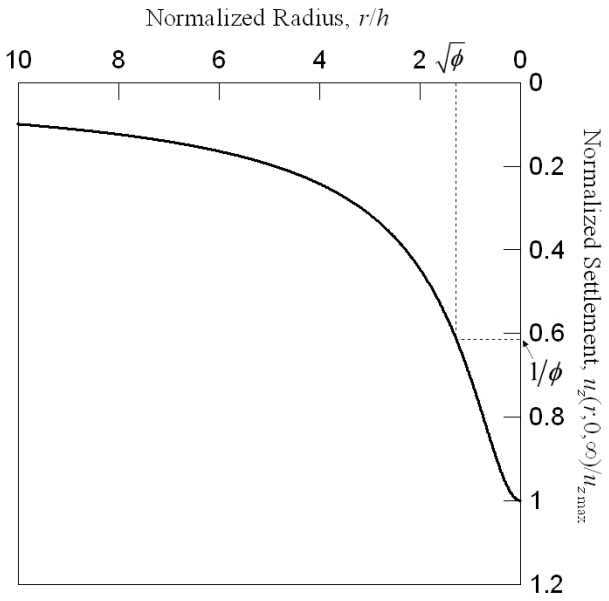

Figure 4. Normalized settlement profile at the ground surface $z = 0$ for pumping at a constant strength.

5. Conclusions

Closed-form solutions of the elastic consolidation due to periodic pumping from pervious saturated elastic half space were obtained by using Laplace-Hankel transformations. Transient ground surface horizontal displacement and settlement of the half space aquifer were investigated. The solutions can be used to evaluate numerical models and numerical simulations of the elastic consolidation settlement near the sink point. The results show:

1. The maximum long-term ground surface horizontal displacement and vertical displacement of the half space due to a point fluid sink at a constant strength are derived from equations (20a) and (20b) by letting $r = \sqrt{\phi}h \approx 1.272h$ and $r = 0$, respectively.
2. It is noticed from equations (21a) and (21b) that the maximum long-term ground surface horizontal displacement and settlement are independent on the pumping depth h of the point sink at a constant strength for the isotropic elastic half space.

Acknowledgements

This work is supported by the National Science Council of Republic of China through grant NSC100-2221-E-216-025.

References

[1] J.F. Poland, *Guidebook to studies of land subsidence due to ground-water withdrawal* (Paris: Unesco, 1984).

[2] M.A. Biot, General theory of three-dimensional consolidation, *Journal of Applied Physics*, 12(2), 1941, 155-164.

[3] M.A. Biot, Theory of elasticity and consolidation for a porous anisotropic solid, *Journal of Applied Physics*, 26(2), 1955, 182-185.

[4] J.R. Booker & J.P. Carter, Analysis of a point sink embedded in a porous elastic half space, *International Journal for Numerical and Analytical Methods in Geomechanics*, 10(2), 1986, 137-150.

[5] J.R. Booker & J.P. Carter, Long term subsidence due to fluid extraction from a saturated, anisotropic, elastic soil mass, *Quarterly Journal of Mechanics and Applied Mathematics*, 39(1), 1986, 85-97.

[6] J.R. Booker & J.P. Carter, Elastic consolidation around a point sink embedded in a half-space with anisotropic permeability, *International Journal for Numerical and Analytical Methods in Geomechanics*, 11(1), 1987, 61-77.

[7] J.R. Booker & J.P. Carter, Withdrawal of a compressible pore fluid from a point sink in an isotropic elastic half space with anisotropic permeability, *International Journal of Solids and Structures*, 23(3), 1987, 369-385.

[8] G.J. Chen, Analysis of pumping in multilayered and poroelastic half space, *Computers and Geotechnics*, 30(1), 2002, 1-26.

[9] G.J. Chen, Steady-state solutions of multilayered and cross-anisotropic poroelastic half-space due to a point sink, *International Journal of Geomechanics*, 5(1), 2005, 45-57.

[10] W. Kanok-Nukulchai & K.T. Chau, Point sink fundamental solutions for subsidence prediction, *Journal of Engineering Mechanics, ASCE*, 116(5), 1990, 1176-1182.

[11] J.-Q. Tarn & C.-C. Lu, Analysis of subsidence due to a point sink in an anisotropic porous elastic half space, *International Journal for Numerical and Analytical Methods in Geomechanics*, 15(8), 1991, 573-592.

[12] J. C.-C. Lu & F.-T. Lin, The transient ground surface displacements due to a point sink/heat source in an elastic half-space, *Geotechnical Special Publication No. 148, ASCE*, 2006, 210-218.

[13] J. C.-C. Lu & F.-T. Lin, Modelling of consolidation settlement subjected to a point sink in an isotropic porous elastic half space, *Proceedings of the 17th IASTED International Conference on Applied Simulation and Modelling*, Corfu, Greece, 2008, 141-146.

[14] J. C.-C. Lu & F.-T. Lin, Analysis of transient ground surface displacements due to an impulsive point sink in an elastic half space, *Proceedings of the IASTED International Conference on Environmental Management and Engineering*, Banff, Alberta, Canada, 2009, 211-217.

[15] I.N. Sneddon, *Fourier transforms* (New York: McGraw-Hill, 1951, 48-70).

[16] A. Erdelyi, W. Magnus, F. Oberhettinger & F.G. Tricomi, *Tables of integral transforms* (New York: McGraw-Hill, 1954).

[17] M. Livio, *The golden ratio: The story of phi, the world's most astonishing number* (New York: Broadway Books, 2002).

[18] R.A. Dunlap, *The golden ratio and Fibonacci numbers* (Singapore: World Scientific Publishing, 1997).

Nomenclature

b_i	Body forces (*Pa/m*)
c	Parameter, $c = k/n\beta\gamma_w$ (m^2/s)
$erf(x)$	Error function (Dimensionless)
$erfc(x)$	Complementary error function (Dimensionless)
$f(t)$	Periodic function (Dimensionless)
$F(s)$	Laplace-Hankel transforms of $f(t)$ (m^2s)
G	Shear modulus of the isotropic porous aquifer (N/m^2)
h	Depth of the periodic sink point (*m*)
$\boldsymbol{i}_r, \boldsymbol{i}_z$	Unit vector in *r*/*z* direction (Dimensionless)
$I_\alpha(x)$	Modified Bessel function of the first kind of order α (Dimensionless)
$J_\alpha(x)$	Bessel function of the first kind of order α (Dimensionless)
k	Permeability of the isotropic porous aquifer (*m*/*s*)
n	Porosity of the porous aquifer (Dimensionless)
p	Excess pore water pressure (N/m^2)
$\tilde{p}$	Laplace-Hankel transforms of p (*Ns*)
q	Rate of water extracted from the saturated porous aquifer per unit volume (1/*s*)
Q_0	Strength of the periodic pumping (m^3/s)
(r, θ, z)	Cylindrical coordinates system (*m*, *radian*, *m*)
s	Laplace transform parameter (s^{-1})
t	Time variable (*s*)
T	Pumping period (*s*)
T_d	Duration of groundwater withdrawal in one period T (*s*)
u_r, u_z	Radial/axial displacement of the porous aquifer (*m*)
$\tilde{u}_r, \tilde{u}_z$	Laplace-Hankel transforms of u_r/u_z (m^3s)
$u_{r\max}, u_{z\max}$	Maximum long-term ground surface horizontal/vertical displacement (*m*)
u_r^∞, u_z^∞	Long-term ground surface horizontal/vertical displacement (*m*)
$\boldsymbol{v}_w, \boldsymbol{v}_s$	Velocity of pore water/solid matrix (*m/s*)
β	Compressibility of pore water (m^2/N)
γ_w	Unit weight of groundwater (N/m^3)
$\delta(x)$	Dirac delta function (m^{-1})
δ_{ij}	Kronecker delta (Dimensionless)
ε	Volume strain of the porous aquifer (Dimensionless)
ε_{ij}	Strain components of the porous aquifer (Dimensionless)
η	Parameter, $\eta = (1-\nu)/(1-2\nu)$ (Dimensionless)
ν	Poisson's ratio of the isotropic porous aquifer (Dimensionless)
ξ	Hankel transform parameter (m^{-1})
τ_{ij}	Total stress components of the porous aquifer (N/m^2)
ϕ	Golden ratio, $\phi \approx 1.6180339887...$ (Dimensionless)

附錄 9

參與本計畫案之兼任研究助理謝適任同學的碩士論文：單井抽水所引致軸對稱彈性沉陷之研究

中 華 大 學

碩 士 論 文

單井抽水所引致軸對稱彈性沉陷之研究

Study on the Axisymmetric Elastic Subsidence Due to Single Well Groundwater Withdrawal

系 所 別：土木工程學系碩士班
學號姓名：M09904006　謝適任
指導教授：呂志宗　　博士

中　華　民　國 102 年 1 月

摘要

本研究旨在探討單井抽水所引致的地表位移與地層超額孔隙水壓變化，係將含水層模擬為均質等向且完全飽和之半無限域，並考慮地表邊界為完全透水與完全不透水兩種情況，研討出穩態之軸對稱彈性壓密沉陷結果。所建立之基本方程式是以 Biot 三維壓密理論為基礎，再根據點抽水問題之基本解與符號運算軟體 Mathematica，推導出線狀抽水所引致的軸對稱壓密沉陷之閉合解。在探討過程中，有考慮抽水深度、取水長度、含水層柏松比、地表滲流邊界條件等的影響，用以推估單井抽水所可能引致之地表水平位移量、垂直位移量及超額孔隙水壓變化量等，其中地表垂直位移即代表沉陷量。本文之研究成果除可進一步了解單井抽水所引致之壓密沉陷行為外，在工程應用上，所研討出之各項閉合解具有計算方法較簡單且計算速度較快之優點。另外，因採用線彈性理論進行沉陷分析，故各種沉陷量之計算結果會偏向保守。

以上所述各項影響因素皆對地層壓密沉陷行為有不同程度的重要影響，由研究結果得知：(1)當含水層之柏松比較大時，含水層容易產生側向變形，故抽水所引致的地表沉陷量會較大。(2)取水長度增加時，抽水量也會增加，故壓密沉陷量也跟著增加。(3)當地表面模擬為不透水邊界時，抽水所引起之負的超額孔隙水壓較不容易消散，含水層中之有效應力上升較多，故抽水所引起的地表沉陷會較大。(4)若考慮點抽水與線狀抽水的抽水量相同，則所引起的最大沉陷量會相同，但於地表大多數位置上，點抽水所引起的沉陷量會較大。(5)因單井抽水所引起的地表水平位移是一軸對稱問題，故地表面在對稱點上之水平位移量應為零，又含水層遠處受抽水擾動的影響很小，故地表遠處之水平位移量亦很小，因此抽水所引起的地表水平位移量會在水井邊逐漸升高後逐步降低。

關鍵詞：壓密沉陷、線狀抽水、點抽水、地下水、Mathematica。

目　　錄

摘要 …… i

目錄 …… ii

表目錄 …… v

圖目錄 …… vi

符號說明 …… xiii

第一章　緒論 …… 1

1.1　研究背景 …… 1

1.2　研究動機與目的 …… 1

1.3　研究方法 …… 2

1.4　研究範圍與限制 …… 2

1.5　論文架構與流程 …… 4

第二章　文獻回顧 …… 6

2.1　前言 …… 6

2.2　地層下陷之定義與成因 …… 7

2.3　地下水 …… 8

2.3.1　地下水之定義與成因 …… 8

2.3.2　地下水層與水井 …… 11

2.3.3　地下水抽取量推估 …… 13

2.3.4　地下水與地層下陷之關聯性與所造成的災害 …… 14

2.3.5　地層下陷之現況與嚴重地層下陷區探討 …… 16

2.3.6　嚴重地層下陷地區劃設作業規範 …… 18

2.3.7　政府補救措施與地下水管制辦法 …… 20

2.4　有效應力 …… 23

2.5　Mathematica 介紹 …… 24

2.6　抽水所引致沉陷之基本理論公式探討 …… 24

2.6.1　前言 …… 25

2.6.2　Biot 於 1941 年所建立之多孔介質彈性力學理論 …… 25

2.6.3 Biot 建立之多孔介質彈性力學理論發展 …… 27
2.7 結語 …… 31
第三章 數學模式分析結果 …… 33
3.1 前言 …… 33
3.2 點抽水問題之閉合解 …… 33
3.2.1 準備工作 …… 33
3.2.2 點抽水之問題之解 …… 35
3.3 線狀抽水問題之解 …… 38
3.4 最大地表位移 …… 40
3.4.1 點抽水問題之地表最大垂直位移 …… 40
3.4.2 點抽水問題之地表最大水平位移 …… 41
3.4.3 線狀抽水問題之地表最大垂直位移 …… 41
3.4.4 線狀抽水問題之地表最大水平位移 …… 42
3.5 結語 …… 43
第四章 參數影響分析 …… 44
4.1 前言 …… 44
4.2 等向性半無限域之點抽水問題結果探討 …… 45
4.2.1 地表模擬為透水情況時點抽水所引致之地表垂直位移 …… 45
4.2.2 地表模擬為透水或不透水情況時點抽水所引致之地表水平位移 … 45
4.2.3 地表模擬為不透水情況時點抽水所引致之地表垂直位移 …… 46
4.3 等向性半無限域之線狀抽水問題結果探討 …… 47
4.3.1 地表模擬為透水情況時線狀抽水所引致之地表垂直位移 …… 47
4.3.2 地表模擬為不透水情況時線狀抽水所引致之地表垂直位移…… 48
4.3.3 地表模擬為透水或不透水情況時線狀抽水所引致之地表水平位移… 49
4.4 半無限域孔隙水壓變化影響結果探討 …… 50

4.4.1 點抽水所引致之含水層超額孔隙水壓 …… 50
4.4.2 現狀抽水所引致之含水層超額孔隙水壓 …… 51
4.5 結語 …… 52
第五章 結論與建議 …… 100
5.1 結論 …… 100
5.2 建議 …… 101
參考文獻 …… 102

表目錄

表 2.1　地下水區劃分說明 …… 10

表 2.2　自然因素與人為因素對地層下陷之發生率的影響比較 …… 15

表 2.3　世界上嚴重地層下陷區的比較 …… 17

表 4.1　土壤之柏松比範圍 …… 44

表 4.2　黏土之柏松比範圍 …… 45

圖目錄

圖 1.1 研究流程圖 …… 5

圖 2.1 雲嘉地區新建造房舍或庭院需墊高基礎 …… 8

圖 2.2 雲嘉地區新建造房舍常需墊高基礎 …… 8

圖 2.3 水井建置示意圖 …… 12

圖 2.4 雲林地區私鑿的水井 …… 16

圖 2.5 民國 100 年度地層下陷檢測概況圖 …… 18

圖 2.6 雲林縣大埤鄉嘉興國小地下水觀測井 1 …… 21

圖 2.7 雲林縣大埤鄉嘉興國小地下水觀測井 2 …… 22

圖 2.8 地下水管制區 …… 22

圖 3.1 點抽水問題示意圖 …… 37

圖 3.2 線狀抽水問題示意圖 …… 38

圖 4.1 地表模擬為透水情況時點抽水問題之無因次化地表沉陷量曲線圖 …… 54

圖 4.2 點抽水問題之無因次化地表水平位移曲線圖 …… 54

圖 4.3 地表模擬為不透水情況時點抽水所引致之無因次化地表沉陷量

(ν = 0.15) …… 55

圖 4.4 地表模擬為不透水情況時點抽水所引致之無因次化地表沉陷量

(ν = 0.2) …… 55

圖 4.5 地表模擬為不透水情況時點抽水所引致之無因次化地表沉陷量

(ν = 0.25) …… 56

圖 4.6 地表模擬為不透水情況時點抽水所引致之無因次化地表沉陷量

(ν = 0.3) …… 56

圖 4.7 地表模擬為不透水情況時點抽水所引致之無因次化地表沉陷量

(ν = 0.35) …… 57

圖 4.8 地表模擬為不透水情況時點抽水所引致之無因次化地表沉陷量
(ν = 0.4) ····· 57
圖 4.9 地表模擬為不透水情況時點抽水所引致之無因次化地表沉陷量
(ν = 0.45) ····· 58
圖 4.10 地表模擬為不透水情況時點抽水所引致之無因次化地表沉陷量
(ν = 0.4999) ····· 58
圖 4.11 地表模擬為透水與不透水情況時點抽水所引致無因次化地表沉陷量比較
圖 ····· 59
圖 4.12 地表模擬為透水情況時線狀抽水所引致之無因次化地表沉陷量
(L/h = 0.1) ····· 59
圖 4.13 地表模擬為透水情況時線狀抽水所引致之無因次化地表沉陷量
(L/h = 0.3) ····· 60
圖 4.14 地表模擬為透水情況時線狀抽水所引致之無因次化地表沉陷量
(L/h = 0.5) ····· 60
圖 4.15 地表模擬為透水情況時線狀抽水所引致之無因次化地表沉陷量
(L/h = 0.8) ····· 61
圖 4.16 地表模擬為透水情況時線狀抽水所引致之無因次化地表沉陷量
(L/h = 1) ····· 61
圖 4.17 地表模擬為透水情況時線狀抽水所引致之無因次化地表沉陷量
(L/h = 0.1~1) ····· 62
圖 4.18 透水情況下點抽水與線狀抽水所引致之無因次化地表沉陷量的比較
····· 62
圖 4.19 地表模擬為不透水情況時線狀抽水所引致之無因次化地表沉陷量
(L/h = 0.1，ν = 0.15) ····· 63
圖 4.20 地表模擬為不透水情況時線狀抽水所引致之無因次化地表沉陷量
(L/h = 0.1，ν = 0.2) ····· 63

圖 4.21 地表模擬為不透水情況時線狀抽水所引致之無因次化地表沉陷量
(L/h = 0.1，ν = 0.25) ····· 64
圖 4.22 地表模擬為不透水情況時線狀抽水所引致之無因次化地表沉陷量
(L/h = 0.1，ν = 0.3) ····· 64
圖 4.23 地表模擬為不透水情況時線狀抽水所引致之無因次化地表沉陷量
(L/h = 0.1，ν = 0.35) ····· 65
圖 4.24 地表模擬為不透水情況時線狀抽水所引致之無因次化地表沉陷量
(L/h = 0.1，ν = 0.4) ····· 65
圖 4.25 地表模擬為不透水情況時線狀抽水所引致之無因次化地表沉陷量
(L/h = 0.1，ν = 0.45) ····· 66
圖 4.26 地表模擬為不透水情況時線狀抽水所引致之無因次化地表沉陷量
(L/h = 0.1，ν = 0.15~0.45) ····· 66
圖 4.27 地表模擬為不透水情況時線狀抽水所引致之無因次化地表沉陷量
(L/h = 0.3，ν = 0.15) ····· 67
圖 4.28 地表模擬為不透水情況時線狀抽水所引致之無因次化地表沉陷量
(L/h = 0.3，ν = 0.2) ····· 67
圖 4.29 地表模擬為不透水情況時線狀抽水所引致之無因次化地表沉陷量
(L/h = 0.3，ν = 0.25) ····· 68
圖 4.30 地表模擬為不透水情況時線狀抽水所引致之無因次化地表沉陷量
(L/h = 0.3，ν = 0.3) ····· 68
圖 4.31 地表模擬為不透水情況時線狀抽水所引致之無因次化地表沉陷量
(L/h = 0.3，ν = 0.35) ····· 69
圖 4.32 地表模擬為不透水情況時線狀抽水所引致之無因次化地表沉陷量
(L/h = 0.3，ν = 0.4) ····· 69
圖 4.33 地表模擬為不透水情況時線狀抽水所引致之無因次化地表沉陷量
(L/h = 0.3，ν = 0.45) ····· 70

圖 4.34 地表模擬為不透水情況時線狀抽水所引致之無因次化地表沉陷量
(L/h = 0.3，ν = 0.15~0.45) ····· 70
圖 4.35 地表模擬為不透水情況時線狀抽水所引致之無因次化地表沉陷量
(L/h = 0.5，ν = 0.15) ····· 71
圖 4.36 地表模擬為不透水情況時線狀抽水所引致之無因次化地表沉陷量
(L/h = 0.5，ν = 0.2) ····· 71
圖 4.37 地表模擬為不透水情況時線狀抽水所引致之無因次化地表沉陷量
(L/h = 0.5，ν = 0.25) ····· 72
圖 4.38 地表模擬為不透水情況時線狀抽水所引致之無因次化地表沉陷量
(L/h = 0.5，ν = 0.3) ····· 72
圖 4.39 地表模擬為不透水情況時線狀抽水所引致之無因次化地表沉陷量
(L/h = 0.5，ν = 0.35) ····· 73
圖 4.40 地表模擬為不透水情況時線狀抽水所引致之無因次化地表沉陷量
(L/h = 0.5，ν = 0.4) ····· 73
圖 4.41 地表模擬為不透水情況時線狀抽水所引致之無因次化地表沉陷量
(L/h = 0.5，ν = 0.45) ····· 74
圖 4.42 地表模擬為不透水情況時線狀抽水所引致之無因次化地表沉陷量
(L/h = 0.3，ν = 0.15~0.45) ····· 74
圖 4.43 地表模擬為不透水情況時線狀抽水所引致之無因次化地表沉陷量
(L/h = 0.8，ν = 0.15) ····· 75
圖 4.44 地表模擬為不透水情況時線狀抽水所引致之無因次化地表沉陷量
(L/h = 0.8，ν = 0.2) ····· 75
圖 4.45 地表模擬為不透水情況時線狀抽水所引致之無因次化地表沉陷量
(L/h = 0.8，ν = 0.25) ····· 76
圖 4.46 地表模擬為不透水情況時線狀抽水所引致之無因次化地表沉陷量
(L/h = 0.8，ν = 0.3) ····· 76

圖 4.47 地表模擬為不透水情況時線狀抽水所引致之無因次化地表沉陷量
(L/h = 0.8，ν = 0.35) ····· 77
圖 4.48 地表模擬為不透水情況時線狀抽水所引致之無因次化地表沉陷量
(L/h = 0.8，ν = 0.4) ····· 77
圖 4.49 地表模擬為不透水情況時線狀抽水所引致之無因次化地表沉陷量
(L/h = 0.8，ν = 0.45) ····· 78
圖 4.50 地表模擬為不透水情況時線狀抽水所引致之無因次化地表沉陷量
(L/h = 0.8，ν = 0.15~0.45) ····· 78
圖 4.51 地表模擬為不透水情況時線狀抽水所引致之無因次化地表沉陷量
(L/h = 1，ν = 0.15) ····· 79
圖 4.52 地表模擬為不透水情況時線狀抽水所引致之無因次化地表沉陷量
(L/h = 1，ν = 0.2) ····· 79
圖 4.53 地表模擬為不透水情況時線狀抽水所引致之無因次化地表沉陷量
(L/h = 1，ν = 0.25) ····· 80
圖 4.54 地表模擬為不透水情況時線狀抽水所引致之無因次化地表沉陷量
(L/h = 1，ν = 0.3) ····· 80
圖 4.55 地表模擬為不透水情況時線狀抽水所引致之無因次化地表沉陷量
(L/h = 1，ν = 0.35) ····· 81
圖 4.56 地表模擬為不透水情況時線狀抽水所引致之無因次化地表沉陷量
(L/h = 1，ν = 0.4) ····· 81
圖 4.57 地表模擬為不透水情況時線狀抽水所引致之無因次化地表沉陷量
(L/h = 1，ν = 0.45) ····· 82
圖 4.58 地表模擬為不透水情況時線狀抽水所引致之無因次化地表沉陷量
(L/h = 1，ν = 0.15~0.45) ····· 82
圖 4.59 地表模擬為不透水情況時線狀抽水所引致之無因次化地表沉陷量
(ν = 0.15，L/h = 0.1~1) ····· 83

圖 4.60 地表模擬為不透水情況時線狀抽水所引致之無因次化地表沉陷量
(ν = 0.2，L/h = 0.1~1) ····· 83
圖 4.61 地表模擬為不透水情況時線狀抽水所引致之無因次化地表沉陷量
(ν = 0.25，L/h = 0.1~1) ····· 84
圖 4.62 地表模擬為不透水情況時線狀抽水所引致之無因次化地表沉陷量
(ν = 0.3，L/h = 0.1~1) ····· 84
圖 4.63 地表模擬為不透水情況時線狀抽水所引致之無因次化地表沉陷量
(ν = 0.35，L/h = 0.1~1) ····· 85
圖 4.64 地表模擬為不透水情況時線狀抽水所引致之無因次化地表沉陷量
(ν = 0.4，L/h = 0.1~1) ····· 85
圖 4.65 地表模擬為不透水情況時線狀抽水所引致之無因次化地表沉陷量
(ν = 0.45，L/h = 0.1~1) ····· 86
圖 4.66 地表模擬為透水與不透水情況時線狀抽水問題無因次化地表沉陷量比較圖(L/h = 1) ····· 86
圖 4.67 線狀抽水所引致之無因次化地表水平位移曲線圖 ····· 87
圖 4.68 地表模擬為透水邊界時點抽水所引致之無因次化孔隙水壓等值曲線圖
····· 88
圖 4.69 地表模擬為不透水邊界時點抽水所引致之無因次化孔隙水壓等值曲線圖
····· 89
圖 4.70 地表模擬為透水邊界時線狀抽水所引致之無因次化孔隙水壓等值曲線圖
(L/h = 0.1) ····· 90
圖 4.71 地表模擬為透水邊界時線狀抽水所引致之無因次化孔隙水壓等值曲線圖
(L/h = 0.3) ····· 91
圖 4.72 地表模擬為透水邊界時線狀抽水所引致之無因次化孔隙水壓等值曲線圖
(L/h = 0.5) ····· 92
圖 4.73 地表模擬為透水邊界時線狀抽水所引致之無因次化孔隙水壓等值曲線圖

(L/h = 0.8) ····· 93
圖 4.74 地表模擬為透水邊界時線狀抽水所引致之無因次化孔隙水壓等值曲線圖
(L/h = 1) ····· 94
圖 4.75 地表模擬為不透水邊界時線狀抽水所引致之無因次化孔隙水壓等值曲線
圖(L/h = 0.1) ····· 95
圖 4.76 地表模擬為不透水邊界時線狀抽水所引致之無因次化孔隙水壓等值曲線
圖(L/h = 0.3) ····· 96
圖 4.77 地表模擬為不透水邊界時線狀抽水所引致之無因次化孔隙水壓等值曲線
圖(L/h = 0.5) ····· 97
圖 4.78 地表模擬為不透水邊界時線狀抽水所引致之無因次化孔隙水壓等值曲線
圖(L/h = 0.8) ····· 98
圖 4.79 地表模擬為不透水邊界時線狀抽水所引致之無因次化孔隙水壓等值曲線
圖(L/h = 1) ····· 99

符號說明

a_s	土壤中固體與固體接觸點面積總和[m^2]；
A, M, N, Q, R, S	Biot 所定義之多孔介質力學常數[kN/m^2]；
$\overline{\mathrm{A}}$	土體的橫斷面積[m^2]；
B	Skempton 孔隙流體壓力常數，即圍壓變化引起的超額孔隙水壓變化量/圍壓變化量[無因次]；
E	含水層之楊氏模數[kN/m^2]；
f_i	徹體力(Body Force) [kN/m^3]；
g	重力加速度[m/s^2]；
G	含水層之剪力模數(Shear Modulus)，$G = E/2(1+\nu)$ [kN/m^2]；
h	抽水深度[m]；
i	水力梯度(Hydraulic Gradient) [無因次]；
k	含水層之滲透係數[m/s]；
L	線狀抽水長度[m]；
n	含水層之孔隙率[無因次]；
p	超額孔隙流體壓力(壓力為正) [kN/m^2]；
q	線狀抽水強度[m^3/sm]；孔隙流體補注變率[$1/s$]；
Q	點抽水強度[m^3/s]；
$R_{(1)}$	距離參數，$R_{(1)}=\sqrt{r^2+(z-h)^2}$ [m]；
$R^*_{(1)}$	距離參數，$R^*_{(1)}=\sqrt{r^2+(z-h)^2}+\lvert z-h\rvert$ [m]；
$R_{(a)}$	距離參數，$R_{(a)}=\sqrt{r^2+(z+h)^2}$ [m]；
$R^*_{(a)}$	距離參數，$R^*_{(a)}=\sqrt{r^2+(z+h)^2}+z+h$ [m]；

R_i 距離參數，$R_i = \sqrt{r^2 + i^2}$，$i = z、z+h、z-h、z+h-L、z-h+L$ $[m]$；

R_i^* 距離參數，$R_i^* = R_i + i$，$i = z+h、z-h、z+h-L、z-h-L$ $[m]$；

r 水平距離座標變數$[m]$；

s 地表至線狀抽水上所選取之點抽水元素的距離$[m]$；

t 時間變數$[s]$；

$u_{i,i}$ 含水層之體積應變量，$u_{i,i} = \frac{\partial u_1}{\partial x_1} + \frac{\partial u_2}{\partial x_2} + \frac{\partial u_3}{\partial x_3} = \frac{\partial u_x}{\partial x} + \frac{\partial u_y}{\partial y} + \frac{\partial u_z}{\partial z}$ [無因次]；

u_r 含水層之水平位移$[m]$；

u_z 含水層之垂直位移$[m]$；

$u_{z\,max}$ 地表模擬為透水時點抽水所引致之最大地表沉陷量$[m]$；

$u_{z\,max\,(L=h)}$ 地表模擬為透水時線狀抽水所引致之最大地表沉陷量$[m]$；

v_i 孔隙流體之流速$[m/s]$；

$\vec{v}_s, \vec{v}_w$ 固體土壤之運動速度與孔隙水之流速$[m/s]$；

z 垂直距離座標變數$[m]$；

希臘字母

α Biot 所定義之多孔介質力學常數$[kN/m^2]$；

β 孔隙水之壓縮係數$[m^2/kN]$；

γ_f 孔隙流體之單位重$[kN/m^3]$；

γ_w 孔隙水之單位重，γ_w= 9,810 $[N/m^3]$；

δ_{ij} Kronecker delta 函數[無因次]；

ε 含水層之體積應變量，$\varepsilon = \frac{\partial u_1}{\partial x_1} + \frac{\partial u_2}{\partial x_2} + \frac{\partial u_3}{\partial x_3}$ [無因次]；

ε_{ij} 含水層之應變量，$\varepsilon_{ij} = \frac{1}{2}\left(\frac{\partial u_i}{\partial x_j} + \frac{\partial u_j}{\partial x_i}\right)$ [無因次]；

ζ 單位多孔介質體積內所增加之孔隙流體體積[無因次]；

η 含水層之材料參數，$\eta = (1-\nu)/(1-2\nu)$ [無因次]；

θ 單位多孔介質體積內所增加之孔隙流體體積[無因次]；

λ 含水層之 Lame 常數，$\lambda = E\nu/[(1+\nu)(1-2\nu)]$ [kN/m^2]；

μ 含水層之剪力模數[kN/m^2]；

ν 含水層於排水情況下所測得之柏松比(Poisson Ratio) [無因次]；

ν_u 含水層於不排水情況下所測得之柏松比[無因次]；

ρ_s, ρ_w 固體土壤與孔隙水之密度[kg/m^3] ；

σ 含水層之總應力，$\sigma = \sigma' + p$ [kN/m^2]；

σ' 含水層之有效應力[kN/m^2]；

τ_{ij} 作用於含水層之總應力[kN/m^2]；

ϕ 黃金比例，ϕ = 1.618… [無因次]。

第一章 緒論

1.1 研究背景

水為維繫所有生態體系運作之所需，地球上的水分布於各個角落：包括海洋、冰川、河川、湖泊、地層及大氣中。而台灣位於西太平洋上，氣候以北迴歸線為界，以北為副熱帶季風氣候、以南為熱帶季風氣候，雖然平均降雨量約為世界平均降雨量之2.6 倍，但由於降雨集中在 5~10 月之豐水期，故每人分配平均降雨量只有世界平均值的 1/6，因此地下水為解決用水問題的辦法之一，但由於大量使用並且管制成效不彰，導致地層下陷問題日益嚴重。Terzaghi 的有效應力觀念可解釋地層下陷之機制，當地下水因人為使用而被抽取出來時，原先由固體土壤與孔隙水共同承擔之荷重，會逐漸移轉至固體土壤上，故造成壓密(Consolidation)現象，所造成的地表下陷情況稱為壓密沉陷(Consolidation Settlement)。地層下陷的過程通常不易被發現，往往在排水設施功能降低、地下管線受損及土地淹水時才被發現，所以有人稱其為沉默的土地危機。台灣因工程上或是經濟上的因素過度抽取地下水且無適當的補注機制，已造成不少縣市深「陷」危機，不只造成國土的流失，且對民生安全的影響甚鉅。例如根據欣傳媒記者蕭介雲在 2012 年 4 月 19 日的報導指出，高鐵在虎尾車站特定區的下陷量已累積達 57.2cm、高鐵與雲 158 線道交接處為 57.6cm、與 78 快速道路交接處達 69.4cm。

1.2 研究動機與目的

地層下陷為目前世界各國普遍遭遇的問題，而地層下陷之成因可從自然與人為兩方面加以探討，過量抽取地下水乃是最嚴重的人為影響因素。地下水並非不可抽用，在台灣地下水也是解決部分季節缺水危機的辦法之一，但如何適量的取用，才不會造成無法挽回的後果是相當重要的。台灣西部沿海由於養殖業的發展，過量抽取地下水，已造成相當嚴重的地層下陷，致使地下水層的水位面下降、海水入侵地下水層、地下水層被汙染、土壤被鹽化、排水不易等惡果。由於地層下陷為不可逆之現象，故應以

嚴肅態度面對。為解決抽水所引致的地層下陷問題，除依賴適當的教育宣導與法規的訂定，改變國人用水習慣與觀念外，亦應從工程上之學理分析層面切入，進行相關之數理分析，藉以瞭解抽水所引致的地層下陷機制，其關鍵課題包括抽水所引致的地層位移變化量、及地層孔隙水壓變化量等的探討，本文擬繪製相關之應用圖表，使有助於瞭解此一問題的關鍵影響因素及其影響結果，研究成果希冀能提供相關主管機關做為訂立相關規範之參考依據。

1.3 研究方法

本文擬採用數學模擬(Mathematical Modelling)的方式進行相關之研究，本文擬推導出問題之理論解析解(Theoretical Analytical Solution)，使用理論解析方式推估合理之壓密沉陷量。數學模式中乃將地表面模擬為一半無限域(Half Space)，地層力學性質與土壤滲流性質皆考慮為均質等向性(Homogeneous Isotropic)，並考慮土壤為完全飽和狀態，且適於引用線彈性飽和多孔介質彈性力學理論建立數學模式。基於此，研討出地層受長期抽水作用影響時之穩態壓密沉陷解析解，其中抽水強度與抽水速率考慮為定值，此外地表邊界則模擬為完全透水與完全不透水兩種情況加以探討。

本文基於 Biot 三維壓密理論，並引用呂志宗(1991)根據多孔介質彈性力學理論所推導出之點抽水所導致地層下陷問題的基本解(Fundament Solution)，利用符號運算軟體 Mathematica 輔助作積分之運算，用以討論因抽水所引起的壓密沉陷問題，所研討出之解包括地層的垂直、水平位移與超額孔隙水壓變化，並繪製出相關之工程應用圖表，各項研究結果均可使用簡單之數學符號加以表達，故稱之為閉合解(Closed-form Solution)。

1.4 研究範圍與限制

本文之研究有考慮以下所示之研究範圍與限制：(1)假設含水層可模擬為一半無限域之均質且完全飽和的多孔介質，本文是將地表模擬為無限延伸之水平面，半無限

域的考慮與擾動效應、尺度效應及邊界效應等有關，均質是指含水地層中之各點的材料性質皆相同。(2)含水層之力學行為與滲流性質皆可模擬為等向性，等向性之力學行為與滲流性質係指在同一個位置上，含水層於任意方向的力學行為與滲流性質皆相同。(3)含水層之力學行為適用於線彈性理論，線彈性是指在小變形理論的前提下，含水層的壓密行為是具有可回復之彈性、且受力與變形具有等比例的線性關係，本文並不考慮塑性變形且含水層無永久之變形。(4)本研究僅考慮抽取之物質為地下水，且抽水強度與抽水速率恆保持為定值，即將抽水行為模擬為持續且不間斷。(5)本文僅探討抽水時因壓密行為所引致的地表長期沉陷量，故所建立的數學模式及其分析結果與時間因子無關。(6)本文將地表邊界模擬為透水邊界時，其意係指地表邊界是模擬為孔隙水壓可以完全消散之情況，該含水層可視為一非拘限含水層；若地表邊界是模擬為不透水情況，則是考慮地表面之孔隙水壓無法消散，該含水層可視為一拘限含水層。另外，地表之力學邊界條件則考慮為無應力變化情況，其意係指地表面之受力無增加或減少的情況。

本文於定義符號之正負意義時，是將正值的孔隙水壓定義為壓力，負值的孔隙水壓定義為吸力；正值的總應力與有效應力定義為壓力，負值的總應力與有效應力則定義為吸力；正值的地表垂直位移是指地表沉陷量，負值的地表水平位移係指朝水井方向移動之位移量。本文是以數學模擬的方式分析問題，故在工程應用上須考慮以上限制條件。本文僅探討出單井抽水所引致的地表水平位移、垂直位移與含水層的超額孔隙水壓變化，尚未討論抽水所引致的地層應力變化問題。

在工程實務上，要完全吻合以上所述適用條件並不容易，但本文之研究成果可應用於以下情況：(1)若能取得含水層的基本水文地質參數資料，即可進行簡易之沉陷量的估算，因本文是採用線彈性理論進行數學模擬，故通常沉陷量估算結果會較大，與工程上常希望進行保守評估相符。(2)本文之研究成果為閉合解，亦為另一種型態的基本解，故可為邊界元素法等數值模擬方法建立研究基礎。

1.5 論文架構與流程

第一章：主要是說明本文之研究背景、研究動機與目的、研究方法、研究範圍與限制、論文架構與流程等。

第二章：利用文獻回顧，蒐集並引用與本文相關之前人的研究與資訊，用以了解關於地下水、地層下陷等之定義、成因與危害等相關資訊，並了解台灣地下水之目前現況與相關法規，最後引用前人所推導之理論解進行後續之探討。

第三章：以點抽水問題之閉合解為基礎，將地層模擬為半無限域、均質且等向性的多孔介質，並將地表之邊界條件分別模擬為透水與不透水兩種情況，進而推導出地表之最大垂直位移、水平位移與超額孔隙水壓等之閉合解。

第四章：主要針對第三章所推導出之閉合解進行參數影響分析，需考慮適當且合理之水文地質及抽水參數，進行數值結果的比較。

第五章：為結論與建議，主要將本文所探討出之各項結果加以歸納整理，並提出後續相關之研究建議、與未來的研究發展方向。

本論文之研究流程乃是先建立研究動機與目的，再蒐集以往相關之研究論文，針對問題提出閉合解，再進行參數影響分析，並針對其結果進行說明，本論文之研究流程圖如圖 1.1 所示。

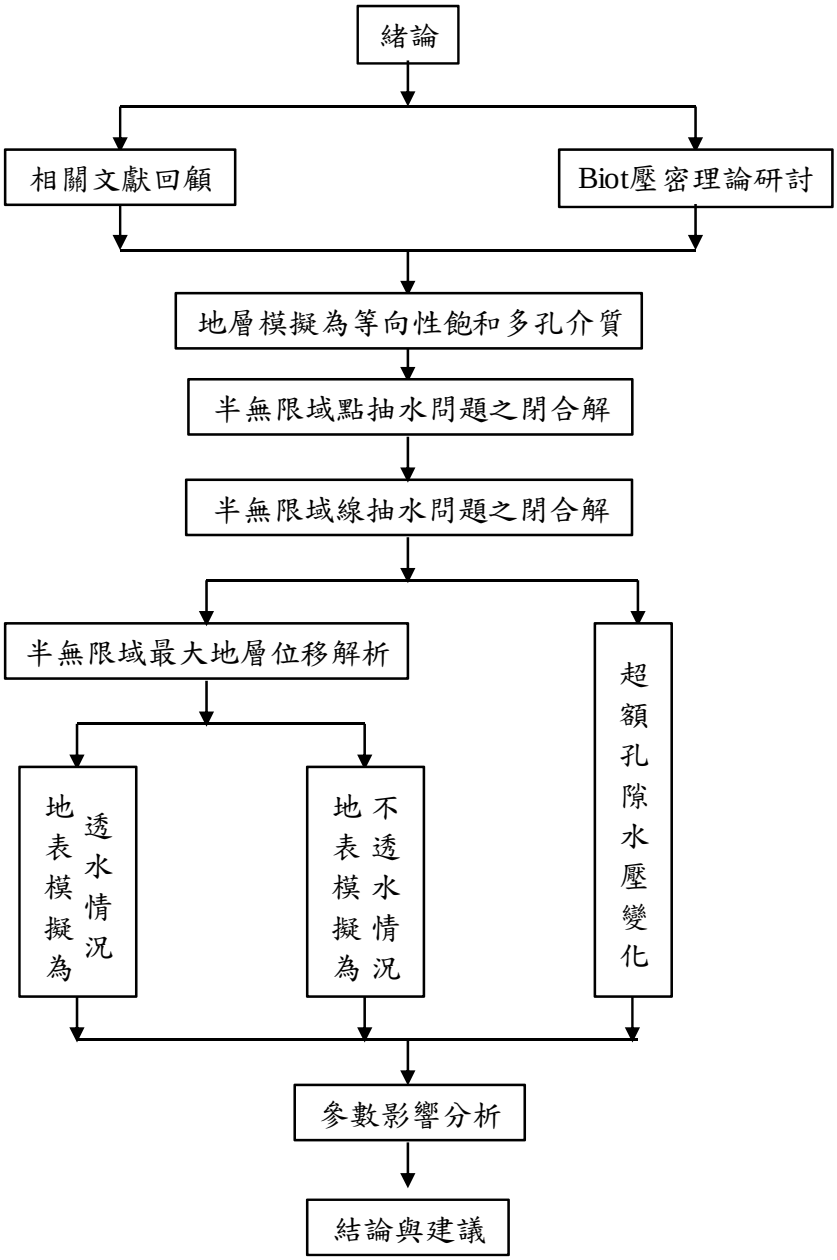
緒論
相關文獻回顧
Biot壓密理論研討
地層模擬為等向性飽和多孔介質
半無限域點抽水問題之閉合解
半無限域線抽水問題之閉合解
半無限域最大地層位移解析
地表模擬為透水情況
地表模擬為不透水情況
超額孔隙水壓變化
參數影響分析
結論與建議

圖 1.1 研究流程圖

第二章 文獻回顧

2.1 前言

台灣的年平均降雨量約達 2500 毫米，屬於世界雨量豐水區之一，卻因山高地險、河川的豐枯季相當明顯且蓄水不易，而在部分季節發生了缺水問題，蘊藏在地底下的地下水變成解決該問題的重要方法之一，更凸顯地下水對台灣的重要性。但多年來過度使用地下水所造成的地層下陷，已成受十分關注的議題。台灣沿海等低窪地區常有淹水問題發生，究其原因常是因為地層下陷導致地表低於海平面，致造成排水不良，每年 5~10 月遇到豐雨季，淹水問題就會更加嚴重，而超抽地下水已公認是造成地層下陷的主因。

目前本國已有許多專家學者探討過這類問題如:杜富麗等(1993)曾探討超抽地下水所引起的地層下陷問題，並提出各種預防及補救措施，曾以模式分析方式建立抽水量與地層下陷預估量的關係，關於模式分析之可靠度及準確度目前仍是各界努力之重點。本文亦採用建立數學模式的分析方式進行相關之研究，旨在探討抽水時所引致的地層下陷與超額孔隙水壓變化，是以呂志宗(1991)所研討出之飽和土層因點抽水所引致的地層壓密沉陷之基本解為研究基礎，進一步討論抽水所引起的地表最大位移量及其發生位置，同時亦探討如何將點抽水問題的壓密沉陷基本解調整為線抽水問題的閉合解，以上問題的研討過程均是將地層的力學行為與滲流性質模擬為等向性。以往亦有許多文獻進行過相關之研究，例如：杜富麗(1993)即曾探討不同抽水型態對地層下陷的影響，建立耦合與非耦合情況下之壓密模式；彭清源(1997)曾探討抽水所引致壓密問題之數值解析方法，並利用近似展開解將耦合的壓密沉陷理論模式改寫為數組簡單的非耦合壓密沉陷理論模式；曾柏領(2007)曾探討抽水所引致的彈性暫態壓密沉陷，並探討管線滲漏所引起的地層位移量變化。

本文在文獻回顧上先介紹地層下陷的定義、成因後，再介紹地下水的定義、地下水與地層下陷的關係、台灣目前下陷之情況、嚴重地層下陷區域、政府目前施救現況與地下水管制辦法等，然後介紹有效應力的概念與 Biot 壓密沉陷理論，最後說明本

研究所使用之理論解析方法與假設條件等。

2.2 地層下陷之定義與成因

地層下陷泛指地層垂直向下移動所呈現的地面沉降現象，是一種因地層內部應力失去平衡所產生的行為，且影響區域以大範圍為主。若將地層下陷影響因素分為自然因素與人為因素兩類，則前者包括板塊運動、火山爆發、岩層溶蝕、地層自然壓密等天然因素，如日本 2011 年所發生的大地震，其所引致的地層下陷曾高達 114 公分(Imakiire 和 Koarai，2012)；又或者因興建人工構造物、地下資源開採或抽取地下水等人為因素，皆會引起地層下陷問題。然而隨著各地之地質條件、作用強度與發展時間等差異性，所產生的情形遂有不同。

地層下陷發生過程不易被發現，往往在排水設施功能減低、地下管線受損及土地淹水時，才會感知其嚴重性，所以有人稱其為沉默的土地危機(柳志錫、杜富麗、洪偉嘉，2003)。如圖 2.1、圖 2.2 所示，為克服地層下陷所引起的排水不良或淹水問題，雲嘉地區新建造的房舍均有墊高基礎之設計。

目前台灣已有許多地區被列為嚴重地層下陷區域，地層下陷嚴重地區是以鄉鎮為劃定單位，凡是達到「地層下陷累積總量」或「近年地層下陷年平均速率」認定標準，且達到「易淹水區域」認定標準之鄉鎮，則該鄉鎮就會被劃定為嚴重地層下陷區，目前已有彰化、雲林、嘉義、台南、屏東等縣市之部分鄉鎮被列為嚴重下陷區(經濟部水利署，地層下陷防治資訊網)。地層下陷發生後，目前的工程技術仍無法完全回復其原貌，所能做的僅有盡力去預防及減緩其下陷速度，放任不管對國土流失將有重大影響，且對我國之社會經濟也是一大威脅。

圖 2.1 雲嘉地區新建造房舍或庭院需墊高基礎(謝適任攝，2012)

圖 2.2 雲嘉地區新建造房舍常需墊高基礎(謝適任攝，2012)

2.3 地下水

2.3.1 地下水之定義與成因

地下水之英譯為 Groundwater，望文生義，其中英文均是表示此為地表以下的水。一般而言地表以下的水，包含土壤或岩石孔隙中的水，在學術領域上多半定義要在地層中達到飽和之水分方可稱為地下水。

地表水受到日曬蒸發後上升至空中，遇冷即凝結為固態或液態下降存於地表，不斷循環形成一水文循環，當降落於地表的水沿著土壤或岩層孔隙滲流而下時，遇到較不易透水的土壤或岩層時，即會開始向上累積並儲存於地層中形成地下水層；也有部分地下水是當沉積岩在地殼變動時，成為封閉在地層內部的水。非拘限含水層(Unconfined Aquifer)之地下水面頂部稱為「地下水位面」，地下水位面通常位於地表下數公尺與數百公尺深，但也會出現幾乎貼近地表面之地下水位面，甚至是自湧式之地下水。地下水的滲流速度會受地面坡度、植物被覆、大地材料與鬆密程度等因素的影響，地下水的抽水量也受地層滲流速度的影響，故水井的取水層會希望其含水層的滲流速度快一些，如砂層、砂礫層等即為滲透性良好的取水層。

台灣本島面積 3 萬 6 千平方公里中，約有 1 萬平方公里有地下水層的分布，所佔比例達總面積的 29%，地下水的主要含水層為鬆散、孔隙較大且未膠結的沖積層，地層若經歷固化成岩層後存於岩縫之中，則可能變為萬年的化石水(宜蘭縣政府，宜蘭縣土壤及地下水汙染整治業務網，2012/9/22 瀏覽)。水利署將全台劃分為 10 個地下水區，如表 2.1 所示，共包含台北盆地、桃園中壢台地、新竹苗栗沿海地區、臺中地區、濁水溪沖積扇、嘉南平原、屏東平原、蘭陽平原、花蓮臺東縱谷區與澎湖地區。

地下水不一定都是淡水(陳文福，2005)，也有因為古世紀海相堆積而鹽分殘留於孔隙中、或人為因素所導致之鹽化，例如：嘉南沿海地區古時為曬鹽區，鹵水經數十年的下滲，導致地下水之鹽分比海水還高。地下水的水質極易受區域內之地質、水源、人類活動、超抽、海水入侵等因素的影響而產生變化，地下水因位於地層中較不易受汙染，但汙染後也較不易回復原狀。

表 2.1 地下水區劃分說明(行政院環境保護署，民國 99 年環境水質監測年報，2010)

水區	總面積 (KM^2)	包含縣市 (測井數)	水區概述
台北盆地	380	臺北市(18)、新北市(30)、桃園縣(3)，共計51口。	主要分布在臺北盆地，涵蓋大漢溪、新店溪與基隆河，地表水沿河床滲入礫石或砂層中形成地下水，降雨或低窪地的積水入滲亦供應部分地下水。
桃園中壢台地	1,090	桃園縣(22)，共計 22 口。	桃園中壢台地為古石門沖積扇的主要部分，沖積扇經造山運動而隆起，並緩緩傾斜形成台地，因台地表面有滲透性不佳的紅土披覆，阻礙地表水的入滲，一般認為地下水主要由大漢溪和南崁溪，沿河道滲入地層中形成。
新竹苗栗沿海地區	900	新竹市(15)、新竹縣(14)、苗栗縣(40)，共計69口。	北以鳳山溪為界，和桃園中壢台地相接，南以大安溪為界，和臺中地區相鄰。本區因地形與地質條件影響，地下水層分布零碎，各屬不同集水區，地下水不相通連。沖積層的地下水主要來自河水補注與雨水入滲，水量充沛，為主要地下水層。
臺中地區	1,180	臺中市(4)、臺中縣(16)、南投縣(2)、彰化縣(2)，共計24口。	由臺中盆地、后里、大肚山、八卦山台地與沿海狹長平原組成。臺中盆地、沿海狹長平原地下水主要來自大甲溪、大肚溪、大安溪水系河床的滲漏而成。后里、大肚山、八卦台地地層表面有紅土分布，下為受紅土浸染的厚層礫岩與砂岩層，蘊藏豐富地下水；惟因地勢高，地下水甚深。
濁水溪沖積扇	1,800	彰化縣(19)、雲林縣(14)、嘉義縣(3)，共計36口	本區為本省最大的沖積扇，地層的孔隙發達，地表水與地下水互相暢流，地下水位淺，地下水極豐富。
屏東平原	2,520	嘉義市(1)、嘉義縣(15)、臺南市(4)、臺南縣(36)、高雄市(13)、高雄縣(21)，共計90口。	北由北港溪左岸起，南迄高屏溪右岸。本區為北港溪、朴子溪、八掌溪、集水溪、曾文溪、鹽水溪與二仁溪所搬運的大量泥砂，淤積河口附近，後因地盤隆起造成廣大沖積平原，地表降雨與河床入滲為地下水的主要來源。
蘭陽平原	400	宜蘭縣(19)，共計 19 口。	呈等邊三角形，北以頭城，南以蘇澳，西以松羅為三個頂點，各邊長約30公里。本區河水部分滲入地下形成地下水，未滲入部分常沿沖積扇表面向下分流，沖積平原內的礫層與砂層為良好地下水層。
花蓮臺東縱谷區	930	花蓮縣(11)、臺東縣(8)，共計19口。	北起花蓮，南迄臺東，介於中央山脈與海岸山脈間，為一南北長約150公里，東西寬2至7公里的狹長縱谷。縱谷內沖積層極厚，主要由變質岩的礫石與砂所組成，孔隙發達，沖積扇的地表水易滲入地層中，形成地下水。
澎湖地區	127	澎湖縣(11)，共計 11 口。	由60餘個島嶼組成，其地層由上而下大致可分為海濱堆積層、石灰岩與澎湖層，其中，海濱堆積層為主要的淺層自由含水層。

地下水的水質特性為水體中包含礦物質，其中以氨、氮、硝酸鹽、氟鹽、鐵、錳、有機碳、鋁、鋅等較為常見，也受當地農業與工業發展的影響而產生汙染。對地下水資源威脅最大的為硝酸鹽，硝酸鹽的來源包括農業化肥、化糞池汙水等，飲水中若硝酸鹽含量過高有可能會造成孕婦流產、藍嬰症與癌症。工業汙染的案例亦有不少，1938年鐘淵曹達工業株式會社在臺南所設立的工廠，主要是為了配合日本海軍生產軍需品，後由台灣省行政長官公署接收後更名稱為臺鹼公司，該公司主要是生產五氯酚(除草劑)等，但在生產過程中會產生戴奧辛，對環境影響甚鉅，故於 1982 年關廠，該工廠早期生產時常採用汞為觸媒，廢水及廢棄物流入地下水層後，已造成鄰近的顯宮、四草、鹿門等三里共 1,282 戶里民的血液中戴奧辛含量偏高，後續整治費用高達新臺幣上百億元。1950 年代在西南沿海地區也曾發生烏腳病，病情為末梢血管堵塞造成患者雙足發黑，其病因為飲用的地下水中含砷、螢光物質或腐質酸所致。

2.3.2 地下水層與水井

水井(Well)如圖 2.3 所示，是汲取地下水資源之主要設施，通常是由地面垂直向下挖掘或鑽鑿一孔達到含水層，並於孔壁四周敷設井框或安裝井管而成。水井之建置因地層情況、用水需求、施工方法等不同條件，分成多種類型，諸如深淺井、群井、小管井、輻射井、橫井等，而其所需費用、抽水量、抽水位及適合之地質及水文條件亦不相同。水井依其用途分有兩類，一般是抽取地下水後加以使用之抽水井，另一為監測地下水之水位或水質的監測井。完整水井井體包含井管、濾料圈、井篩及沈砂管等裝置。井管是井體最主要的部分，應有足夠的強度以承受周圍地層的側向土壓、地下含水層的靜水壓力及下管時的施工外力等，同時又必須不易與地層材料、其他流體起化學反應。若井管無法承受這些壓力，井體就容易坍塌，若容易與其他物質反應，則容易腐蝕或積垢，因此其材質常是影響水井使用壽命的重要因素。濾圈(Filter Pack)之主要功能為避免含水層中的細顆粒土壤隨地下水流入井管而造成土壤流失，或將濾管阻塞致地下水無法順暢地流入井管中，因此在埋設井管後，會於井孔與井管間填充

濾料形成一濾料圈（或稱礫石圈，Gravel Pack）。井篩(Screen)的主要功用為提供通過濾圈之地下水進入井管中之通道，井篩長度及篩孔大小會影響出水量之多寡，也影響井管的整體強度。井篩形式繁多，有切縫式、鑽孔繞線式、百葉窗式等。沈砂管則為水井最底部之一段井管，銜接於最下層之濾水管下方，深置於不透水層內，管底封閉，與井外不相通，其主要功用為備供沈積侵入井體之細緻顆粒，使不致於積塞井管。皂土(Bentonite)之功能為封阻隔絕所監測之含水層與其他含水層間之連通性，避免雨水、地面水或不同含水層之地下水混流，影響水位或水質監測之正確性(經濟部水利署、國立成功大學，地層下陷防治服務團)。

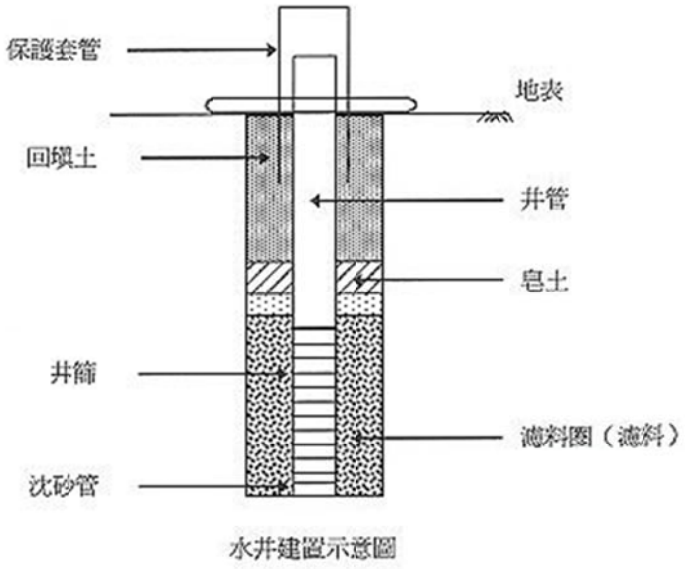

圖 2.3 水井建置示意圖

(經濟部水利署、國立成功大學，地層下陷防治服務團，2012/9/6 瀏覽)

地層按其滲透性可分為透水層與阻水層(單信瑜，2005)，含水層與阻水層之間的劃分是相對的，僅取決於地層透水性的大小。所謂含水層是指儲存有地下水並在自然條件或人為條件下，能流出水來的土層或岩層，如砂層、砂礫層等，是地下水貯存和流動的地方。有些岩層和黏土層雖然富含地下水，但幾乎不透水或透水性很低。一般來說滲透係數較小之地層稱為阻水層或拘限層，也可稱為不透水層，如黏土、頁岩等。

地面以下的第一個含水層，通常稱為非拘限含水層(Unconfined Aquifer)、或自由含水層(Phreatic Aquifer)，這個含水層中有一個『地下水位面』，地下水位面是指地下水的上部邊界，此水位面上的壓力為大氣壓力。若將水井打到此含水層中，則井中的水位面與地下水位面同高。通常地下水的含水層底部是低透水性的黏土或岩層，含水層本身則為透水性良好的土壤，在非拘限含水層以下，被兩層拘限層所包夾的含水層，稱為拘限含水層(Confined Aquifer)，若僅將水井打到該類含水層，其井中水位面會高於原先含水層之上方邊界，直至與大氣壓力產生平衡。無論是拘限或是非拘限含水層都會因人為鑿井抽水而造成水位或水壓降低，而形成一個以抽水井為中心的漏斗形曲面，一般稱之為洩降錐(Cone of Drawdown 或 Cone of Depression)。

2.3.3 地下水抽取量推估

地下水抽取推估方法有許多種，馮寶蓮(2006)使用經驗法、現地流量法與用電量法等三種方法，進行台南縣及高雄縣部分地區之抽水量的推估，亦即(1)經驗法：乃依據經濟部水利署所擬之「水井調查手冊(草案)」，所提出之抽水機進水口管徑與抽水量關係，查出每口水井之抽水量後推估計算地下水之總抽取量。(2)現地流量法：水井清查完成後，依各類用水不同，隨機抽樣於現地進行流量率定試驗，計算抽樣水井每分鐘抽水量後測估地下水之抽取量。(3)用電量法：係使用當地抽水馬達用電量進行地下水之抽取量的推估計算。因經驗法所推估之用水時數較不完整，僅供參考對照用，現地水井量測法在水井特性掌握上較經驗法可靠，而用電量法則可以清楚反映水井使用之真實情況，誤差範圍僅限某些較難調查之區，故可靠度為三者之最。

湯珠孝(2010)曾提出應用地下水歷線分析法推估屏東平原補注量及抽水量，該方法在降雨量豐、枯水期分明的區域，可以快速概估該區域補注量與抽水量，並可計算安全出水量。徐年盛等(2011)也曾提出應用地下水歷線及同位素分析法估算地下水系統之水文平衡情形，可推估各補注源之比例與補注量，依其方法對地下水之蓄水量歷線進行推估，結果顯示西元 1999 年至 2008 年之年平均蓄水變化量為 0.11 億噸，年

平均抽水量為14.08億噸,年平均補注量為17.57億噸,總補注中雨水占整體之55.9%，河水補注占整體之 14.3%，而區外補注達 29.8%。

丁崇峰等(2006)在水資源供需平衡條件下，利用相關統計資料，建立地下水抽取量的推估方法，藉由一維垂直入滲及二維河岸滲漏模式推估補注量，以推算地下水超抽量，並輔以他人所做之統計結果進行比較。結果顯示，民國 81~90 年間雲彰地區，兩地之超抽水量約在 0.5~6.7 億立方公尺。

而在數值模擬上則有引用 MODFLOW 地下水模式進行推估的方法。經濟部水利署水資源科技模式庫中曾介紹,MODFLOW 地下水模式是由美國地質調查所 Michael (1988)及 Arlen(1996)二人所發展之數值模式,其名來自於「模組化三維地下水流模式」(Modular Three-dimensional Groundwater Flow Model)之縮寫(McDonald 和 Harbaugh，1988，1996)。可應用於一維、二維及大部分的三維地下水流問題，無論是穩態、暫態、拘限含水層與非拘限含水層皆可加以模擬。侯依浩等人(2010)曾利用 MODFLOW 地下水流數值模擬軟體，建構濁水溪沖積扇之地下水流數值模型。張正緯等(2009)使用有限解析法與垂直分層技巧,發展一套可以根據地質分塊計算大範圍的三維地下水模式，補足 MODFLOW 在非拘限含水層之自由液面準確性計算不佳的問題。

2.3.4 地下水與地層下陷之關連性與所造成的災害

如表 2.2 所示，有 90%的地層下陷問題是因人類開發地下資源不當所致，此可以有效應力觀念的力學作用機制加以解釋：地下水超抽會引起地下水壓降低，因而荷重會轉移至土體上，造成地層的緊密度增加，故導致局部或區域性的地層下陷後果。地層下陷的現象為不可逆之反應，且目前技術並無法使已下沉之地表回復原貌，故須加以管控與限制地下水的開發，以減緩這個過程。

國立成功大學地層下陷防治服務團隊在民國 89 年到 98 年間,共清查了宜蘭縣、台北市、新竹縣市、苗栗縣、彰化縣、雲林縣、嘉義縣市、台南縣市、高雄縣市及屏東縣等 14 個縣市地區的水井數已超過 30 萬口，其中僅有約 1.8 萬口水井為具有水權

或有臨時用水執照，亦即僅約有 6%為合法水井。如圖 2.4 所示，部分地區私設水井的情況相當普遍。

表 2.2 自然因素與人為因素對地層下陷之發生率的影響比較(Freeze，2000)

地陷原因 / 比較項目	海水面上升	沉積物自然壓實	開採地下流體
地層下陷量(公分/年)	0.0~0.5	0.0~0.5	0.0~10.0
發生率(%)	5	5	90

超抽地下水所引發的地層下陷問題對土地、環境、工程建設、水資源利用、國土規劃、社會經濟與法令政策等等，均有相當重大的影響。此外，地層下陷通常會在密集抽水區域形成下陷中心並向四周擴散出去，有時候影響可能達數百平方公里。其對結構物的影響包括基礎會產生差異沉陷或承載力下降等，地下維生管線上也可能因受擠壓變形致不堪使用；部分沿海地區受地層下陷的影響，已造成海水入侵，其原因是淡水密度較低會浮在海水上，當大量抽取淡水時會造成淡水與海水之交界面不斷下降，使得海水發生入侵含水層的現象。海水入侵地下水層會導致土壤與水質的鹽化，造成地表植被及耕作的枯死。地層及土壤一旦被鹽化，就算是停抽地下水，讓地下水位回升，迫使海水退出地下水層，但地層及土壤已受鹽害，這是一個極難復原的災害。地層下陷後，部分低窪地區長年積水不退，不但造成土地利用上極大的不便，臨海地區更屢屢發生海水倒灌，使得土壤鹽害更加嚴重。對於交通層面來說亦已造成影響，高鐵啟用不到十年，但據蘋果日報記者李姿慧於 2012 年 4 月 2 日的報導，高鐵雲林沿線的地層下陷情況仍止不住，依監測資料顯示，高鐵跨台 78 線處兩年內之下陷量已達 14 公分，且多數路段雖有下陷趨緩之勢，但仍是警訊，若不改善，高鐵未來僅能開到台中，影響行車安全甚鉅。陳文福(2005)在台灣的地下水一書中提到：西部沿海一帶養殖業的年產值約有 270 億元，淨利約 45 億元，但政府後續所需投入的安全維

護費用甚高，例如：增建海堤、改建排水設施等均須耗費鉅資，若要依賴填土填回原地層高度，即需花費 800 億元以上的代價，因此如何合理的使用地下水是十分重要的課題。

圖 2.4 雲林地區私鑿的水井(謝適任攝，2012)

2.3.5 地層下陷之現況與嚴重地層下陷區域探討

如表 2.3 所示，許多國家都需面對地層下陷的問題。辜樹仁(2012)在天下雜誌 492 期的專題報導中指出：大陸上海市在 60 年內之地層下陷量已達 2.5 公尺，同時在大陸另有 49 個城市也遭遇相同的問題，總下陷面積已達 7.9 萬平方公里，比兩個台灣還大，其起因包括推動大量的基礎建設與興建超高樓層建築等。如圖 2.5 所示，依經濟部水利署地層下陷防治資訊網的資料顯示，歷年來全台各地除花蓮台東外皆有地層下陷的問題，目前彰化、雲林、嘉義、屏東等地區還在持續下陷，持續下陷的面積以雲林縣的 397.6 平方公里最為嚴重，最大下陷量則是以屏東的 3.39 公尺最為嚴重，而民國 100 年的最大下陷速率則以雲林與屏東的每年 6.8 公分為最快。

屏東地區在 1970 年後成為養殖漁業的重要地區，魚塭面積大量增加，1980 年台灣遇到大乾旱，屏東地區也在當年創下了一年下沉 68.9 公分的驚人紀錄；另 1994 年

也遇到乾旱，但並未下沉得如此嚴重，據推論應是 1980 年的大量抽水，取走孔隙中的水分已造成地層過度壓實。桃園地區雖也大量抽取地下水，卻未發生如此嚴重的下陷，因桃園地區為隆起的台地，地層已被壓縮過一次，故地層下陷也與當地之地質有關。

經濟部於民國 94 年 12 月公告並劃分嚴重地層下陷區域，其係以鄉鎮為單位加以劃定，凡是達到「地層下陷累積總量」或「近年地層下陷年平均速率」認定標準，且達到「易淹水區域」認定標準之鄉鎮，則該鄉鎮即被劃定為嚴重地層下陷區，其中包含彰化、雲林、台南、屏東等縣市，共涵蓋 24 個鄉鎮地區，詳細規定如 2.3.6 節所示。

表 2.3 世界上嚴重地層下陷區的比較(柳志錫、杜富麗、洪偉嘉，2003)

地區	最大下陷量(公尺)	下陷面積(平方公里)	發生期間
日本東京	4	190	1920~1970+
日本大阪	3	190	1928~1968
墨西哥墨西哥市	9	130	1938~1970+
美西亞歷桑大中部	2.3	130	1961~1969+
加州 Santa Clara 谷	4	650	1920~1970
San Joaquin 谷	2.9~9	11,000	1935~1970+
拉斯維加斯	1	500	1935~1963
大陸上海市	2.9	1,069	1963~1989

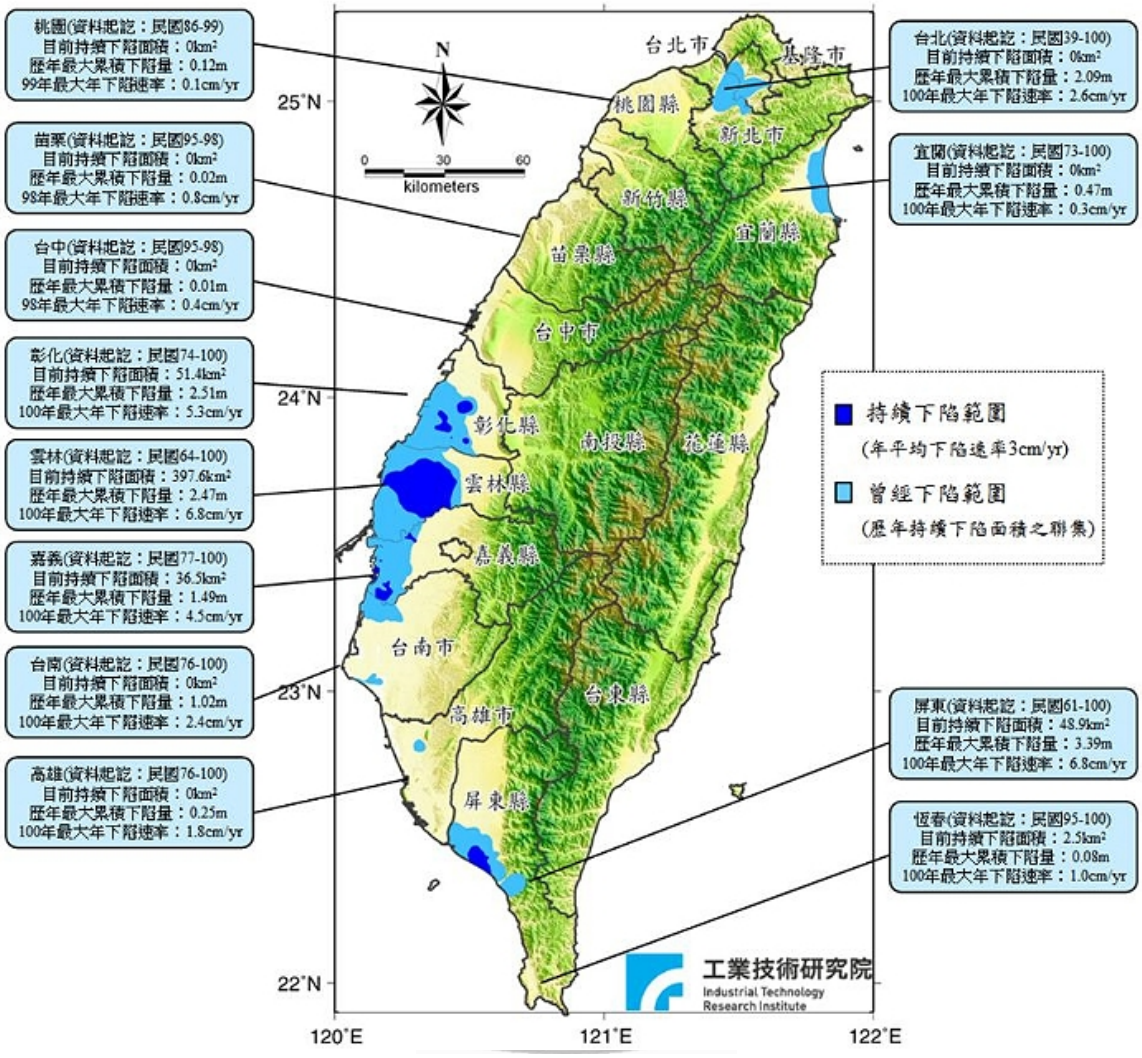

圖 2.5 民國 100 年度地層下陷檢測概況圖

(經濟部水利署，全球資訊網，基本水利資訊 -- 地層下陷，2013/1/21 瀏覽)

2.3.6 嚴重地層下陷地區劃設作業規範

民國 94 年 10 月 28 日，經濟部經授水字第 09420219000 號令，訂定嚴重地層下陷地區之劃設作業，如以下所示。

一、經濟部（以下簡稱本部）為辦理行政院核定之國土復育策略方案暨行動計畫，進行嚴重地層下陷地區劃設作業，特訂定本規範。

二、本規範劃設之嚴重地層下陷地區，係考量地層下陷累積總量、下陷年平均速率達一定程度以上，且對防洪、排水、禦潮或環境產生重大影響等相關因素劃定公告，

並刊登政府公報；變更時亦同。前項嚴重地層下陷地區，本部得每五年或依實際狀況檢討變更之。

三、本規範用詞定義如下：

(一)累積下陷量：指地面某定點自有檢測資料開始歷年高程之下陷總量。

(二)近年地層下陷年平均速率：指近五年內地面某定點之年平均下陷量。

四、劃設或變更嚴重地層下陷地區之參據資料如下：

(一)地層下陷資料：符合二等水準點閉合標準之地面高程檢測資料及本部水利署管理之地層下陷監測井資料。

(二)易淹水區域資料：以本部水利署繪製之感潮線、台灣地區常淹水地區及颱風豪雨水災常淹水地區等區域之聯集範圍為主，各縣（市）政府淹水地區調查資料為輔。

五、網格數據取得：將擬檢討地區分割為長寬各一公里之正方形網格，並將具有參據之累積下陷量與近年地層下陷年平均速率地層下陷檢測資料，經空間內插方法分配於網格。

六、網格狀態判釋原則如下：

(一)地層下陷明顯網格

符合下列任一目規定之網格，該網格即為地層下陷明顯網格：

1、累積下陷量達五十公分以上者。

2、近年地層下陷年平均速率達每年十公分以上者。

(二)嚴重地層下陷網格：前款地層下陷明顯網格，經判釋後位於易淹水區域內，該網格列為嚴重地層下陷網格。

七、嚴重地層下陷地區之劃設原則如下：

(一)經檢討嚴重地層下陷網格範圍達全鄉（鎮、市、區）面積百分之七十以上者，以全鄉（鎮、市、區）列為嚴重地層下陷地區。

(二)經檢討嚴重地層下陷網格範圍達全鄉（鎮、市、區）面積百分之三十以上，未達百分之七十者，得依應列入嚴重地層下陷地區範圍周邊之明顯地形、地貌、排水、道路或地段分界劃設為嚴重地層下陷地區範圍。但該劃設為嚴重地層下陷範圍不得小於應列入之嚴重地層下陷網格範圍。

(三)經檢討嚴重地層下陷網格範圍未達全鄉（鎮、市、區）面積百分之三十者，該鄉（鎮、市、區）不予列入嚴重地層下陷地區。

(四)本部依據農地釋出方案於八十八年一月二十八日以經（八八）水字第八八二六○○三○號公告之嚴重地層下陷區直接納入嚴重地層下陷地區範圍內。

八、嚴重地層下陷地區已完成防洪排水與防災設施之興建及改善工程，明顯可降低洪氾、暴潮或淹水災害發生頻率者，得依實際改善情況檢討修正嚴重地層下陷地區範圍。

九、進行劃設作業時，該鄉（鎮、市、區）於前五年均無符合第四點資料者，則視為資料不足，暫不予以檢討，俟資料完備後再依本規範辦理劃設作業。

2.3.7 政府施救措施與地下水管制辦法

由於地層下陷為不可逆之行為，只能採取預防與減緩沉降為主，經濟部、內政部等單位於民國 85 年開始陸續推動地層下陷防治工作，工研院能資所受經濟部水利署委託在部分地區設立地下水觀測網(經濟部水利署,地下水觀測網， 2012/9/22 瀏覽)，時時監測其地下水位的變化，如圖 2.6 與圖 2.7 所示。民國 87 年由經濟部水利署委託國立成功大學成立的地層下陷防治服務團隊(經濟部水利署，地層下陷防治智識服務計畫，2009)，以專職的人力協助中央業務主管機關進行相關業務的推動、協調、溝通、整合及執行，並建立幕僚技術，協助處理敏感地帶或地區之地層下陷問題，並提出對策加以分析及研討,也對地下水管制區與相關環境敏感地區的變化進行監控防治等，並定期舉辦多種活動，藉簡單的觀念宣導建立防治地層下陷的概念，使社會大眾更加清楚了解與重視相關問題。馬英九總統透過行政院經濟建設委員會，在 2008 年 12 月提出的「愛台 12 建設」計畫中(行政院經濟建設委員會,愛台 12 建設總體計畫，2013/1/21 瀏覽)，在防洪治水議題中曾明列「加強地下水補注，有效改善地層下陷」的目標，期望把全台持續下陷面積控制在 800 平方公里以內，深地層的最大平均壓縮速率控制在每年 5 公分內，並倡導改用海水供應養殖漁業的需要，以減少地下水的抽取量。

民國 87 年經濟部曾提出高屏大湖計畫，又名吉洋人工湖計畫，希冀能藉由該計畫調節荖濃溪豐枯期的水量，解決高屏地區的缺水危機，並補注地下水層(經濟部水利署，高屏大湖(第一階段工程)可行性研究，2008)。由「高屏大湖工程計畫－地下水文監測追蹤與檢討評估（99 年度）」的成果報告(經濟部水利署南區水資源局，2010)得知：由於荖濃溪的溪水含泥量過高，河水懸浮固體濃度偏高，底泥經篩分析與比重計分析後粒徑屬細沙、粉土與黏土，水力傳導係數為 1.3~1.7x10^{-6} 公尺/秒，屬低滲透性，入滲量會因孔隙堵塞而遞減，又該計畫牽涉環境保護等因素的考量，對當地居民的影響甚鉅，本計畫是否繼續推動，尚在評估中。

經濟部在民國 91 年 2 月曾訂定並發布地下水管制辦法，並於 95 年 2 月加以修正，全文共計 18 條。該辦法為依照水利法第 47 條之第一項規定訂定之，當主管機關考量地層下陷程度、地下水變化、地質條件等因素後，可據以劃定地下水管制區，該法在第五條有詳細規定管制區內鑿井引水需符合其規定，並經由主管機關核定後方可發放水權狀，並規定使用期限與使用量，管制範圍如圖 2.8 所示。

圖 2.6 雲林縣大埤鄉嘉興國小地下水觀測井 1(謝適任攝，2012)

圖 2.7 雲林縣大埤鄉嘉興國小地下水觀測井 2(謝適任攝，2012)

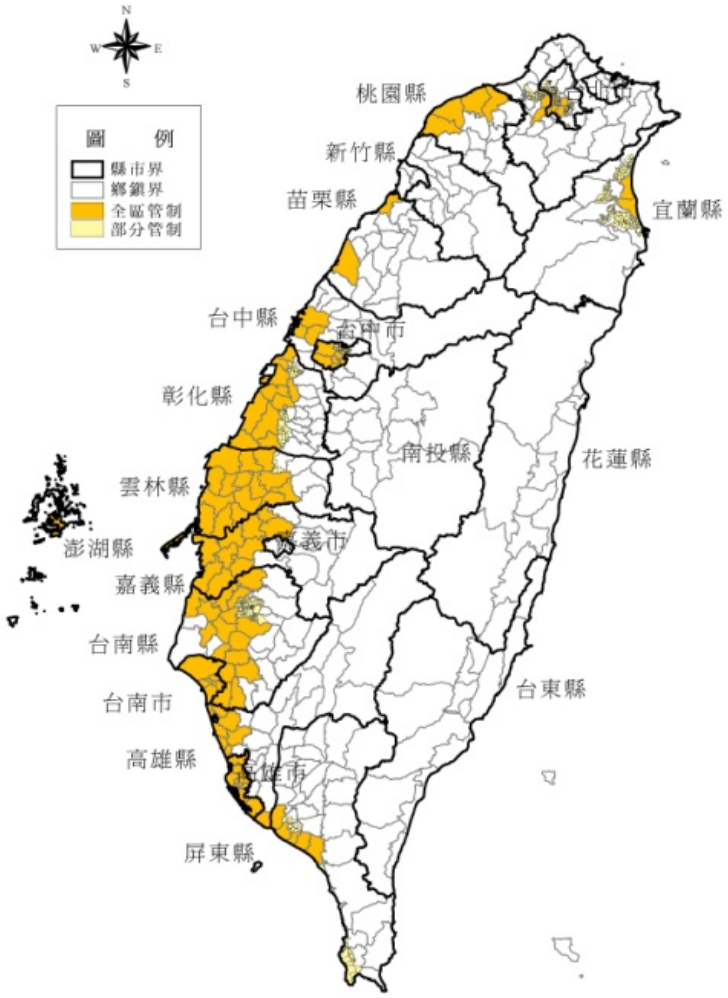

圖 2.8 地下水管制區
(經濟部水利署，全球資訊網，檔案下載 -- 水文技術組，2012/11/3 瀏覽)

2.4 有效應力

土壤結構為三相系統(Das，2005，2008)，由固體、液體與氣體所組成，固體土體形成孔隙排列，孔隙由水與空氣所佔據，當土壤受壓時，壓力也為三者所共同分擔，一般多半都是以總應力來推估土體受壓情形。一般而言，土壤與水可視為不可壓縮性質，但水無法承受剪力；除非在密閉空間內，不然空氣無法承受任何作用力。為了分析土體的壓縮、承載情況與應力分布特性，故有學者提出 Terzaghi 的有效應力觀念，如式(2.1)所示：

$$\sigma = \sigma' + p \text{，} \tag{2.1}$$

其中σ = 總應力，σ' = 有效應力，p = 孔隙水壓。

Skempton(1960)將其理論加以延伸，提出式(2.2)：

$$\sigma = \sigma' + \frac{p(\overline{\mathrm{A}} - a_s)}{\overline{\mathrm{A}}} = \sigma' + p(1 - a_s') \text{，} \tag{2.2}$$

其中$\overline{\mathrm{A}}$=土體的橫斷面積，a_s=土壤中固體與固體接觸點面積之總和，$a_s' = \frac{a_s}{\overline{\mathrm{A}}}$=每單位土壤橫斷面積內屬固體與固體接觸部分的面積。

有效應力為土壤橫斷面上，每單位土壤面積內，土壤固體顆粒形成之架構所承受之應力。土體中的有效應力會影響其體積變化與強度，有效應力增加會導致土壤顆粒更緊密的結合在一起，造成壓密之現象。有效應力的觀念為大地工程中最重要的觀念之一，土壤的壓縮性與抗剪強度等，多半皆與有效應力有關，在解決擋土結構所承受的橫向土壓力、基礎承載力與沉陷、邊坡穩定上皆有相關。

地震過後的土壤液化現象，也可依有效應力觀念加以說明。當地層受強烈地震影響時，土壤的顆粒會因震動更緊密結合在一起，土壤中之孔隙水壓因無法消散，而累積向地表宣洩之壓力，最後挾帶地層內之泥沙噴出地表形成噴砂孔，導致土壤的有效

應力大幅降低而影響土壤之承載力，造成上部結構的破壞，土壤液化通常好發於年輕的沖積地層或海埔新生地等疏鬆的沙土層。

2.5 Mathematica 介紹

Mathematica 為符號運算軟體(洪維恩，2001)，係美國 Wolfram 公司於 1988 年所開發出之數學運算軟體，不僅能運用於積分、微分、解析微分方程式等符號運算，亦可將結果以圖示方式予以可視化。Mathematica 能快速分析數據、驗證理論假設並整理研究之成果，已被廣泛應用在教學與研究方面，本文亦藉此套軟體輔助進行積分的運算。涂凱嵐(2010)曾提到 Mathematica 4.0 版本共有六點使用上較不便利的部分，包括：

1. 進行計算時，計算若有出錯，需將程式關閉後再重新啟動，否則程式會使用前面所宣告之數值繼續運算。
2. Mathematica 所推導出之結果無法與 MS Word 的方程式編輯器相容。
3. 使用 Mathematica 進行等壓線繪圖時，需於官方網站下載相關輔助軟件，對於初次使用的使用者而言，較難蒐尋到該輔助軟件。
4. Mathematica 之繪圖，部分結果需以人工方式進行幕後製作。
5. Mathematica 運算過於複雜的算式，需要拆分為較小之計算單元再進行組合。
6. Mathematica 所計算的結果化簡後，仍會有計算式無法以該軟體作最精簡之化簡，需藉由人工化簡才能獲得較簡易之計算結果。

本研究在使用 Mathematica 符號運算軟體進行相關計算之過程中，亦需面對以上所述六點的困擾，另外發現使用 Full Simplify 化簡功能或進行較多運算時，偶爾會發生運算時間極長的情況，強制關閉會造成運算檔案的損毀，需重新開啟並全部重新輸入運算式。

2.6 抽水所引致沉陷之基本理論公式探討

2.6.1 前言

如前所述，土壤結構為三相系統，是由固體、液體與氣體所組成，固體的土體顆粒會形成空隙且隨機的排列，而空隙會被水與空氣所佔據，當土壤受壓時，也會由這三者共同分擔。當地下水被抽取後，原本由水所承受的壓應力會轉至土壤顆粒造成壓密。呂志宗(1991)提到 Terzaghi 於 1923 年首先提出單向度壓密理論，其一維壓密理論之基本假設為：

1. 土壤為均質且完全飽和。
2. 固體土壤顆粒與孔隙水不可壓縮。
3. 孔隙水在孔隙中流動符合 Darcy 定律。
4. 土壤孔隙率不隨介質內部有效應力大小而改變。
5. 土壤體積的縮小是因為孔隙被壓縮所致。
6. 土壤之力學性質與滲流性質皆考慮為均質且等向性。

實際上土壤的壓縮性和水分排出並非單向，故以上所述 Terzaghi 的單向度壓密理論之基本假設僅適用於特殊壓密情況下。呂志宗(1991)曾提及：「Terzaghi 的壓密理論過度簡化問題，對於一維壓密沉陷而言問題不大，但若欲應用在解析三維壓密沉陷問題時，實需斟酌。雖然 Terzaghi 的單向度壓密理論簡易，而常被工程界應用於壓密沉陷分析，然而以較嚴謹之 Biot 三維壓密理論解析壓密沉陷問題，為深入研究此類問題之所需。」本文在研究與建立問題之基本方程式時，係使用 Biot(1941)所建立之三維壓密理論，學理上亦稱之為多孔介質彈性力學理論 (Poroelasticity)。

2.6.2 Biot 於 1941 年所建立之多孔介質彈性力學理論

Biot 於 1941 年首先提出土壤的三維多孔介質彈性力學理論，其基本假設為考慮孔隙水與固體土壤顆粒皆可壓縮，土壤為均質且等向性之多孔隙介質，並假設孔隙水在孔隙中的流動符合 Darcy 定律，在探討多孔介質之組成律關係時，若考慮固體介質

與孔隙流體間的互制作用關係，且模擬多孔介質為等向性之飽和線彈性體，則其組成律關係可表示為：

$$\tau_{ij} = \lambda u_{k,k}\delta_{ij} + \mu\left(u_{i,j} + u_{j,i}\right) - \alpha p\delta_{ij} \tag{2.3}$$

$$\theta = \alpha u_{k,k} + \frac{1}{Q}p \tag{2.4}$$

其中

τ_{ij} = 作用於多孔介質之總應力；

θ = 單位多孔介質體積內所增加之孔隙流體體積；

p = 超額孔隙流體壓力 (壓力為正)；

$u_{i,i} = \frac{\partial u_1}{\partial x_1} + \frac{\partial u_2}{\partial x_2} + \frac{\partial u_3}{\partial x_3} = \frac{\partial u_x}{\partial x} + \frac{\partial u_y}{\partial y} + \frac{\partial u_z}{\partial z}$ = 多孔介質之體積應變量；

δ_{ij} = Kronecker delta 函數；

μ = 含水層之剪力模數；

λ = Lame 常數 = $\frac{E\nu}{(1+\nu)(1-2\nu)}$；

ν = 含水層於排水情況下所測得之柏松比；

Q、α = 固體介質與孔隙流體間之互制作用係數。

因考慮孔隙流體的流動符合 Darcy 定律，則：

$$v_i = -\frac{k}{\gamma_f}p_{,i} \tag{2.5}$$

其中

v_i = 孔隙流體之流速；

k = 多孔介質之滲透係數；

γ_f = 孔隙流體之單位重；

$p_{,i} = \frac{\partial \mathrm{p}}{\partial x_i}$ (i = 1,2,3) = 超額孔隙流體壓力之壓力梯度。

將 Darcy 定律式代入考慮多孔介質徹體力(Body Force) f_i與孔隙流體補注變率 q 之力平衡方程式(2.6)與流量連續方程式(2.7)中：

$$\tau_{ij,j} + f_i = 0 \tag{2.6}$$

$$\dot{\theta} + v_{k,k} = q \tag{2.7}$$

則理論模式之基本方程式可表示為：

$$(\lambda + \mu)u_{k,ki} + \mu u_{i,kk} - \alpha p_{,i} + f_i = 0 \tag{2.8}$$

$$-\frac{k}{\gamma_f} p_{,kk} + \alpha \dot{u}_{k,k} + \frac{1}{Q}\dot{p} - q = 0 \tag{2.9}$$

其中$\dot{u}_{k,k} = \frac{\partial u_{k,k}}{\partial t}$。上式即引用$\alpha$、$\mu$、$\lambda$、$Q$等基本力學常數建立基本方程式，以試驗獲取這些力學常數時，須考慮固體介質與孔隙流體間之互制力學行為的變化。而 n、k、γ_f等係數，則是屬於土壤之物理性質或孔隙水之水利常數。

2.6.3 Biot 建立之多孔介質彈性力學理論發展

Biot 於 1955 年引入孔隙率(Porosity) n 的觀念，說明作用於多孔隙介質之孔隙流體壓力變化量，再以孔隙流體與固體介質間會產生相對位移的現象來分析多孔隙介質的位移變化，並將其理論推廣至異向性介質的情況。若考慮多孔介質為等向性之飽和線彈性體，則其組成律關係可表示為：

$$\tau_{ij} = \lambda u_{k,k}\delta_{ij} + \mu\left(u_{i,j} + u_{j,i}\right) - n\frac{Q+R}{R} p\delta_{ij} \tag{2.10}$$

$$\theta = n\frac{Q+R}{R} u_{k,k} + \frac{n^2}{R} p \tag{2.11}$$

式中τ_{ij}、θ、u_i、p、δ_{ij}、μ、λ之定義與式(2.3)與式(2.4)相同，Q 與 R 分別為新定義之固體介質與孔隙流體間的互制作用參數，亦即此力學常數 Q 與式(2.4)之定義並不

相同，上式所引用之力學常數 R、μ、λ、Q 與 Biot(1941)文獻中所出現之力學常數 A、N、S 的關係為：

$$\mu = N \tag{2.12}$$

$$\lambda = S = A - \frac{Q^2}{R} \tag{2.13}$$

將 Darcy 定律式(2.5)、式(2.10)、式(2.11)代入力平衡方程式(2.6)與流量連續方程式(2.7)中，則理論模式之基本方程式可表示為：

$$(\lambda + \mu)u_{k,ki} + \mu u_{i,kk} - n\frac{Q+R}{R}p_{,i} + f_i = 0 \tag{2.14}$$

$$-\frac{k}{\gamma_f}p_{,kk} + n\frac{Q+R}{R}\dot{u}_{k,k} + \frac{Q^2}{R}\dot{p} - q = 0 \tag{2.15}$$

Biot 於 1956 年為了研討介紹多孔隙介質之彈性動力學模式，曾引用基本力學常數α、μ、λ、M建立理論模式之基本方程式，其中互制力學常數 M 與 Biot 於 1941 年所定義之力學常數 Q 相同，並仍沿用在 1955 年所介紹之相對位移的觀念建立基本方程式。為方便比較，故相關方程式的表示方式盡量與 2.6.2 節相同，其中在單位多孔隙介質體積內增加之孔隙流體體積θ改以ζ表示。若考慮多孔介質為等向性之飽和線彈性體，則其組成律關係可表示為：

$$\tau_{ij} = \lambda u_{k,k}\delta_{ij} + \mu\left(u_{i,j} + u_{j,i}\right) - \alpha p\delta_{ij} \tag{2.16}$$

$$\theta = \zeta = \alpha u_{k,k} + \frac{1}{M}p \tag{2.17}$$

式中各項物理量或參數符號皆與 2.6.2 節所述相同。將 Darcy 定律式(2.5)、式(2.16)、式(2.17)代入力平衡方程式(2.6)與流量連續方程式(2.7)中，則理論模式之基本方程式可表示為：

$$(\lambda+\mu)u_{k,ki}+\mu u_{i,kk}-\alpha p_{,i}+f_i=0 \tag{2.18}$$

$$-\frac{k}{\gamma_f}p_{,kk}+\alpha\dot{u}_{k,k}+\frac{1}{M}\dot{p}-q=0 \tag{2.19}$$

再將相關力學常數加以比較後可知：

$$M=Q=\frac{R}{n^2} \tag{2.20}$$

$$\alpha=n\frac{Q+R}{R} \tag{2.21}$$

多孔隙介質壓密理論經過 20 餘年的發展後已漸廣為應用，其中所引用的多孔介質彈性力學參數已經容易由基本力學試驗得知。1976 年由 Rice 與 Cleary 引用流體不排出情況下所測得的波松比ν_u、與 Skempton 孔隙流體壓力常數 *B*(即圍壓變化引起的超額孔隙水壓變化量/圍壓變化量)，改寫 Biot 於 1941 年所建立之理論模式中所使用的基本力學常數，所使用的基本力學常數包括ν_{u}、μ、λ、*B*。若考慮多孔介質為等向性之飽和線彈性體，則其組成律關係可表示為：

$$\tau_{ij}=\lambda u_{k,k}\delta_{ij}+\mu\left(u_{i,j}+u_{j,i}\right)-\frac{3(\nu_u-\nu)}{B(1-2\nu)(1+\nu_u)}p\delta_{ij} \tag{2.22}$$

$$\theta=\frac{3(\nu_u-\nu)}{B(1-2\nu)(1+\nu_u)}u_{k,k}+\frac{9(\nu_u-\nu)(1-2\nu_u)}{2\mu B^2(1-2\nu)(1+\nu_u)^2}p \tag{2.23}$$

式中ν_u= 含水層於不排水情況下所測得之柏松比；其他各項物理量或參數符號皆與 2.6.2 節相同，其中ν為考慮流體在排出情況下所測得之多孔隙介質的波松比，其與力學常數μ、λ的關係為：

$$\nu=\frac{\lambda}{2(\lambda+\mu)} \tag{2.23}$$

將 Darcy 定律式(2.5)、式(2.22)、式(2.23)代入力平衡方程式(2.6)與流量連續方程式(2.7)中，則理論模式之基本方程式可表示為：

$$(\lambda+\mu)u_{k,ki}+\mu u_{i,kk}-\frac{3(\nu_u-\nu)}{B(1-2\nu)(1+\nu_u)}p_{,i}+f_i=0 \tag{2.24}$$

$$-\frac{k}{\gamma_f}p_{,kk}+\frac{3(\nu_u-\nu)}{B(1-2\nu)(1+\nu_u)}\dot{u}_{k,k}+\frac{9(\nu_u-\nu)(1-2\nu_u)}{2\mu B^2(1-2\nu)(1+\nu_u)^2}\dot{p}-q=0 \tag{2.25}$$

Bear 與 Verruijt 於 1987 年引用地下水流動觀點，重新建構 Biot 三維壓密理論，在探討地層壓密沉陷的現象時，將其變形過程視為另一種流體的流動，所以固體介質的變化與地下流體流動需皆滿足質量守恆定理，理論模式之基本假設為：

一、土壤完全飽和。

二、孔隙水為可壓縮流體，並且壓縮流體密度的改變主要與孔隙水壓的改變有關。

三、土壤之固體顆粒不可壓縮。

四、孔隙水在孔隙中流動須符合 Darcy 定律。

五、孔隙率 n 主要受介質之有效應力的影響。

根據以上假設，由質量守恆定律得知，固體介質的變化與地下流體流動需皆滿足質量守恆定理，即：

$$\nabla\cdot(n\rho_w\vec{v}_w)+\frac{\partial(n\rho_w)}{\partial t}=0 \tag{2.26}$$

$$\nabla\cdot[(1-n)\rho_w\vec{v}_s]+\frac{\partial[(1-n)\rho_s]}{\partial t}=0 \tag{2.27}$$

其中

ρ_s、ρ_w = 固體土壤與孔隙水之密度；

$\vec{v}_s$、$\vec{v}_w$ = 固體土壤之運動速度與孔隙水流速。

根據基本假設，式(2.26)、式(2.27)可改寫為：

$$\nabla\cdot[n(\vec{v}_w-\vec{v}_s)]+\frac{\partial\varepsilon}{\partial t}+n\beta\frac{\partial p}{\partial t}=0 \tag{2.28}$$

其中ε為土壤介質之體積應變量；β為孔隙水之壓縮係數，其係定義為：

$$\beta = \frac{1}{\rho_w}\frac{\partial \rho_w}{\partial p} \tag{2.29}$$

設孔隙水的流動符合 Darcy 定律：

$$n(\vec{v}_w - \vec{v}_s) = -\frac{k}{\gamma_w}\nabla p \tag{2.30}$$

其中

k = 含水層滲透係數；

γ_w = 孔隙水之單位體積重 = $\rho_w g$，g為重力加速度。

將 Darcy 定律式(2.30)代入式(2.28)，可將質量守恆方程式改寫為：

$$-\frac{k}{\gamma_w}\nabla^2 p + \frac{\partial \varepsilon}{\partial t} + n\beta\frac{\partial p}{\partial t} = 0 \tag{2.31}$$

再引用 Terzaghi 的有效應力觀念將多孔介質之組成律表示為：

$$\tau_{ij} = 2\mu\varepsilon_{ij} + \lambda\varepsilon\delta_{ij} + p\delta_{ij} \tag{2.32}$$

式中各項物理量或參數符號皆與 2.6.2 節相同，式(2.32)需滿足力平衡方程式，即 $\tau_{ij,j} = 0$，由應變位移的線性關係式(2.32)配合力平衡方程式，可得以介質位移和孔隙水壓力為變數之基本方程式：

$$\mu\nabla^2 u_i + \mu(2\eta - 1)\varepsilon_{,i} - p_{,i} = 0 \tag{2.33}$$

式中$\eta = \frac{1-\nu}{1-2\nu}$。式(2.31)與式(2.33)構成飽和等向性多孔介質之基本方程式。

2.7 結語

本研究是採用數學模擬方式，研討出抽水所引致地層下陷問題之三維壓密解析解，

故針對地層下陷相關議題進行深入之文獻回顧。於後續研究中，擬將含水層模擬為一飽和之半無線域多孔介質，再採用呂志宗(1991)所研討出之點抽水所引致的三維壓密沉陷基本解，探討線形抽水所引起的地表垂直位移、水平位移與超額孔隙水壓。研究過程中，需引用符號運算軟體 Mathematica 做適當之線積分運算，故亦針對該軟體之優缺點進行深入的研討，相關之應用將呈現於論文第三章與第四章。

第三章　數學模式分析結果

3.1 前言

本章節係引用呂志宗(1991)的研究成果進行後續之相關研究，其研究是採用積分轉換方法對點抽水問題之數學模式進行解析，推導出半無限域地層受點抽水影響之穩態及暫態基本解。本文擬採用其所推導出之點抽水問題的穩態基本解，進一步研討出線狀抽水問題之穩態閉合解。本文是將地層模擬成均質等向性之線彈性飽和多孔介質，分別將地表邊界模擬成透水與不透水邊界兩種情況，然後做適當之座標轉換與線積分，再於第四章進行參數影響分析。所研討出之結果包括抽水所引起的地表最大垂直暨水平位移量及其發生位置，關於地層孔隙水壓之變化情況亦加以探討。

3.2 點抽水問題之閉合解

3.2.1 準備工作

本文所考慮的基本假設為：

一、模擬地層為均質之線彈性飽和多孔隙介質，分別考慮地層之力學行為與滲流性質皆為等向性，等向性係指地層於任意方向的性質皆相同。

二、忽略與時間有關之暫態行為，僅考慮穩態情況下，地層長期壓密行為與滲流行為之變化，故問題之數學模式與時間變數無關。

三、考慮孔隙水滲流遵守 Darcy 定律與質量守恆定律，地層力學行為變化服從牛頓第二定律、地層組成律與虎克定律等，且地層之壓密行為適於以線彈性飽和多孔介質彈性力學理論進行數學模擬。

四、考慮抽水強度與抽水速率恆保持定值，抽水時假設含水層中之地下水補注量與抽水量相等，故可考慮抽水行為持續且不間斷。

五、模擬地層為一半無限域，地表邊界為一無限延伸之水平面。若抽水所引致三維壓密沉陷問題之擾動效應、尺度效應及邊界效應等，符合一定距離以外對含水層的

影響已相當微小的考量時，半無限域地層的模擬方式即適用於現地情況。

六、考慮地表邊界為完全透水與完全不透水兩種邊界情況，是因考慮地表面可能會覆蓋著綠地、景觀植物、透水磚等透水性較佳之材料，故可將地表邊界模擬為透水情況；另外，也考慮地表邊界有可能大範圍鋪設柏油、混凝土或是有地上物等不利於水滲漏至地表以下之情況，故將地表模擬為不透水情況較為合適。

七、地表之力學邊界條件則考慮為無應力變化情況，其意係指地表面之受力無增加或減少的情況。

本文是將地層模擬為一半無限域，再討論抽水時所引致之地層力學與滲流行為等，因係考慮地層之長期壓密沉陷行為，所以在數學模式中並不考慮時間因素的影響。今若考慮地表邊界上($z = 0$)無應力變化且為透水情況，則地表邊界條件可表示為：

$$\sigma'_{rz}(r,0) = G\left[\frac{\partial u_r(r,0)}{\partial z} + \frac{\partial u_z(r,0)}{\partial r}\right] = 0 \tag{3.1a}$$

$$\sigma'_{zz}(r,0) = \frac{2G}{1-2\nu}\left[\frac{\partial u_r(r,0)}{\partial r} + \frac{\partial u_r(r,0)}{\partial r}\right] + \frac{2G(1-\nu)G}{1-2\nu}\frac{\partial u_z(r,0)}{\partial z} = 0 \tag{3.1b}$$

$$p(r,0) = 0 \tag{3.1c}$$

其中$p(r,0) = 0$亦可解釋為地表邊界上無壓力差或孔隙水壓可完全消散情況。

若將地表邊界模擬為無應力變化且為不透水情況，則地表邊界條件可表示為：

$$\sigma'_{rz}(r,0) = G\left[\frac{\partial u_r(r,0)}{\partial z} + \frac{\partial u_z(r,0)}{\partial r}\right] = 0 \tag{3.2a}$$

$$\sigma'_{zz}(r,0) = \frac{2G}{1-2\nu}\left[\frac{\partial u_r(r,0)}{\partial r} + \frac{\partial u_r(r,0)}{\partial r}\right] + \frac{2G(1-\nu)G}{1-2\nu}\frac{\partial u_z(r,0)}{\partial z} = 0 \tag{3.2b}$$

$$\frac{\partial p(r,0)}{\partial z} = 0 \tag{3.2c}$$

以下針對式(3.2c)中$\frac{\partial p(r,0)}{\partial z} = 0$之工程意義加以說明，由 Darcy 定律 $Q = kiA$ 且壓力梯度 $i = -\frac{\partial p(r,z)}{\partial z}$得知，Darcy 定律式可改寫為 $Q = -k\frac{\partial p(r,z)}{\partial z}A$。當考慮地表邊界無滲流

量 Q 時，因地層滲透係數 k 不為零，且水流通過的截面積 A 之值亦不為零，故 Darcy 定律式中之$\frac{\partial p(r,z)}{\partial z}=0$，亦即在不透水邊界上的超額孔隙水壓之壓力梯度為零或孔隙水壓呈無法消散之情況。

為解析出問題之閉合解，數學模式中需建立另一組合理之無限深遠處($z\to\infty$)的合適邊界條件。因含水層是模擬為一半無限域，故在無限深遠處之所有物理變量可考慮為均不受抽水的影響，亦即：

$$\lim_{z\to\infty}\{u_r(r,z)\}\to 0 \tag{3.3a}$$

$$\lim_{z\to\infty}\{u_z(r,z)\}\to 0 \tag{3.3b}$$

$$\lim_{z\to\infty}\{p(r,z)\}\to 0 \tag{3.3c}$$

本文是考慮未抽水前，問題之初始應力、位移、超額孔隙水壓等均處於平衡狀態，開始抽水後會形成一擾動作用源，此擾動作用源會引起地層之三維壓密沉陷現象，本研究是擬探討長期穩定抽水所引起的含水層水平位移、垂直位移和超額孔隙水壓等，故問題之數學模式與時間變數無關聯。當抽水作用發生時，因含水層中之孔隙流體壓力下降時，會伴隨有效應力逐漸增加，故引致含水層的壓密沉陷現象。

本文是將含水層模擬為等向性，所謂的等向性含水層是指含水層於任意方向的性質皆相同。如式(3.1c)與式(3.2c)所示，本文是將地表模擬為透水與不透水兩種情況。將地表模擬為透水情況的考慮，是因為地表可能會覆以透水磚、綠地或景觀植物等；而將地表模擬為不透水情況時，則是考慮地表可能覆蓋著柏油路、混凝土或建築物等。針對以上兩種情況進行分析與探討，將有助於進一步了解抽水所引致之壓密沉陷問題。

3.2.2 點抽水之問題之解

本研究根據呂志宗(1991)所研討出之點抽水問題的基本解進行後續之研討，茲考慮將座標 z 軸通過抽水點，則問題可簡化為軸對稱問題，故可以軸對稱圓柱座標系統 (r,z)表示三維壓密理論之基本方程式，所分析之點抽水問題如圖 3.1 所示。

如前所述，含水層力學行為與滲流性質均模擬為等向性。基於此，當地表模擬為透水情況時，含水層因抽水所引致之水平位移、垂直位移和超額孔隙水壓等可分別表示為：

$$u_r(r,z)=\frac{Q\gamma_w}{16\pi G\eta k}\left[-\frac{r}{R_{(1)}}+\frac{r}{R^*_{(a)}}-\frac{2\eta+1}{2\eta-1}\frac{hr}{R_{(a)}R^*_{(a)}}+\frac{rz}{R_{(a)}R^*_{(a)}}+\frac{2hrz}{R^3_{(a)}}\right] \quad (3.4a)$$

$$u_z(r,z)=\frac{Q\gamma_w}{16\pi G\eta k}\left[-\frac{z-h}{R_{(1)}}+\frac{2\eta+1}{2\eta-1}\frac{h}{R_{(a)}}+\frac{z}{R_{(a)}}+\frac{2hz(z+h)}{R^3_{(a)}}\right] \quad (3.4b)$$

$$p(r,z)=-\frac{Q\gamma_w}{4\pi k}\left[\frac{1}{R_{(1)}}-\frac{1}{R_{(a)}}\right] \quad (3.4c)$$

其中

u_r = 含水層之水平位移；

u_z = 含水層之垂直位移；

p = 超額孔隙水壓；

r = 水平距離座標變數；

z = 垂直距離座標變數；

h = 抽水深度；

Q = 點抽水量；

γ_w = 水的單位重；

G = 含水層之剪力模數(Shear Modulus)；

v = 柏松比(Poisson Ratio)；

η = $\frac{1-v}{1-2v}$；

k = 含水層之滲透係數；

$R_{(1)}=\sqrt{r^2+(z-h)^2}$；

$R^*_{(1)}=\sqrt{r^2+(z-h)^2}+|z-h|$；

$R_{(a)}=\sqrt{r^2+(z+h)^2}$；

$R^*_{(a)}=\sqrt{r^2+(z+h)^2}+z+h$。

當地表模擬為不透水情況，仍考慮含水層力學與滲流性質均模擬為等向性，則抽水所引致含水層之水平位移、垂直位移和超額孔隙水壓等可分別表示為：

$$u_r(r,z)=\frac{Q\gamma_w}{16\pi G\eta k}\left[-\frac{r}{R_{(1)}}+\frac{r}{R^*_{(a)}}-\frac{2\eta+1}{2\eta-1}\frac{hr}{R_{(a)}R^*_{(a)}}+(-4\eta+1)\frac{rz}{R_{(a)}R^*_{(a)}}+\frac{2hrz}{R^3_{(a)}}\right] \quad (3.5a)$$

$$u_z(r,z)=\frac{Q\gamma_w}{16\pi G\eta k}\left[-\frac{z-h}{R_{(1)}}+\frac{2\eta+1}{2\eta-1}\frac{h}{R_{(a)}}+(-4\eta+1)\frac{z}{R_{(a)}}+\frac{2hz(z+h)}{R^3_{(a)}}+4\eta\sinh^{-1}\frac{z+h}{r}\right] \quad (3.5b)$$

$$p(r,z)=-\frac{Q\gamma_w}{4\pi k}\left[\frac{1}{R_{(1)}}+\frac{1}{R_{(a)}}\right] \quad (3.5c)$$

其中所示各項物理量或參數符號皆與式(3.4a)~(3.4c)相同。以上所示點抽水問題之基本解，可作為本文後續探討如圖 3.2 所示線狀抽水問題之基礎。

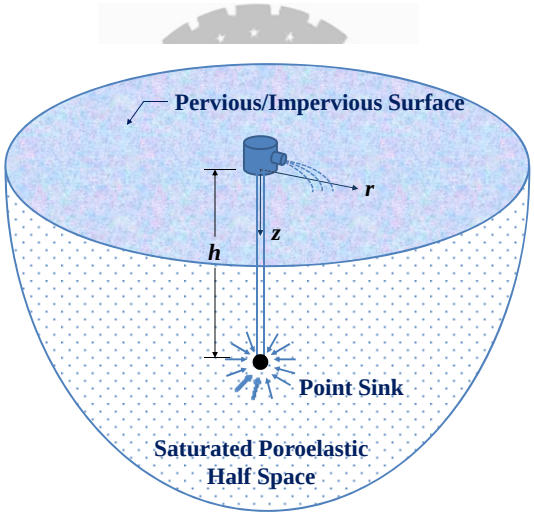

圖 3.1　點抽水問題示意圖

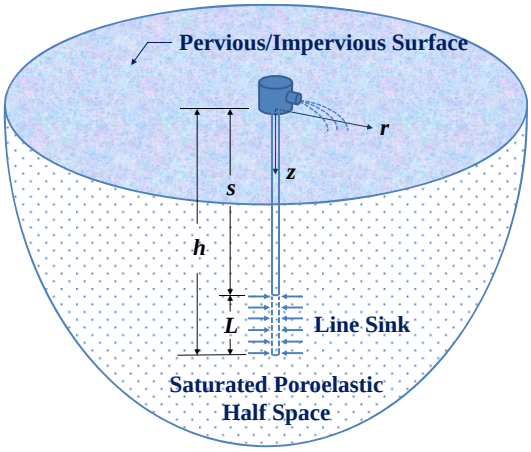

圖 3.2　線狀抽水問題示意圖

3.3 線狀抽水問題之解

為推求如圖 3.2 所示之含水層受線狀抽水影響時的穩態閉合解，可先考慮在線上取 ds 的長度（相當於點抽水之元素）、線抽水之強度為 q（單位：m^3/sm）、地表至點抽水元素之距離為 s，則 qds 相當於點抽水之強度 Q（單位：m^3/s），s 相當於點抽水深度 h。只要再針對線狀抽水長度進行積分，即可研討出線狀抽水問題的閉合解，解析過程會使用 Mathematica 數學符號運算軟體進行積分運算。

茲考慮線狀抽水長度為 L，基於式(3.4a)~(3.4c)、式(3.5a)~(3.5c)，將其中之符號 Q 改寫為 qds、變數 h 改寫為 s，且$R_{(1)}=\sqrt{r^2+(z-s)^2}$、$R^*_{(1)}=\sqrt{r^2+(z-s)^2}+|z-s|$、$R_{(a)}=\sqrt{r^2+(z+s)^2}$。基於此，再對其中之變數 s 進行[h-L,h]範圍之線積分，即可研討出線狀抽水所引起的地層水平位移、垂直位移和超額孔隙水壓，如以下所示：

$$u_r(r,z)=\frac{q\gamma_w}{16\pi G\eta k}\int_{h-L}^{h}\left(-\frac{r}{R_{(1)}}+\frac{r}{R^*_{(a)}}-\frac{2\eta+1}{2\eta-1}\frac{sr}{R_{(a)}R^*_{(a)}}+\frac{rz}{R_{(a)}R^*_{(a)}}+\frac{2srz}{R^3_{(a)}}\right)ds \tag{3.6a}$$

$$u_z(r,z)=\frac{q\gamma_w}{16\pi G\eta k}\int_{h-L}^{h}\left(-\frac{z-s}{R_{(1)}}+\frac{2\eta+1}{2\eta-1}\frac{s}{R_{(a)}}+\frac{z}{R_{(a)}}+\frac{2sz(z+s)}{R^3_{(a)}}\right)ds \tag{3.6b}$$

$$p(r,z)=-\frac{q\gamma_w}{4\pi k}\int_{h-L}^{h}\left(\frac{1}{R_{(1)}}-\frac{1}{R_{(a)}}\right)ds \tag{3.6c}$$

其中

$R_{(1)}=\sqrt{r^2+(z-s)^2}$；

$R^*_{(1)}=\sqrt{r^2+(z-s)^2}+|z-s|$；

$R_{(a)}=\sqrt{r^2+(z+s)^2}$；

$R^*_{(a)}=\sqrt{r^2+(z+s)^2}+(z+s)$。

式(3.6a)~(3.6c)進行線積分之結果如以下所示：

$$u_r(r,z)=\frac{q\gamma_w}{8\pi G\eta k}\left\{\frac{h^3+zh^2+(r^2-2z^2)h-2z(r^2+z^2)}{rR_{z+h}}-\frac{2[(h-L)^3+z(h-L)^2+(r^2-2z^2)(h-L)-2z(r^2+z^2)]}{rR_{z+h-L}}+\right.$$
$$\left.\frac{r}{2}\left[ln\frac{\sqrt{r^2+(z-h+L)^2}-(z-h+L)}{\sqrt{r^2+(z-h)^2}-(z-h)}+(1-2\nu)ln\frac{R^*_{z+h-L}}{R^*_{z+h}}\right]+\frac{3(R_z^2+h^2)+4hz}{R_{z+h}}-\right.$$
$$\left.\frac{3[R_z^2+(h-L)^2]+4(h-L)z}{R_{z+h-L}}\right\} \quad (3.7a)$$

$$u_z(r,z)=\frac{q\gamma_w}{16\pi G\eta k}\left\{R_{z-h}-R_{z-h+L}+4\nu\left(R_{z+h-L}-R_{z+h}+zln\frac{R^*_{z+h}}{R^*_{z+h-L}}\right)+\frac{3(R_z^2+h^2)+4hz}{R_{z+h}}-\right.$$
$$\left.\frac{3[R_z^2+(h-L)^2]+4(h-L)z}{R_{z+h-L}}\right\} \quad (3.7b)$$

$$p(r,z)=\frac{q\gamma_w}{4\pi k}\{\ln(R^*_{z+h}*R^*_{z-h})+ln\frac{R^*_{z+h-L}}{R^*_{z-h-L}}\} \quad (3.7c)$$

式中

$R_i=\sqrt{r^2+i^2}$，$i=z$、$z+h$、$z-h$、$z+h-L$、$z-h+L$；

$R^*_i=R_i+i$，$i=z+h$、$z+h-L$。

其餘各項物理量或參數符號皆與 3.2 節相同。

若考慮地表為不透水情況，則線狀抽水所引致的地層水平位移、垂直位移、和超額孔隙水壓可表示為：

$$u_r(r,z)=\frac{q\gamma_w}{8\pi G\eta k}\left\{\frac{h^3+zh^2+(r^2-2z^2)h-2z(r^2+z^2)}{rR_{z+h}}-\frac{2[(h-L)^3+z(h-L)^2+(r^2-2z^2)(h-L)-2z(r^2+z^2)]}{rR_{z+h-L}}+\right.$$

$$\frac{r}{2}\left[ln\frac{\sqrt{r^2+(z-h+L)^2}-(z-h+L)}{\sqrt{r^2+(z-h)^2}-(z-h)}+(1-2\nu)ln\frac{R^*_{z+h-L}}{R^*_{z+h}}\right]+\frac{3\left(R_z^2+h^2\right)+4hz}{R_{z+h}}-$$

$$\frac{3\left[R_z^2+(h-L)^2\right]+4(h-L)z}{R_{z+h-L}}\Bigg\} \tag{3.8a}$$

$$u_z(r,z)=\frac{q\gamma_w}{16\pi G\eta k}\Bigg\{R_{z-h}-R_{z-h+L}+4\nu\left(R_{z+h-L}-R_{z+h}+zln\frac{R^*_{z+h}}{R^*_{z+h-L}}\right)+\frac{3\left(R_z^2+h^2\right)+4hz}{R_{z+h}}-$$

$$\frac{3\left[R_z^2+(h-L)^2\right]+4(h-L)z}{R_{z+h-L}}\Bigg\} \tag{3.8b}$$

$$p(r,z)=\frac{q\gamma_w}{4\pi k}[\ln(R^*_{z+h}*R^*_{z-h})-ln\frac{R^*_{z+h-L}}{R^*_{z-h-L}}] \tag{3.8c}$$

其中所示各項物理量或參數符號皆與 3.2 節相同。

3.4 最大地表位移

3.4.1 點抽水問題之地表最大垂直位移

本文是考慮地層力學與滲流性質均模擬為等向性，若地表模擬為透水情況，則地表最大垂直位移發生於地表對稱軸位置上，即$r=0$、$z=0$位置上。由式(3.4b)知地表最大垂直沉陷量$u_{z\,max}$為：

$$u_{z\,max}=u_z(0,0)=\frac{Q\gamma_w(1-2\nu)}{4\pi Gk} \tag{3.9}$$

由上式獲悉，地表最大垂直位移主要是受抽水量 Q、地層剪力模數 G、含水層滲透係數 k、地層柏松比ν等各項參數的影響。

若考慮地表為不透水情況，則地表最大垂直位移亦發生於地表對稱軸位置上，由式(3.5b)可知地表最大垂直沉陷量$u_{z\,max}$為：

$$u_{z\,max}=\lim_{r\to 0}u_z(r,0)=\lim_{r\to 0}\frac{Q\gamma_w}{4\pi Gk}\left[\frac{1-2\nu}{\sqrt{1+(\frac{r}{h})^2}}-\sinh^{-1}(\frac{1}{\frac{r}{h}})\right] \tag{3.10}$$

其中所示各項物理量或參數符號皆與 3.2 與 3.3 節相同。

3.4.2 點抽水問題之地表最大水平位移

由式(3.4a)與式(3.5a)得知，當考慮地表水平位移問題時，可考慮其中之垂直座標變數 $z = 0$，且依所建立之數學模式，無論模擬地表為透水或是不透水，所研討出之地表水平位移的閉合解皆相同。因地表最大水平位移發生位置之斜率為零，故尋找地表最大水平位移發生位置的方法是對地表水平位移曲線中之變數 r 作微分，然後讓微分結果為零。基於此，發現地表最大水平位移發生位置與黃金比例ϕ有相關，即當地表面$r = \sqrt{\phi}h$時，會發生地表最大水平位移。而所引起的地表最大水平位移量$u_{r\,max}$為：

$$u_{r\,max} = u_r\left(\sqrt{\phi}h, 0\right) = -\frac{Q\gamma_w(1-2\nu)}{4\pi Gk}\frac{1}{\phi^{2.5}} \tag{3.11}$$

其中之負號表示地表水平位移會朝對稱軸方向移動；黃金比例ϕ可表為：

$$\phi = \frac{1+\sqrt{5}}{2} = \sqrt{1+\phi} = 1 + \frac{1}{1+\frac{1}{1+\frac{1}{1+\frac{1}{\cdots}}}} = \sqrt{1+\sqrt{1+\sqrt{1+\sqrt{1+\cdots}}}} \tag{3.12}$$

3.4.3 線狀抽水問題之地表最大垂直位移

若考慮地表為透水情況，則線狀抽水問題之地表垂直位移可由令式(3.7b)中之變數r =0 推導出，結果如以下所示：

$$u_z(r,0) = \frac{q\gamma_w(1-2\nu)}{4\pi Gk}\left[\sqrt{r^2+h^2} - \sqrt{r^2+(h-L)^2}\right] \tag{3.13}$$

再令其中之變數 $z = 0$，即可推導出地表模擬為透水情況下，線狀抽水所引致之地表最大垂直位移量$u_{z\,max\ (L=h)}$：

$$u_{z\,max\,(L=h)} = u_z(0,0) = \frac{q\gamma_w(1-2\nu)}{4\pi Gk}[\mathrm{h} - |h-L|] = \frac{q\gamma_w L(1-2\nu)}{4\pi Gk} \tag{3.14}$$

若地表模擬為不透水情況，則線抽水問題之地表垂直位移可由令式(3.8b)中之變數r = 0 推導出：

$$u_z(r,0) = \frac{q\gamma_w}{4\pi Gk}\left[2\nu\sqrt{r^2+(h-L)^2} - 2\nu\sqrt{r^2+h^2} + sinh^{-1}\frac{h}{r} + (L-h)sinh^{-1}\frac{h-L}{r}\right] \tag{3.15}$$

再令其中之變數 z = 0，即可推導出地表模擬為不透水情況下，線狀抽水所引致之地表最大垂直位移$u_{z\,max\,(L=h)}$：

$$u_{z\,max\,(L=h)} = u_z(0,0) = \lim_{r\to 0}\frac{q\gamma_w}{4\pi Gk}\left[2\nu\sqrt{r^2+(h-L)^2} - 2\nu\sqrt{r^2+h^2} + sinh^{-1}\frac{h}{r} + (L-h)sinh^{-1}\frac{h-L}{r}\right] \tag{3.16}$$

式(3.13)~(3.16)中各項物理量或參數符號之定義皆與 3.2 節相同。

3.4.4 線狀抽水問題之地表最大水平位移

由 3.4.2 節的研討知，地表模擬為透水或不透水情況下之地表水平位移的解皆相同，今令式(3.7a)或(3.8a)中之垂直座標變數 z = 0 得知：

$$u_r(r,0) = -\frac{q\gamma_w(1-2\nu)}{8\pi Gk}\left[\frac{L(2h-L)}{r} - \frac{h\sqrt{r^2+h^2}}{r} + \frac{(h-L)\sqrt{r^2+(h-L)^2}}{r} + rln\frac{\sqrt{r^2+h^2}+h}{\sqrt{r^2+(h-L)^2}+h-L}\right] \tag{3.17}$$

式中各項物理量或參數符號之定義皆與 3.2 節相同。理論上仍可引用 3.4.2 節的方法尋找地表最大水平位移發生位置及地表最大水平位移量，亦即可考慮地表最大水平位移發生位置之斜率應為零，故尋找地表最大水平位移發生位置的方法應是對地表水平位移曲線式(3.17)中之變數 r 作微分，然後讓微分結果為零。然而對式(3.17)進行微分

後發現，其微分結果較為複雜，初步研判應無法像尋找點抽水所引致之地表最大水平位移一般，整理出可以簡單函數及黃金比例方式加以表達的關係式，此一部分之研討，尚待後續之研究繼續加以努力。

3.5 結語

本章節係根據點抽水問題之基本解，分別研討出模擬地表為透水與不透水兩種情況時，長期抽水所引致的穩態壓密沉陷問題的閉合解，其中關於抽水井之抽水是模擬為線狀抽水型態，所研討出之解包括抽水所引起的地層垂直位移、水平位移與超額孔隙水壓變化等，並進一步推求出所引致之地表最大沉陷量、最大水平位移量及其發生位置，於下一章節中將進一步進行參數影響分析。

第四章 參數影響分析

4.1 前言

為清楚了解各種參數對數值結果的影響，本章擬根據前章所推導出之結果進行參數影響分析，研討過程會盡量採用無因次化的原則，因為無因次化的圖表可以增加各種圖表的代表性與應用範圍。本研究是將地層力學性質與滲透行為均模擬為等向性，而地表邊界則分別模擬為完全透水與完全不透水兩種情況，所繪製的圖表內容包括點抽水與線狀抽水問題所導致的地表垂直位移量、水平位移量與地層超額孔隙水壓等，研究結果可作為工程應用上之參考。

本文在進行地表水平暨垂直位移量之無因次化時，乃是以地表模擬為透水邊界時之最大沉陷量$u_{z\,max}$為無因次化的基準量。點抽水問題之部分繪圖結果與參考文獻(Booker 和 Carter，1986)中之圖表相似，故亦會與該文獻之繪圖結果加以比較，以確定本章之各項研究結果正確無誤。關於無因次化之基準量不考慮不透水地表面上之最大沉陷量的原因，是因在該不透水條件下，其地表最大沉陷量會有發散情況。

由表 4.1 與表 4.2 得知，不同性質土壤之柏松比的變化範圍約為 0.15 至 0.5 之間，因此於參數影響分析的過程中，地層柏松比ν擬分別考慮為 0.15、0.2、0.25、0.3、0.35、0.4、0.45、0.4999 等八種情況，如圖 2.4 之抽水井，經訪查得知，其井深 h 約 65 公尺、取水長度 L 約 10 公尺，亦即取水長度與井深的比值L/h約為 0.15。本章在進行參數影響分析時，擬將取水長度L與井深h的比值L/h分別模擬為 0.1、0.3、0.5、0.8、1.0 等五種情況。

表 4.1　土壤之柏松比範圍（Das，2008）

土壤種類	柏松比範圍
疏鬆砂(Loose Sand)	0.2~0.4
中等緊密砂(Medium Dense Sand)	0.25~0.4
緊密砂(Dense Sand)	0.3~0.45
粉土質砂(Silty Sand)	0.2~0.4
砂及礫石(Sand and Gravel)	0.15~0.35

表 4.2　黏土之柏松比範圍（施俊如，2000）

土壤種類	柏松比範圍
軟黏土(Soft Clay)	0.15~0.25
中等黏土(Medium Clay)	0.2~0.5

4.2 等向性半無限域之點抽水問題探討

4.2.1 地表模擬為透水情況時點抽水所引致之地表垂直位移

本單元擬根據第三章之說明，討論點抽水所引致之地表（$z=0$）垂直位移，該地表垂直位移即為地盤下陷量。茲引用無因次化的概念，並以地表模擬為透水邊界時之最大沉陷量$u_{z\,max}$為無因次化的基準量，則可將由式(3.4b)所得出之地表垂直位移予以無因次化。另外，由式(3.9)知，地表模擬為透水時之最大地表沉陷量$u_{z\,max}=\frac{Q\gamma_w(1-2\nu)}{4\pi Gk}$。基於此，可得：

$$\frac{u_z(r,0)}{u_{z\,max}\text{ of Pervious Half Space}}=\frac{u_z(r,0)}{u_z(0,0)}=\frac{1}{\sqrt{\left(\frac{r}{h}\right)^2+1}} \tag{4.1}$$

本文是採用 Mathematica 軟體進行繪圖，茲代入適當之水文地質參數後，可繪出圖 4.1，由圖 4.1 可知，單點抽水所引起的地表最大垂直位移發生在地表$r=0$的對稱軸位置上。

4.2.2 地表模擬為透水或不透水情況時點抽水所引致之地表水平位移

本單元擬根據第三章之說明，討論點抽水所引起的地表水平位移。由第三章之研討知，地表邊界模擬為透水與不透水兩種邊界時，所研討出之地表水平位移完全相同，因此可一併討論之。本單元仍以地表邊界模擬為透水時之最大沉陷量$u_{z\,max}$為無因次化的基準量，基於此，無因次化之地表水平位移可表為：

$$\frac{u_r(r,0)}{u_{z\,max}\text{ of Pervious Half Space}}=\frac{u_r(r,0)}{u_z(0,0)}=-\frac{hr}{\sqrt{r^2+h^2}\left(\sqrt{r^2+h^2}+h\right)}=-\frac{\frac{r}{h}}{\sqrt{\left(\frac{r}{h}\right)^2+1}\left(\sqrt{\left(\frac{r}{h}\right)^2+1}+1\right)} \quad (4.2)$$

茲引用 Mathematica 軟體進行 2D 繪圖，所得結果如圖 4.2 所示。由圖 4.2 與 3.4.2 節的討論知，單點抽水所引致地表最大水平位移位於$r=\sqrt{\phi}h\backsimeq 1.272h$的位置上，且地表最大水平位移量約為最大地表最大沉陷量的 0.3 倍。另外，由式(3.11)知，地表模擬為透水或不透水時之最大地表水平位移量$u_{r\,max}=u_r\left(\sqrt{\phi}h,0\right)=-\frac{Q\gamma_w(1-2\nu)}{4\pi Gk}\frac{1}{\phi^{2.5}}$。

4.2.3 地表模擬為不透水情況時點抽水所引致之地表垂直位移

如 4.2.1 單元所引述的概念，擬以地表模擬為透水邊界時之最大沉陷量$u_{z\,max}$為無因次化的基準量，茲先引用式(3.5b)得出地表垂直位移再予以無因次化，可得：

$$\frac{u_z(r,0)}{u_{z\,max}\text{ of Pervious Half Space}}=\frac{u_z(r,0)}{u_z(0,0)}=\frac{1}{\sqrt{\left(\frac{r}{h}\right)^2+1}}-\frac{1}{1-2\nu}\sinh^{-1}\frac{1}{\frac{r}{h}} \quad (4.3)$$

再引用 Mathematica 軟體進行 2D 繪圖，模擬含水地層之柏松比ν分別為 0.15、0.2、0.25、0.3、0.35、0.4、0.45、0.4999，研討結果如圖 4.3~4.10 所示。由圖 4.3~4.10 知，柏松比ν越大時，抽水所引起的地表沉陷量會越大；又當$\nu=0.4999$（即接近 0.5）時，模式分析所得之不透水地表邊界之沉陷量相當大，其原因可由波松比ν的定義得知：當波松比ν變大時，有較大的變形，故反映出較大之地表沉陷量。本文於後續相關之研討，將不再考慮$\nu=0.4999$的情況。由圖 4.3 得知，當含水層之柏松比ν較小(ν = 0.15)且地表模擬為完全不透水邊界時，抽水所引致之最大沉陷量約為地表模擬為完全透水邊界時的 6 倍；又由圖 4.9 知，當含水層之柏松比ν = 0.45 且地表模擬為完全不透水邊界時，抽水所引致的最大沉陷量約為地表模擬為完全透水邊界時的 43 倍，亦即當含水層之柏松比由ν = 0.15 增至ν = 0.45 時，點抽水所引起的沉陷量約增加 7 倍。由以上研討知，地表滲流邊界條件的考慮方式，以及含水地層的柏松比之模擬方式，均

對點抽水所引致的地表沉陷有相當顯著的影響。

圖 4.11 是地表模擬為透水與不透水情況時，點抽水所引致的地表沉陷量之比較圖，由圖 4.11 知：(1)不透水情況下點抽水所引致的地表沉陷會較大，這是因為當地表面模擬為不透水邊界時，抽水會引起較大之負的超額孔隙水壓力，導致含水層之有效應力增加較多，故地表沉陷量會變大。(2)地層柏松比越大，抽水所引致的地表沉陷量會越大，這是因為含水層之柏松比變大時，地層較容易產生變形，故反映出較大之地表沉陷量。

4.3 等向性半無限域之線狀抽水問題探討

4.3.1 地表模擬為透水情況時線狀抽水所引致之地表垂直位移

本單元亦擬根據第三章之說明，討論點抽水所引致之地表（$z=0$）垂直位移。茲引用無因次化的概念，並以抽水長度 L 等於水井深度 h 時，地表模擬為透水邊界下之最大沉陷量$u_{z\,max\,(L=h)}$為無因次化的基準量，則可將由式(3.7b)所得出之地表垂直位移予以無因次化。基於此，可得：

$$\frac{u_z(r,0)}{u_{z\,max\,(L=h)}\text{of Pervious Half Space}}=\sqrt{\left(\frac{r}{h}\right)^2+1}-\sqrt{\left(\frac{r}{h}\right)^2+\left(1-\frac{L}{h}\right)^2} \tag{4.4}$$

由式(3.14)知，$u_{z\,max\,(L=h)}=\frac{q\gamma_w L(1-2\nu)}{4\pi Gk}$。

於進行參數影響分析時，擬考慮取水長度L與井深h的比值L/h分別為 0.1、0.3、0.5、0.8、1，所得結果如圖 4.12 ~4.17 所示。當線抽水強度L/h = 1 時，會在地表產生最大沉陷量$u_{z\,max\,(L=h)}$，即地表沉陷量與抽水強度L/h有關。由圖 4.12 的觀察得知，當線抽水強度L/h = 0.1 時，地表沉陷量約為地表最大沉陷量$u_{z\,max\,(L=h)}$的 0.005 倍；又由圖 4.15 的觀察得知，當線抽水強度L/h = 0.8 時，地表沉陷量約為地表最大沉陷量$u_{z\,max\,(L=h)}$的 0.4 倍。圖 4.17 是將上述五個參數的影響繪製在一起，由此圖可知，當線抽水強度由L/h = 0.8 增至 1.0 時，抽水所引致的最大地表沉陷量約會增加 1.5

倍。

圖 4.18 為透水情況下點抽水與線狀抽水所引致沉陷量的比較，比較過程中是考慮點抽水的抽水量 Q 等於所對應之線狀抽水的抽水量 qL(且模擬$L/h = 1$)。由圖 4.18 可知，若所考慮的抽水量相同，則在對稱軸上點抽水與線狀抽水所引起的最大沉陷量會相同，但除了對稱軸位置以外之地表面，所呈現的地層下陷均以點抽水情況較嚴重，例如在 $r/h = 1$ 之地表面位置上，地表沉陷量結果約有兩倍的差距。

4.3.2 地表模擬為不透水情況時線狀抽水所引致之地表垂直位移

如 4.3.1 單元所引述的概念，擬以地表模擬為透水邊界時之最大沉陷量$u_{z\,max\,(L=h)}$為無因次化的基準量，茲引用由式(3.8b)所得出之地表垂直位移並予以無因次化，可得：

$$\frac{u_z(r,0)}{u_{z\,max\,(L=h)}\ \text{of Pervious Half Space}} = \frac{1}{\frac{L}{h}}\frac{1}{(1-2\nu)}\{2\nu\left(\sqrt{\left(\frac{r}{h}\right)^2+\left(1-\left(\frac{L}{h}\right)^2\right)}-\sqrt{\left(\frac{r}{h}\right)^2+1}\right)+$$

$$\sinh^{-1}\frac{1}{\frac{r}{h}}+\left(\frac{L}{h}-1\right)\sinh^{-1}\frac{1-\frac{L}{h}}{\frac{r}{h}}\} \qquad (4.5)$$

由式(3.14)的研討知，上式中之$u_{z\,max\,(L=h)} = \frac{q\gamma_w L(1-2\nu)}{4\pi Gk}$。

於進行參數影響分析時，考慮取水長度L與井深h的比值L/h分別為 0.1、0.3、0.5、0.8、1，含水層之柏松比ν則分別模擬為 0.15、0.2、0.25、0.3、0.35、0.4、0.45，所得結果如圖 4.19~圖 4.58 所示。當取水長度L與井深h的比值L/h = 0.1、ν = 0.1~0.45 時相關之沉陷量數值變化結果如圖 4.19~圖 4.26 所示；L/h = 0.3、ν = 0.1~0.45 時，相關之沉陷量數值變化結果如圖 4.27~圖 4.34 所示。依此類推，L/h = 0.5、ν = 0.1~0.45 時，相關之沉陷量數值變化結果如圖 4.35~圖 4.42 所示；L/h = 0.8、ν = 0.1~0.45 時，相關之沉陷量數值變化結果如圖 4.43~圖 4.50 所示；L/h = 1、ν = 0.1~0.45 時，相關之沉陷量數值變化結果如圖 4.51~圖 4.58 所示。

圖 4.19~圖 4.58 之圖組的討論過程中，是分別固定取水長度L與井深h的比值L/h，

再改變含水層之柏松比。而圖 4.59~圖 4.65 的討論方式，則是分別固定含水層之柏松比，再改變取水長度L與井深h的比值L/h。基於此，圖 4.59~圖 4.65 均係討論含水層柏松比ν = 0.15~0.45 時，取水長度L與井深h的比值L/h分別為 0.1、0.3、0.5、0.8、1.0 時，線狀抽水所引起的壓密沉陷行為。

各項數值結果均呈：(1)含水層之柏松比增加時地表沉陷量也增加，這是因為含水層之柏松比變大時，地層較容易產生變形，故反映出較大之地表沉陷量。(2)取水長度L與井深h的比值L/h增加時，地表沉陷量也呈增加的現象，這是因為取水長度L增加時，抽水量也會增加，故壓密沉陷量也會增加。例如由圖 4.58 知，當模擬取水長度L與井深h的比值$L/h = 1$、含水層之柏松比$\nu = 0.45$ 時，抽水所引致的地表沉陷量約為模擬含水層之柏松比$\nu = 0.35$ 時的兩倍。又由圖 4.65 知，當模擬含水層之柏松比$\nu = 0.45$、取水長度L與井深h的比值$L/h = 1$ 時，抽水所引致的地表沉陷量約為模擬$L/h = 0.1$ 時的兩倍。

由圖 4.66 知：(1) 地表模擬為不透水情況時，線狀抽水所引致的地表沉陷會較大，這是因為當地表面模擬為不透水邊界時，抽水會引起較大之負的超額孔隙水壓力，故會引起含水層之有效應力增加，導致地表沉陷量變大。(2)取水長度L與井深h的比值L/h增加時地表沉陷量也增加的現象，這是因為取水長度L增加時，抽水量會增加，故壓密沉陷量也會增加之故。

本單元之研究成果與曾鈞敏(2009)的研究成果亦有相似之處，其研究中曾指出：「相同地質參數條件下，拘限含水層之土體變形範圍大於非拘限含水層。」因拘限含水層具有不透水之邊界，抽水所引致之負的超額孔隙水壓無法在不透水之邊界面上消散，故導致含水層之有效應力上升較多，因而引起較大範圍之土體變形。

4.3.3 地表模擬為透水或不透水情況時線狀抽水所引致之地表水平位移

本單元亦擬根據第三章之說明，討論線狀抽水所引起的地表水平位移。由第三章之研討知，地表邊界模擬為透水與不透水邊界時，所研討出之地表水平位移完全相同，

因此可一併討論之。本單元仍以地表邊界模擬為透水時之最大沉陷量$u_{z\,max\,(L=h)}$為無因次化的基準量，基於此，無因次化之地表水平位移可表為：

$$\frac{u_r(r,0)}{u_{z\,max\,(L=h)}\text{of Pervious Half Space}}=\frac{u_r(r,0)}{u_z(0,0)}=\frac{-\left[\frac{L(2h-L)}{r}-\frac{h\sqrt{r^2+h^2}}{r}+\frac{(h-L)\sqrt{r^2+(h-L)^2}}{r}+rln\frac{\sqrt{r^2+h^2}+h}{\sqrt{r^2+(h-L)^2}+h-L}\right]}{2h} \tag{4.6}$$

由上式知，進行無因次化後，線狀抽水所引致之地表水平位移與水文地質參數G、ν、k等無關，相關之數值結果繪製於圖 4.67。由圖 4.67 知：(1)取水長度L與井深h的比值L/h增加時，抽水所引起的地表水平位移量會跟著增加，因L/h的比值增加代表抽水量亦呈增加之勢。(2)抽水所引起的地表水平位移量會在水井邊逐漸升高後逐步降低，這是因為單井抽水所引起的地表水平位移是一軸對稱問題，故地表面在對稱點上之水平位移量應為零；另外，含水層遠處受抽水擾動的影響很小，故地表遠處之水平位移量亦很小。(3)線狀抽水時，地表最大水平位移發生位置約位於$r/h=1$的位置上，此與點抽水所引致地表最大水平位移是落在$r=\sqrt{\phi}h\backsimeq 1.272h$位置上之結論相當接近。

本單元之研究成果與曾鈞敏(2009)的研究成果亦有相似之處，其研究中曾指出：「無論拘限或非拘限含水層於抽水後，水平位移量在抽水點源邊會逐漸升高後逐步降低。」本研究在此一研究重點上之結論與其一致。

4.4 半無限域孔隙水壓變化影響結果探討

4.4.1 點抽水所引致之含水層超額孔隙水壓

本節研討重點為探討地表模擬為透水狀態與不透水狀態下之超額孔隙水壓的差異變化。由式(3.4c)知，透水情況下超額孔隙水壓之無因次化結果為：

$$\frac{p(r,z)}{\frac{Q\gamma_w h}{4\pi k}}=-\frac{1}{\sqrt{\left(\frac{z}{h}-1\right)^2+\left(\frac{r}{h}\right)^2}}+\frac{1}{\sqrt{\left(\frac{z}{h}+1\right)^2+\left(\frac{r}{h}\right)^2}} \tag{4.7}$$

土壤之超額孔隙水壓係因點抽水後流體自含水層中流入抽水點所致，根據方程式(4.7)所繪製之超額孔隙水壓如圖 4.68 所示，圖 4.68 分別採立體圖與平面等值曲線圖表示之。

由式(3.5c)知，若模擬地表面為不透水邊界，則無因次化之超額孔隙水壓結果為：

$$\frac{p(r,z)}{\frac{Q\gamma_W h}{4\pi k}} = -\frac{1}{\sqrt{\left(\frac{z}{h}-1\right)^2+\left(\frac{r}{h}\right)^2}} - \frac{1}{\sqrt{\left(\frac{z}{h}+1\right)^2+\left(\frac{r}{h}\right)^2}} \tag{4.8}$$

根據式(4.8)所繪製之超額孔隙水壓如圖 4.69 所示，圖 4.69 亦分別採立體圖與平面等值曲線圖表示之，超額孔隙水壓呈負值的工程意義是代表吸力狀態。

由圖 4.68 與圖 4.69 之比較得知，當地表邊界模擬為不透水時，所引致之負的超額孔隙水壓會較大，這是因為此時超額孔隙水壓無法透過地表消散所致。因水的負壓較高，故含水層的有效應力亦會較高，所反映出之地表沉陷亦會較大，如圖 4.11 所示。

4.4.2 線狀抽水所引致之含水層超額孔隙水壓

本單元擬探討含水層因線狀抽水所引起的超額孔隙水壓p，由式(3.7c)知，地表模擬為透水情況下，線狀抽水所引起的含水層超額孔隙水壓之無因次化結果為：

$$\frac{p(r,z)}{\frac{q\gamma_W}{4\pi k}} = ln(R^*_{z+h} * R^*_{z-h}) + ln\frac{R^*_{z+h-L}}{R^*_{z-h-L}} \tag{4.9}$$

其中 $R^*_i = R_i + i$，$i = z+h、z-h、z+h-L、z-h-L$ ； $R_i = \sqrt{r^2+i^2}$ ，$i = z、z+h、z-h、z+h-L、z-h+L$。所繪製之相關數值結果如圖 4.70~4.74 所示。

若地表邊界是模擬為不透水情況，則由式(3.8c)知，線狀抽水所引起的含水層超額孔隙水壓之無因次化結果為：

$$\frac{p(r,z)}{\frac{q\gamma_w}{4\pi k}} = \ln(R^*_{z+h} * R^*_{z-h}) - ln\frac{R^*_{z+h-L}}{R^*_{z-h-L}} \quad (4.10)$$

其中R^*_i的定義與式(4.9)相同。所繪製之相關數值結果如圖 4.75~4.79 所示。

研討並比較圖 4.68~4.79 知：(1)若地表邊界模擬為透水情況，則抽水所引致的超額孔隙水壓會在地表邊界上完全消散，因此所呈現出之含水層負的超額孔隙水壓會較小。反之，若將地表邊界模擬為不透水，則抽水所引致之負的超額孔隙水壓會較大，這是因為超額孔隙水壓無法透過地表消散所致。(2)取水長度L與井深h的比值L/h增加時，含水層超額孔隙水壓也會有增加的現象，這是因為取水長度L增加時，代表抽水量亦呈增加的趨勢，故含水層超額孔隙水壓也會增加。

4.5 結語

本章各節旨在探討：(1)將抽水行為模擬為點抽水和線狀抽水時的數值結果之差異性。(2)將地表模擬為透水和不透水時的數值結果之差異性。(3)含水層柏松比對抽水所引致壓密行為的影響。(4)取水長度L與井深h的比值對抽水所引致壓密行為的影響。(5)抽水所引致之地表水平位移變化趨勢。所進行之參數影響分析的數值結果包括地表水平位移、垂直位移及地層超額孔隙水壓。經由研究成果顯示，將抽水行為模擬為點抽水或線狀抽水、地表滲流邊界條件、含水層柏松比、取水長度L與井深h等，均是影響抽水所引致地層壓密沉陷行為的重要原因。重要之研究成果說明如下：

1. 關於將抽水行為模擬為點抽水和線狀抽水時的數值結果之差異性：圖 4.18 為透水情況下點抽水與線狀抽水所引致沉陷量的比較，比較過程中是考慮點抽水的抽水量 Q 等於所對應之線狀抽水的抽水量 qL（且L/h 考慮為 1），由圖 4.18 可知點抽水與線狀抽水所引起的最大沉陷量會相同，但大多數情況下點抽水所引起的沉陷量會較大，例如在 $r/h = 1$ 位置上之地表沉陷量結果約有兩倍的差距。
2. 關於將地表模擬為透水和不透水時的數值結果之差異性：地表模擬為不透水情況下所引致的地表沉陷會較大，這是因為當地表面模擬為不透水邊界時，抽水所引起之負的超額孔隙水壓無法消散，含水層之有效應力因而升高，壓密沉陷之效應

變大，故所導致的地表沉陷量會變大。

3. 關於含水層柏松比對抽水所引致壓密行為的影響：當含水層之柏松比較大時，抽水所引致的地表沉陷量會較大，其原因可由柏松比ν的定義得知：當柏松比ν變大時，有較大的變形，故含水層柏松比變大時會反映出較大之地表沉陷。
4. 關於取水長度L與井深h的比值對抽水所引致壓密行為的影響：取水長度L與井深h的比值L/h增加時地表沉陷量也有增加的現象，這是因為L/h增加時，代表取水長度L增加，亦即抽水量在增加，故壓密沉陷量也會增加。
5. 抽水所引起的地表水平位移量會在水井邊逐漸升高後逐步降低，這是因為單井抽水所引起的地表水平位移是一軸對稱問題，故地表面在對稱點上之水平位移量應為零；另外，含水層遠處受抽水擾動的影響很小，故地表遠處之水平位移量亦很小。另外，線狀抽水時，地表最大水平位移發生位置約位於$r/h = 1$的位置上，此與點抽水所引致地表最大水平位移是落在$r = \sqrt{\phi}h \simeq 1.272h$位置上之結論相當接近。

本章之研究成果與曾鈞敏(2009)的研究成果亦有相似之處：(1)無論拘限或非拘限含水層於抽水後，水平位移量在抽水點源邊會逐漸升高後逐步降低。(2)相同地質參數條件下，拘限含水層之土體變形範圍大於非拘限含水層。本研究在這兩項研究重點上之結論與其一致。

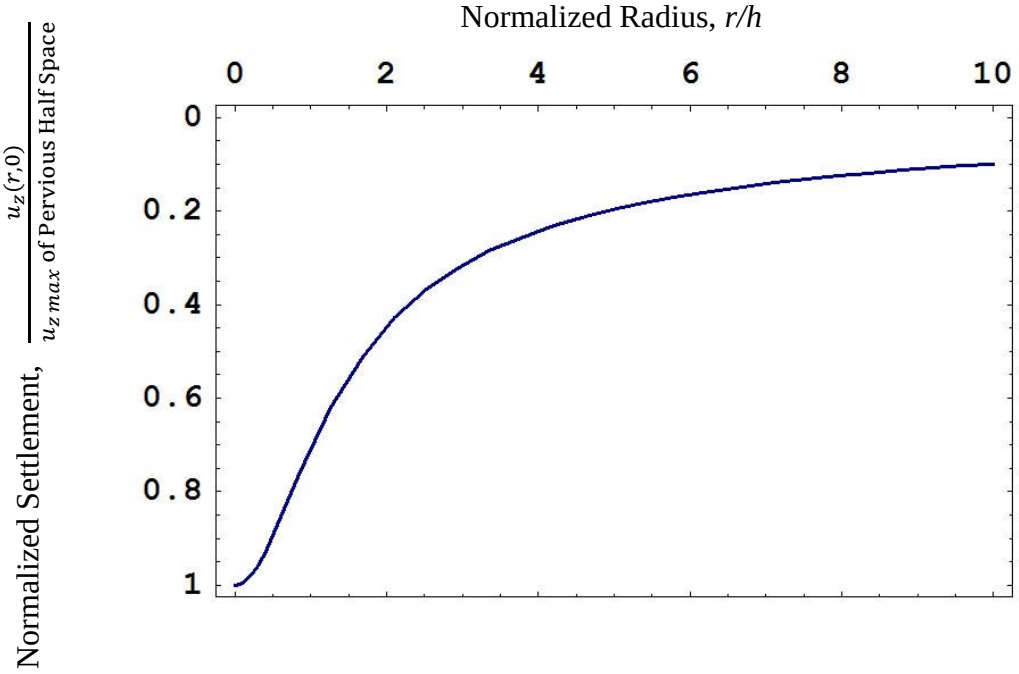

圖 4.1 地表模擬為透水情況時點抽水問題之無因次化地表沉陷量曲線圖

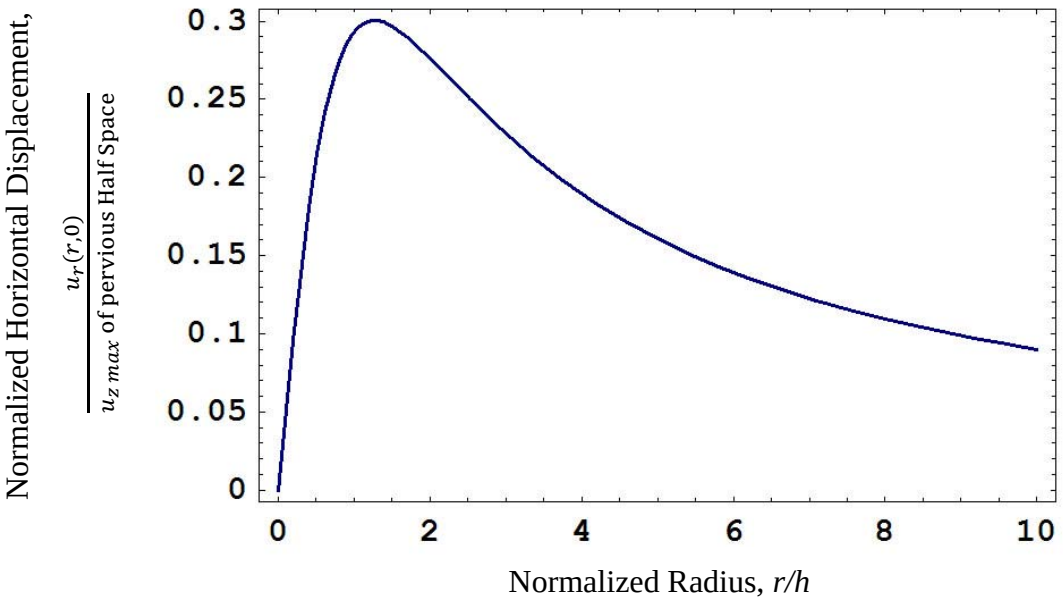

圖 4.2 點抽水問題之無因次化地表水平位移曲線圖

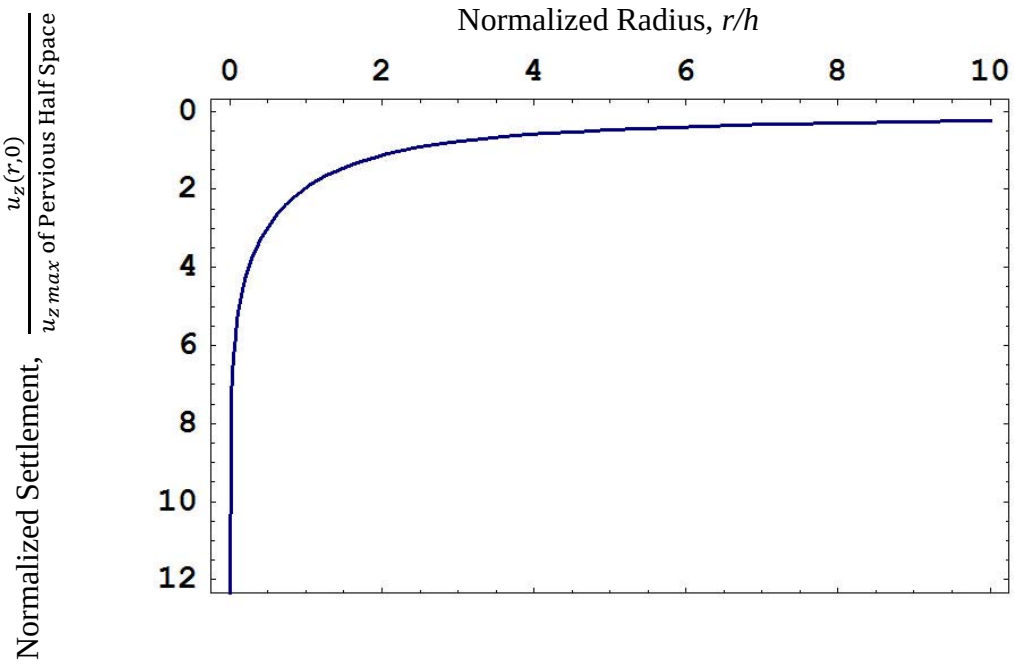

圖 4.3 地表模擬為不透水情況時點抽水所引致之無因次化地表沉陷量(ν = 0.15)

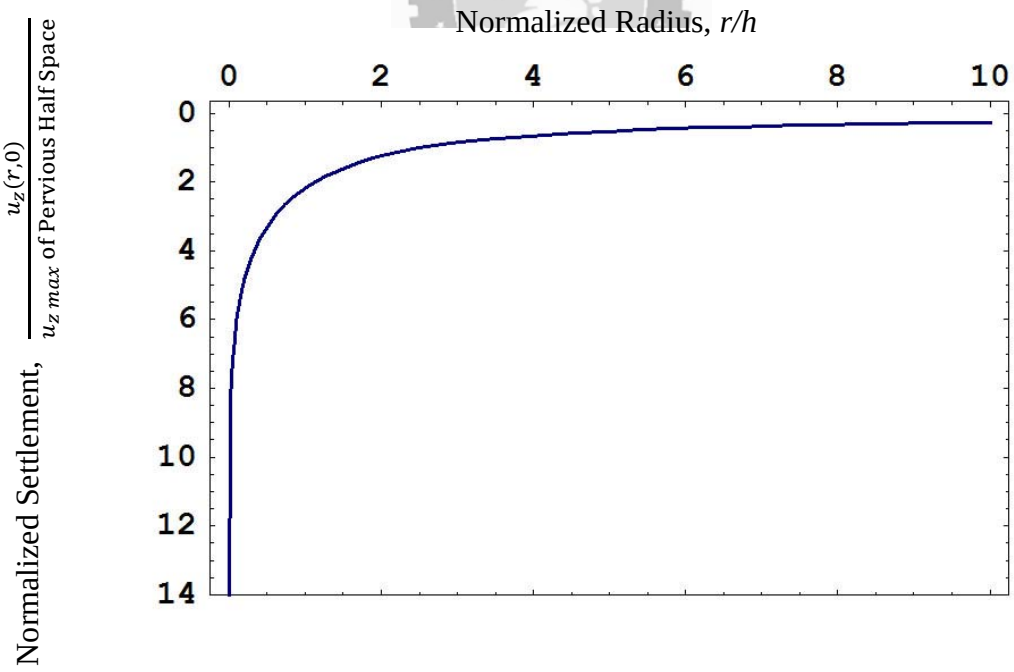

圖 4.4 地表模擬為不透水情況時點抽水所引致之無因次化地表沉陷量(ν = 0.2)

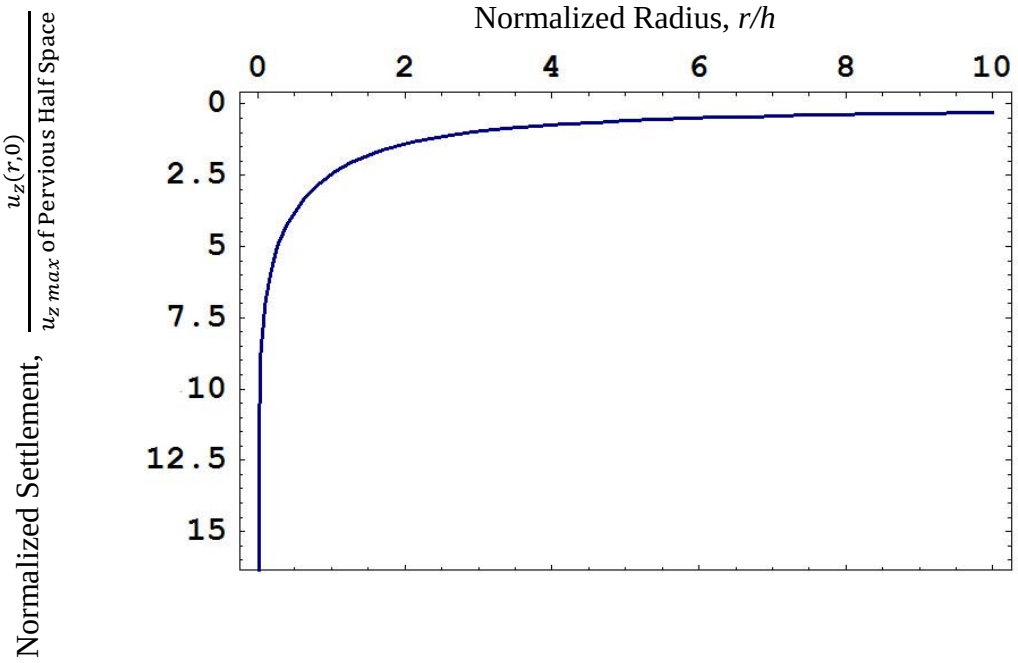

圖 4.5 地表模擬為不透水情況時點抽水所引致之無因次化地表沉陷量(ν = 0.25)

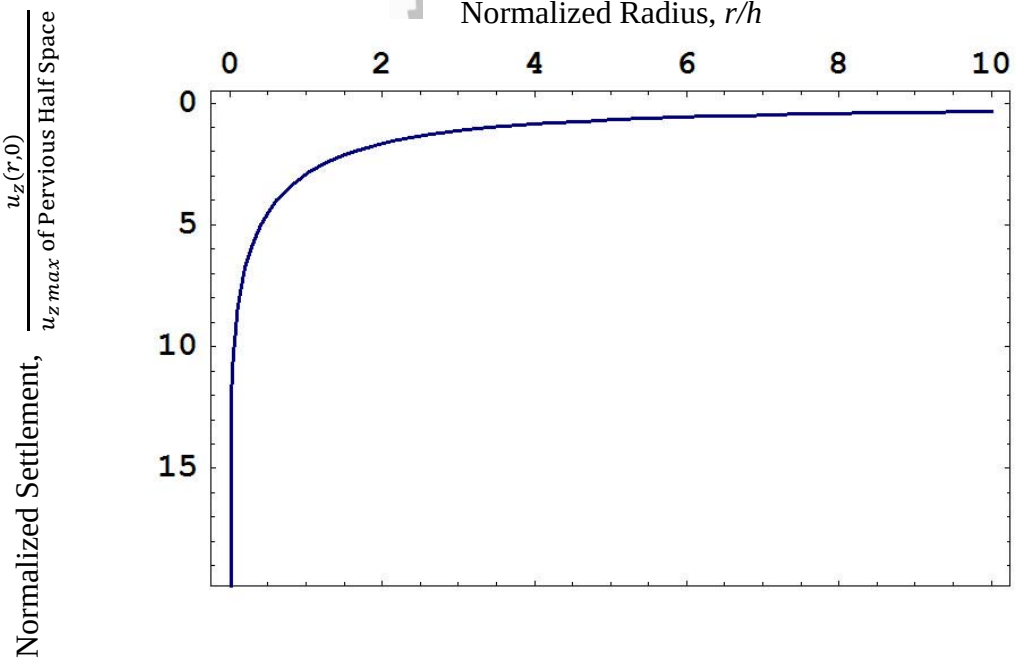

圖 4.6 地表模擬為不透水情況時點抽水所引致之無因次化地表沉陷量(ν = 0.3)

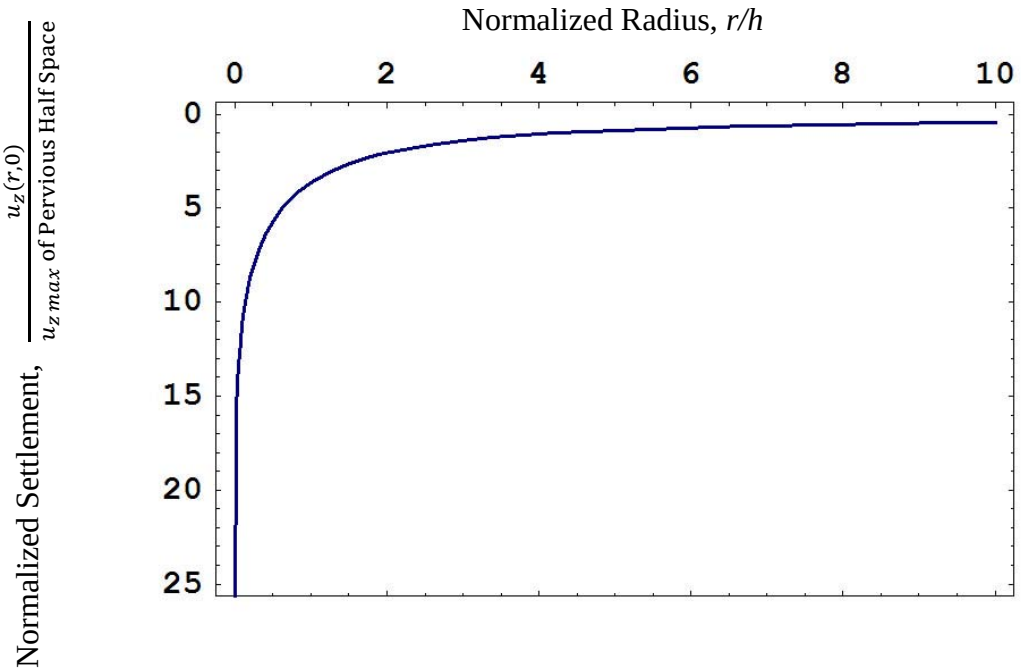

圖 4.7 地表模擬為不透水情況時點抽水所引致之無因次化地表沉陷量(ν = 0.35)

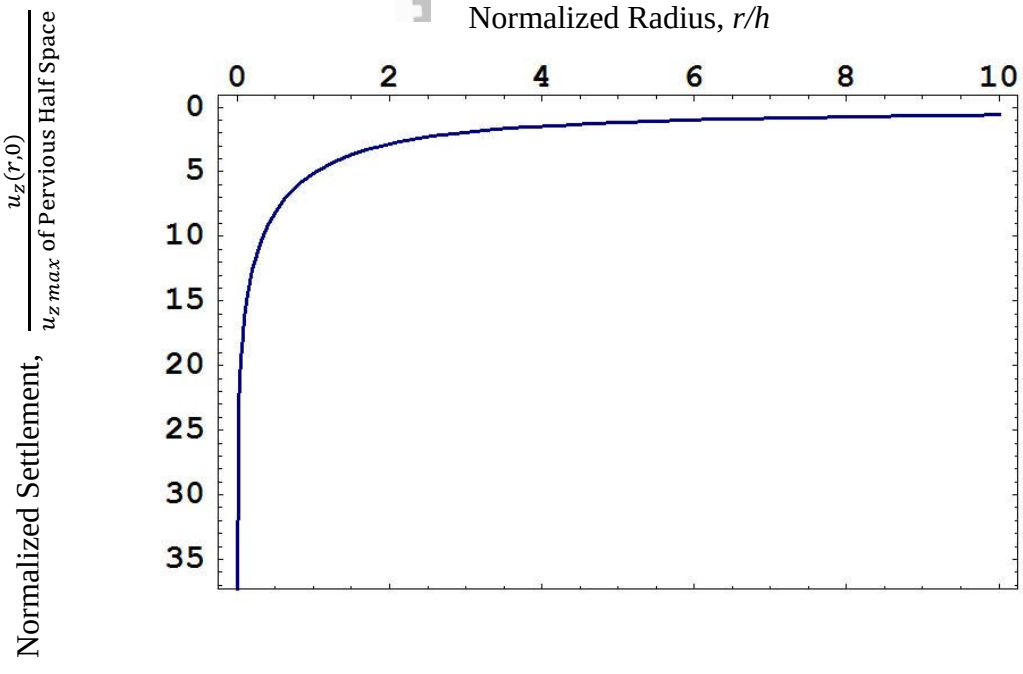

圖 4.8 地表模擬為不透水情況時點抽水所引致之無因次化地表沉陷量(ν = 0.4)

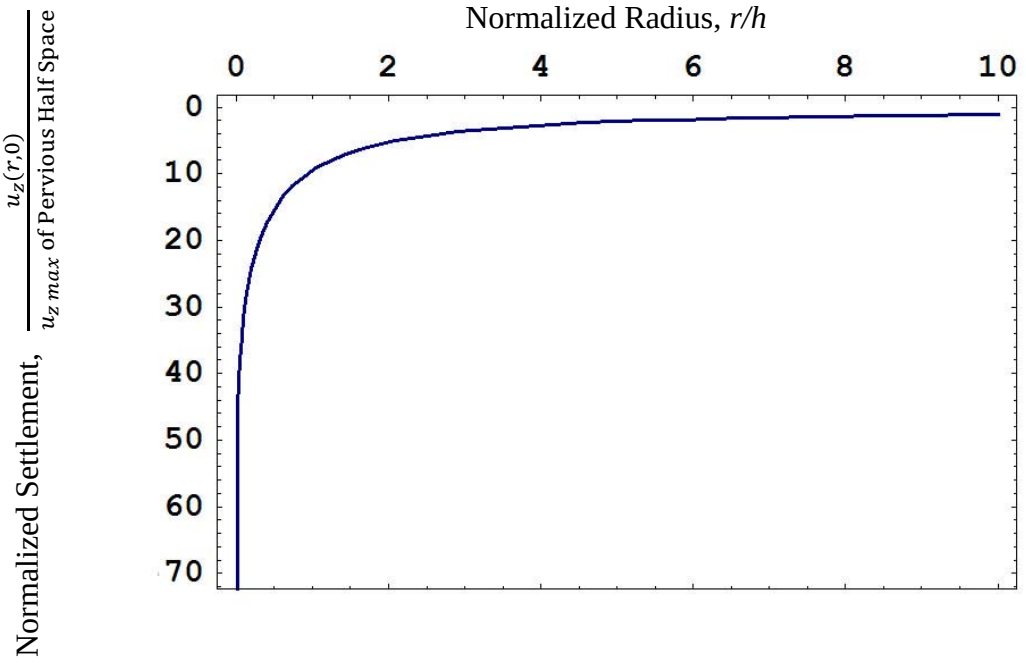

圖 4.9 地表模擬為不透水情況時點抽水所引致之無因次化地表沉陷量(ν = 0.45)

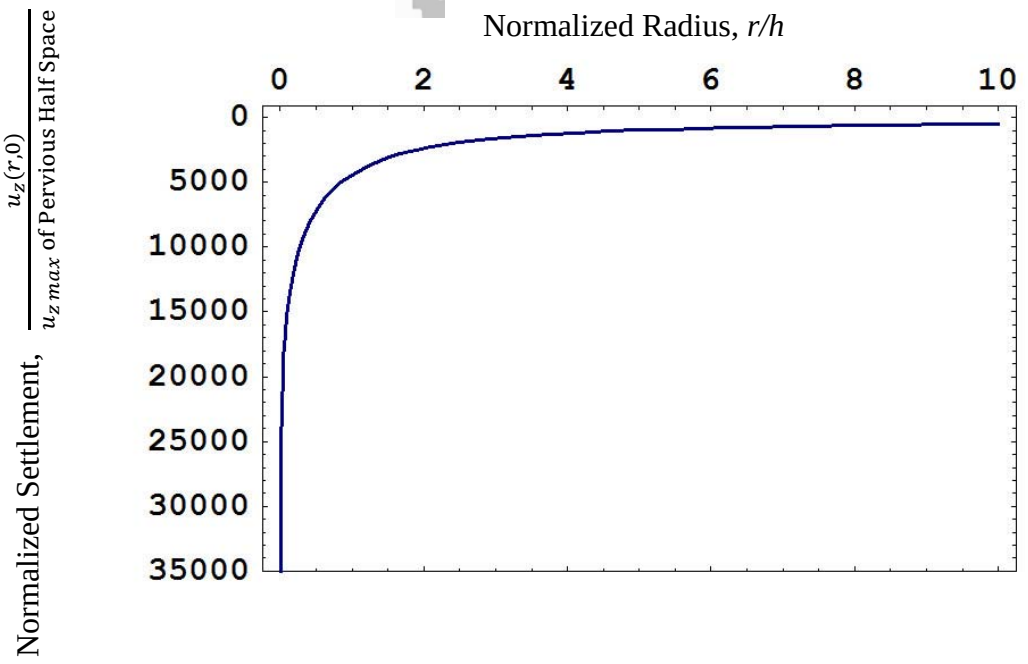

圖 4.10 地表模擬為不透水情況時點抽水所引致之無因次化地表沉陷量(ν = 0.4999)

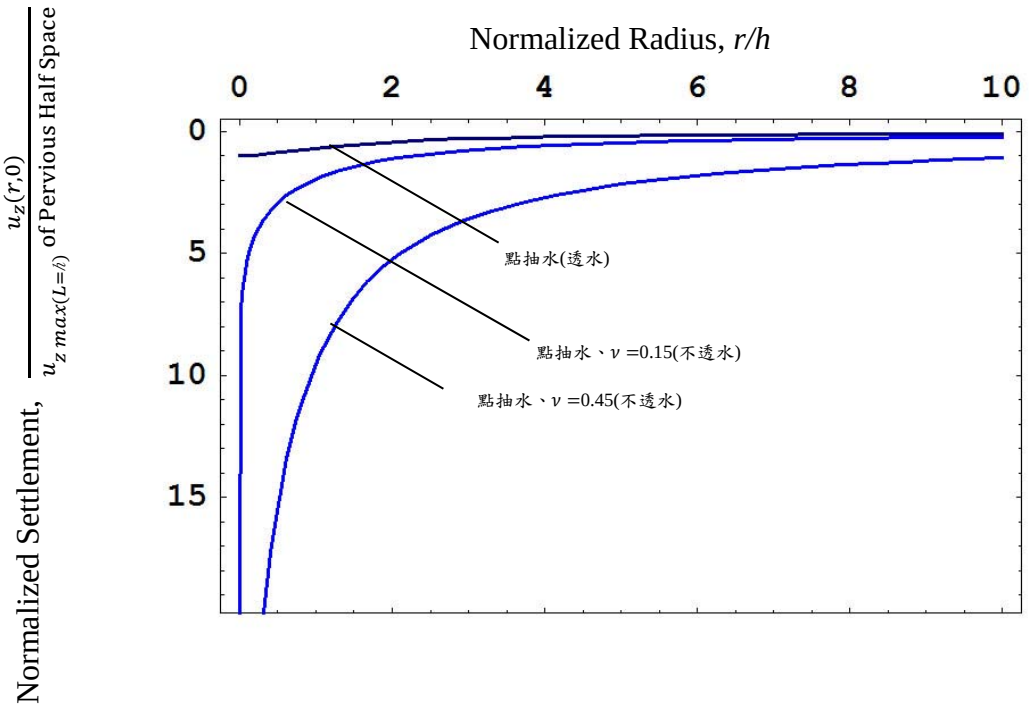

圖 4.11 地表模擬為透水與不透水情況時點抽水所引致無因次化地表沉陷量比較圖

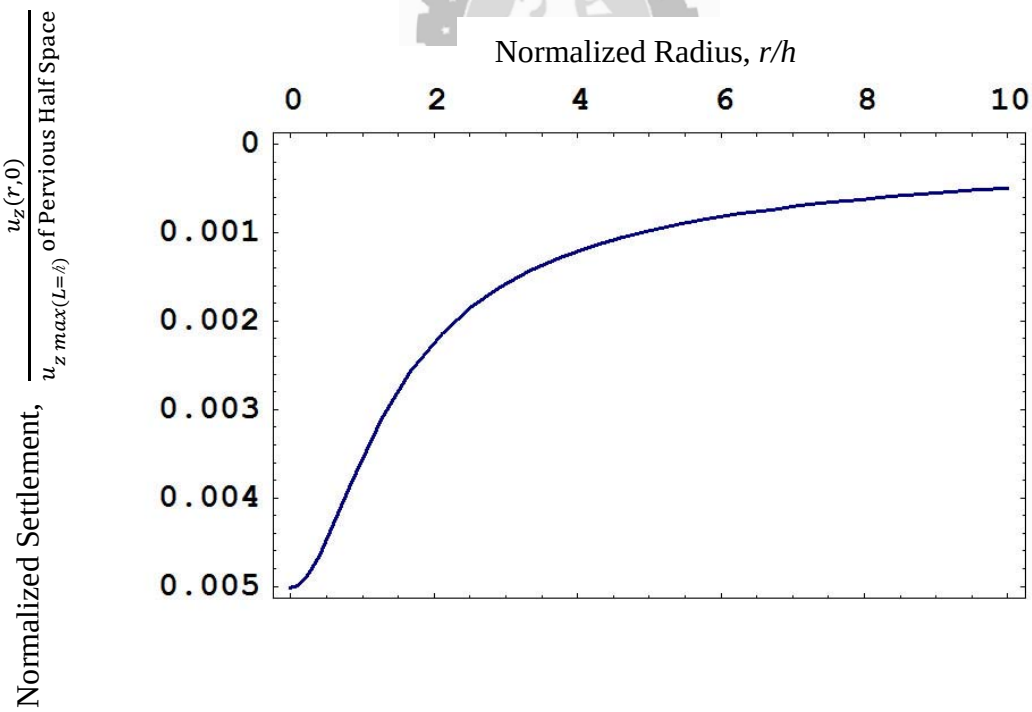

圖 4.12 地表模擬為透水情況時線狀抽水所引致之無因次化地表沉陷量(L/h = 0.1)

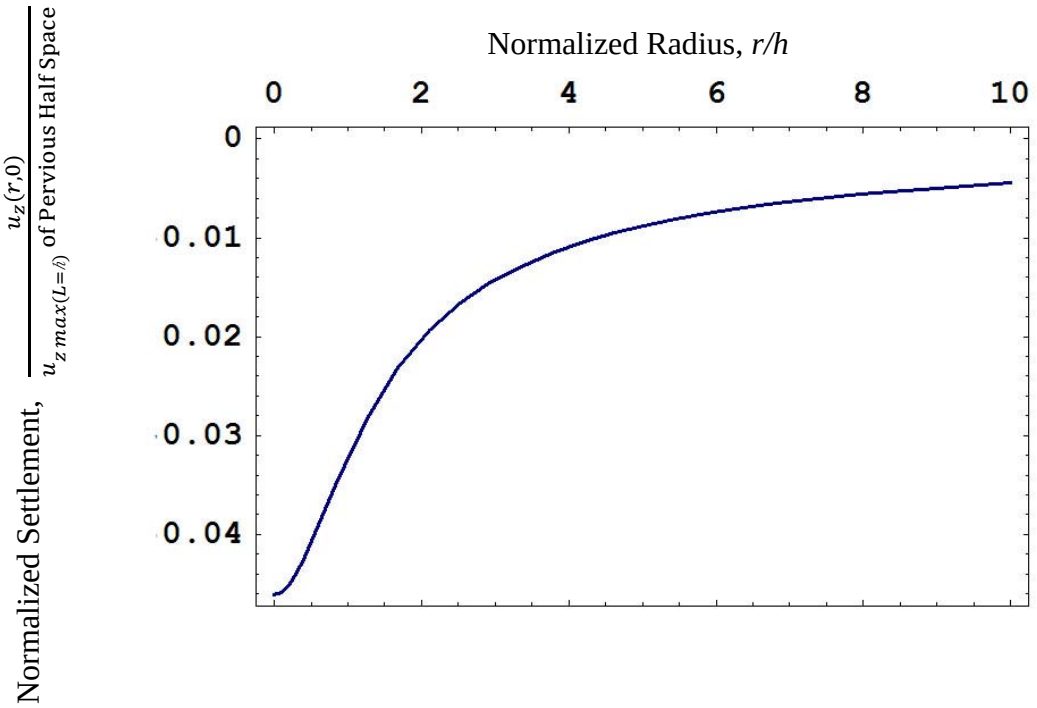

圖 4.13 地表模擬為透水情況時線狀抽水所引致之無因次化地表沉陷量(L/h = 0.3)

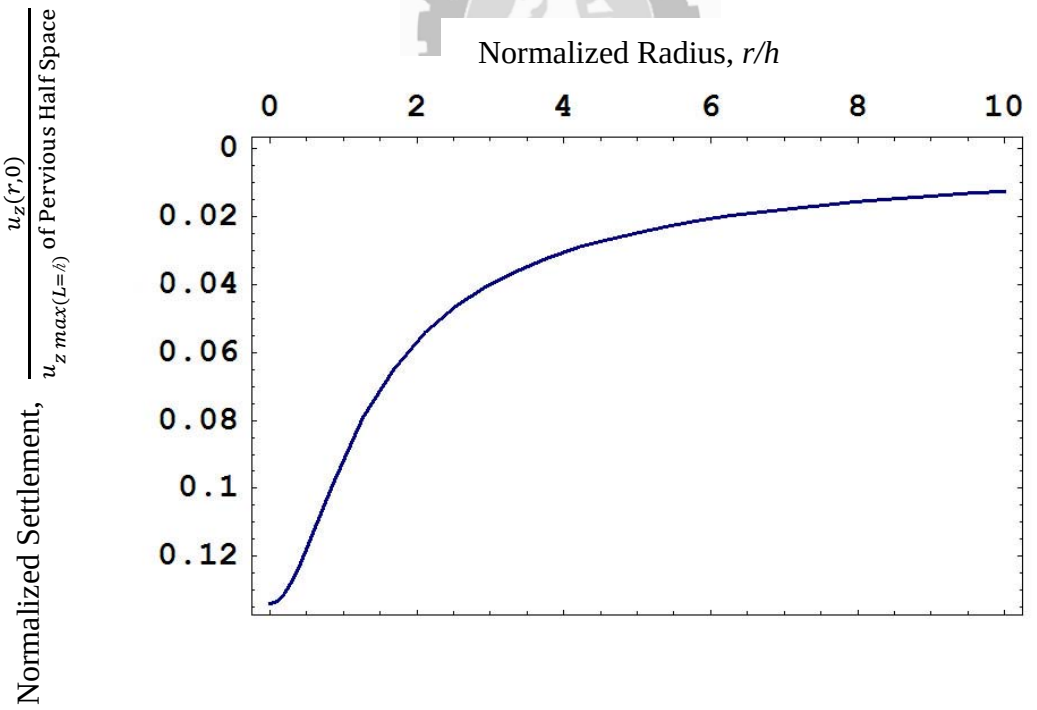

圖 4.14 地表模擬為透水情況時線狀抽水所引致之無因次化地表沉陷量(L/h = 0.5)

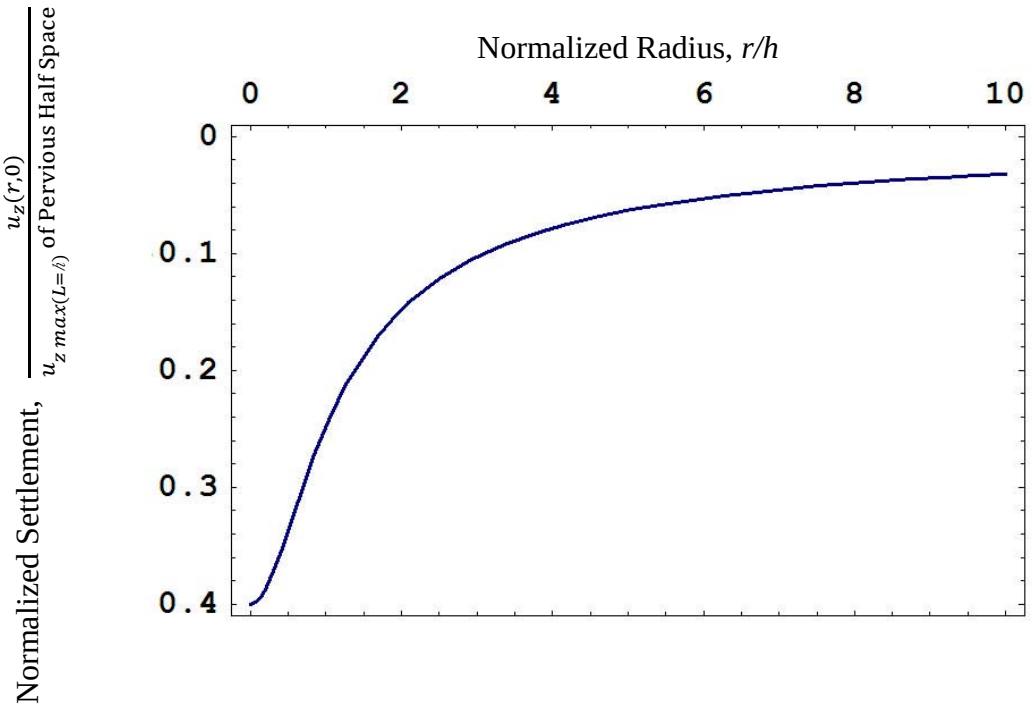

圖 4.15 地表模擬為透水情況時線狀抽水所引致之無因次化地表沉陷量(L/h = 0.8)

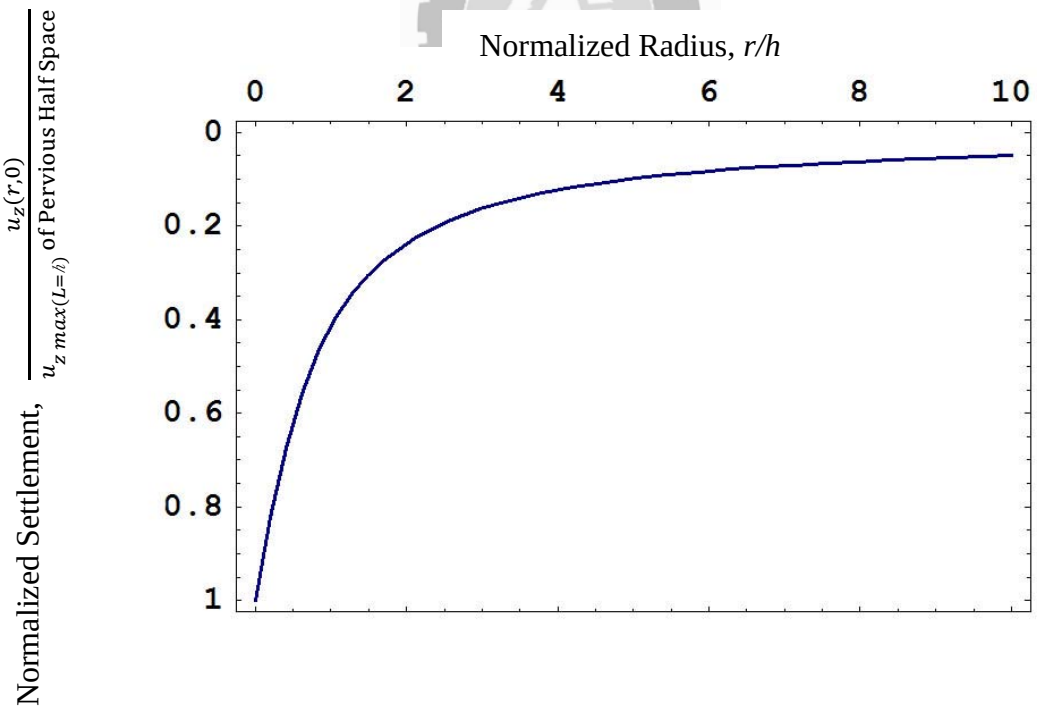

圖 4.16 地表模擬為透水情況時線狀抽水所引致之無因次化地表沉陷量(L/h = 1)

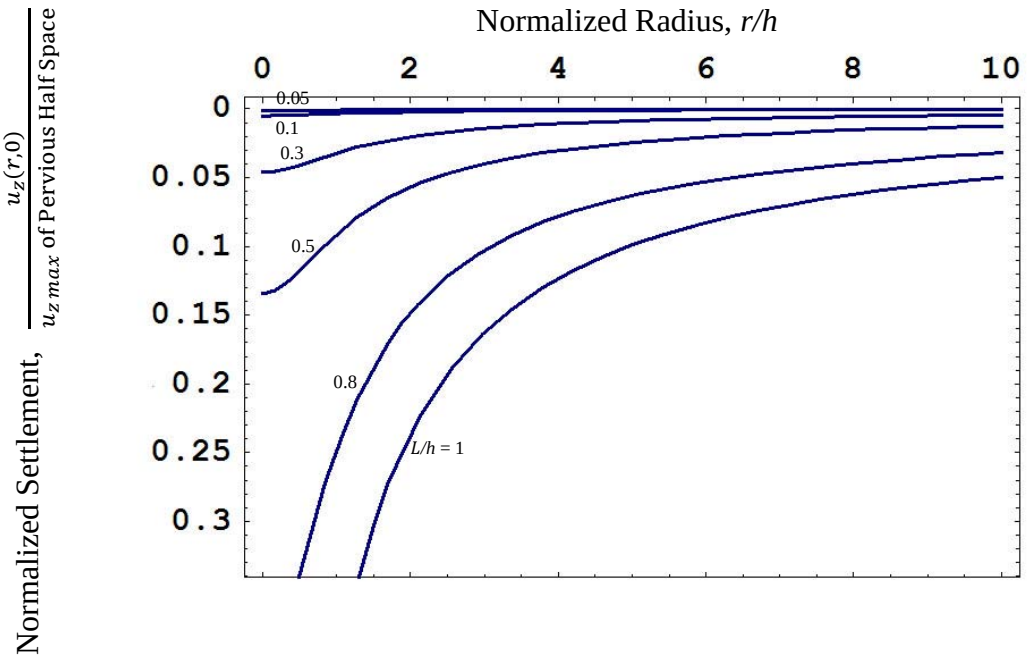

圖 4.17 地表模擬為透水情況時線狀抽水所引致之無因次化地表沉陷量(L/h = 0.1~1)

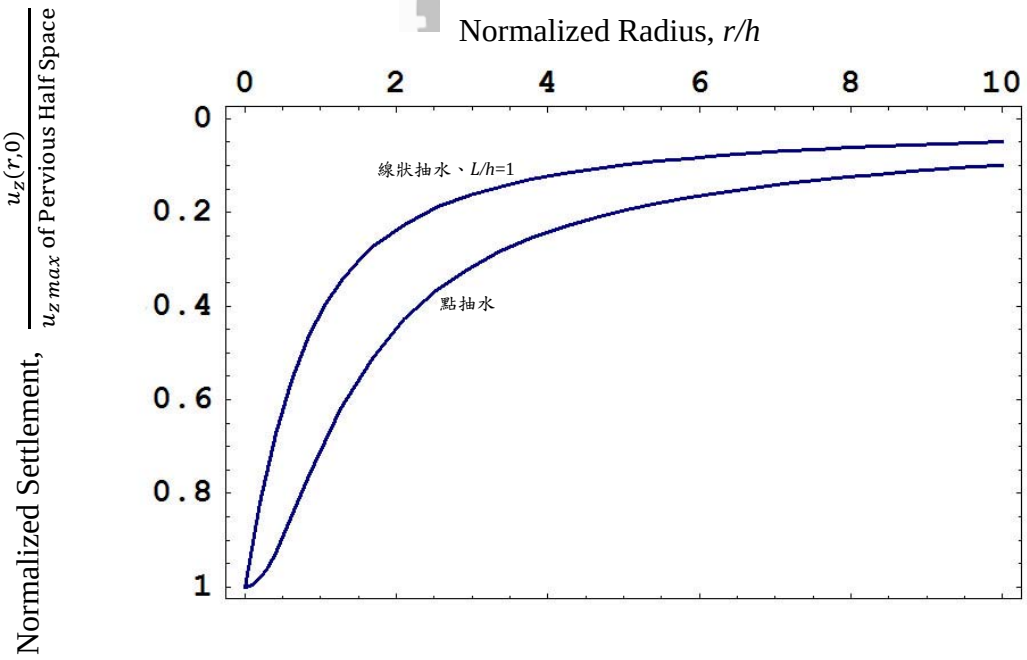

圖 4.18 透水情況下點抽水與線狀抽水所引致之無因次化地表沉陷量的比較

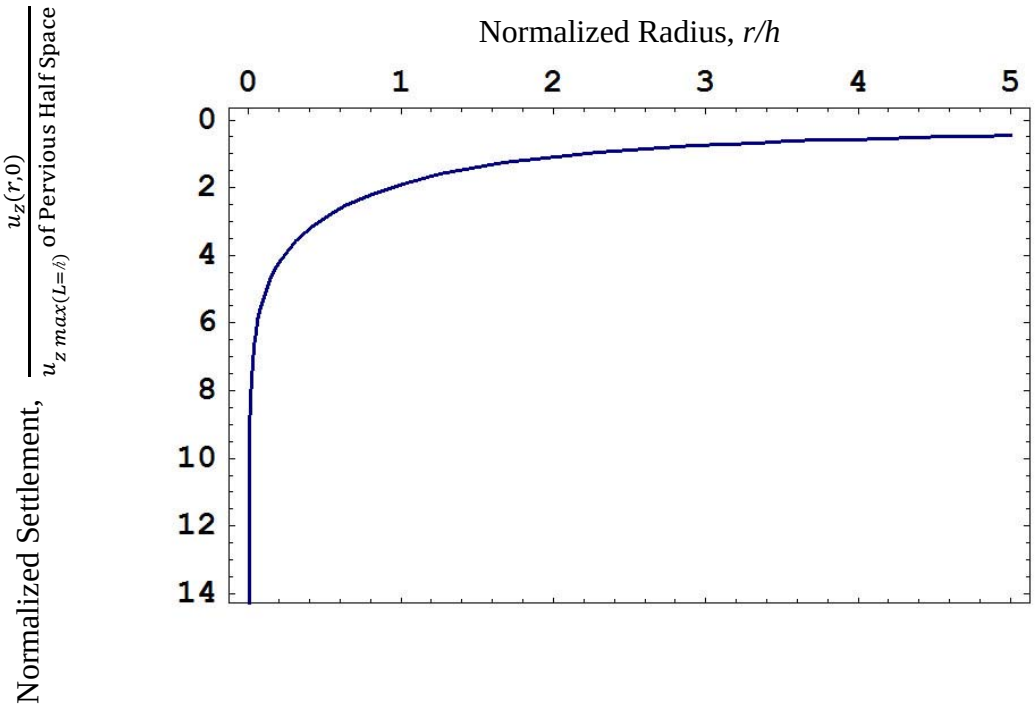

圖 4.19 地表模擬為不透水情況時線狀抽水所引致之無因次化地表沉陷量

(L/h = 0.1，ν = 0.15)

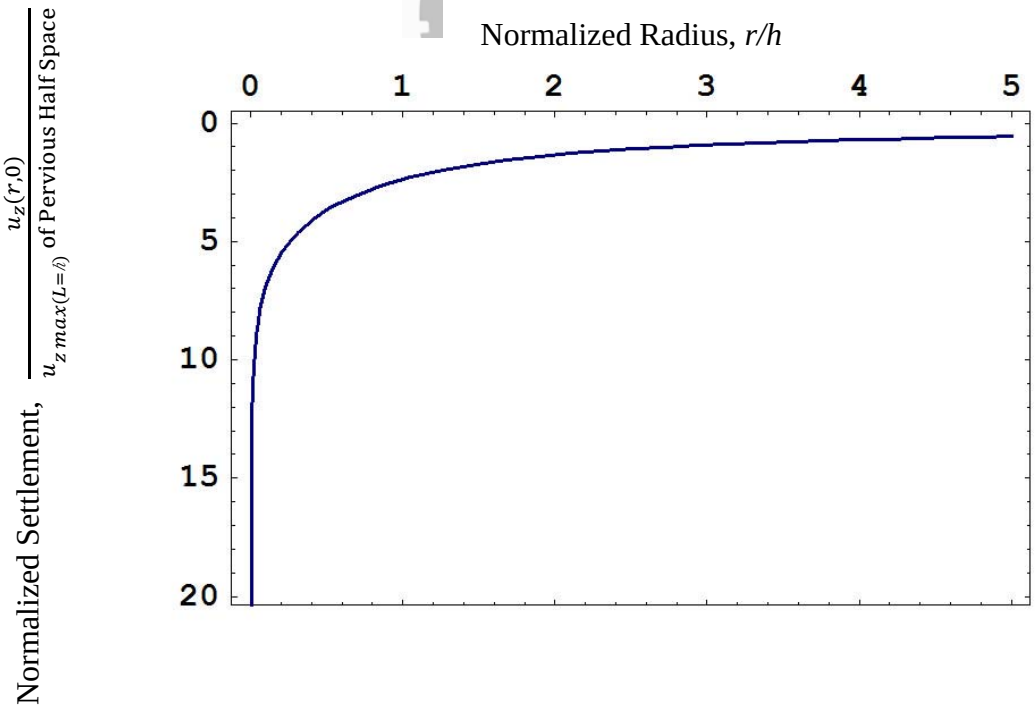

圖 4.20 地表模擬為不透水情況時線狀抽水所引致之無因次化地表沉陷量

(L/h = 0.1，ν = 0.2)

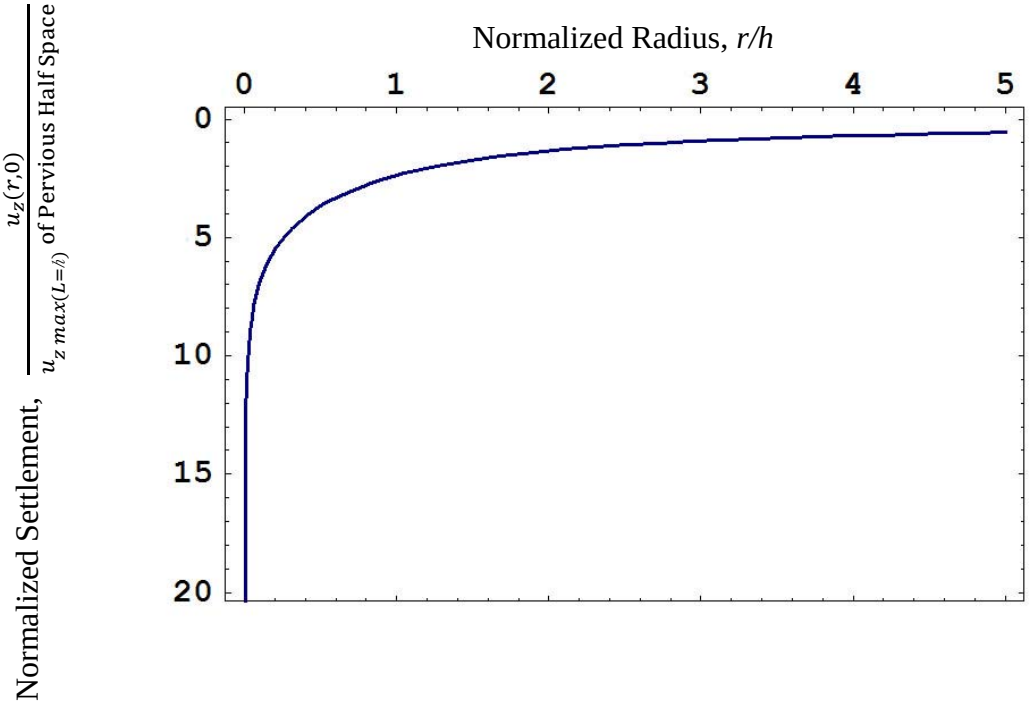

圖 4.21 地表模擬為不透水情況時線狀抽水所引致之無因次化地表沉陷量

(L/h = 0.1，ν = 0.25)

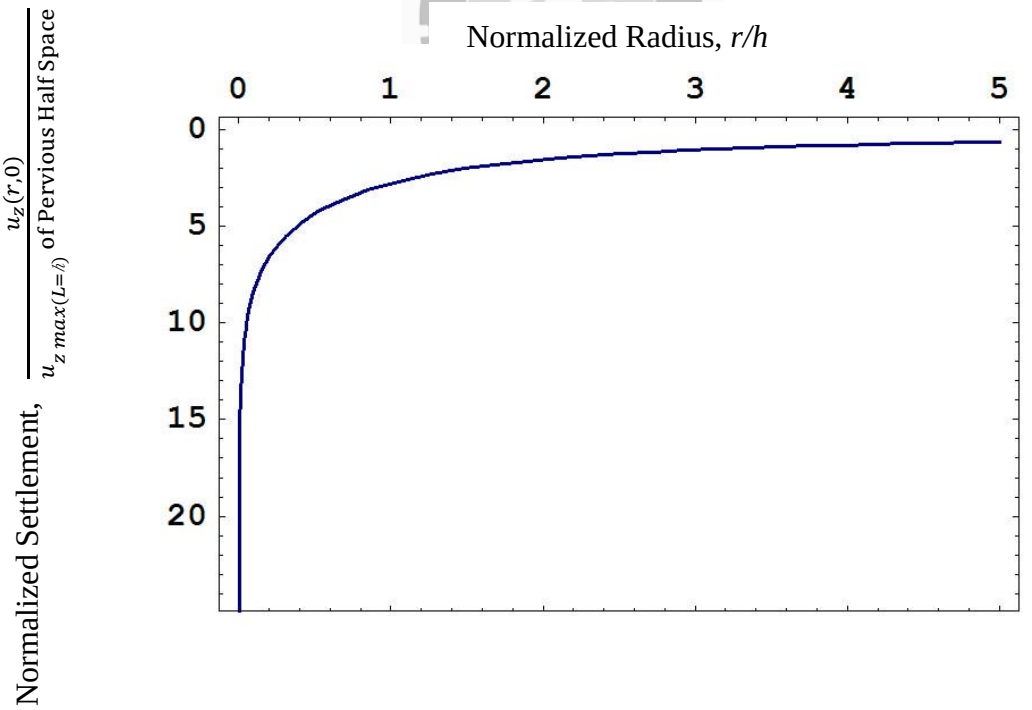

圖 4.22 地表模擬為不透水情況時線狀抽水所引致之無因次化地表沉陷量

(L/h = 0.1，ν = 0.3)

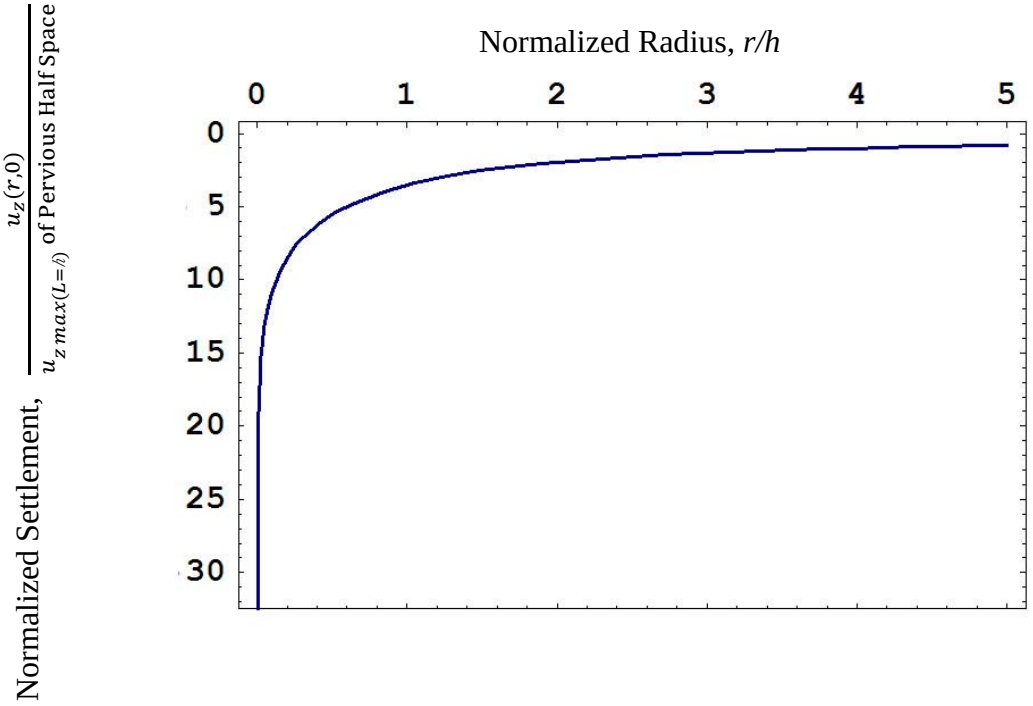

圖 4.23 地表模擬為不透水情況時線狀抽水所引致之無因次化地表沉陷量

(L/h = 0.1，ν = 0.35)

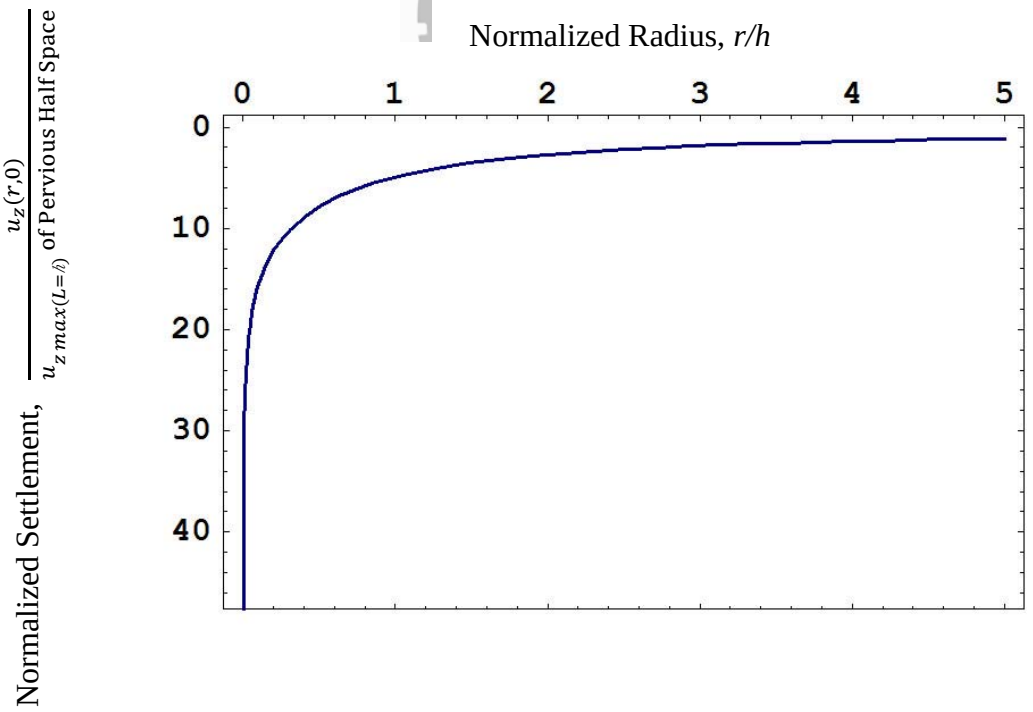

圖 4.24 地表模擬為不透水情況時線狀抽水所引致之無因次化地表沉陷量

(L/h = 0.1，ν = 0.4)

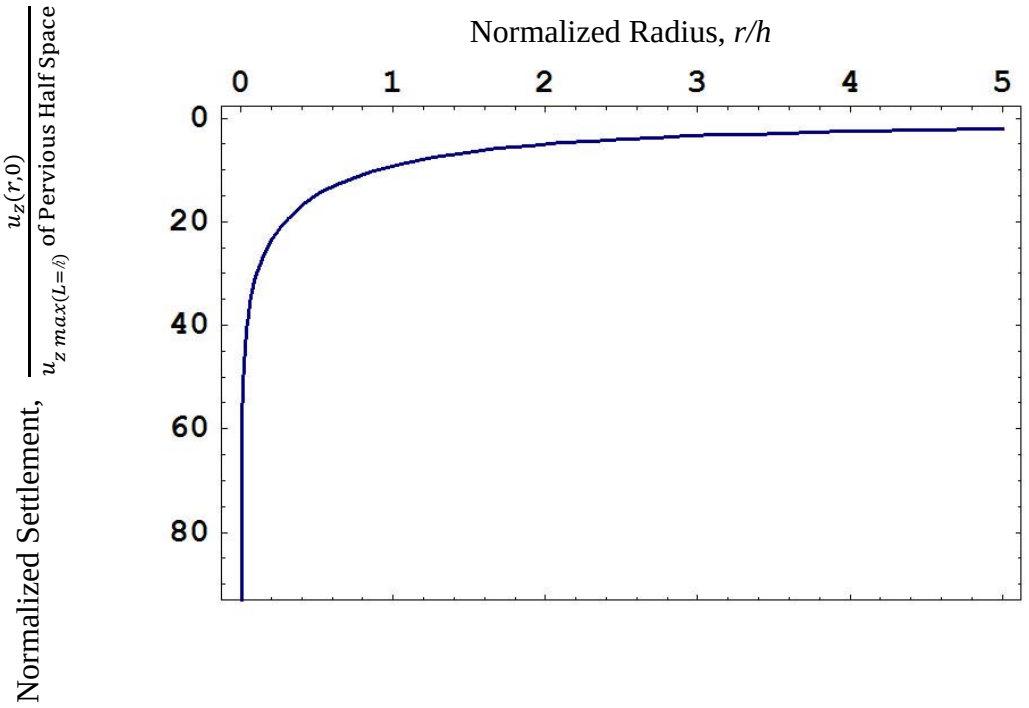

圖 4.25 地表模擬為不透水情況時線狀抽水所引致之無因次化地表沉陷量

(L/h = 0.1，ν = 0.45)

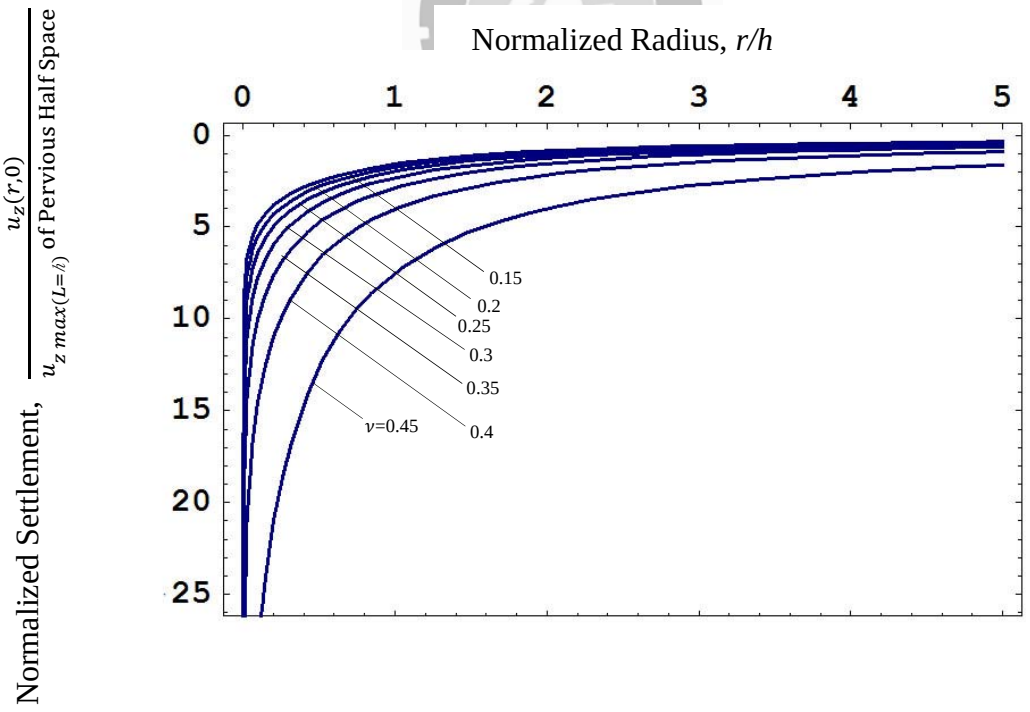

圖 4.26 地表模擬為不透水情況時線狀抽水所引致之無因次化地表沉陷量

(L/h = 0.1，ν = 0.15~0.45)

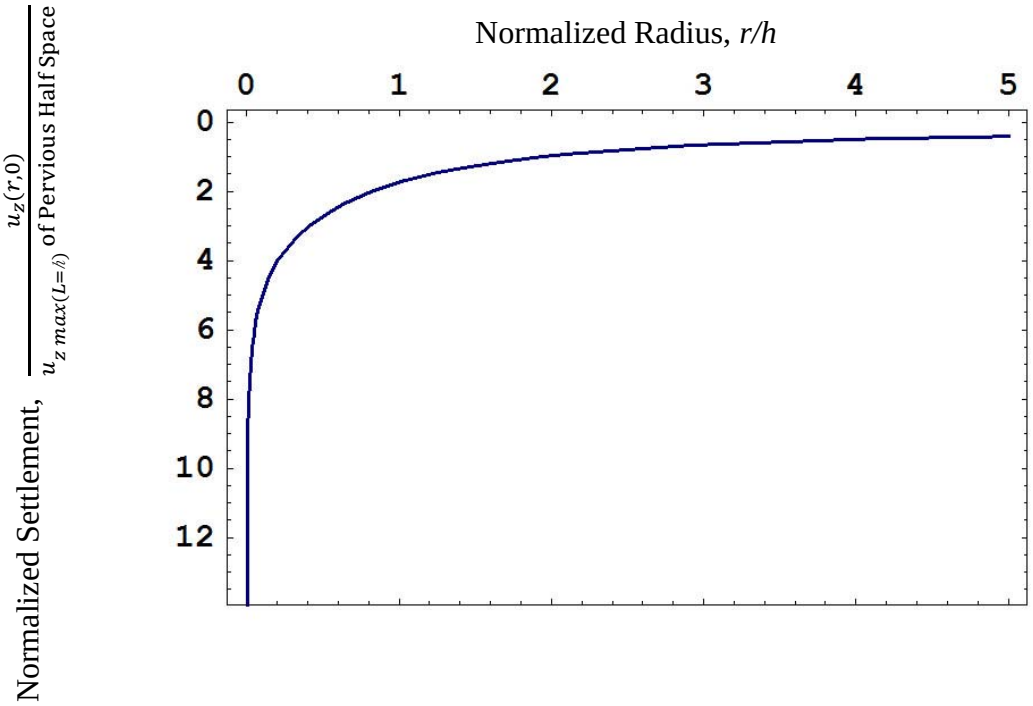

圖 4.27 地表模擬為不透水情況時線狀抽水所引致之無因次化地表沉陷量

(L/h = 0.3，ν = 0.15)

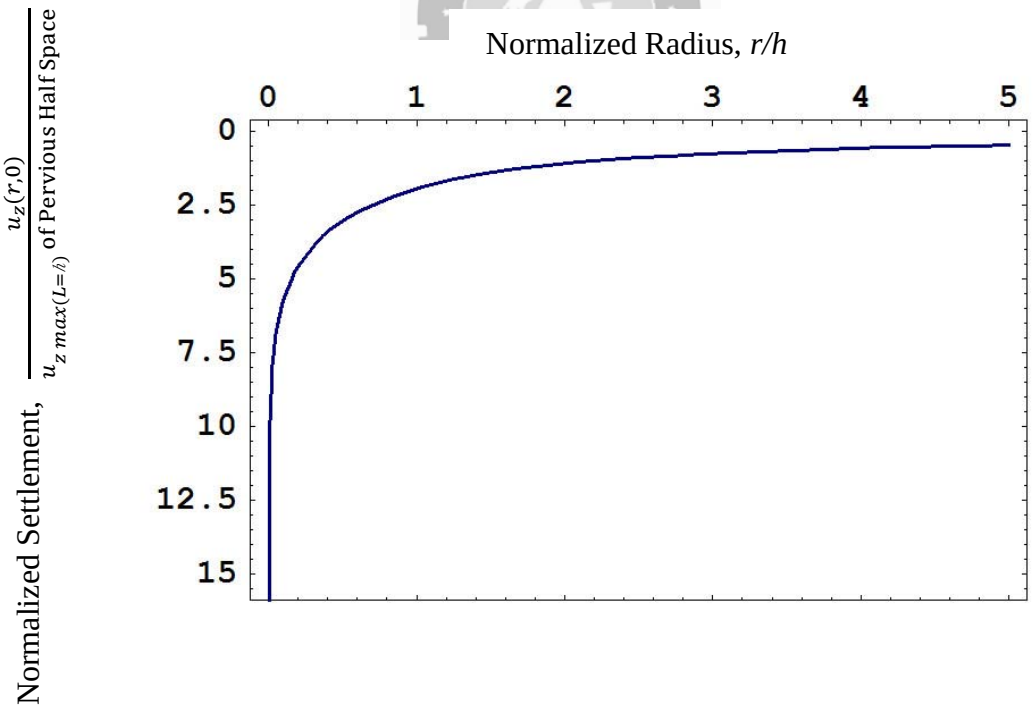

圖 4.28 地表模擬為不透水情況時線狀抽水所引致之無因次化地表沉陷量

(L/h = 0.3，ν = 0.2)

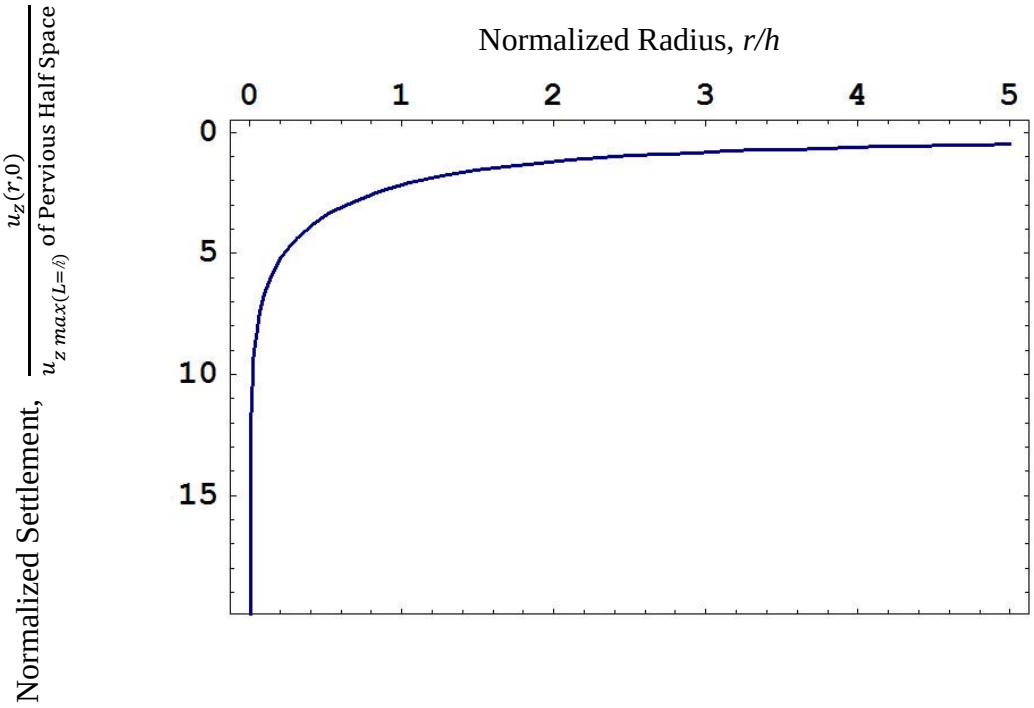

圖 4.29 地表模擬為不透水情況時線狀抽水所引致之無因次化地表沉陷量

(L/h = 0.3，ν = 0.25)

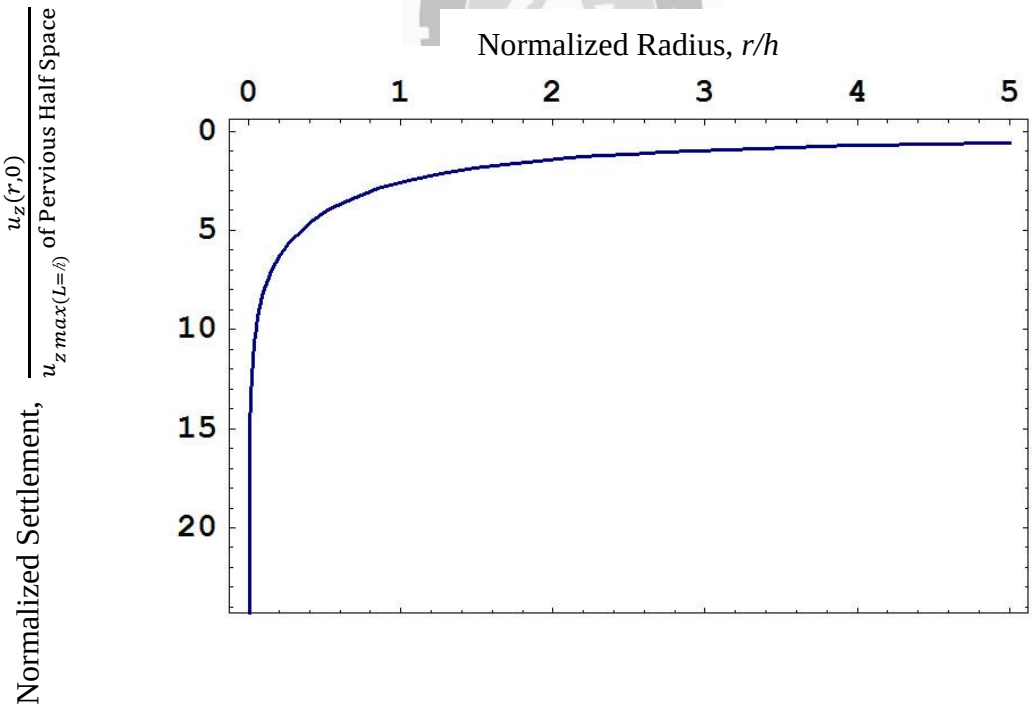

圖 4.30 地表模擬為不透水情況時線狀抽水所引致之無因次化地表沉陷量

(L/h = 0.3，ν = 0.3)

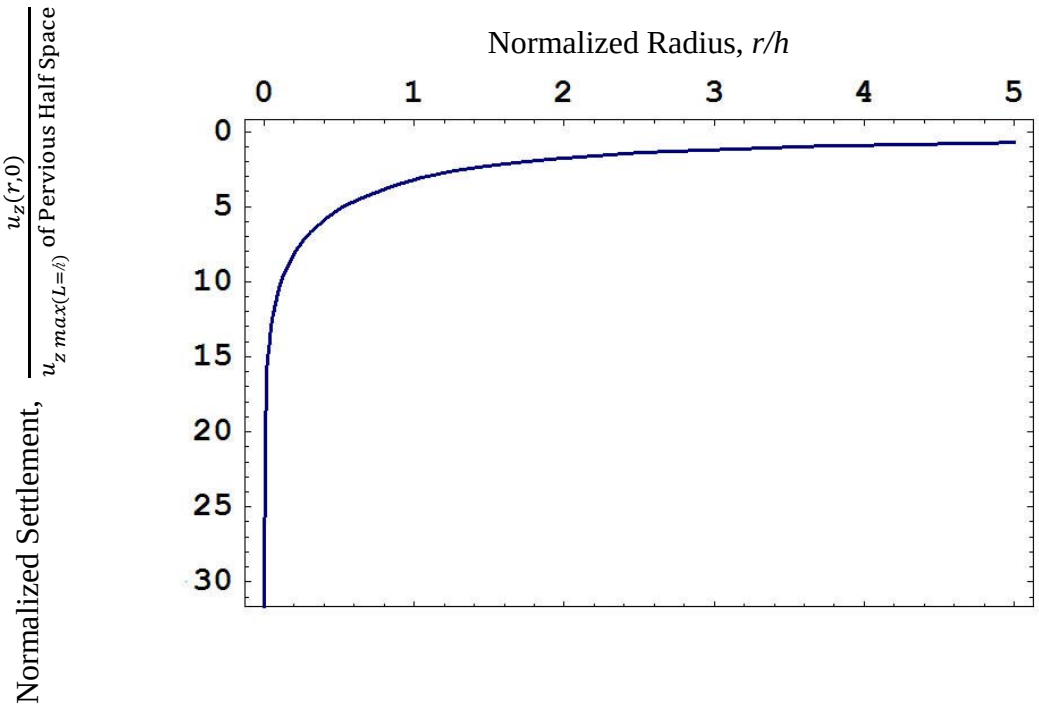

圖 4.31 地表模擬為不透水情況時線狀抽水所引致之無因次化地表沉陷量

(L/h = 0.3，ν = 0.35)

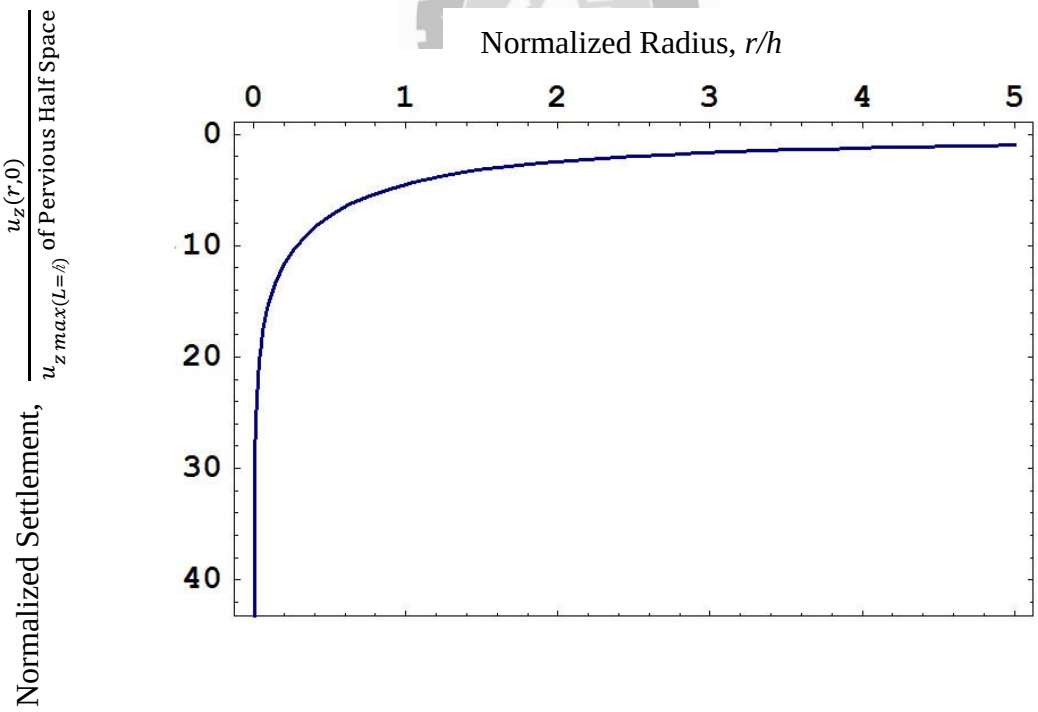

圖 4.32 地表模擬為不透水情況時線狀抽水所引致之無因次化地表沉陷量

(L/h = 0.3，ν = 0.4)

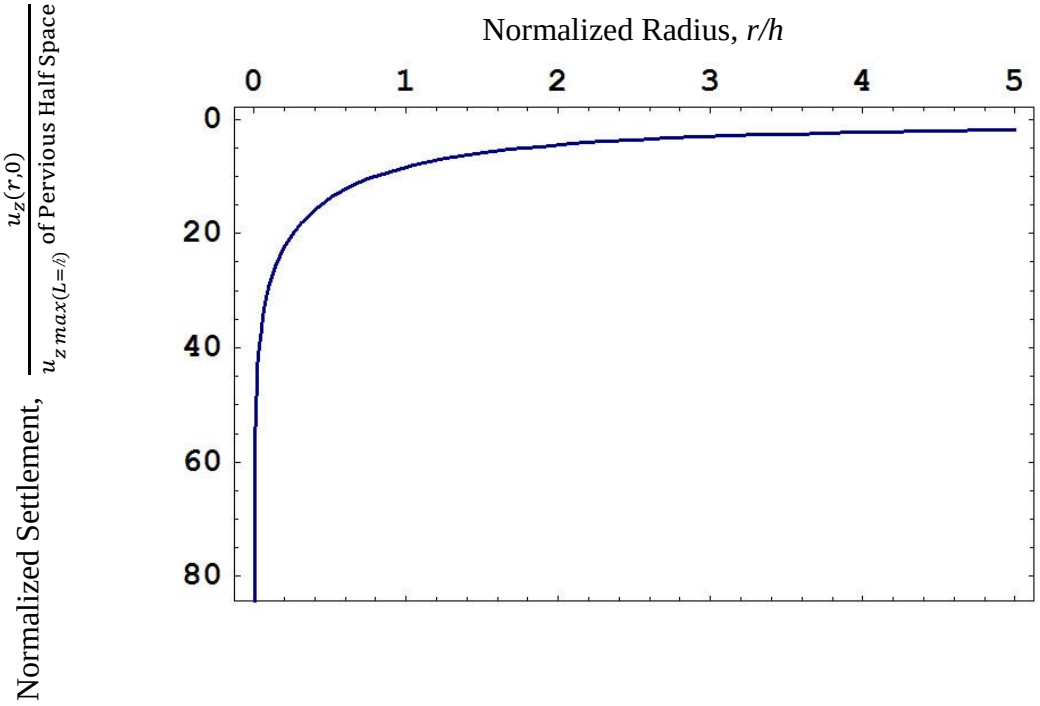

圖 4.33 地表模擬為不透水情況時線狀抽水所引致之無因次化地表沉陷量

(L/h = 0.3，ν = 0.45)

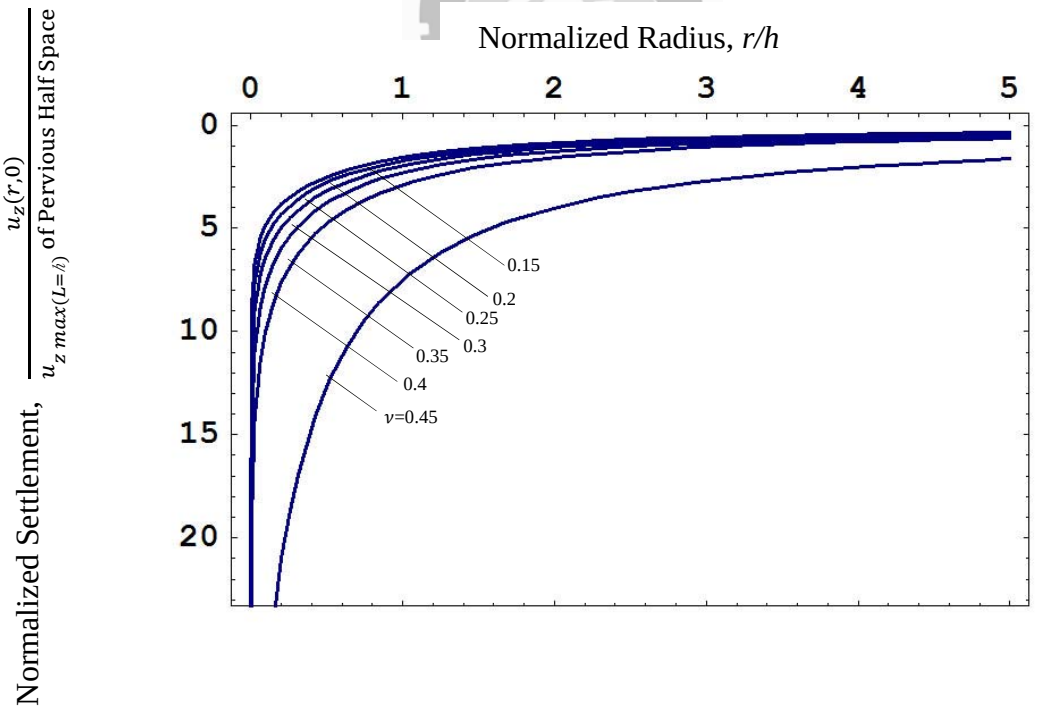

圖 4.34 地表模擬為不透水情況時線狀抽水所引致之無因次化地表沉陷量

(L/h = 0.3，ν = 0.15~0.45)

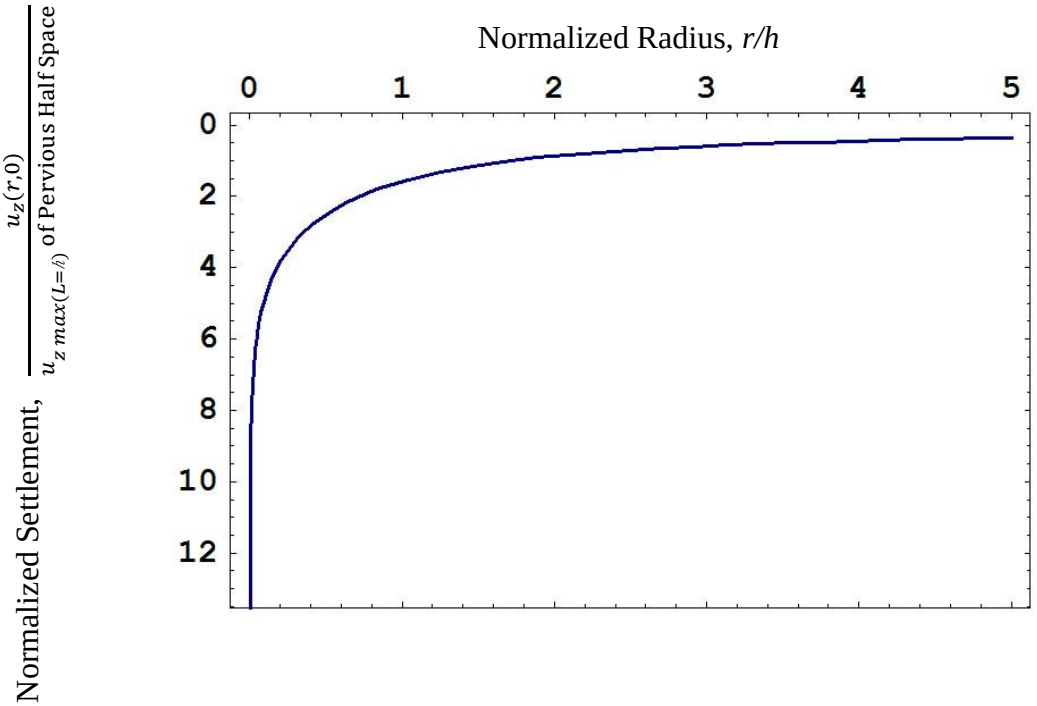

圖 4.35 地表模擬為不透水情況時線狀抽水所引致之無因次化地表沉陷量

(L/h = 0.5，ν = 0.15)

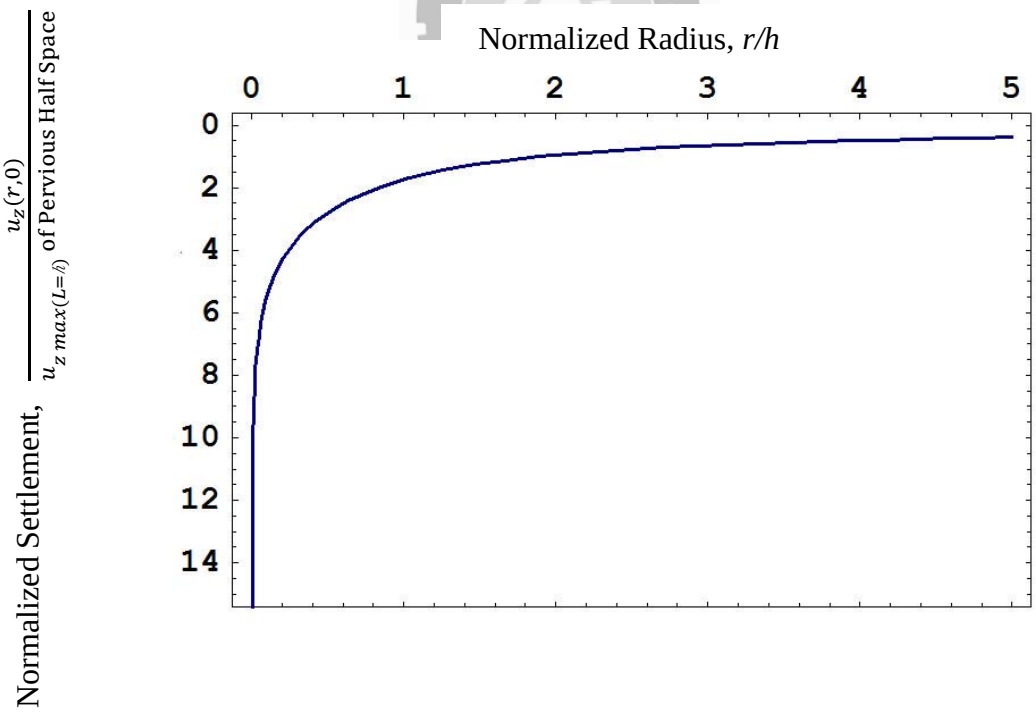

圖 4.36 地表模擬為不透水情況時線狀抽水所引致之無因次化地表沉陷量

(L/h = 0.5，ν = 0.2)

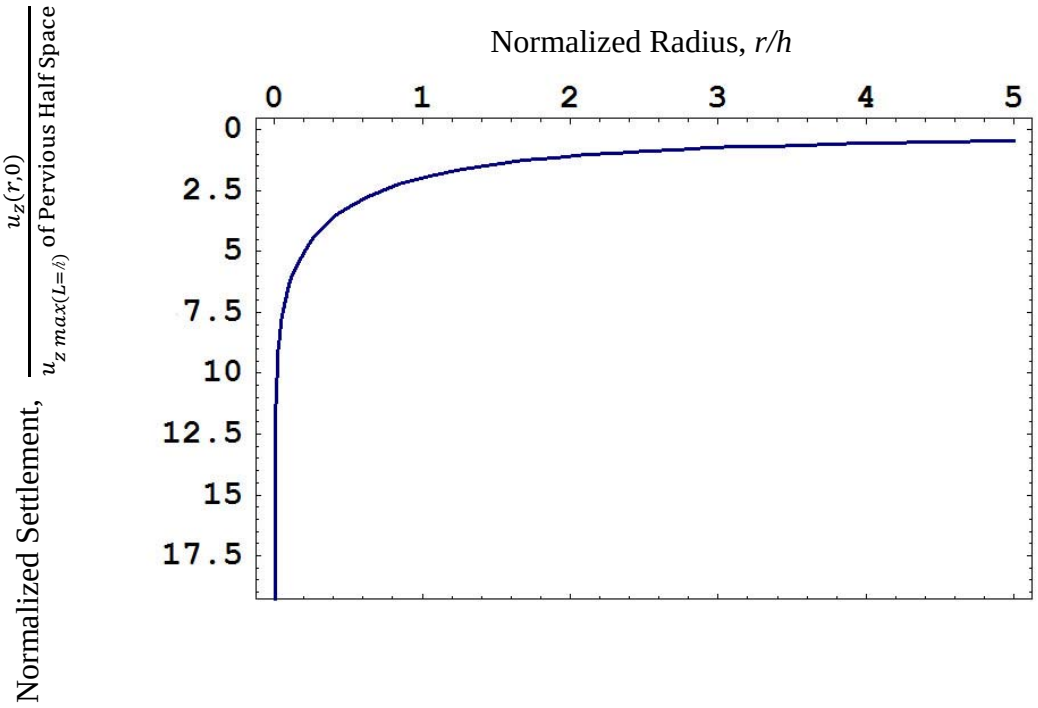

圖 4.37 地表模擬為不透水情況時線狀抽水所引致之無因次化地表沉陷量

(L/h = 0.5，ν = 0.25)

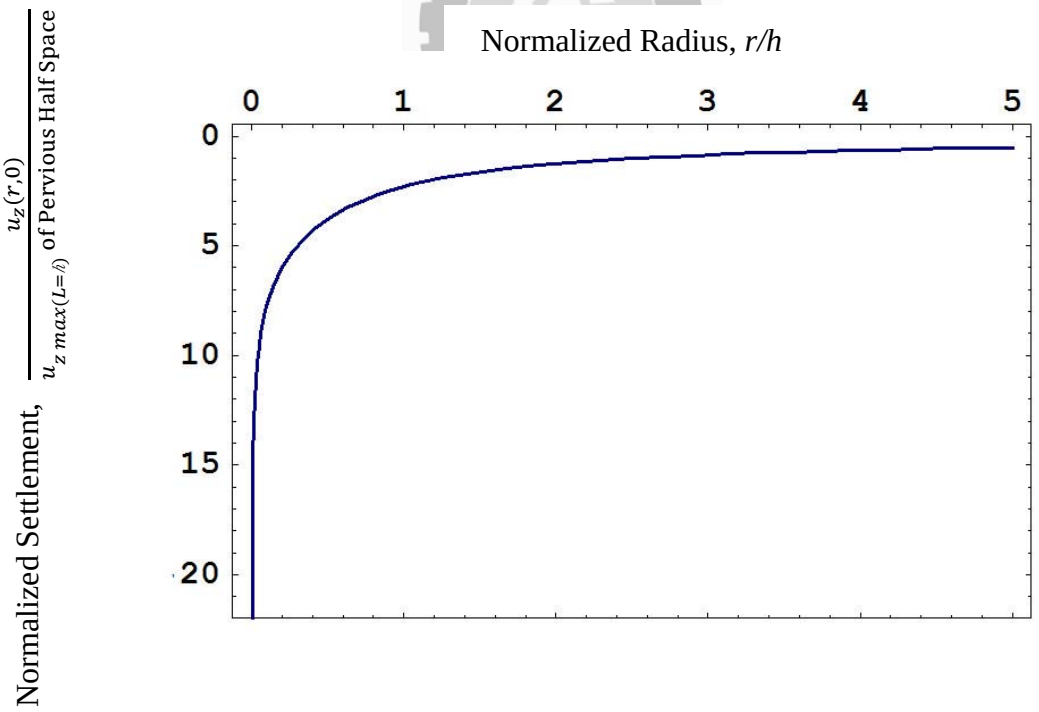

圖 4.38 地表模擬為不透水情況時線狀抽水所引致之無因次化地表沉陷量

(L/h = 0.5，ν = 0.3)

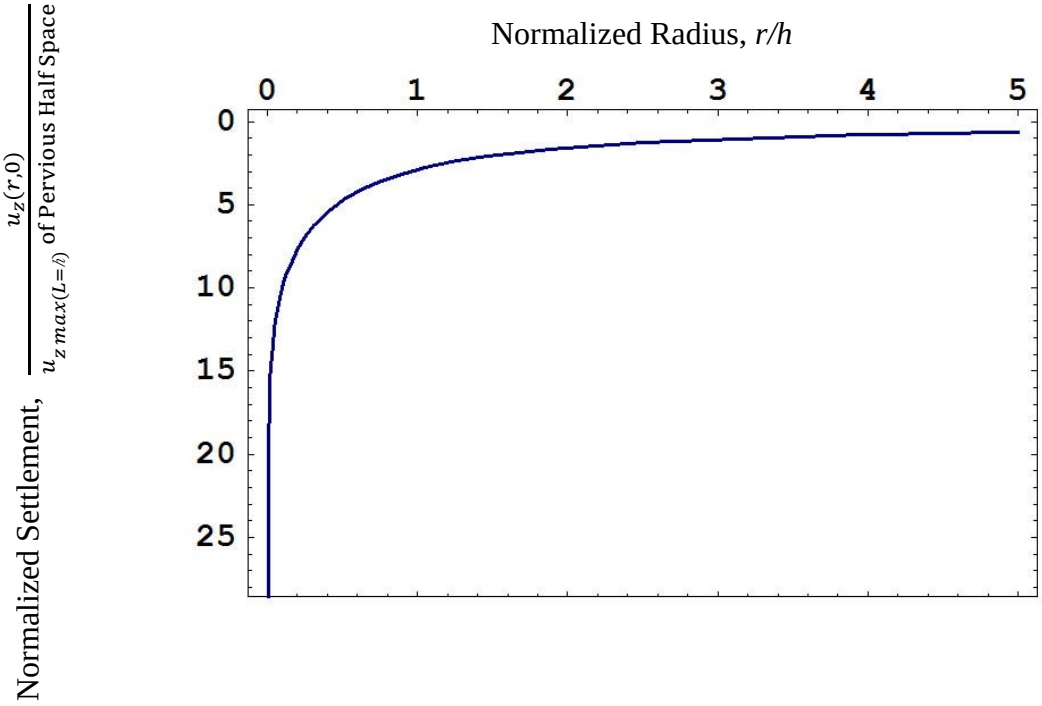

圖 4.39 地表模擬為不透水情況時線狀抽水所引致之無因次化地表沉陷量

(L/h = 0.5，ν = 0.35)

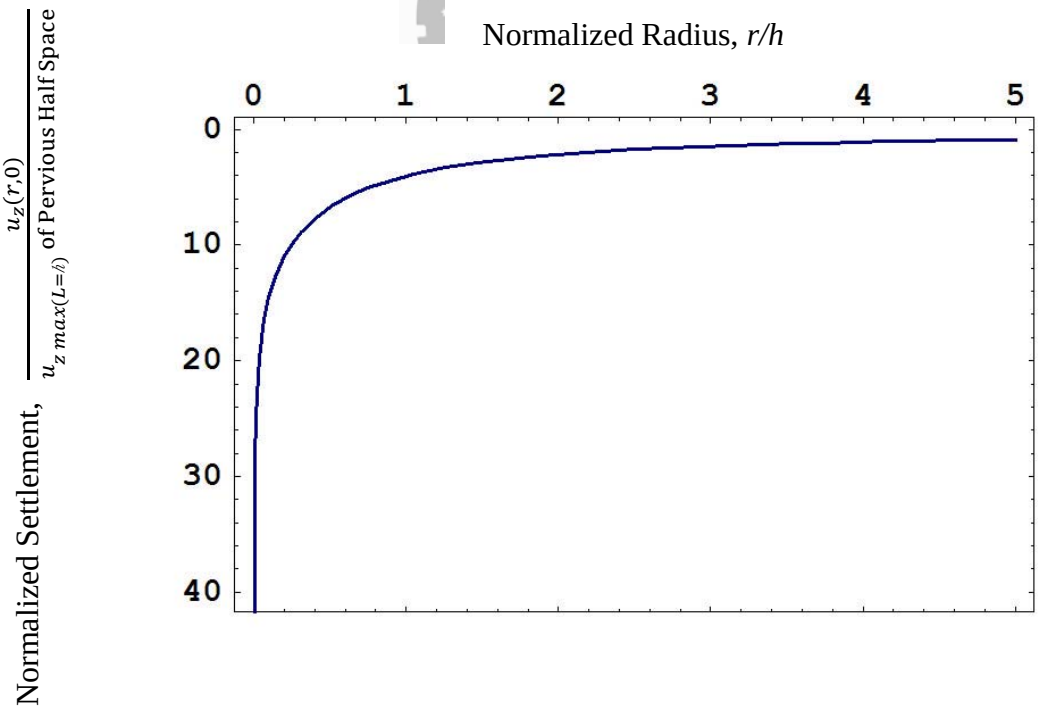

圖 4.40 地表模擬為不透水情況時線狀抽水所引致之無因次化地表沉陷量

(L/h = 0.5，ν = 0.4)

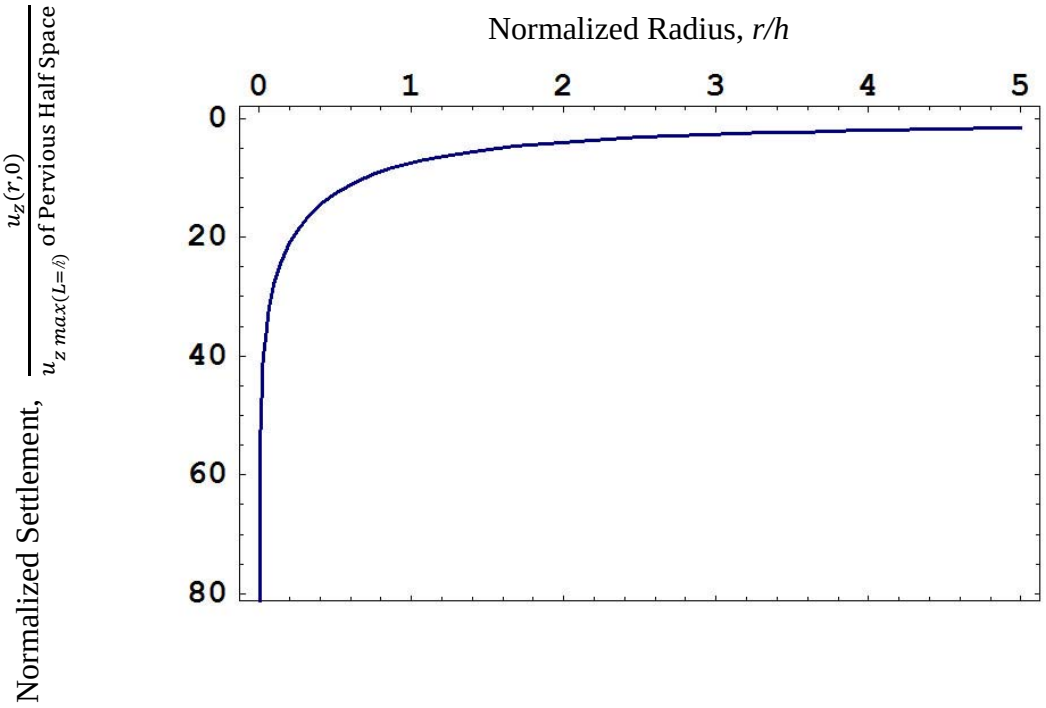

圖 4.41 地表模擬為不透水情況時線狀抽水所引致之無因次化地表沉陷量

(L/h = 0.5，ν = 0.45)

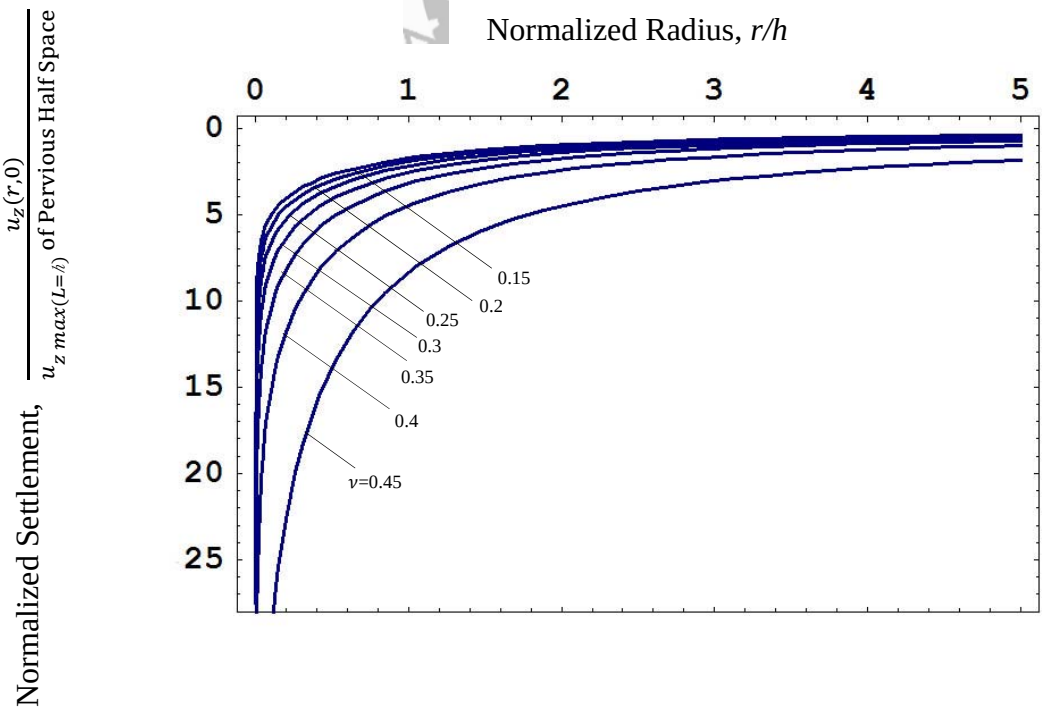

圖 4.42 地表模擬為不透水情況時線狀抽水所引致之無因次化地表沉陷量

(L/h = 0.3，ν = 0.15~0.45)

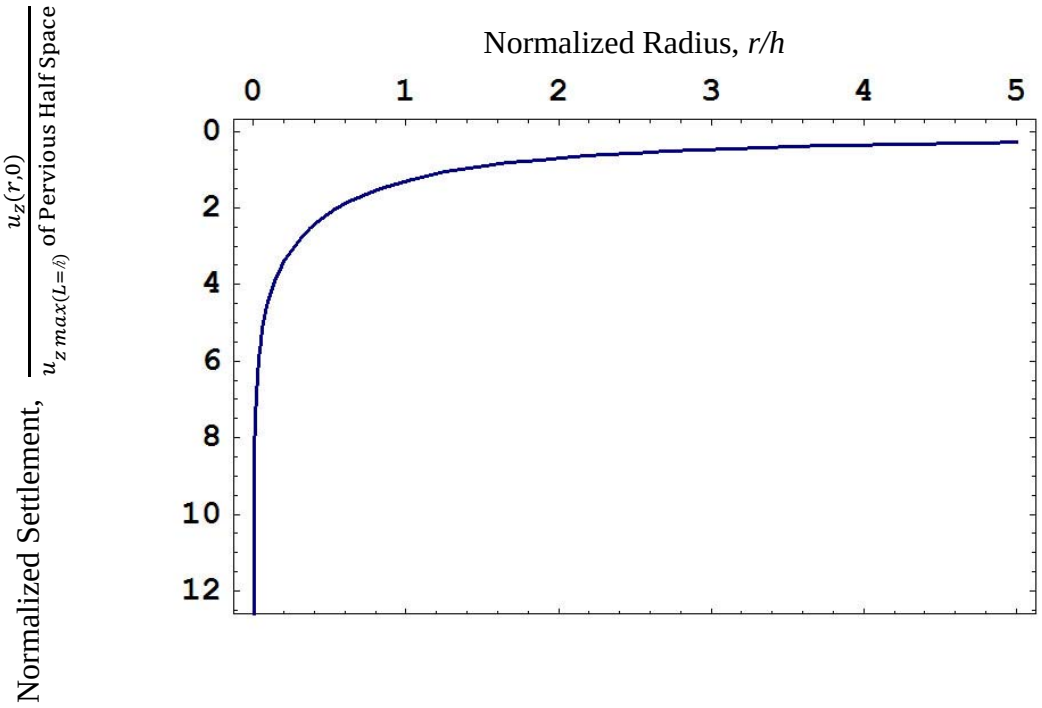

圖 4.43 地表模擬為不透水情況時線狀抽水所引致之無因次化地表沉陷量

(L/h = 0.8，ν = 0.15)

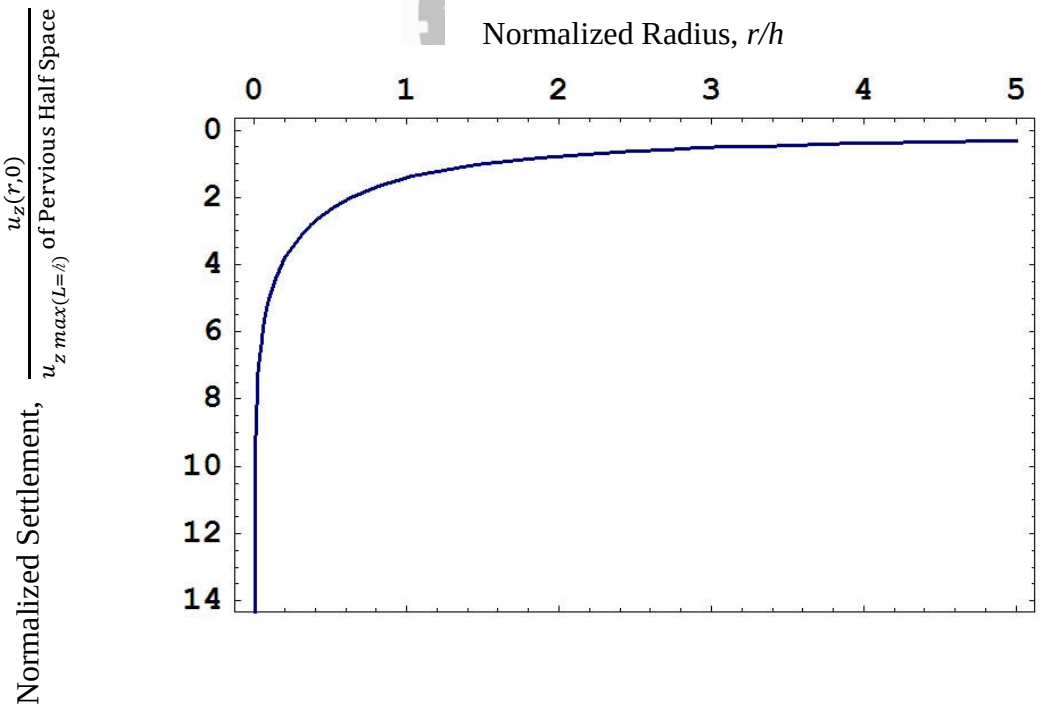

圖 4.44 地表模擬為不透水情況時線狀抽水所引致之無因次化地表沉陷量

(L/h = 0.8，ν = 0.2)

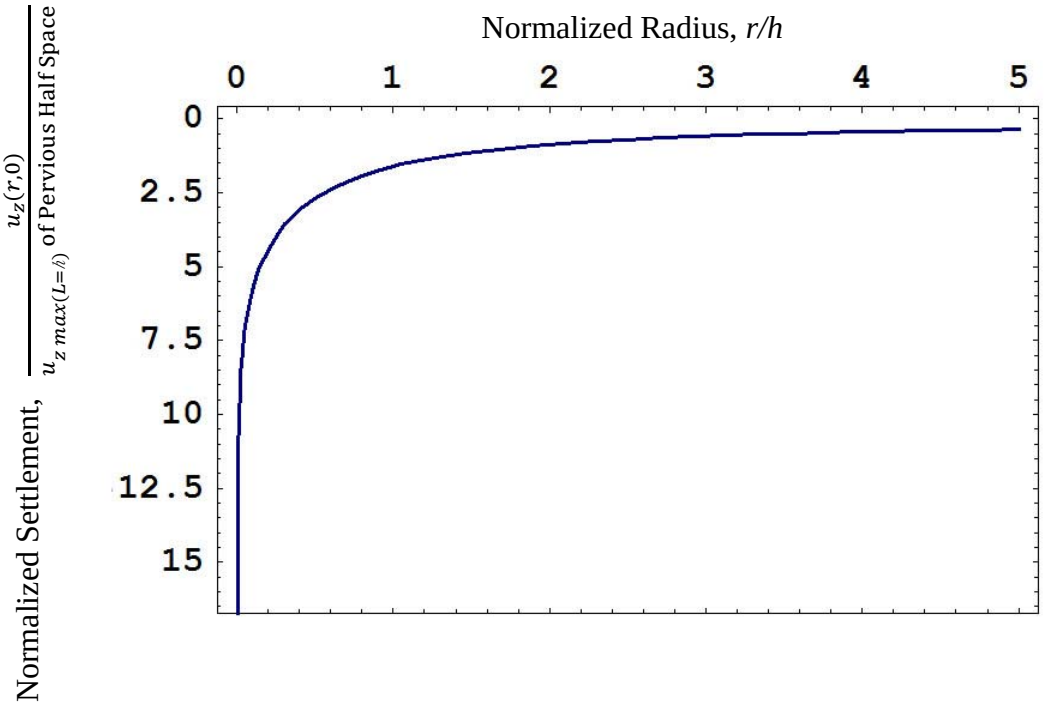

圖 4.45 地表模擬為不透水情況時線狀抽水所引致之無因次化地表沉陷量

(L/h = 0.8，ν = 0.25)

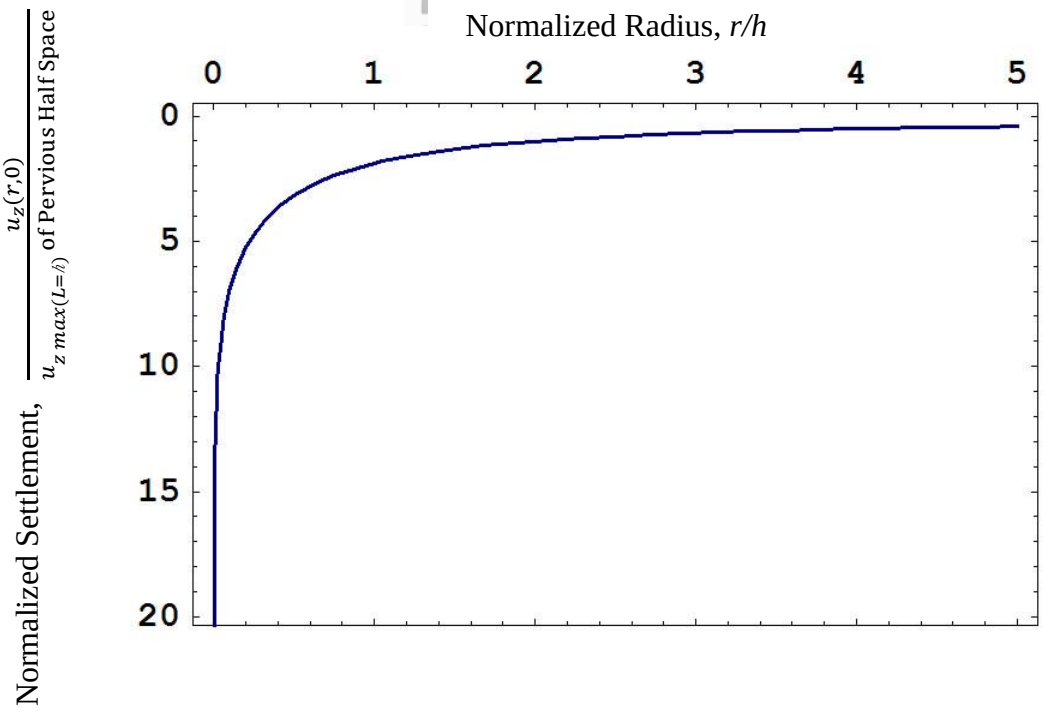

圖 4.46 地表模擬為不透水情況時線狀抽水所引致之無因次化地表沉陷量

(L/h = 0.8，ν = 0.3)

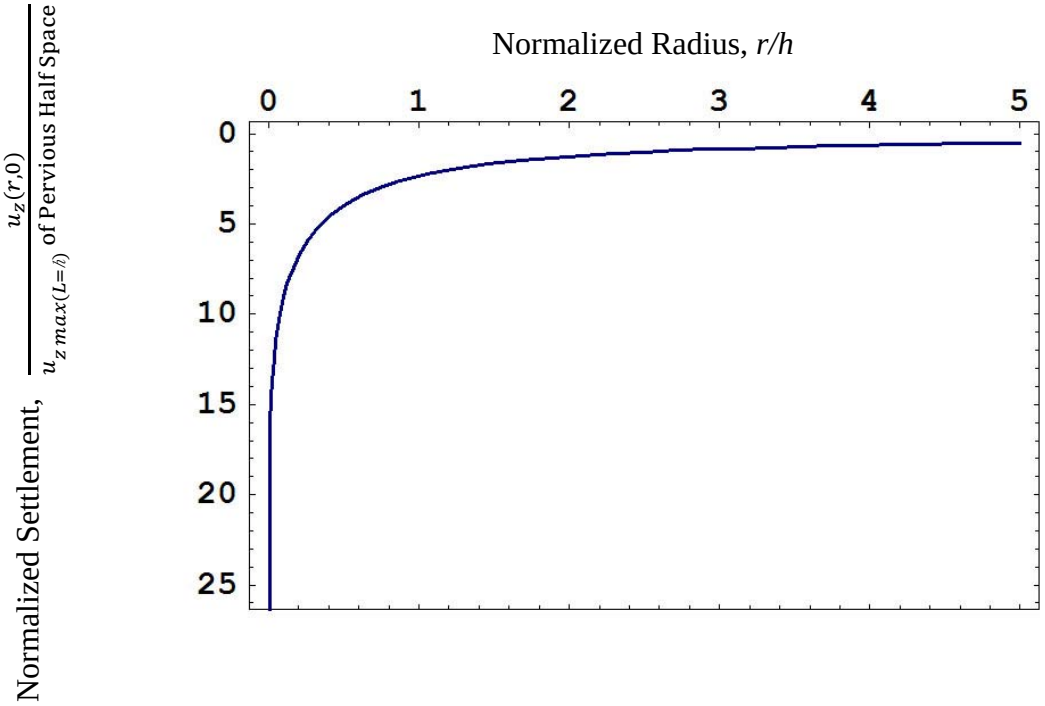

圖 4.47 地表模擬為不透水情況時線狀抽水所引致之無因次化地表沉陷量

(L/h = 0.8，ν = 0.35)

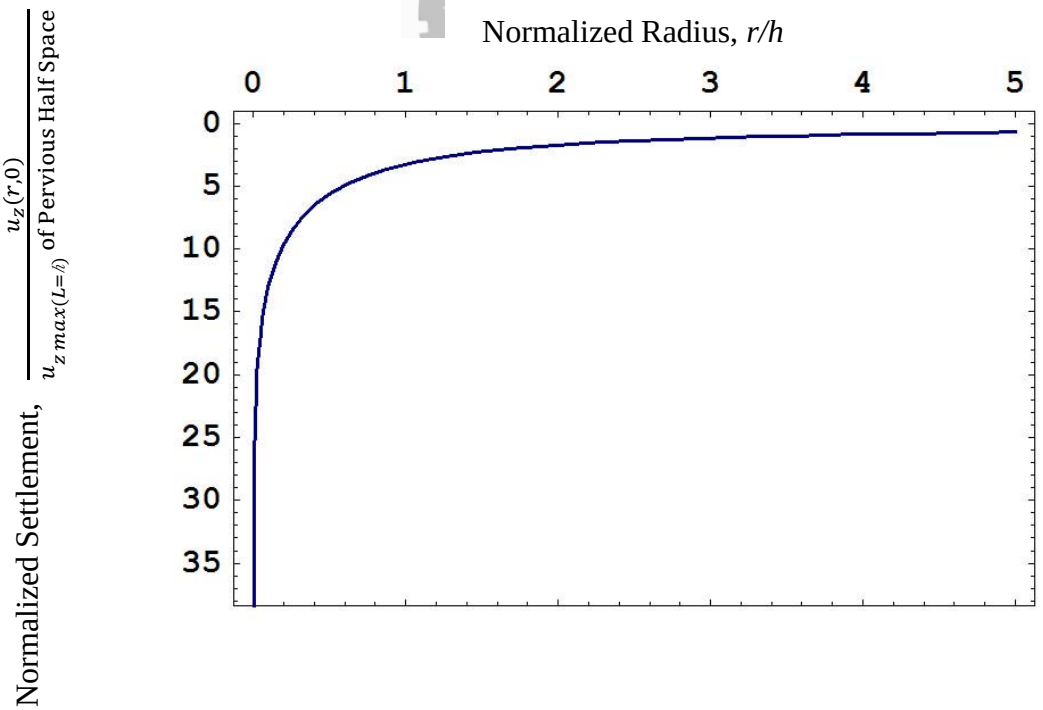

圖 4.48 地表模擬為不透水情況時線狀抽水所引致之無因次化地表沉陷量

(L/h = 0.8，ν = 0.4)

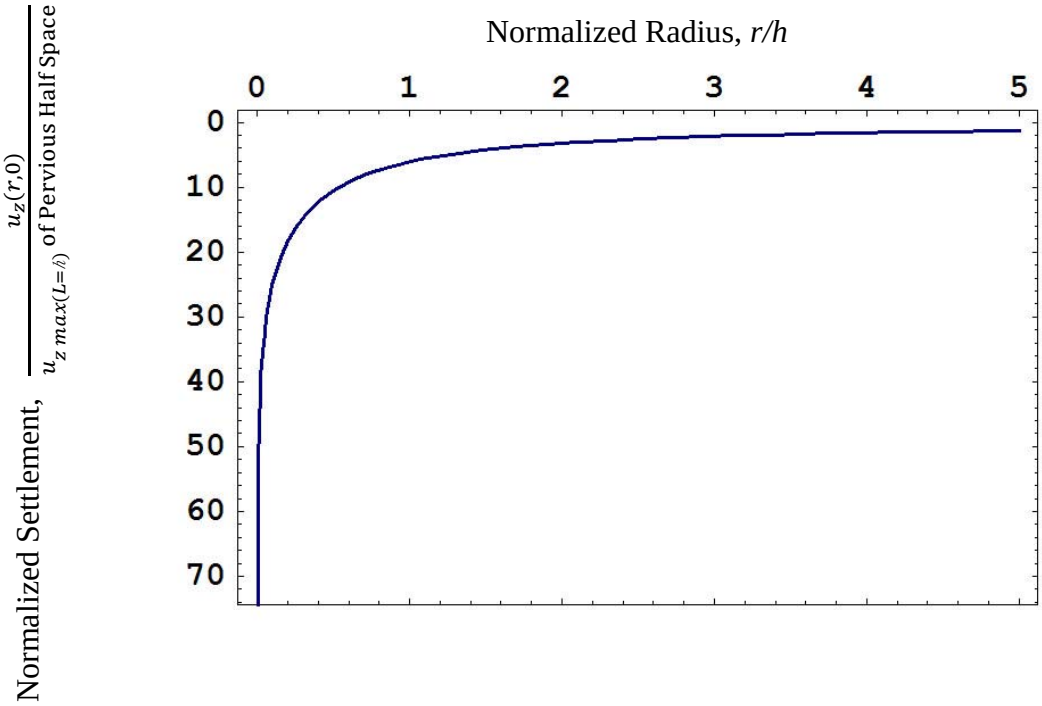

圖 4.49 地表模擬為不透水情況時線狀抽水所引致之無因次化地表沉陷量

(L/h = 0.8，ν = 0.45)

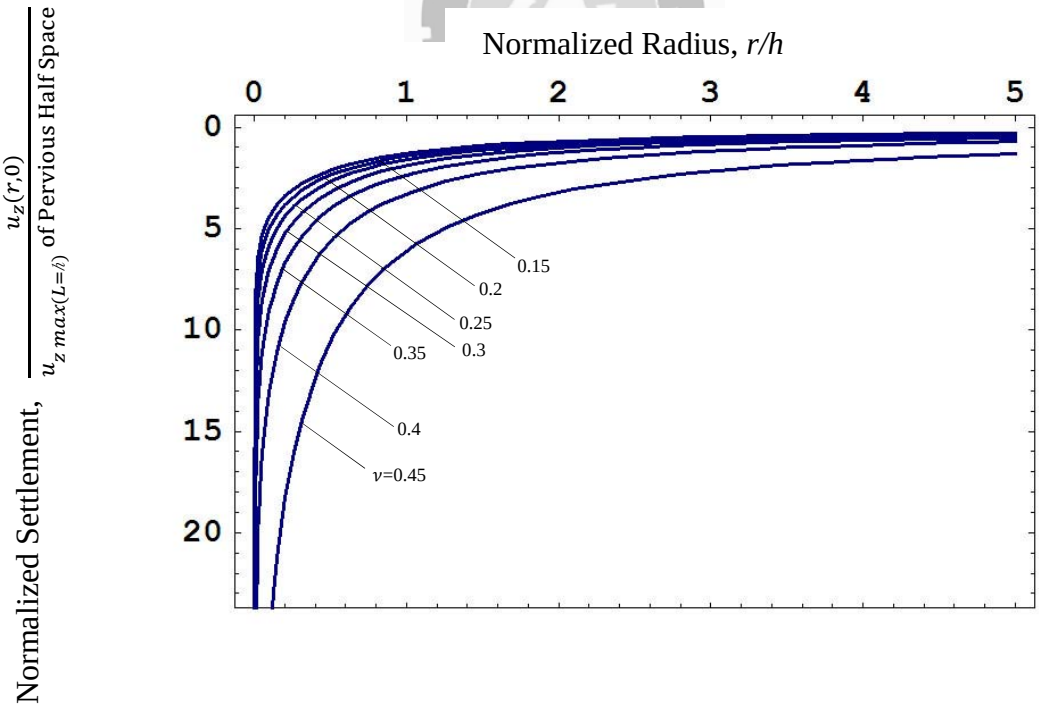

圖 4.50 地表模擬為不透水情況時線狀抽水所引致之無因次化地表沉陷量

(L/h = 0.8，ν = 0.15~0.45)

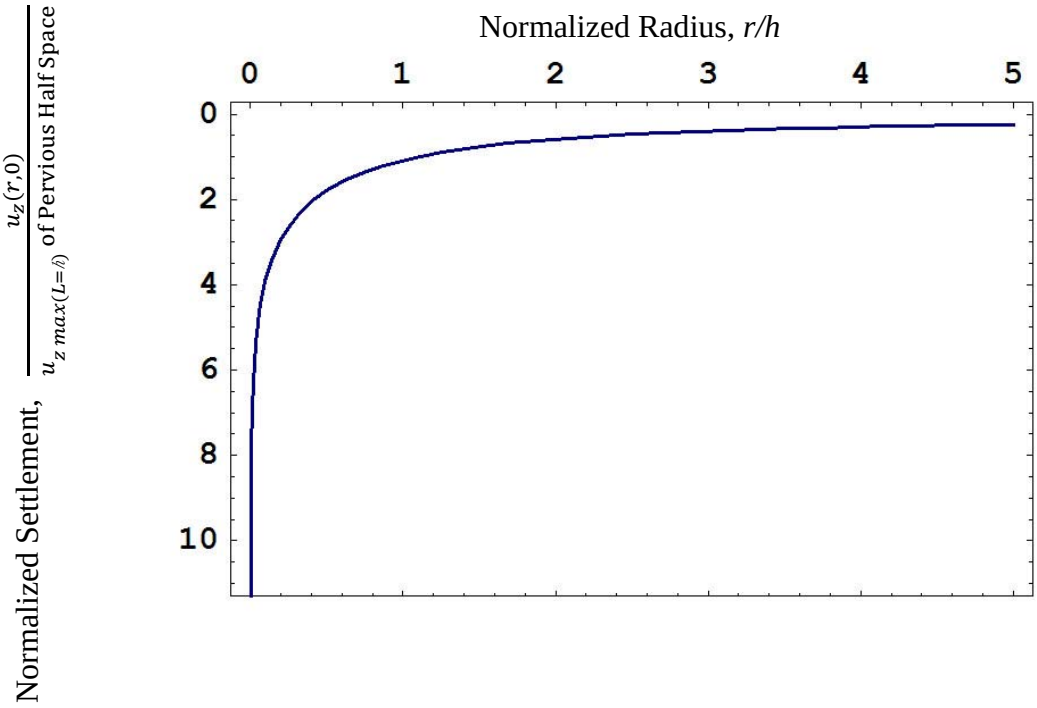

圖 4.51 地表模擬為不透水情況時線狀抽水所引致之無因次化地表沉陷量

(L/h = 1，ν = 0.15)

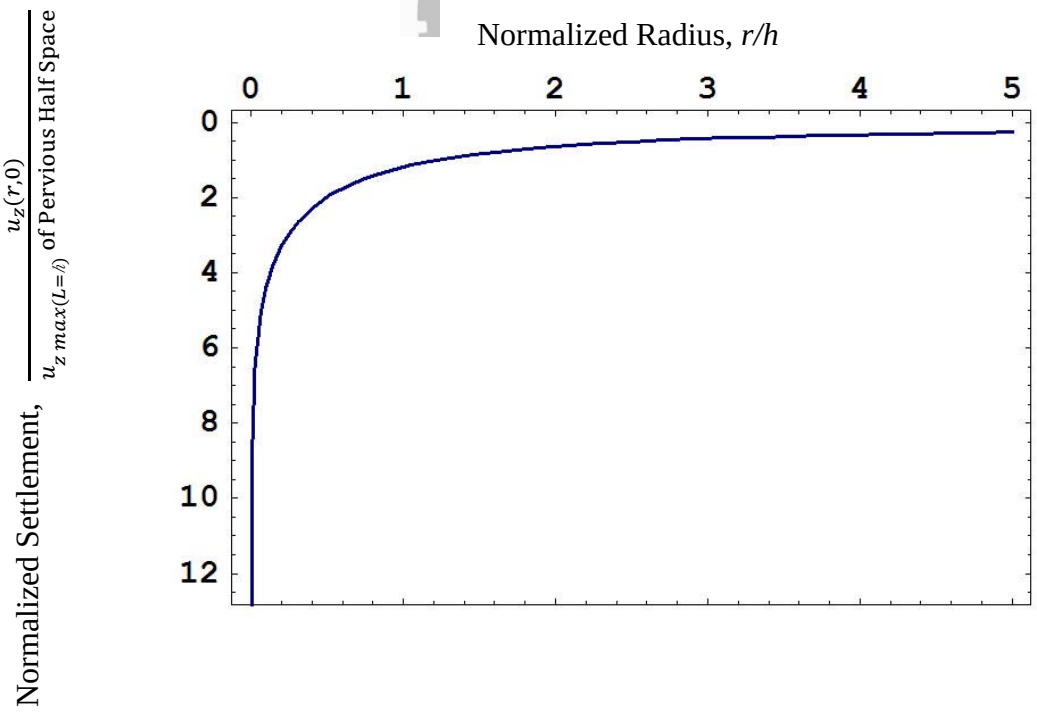

圖 4.52 地表模擬為不透水情況時線狀抽水所引致之無因次化地表沉陷量

(L/h = 1，ν = 0.2)

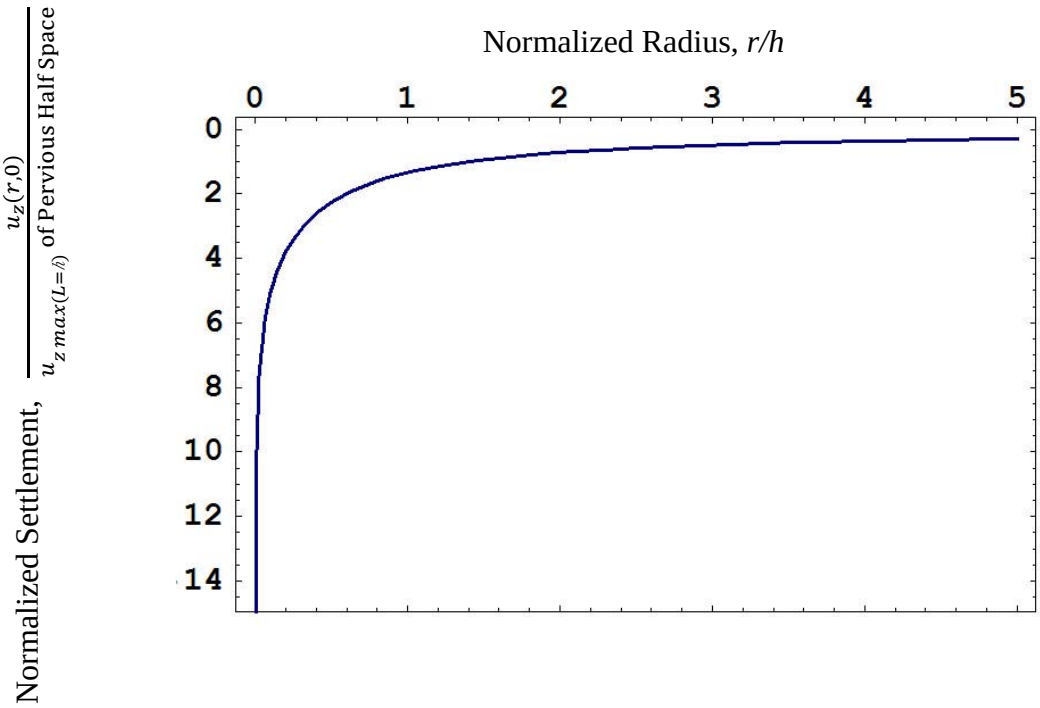

圖 4.53 地表模擬為不透水情況時線狀抽水所引致之無因次化地表沉陷量

(L/h = 1，ν = 0.25)

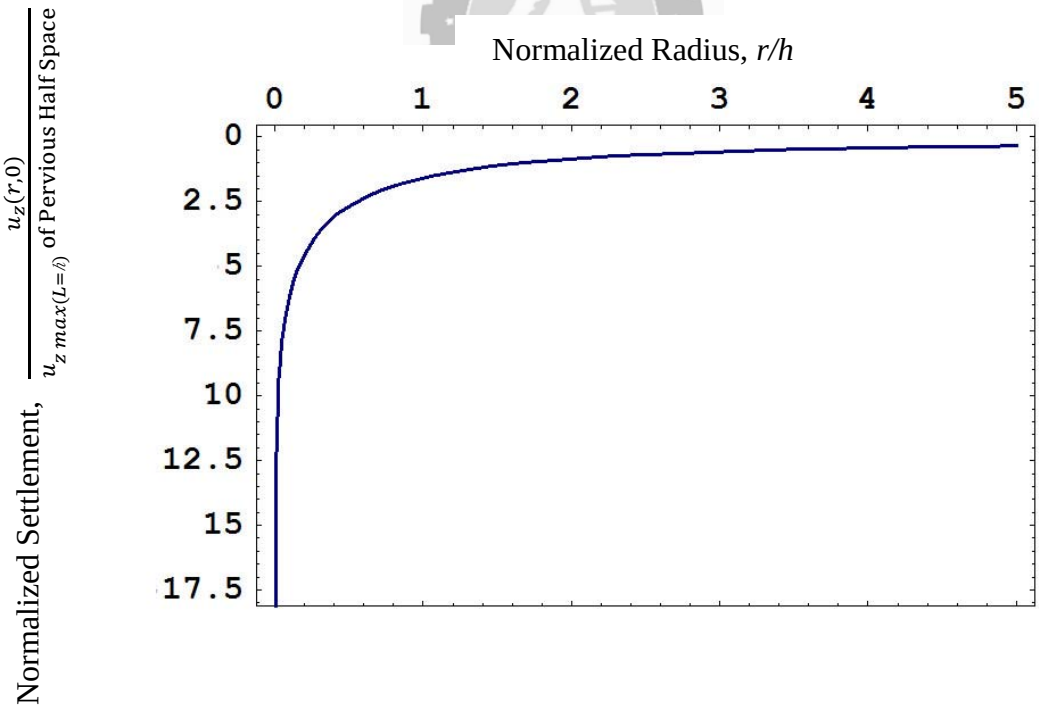

圖 4.54 地表模擬為不透水情況時線狀抽水所引致之無因次化地表沉陷量

(L/h = 1，ν = 0.3)

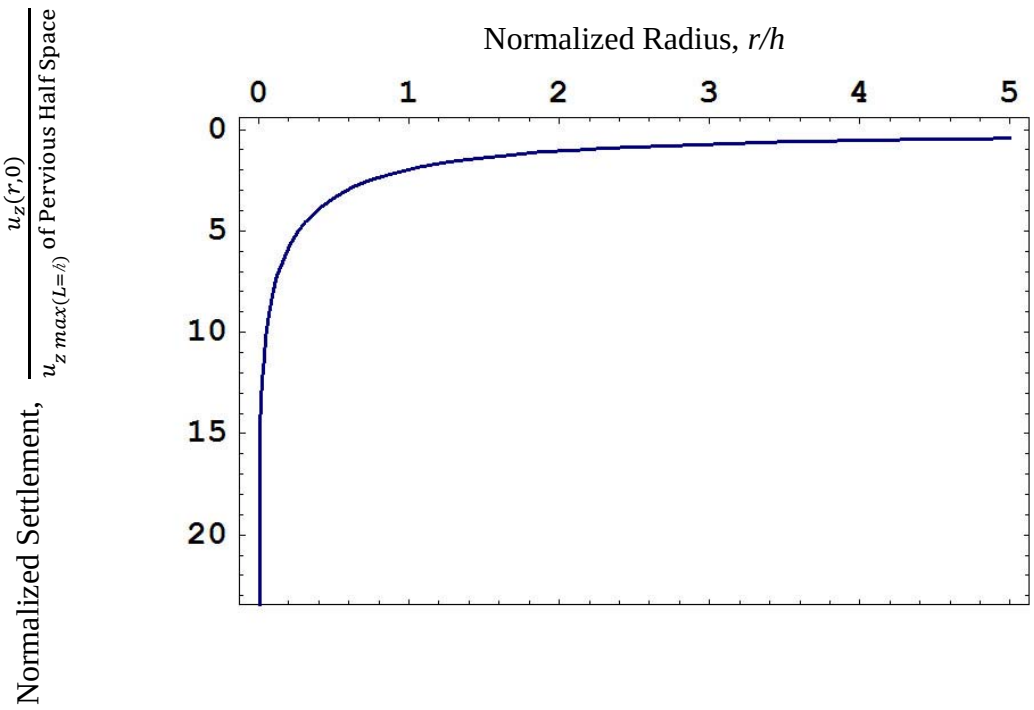

圖 4.55 地表模擬為不透水情況時線狀抽水所引致之無因次化地表沉陷量

(L/h = 1，ν = 0.35)

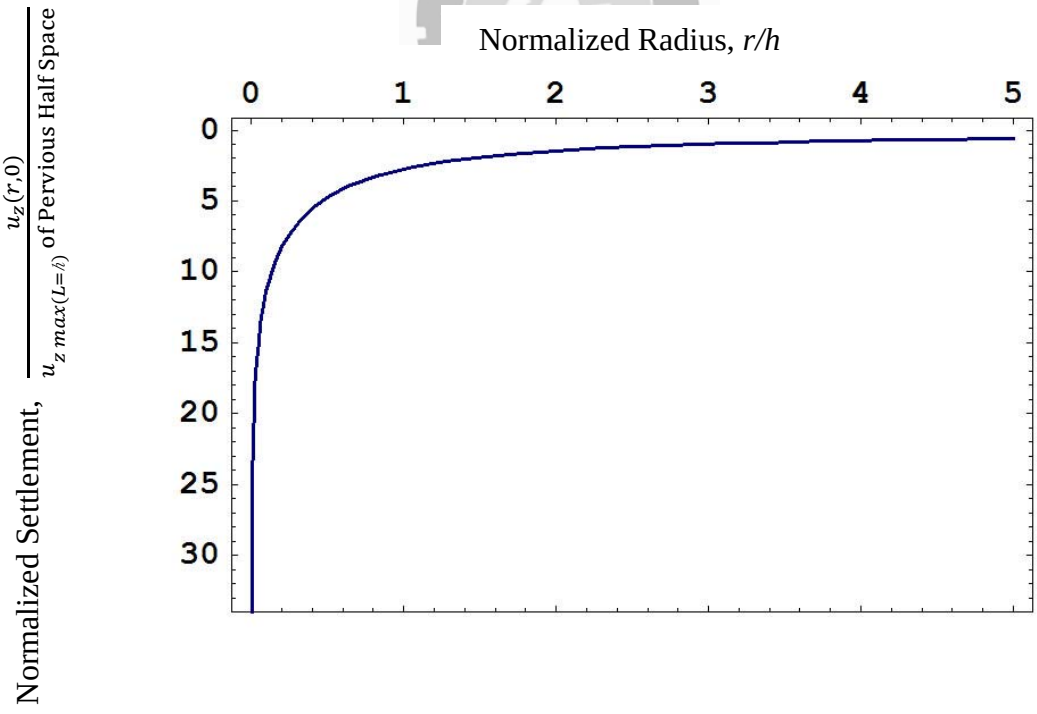

圖 4.56 地表模擬為不透水情況時線狀抽水所引致之無因次化地表沉陷量

(L/h = 1，ν = 0.4)

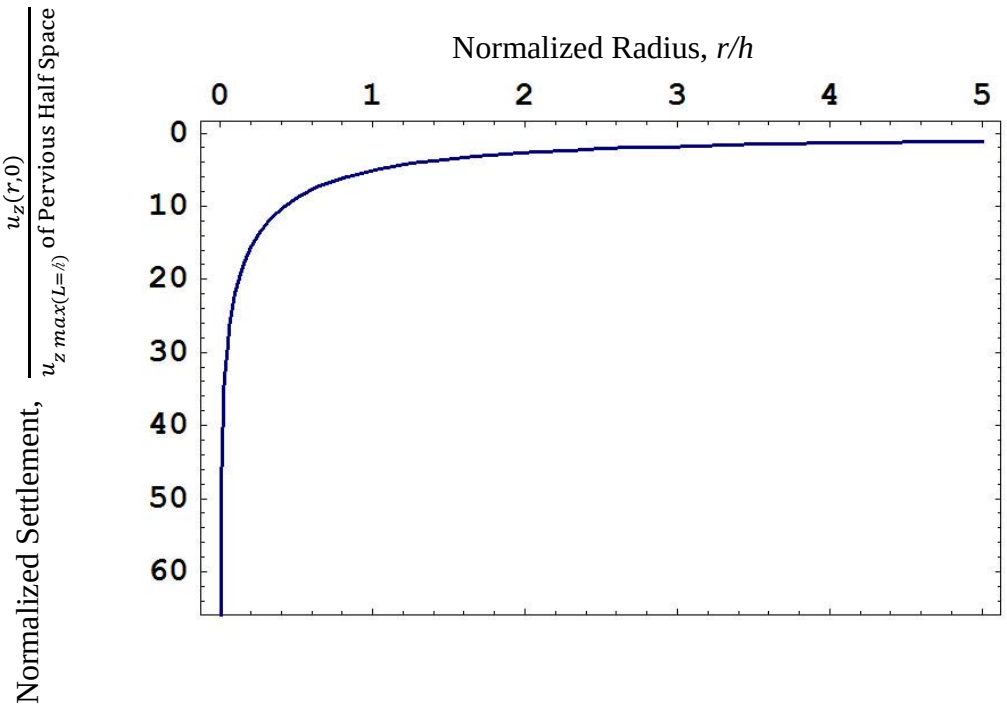

圖 4.57 地表模擬為不透水情況時線狀抽水所引致之無因次化地表沉陷量

(L/h = 1，ν = 0.45)

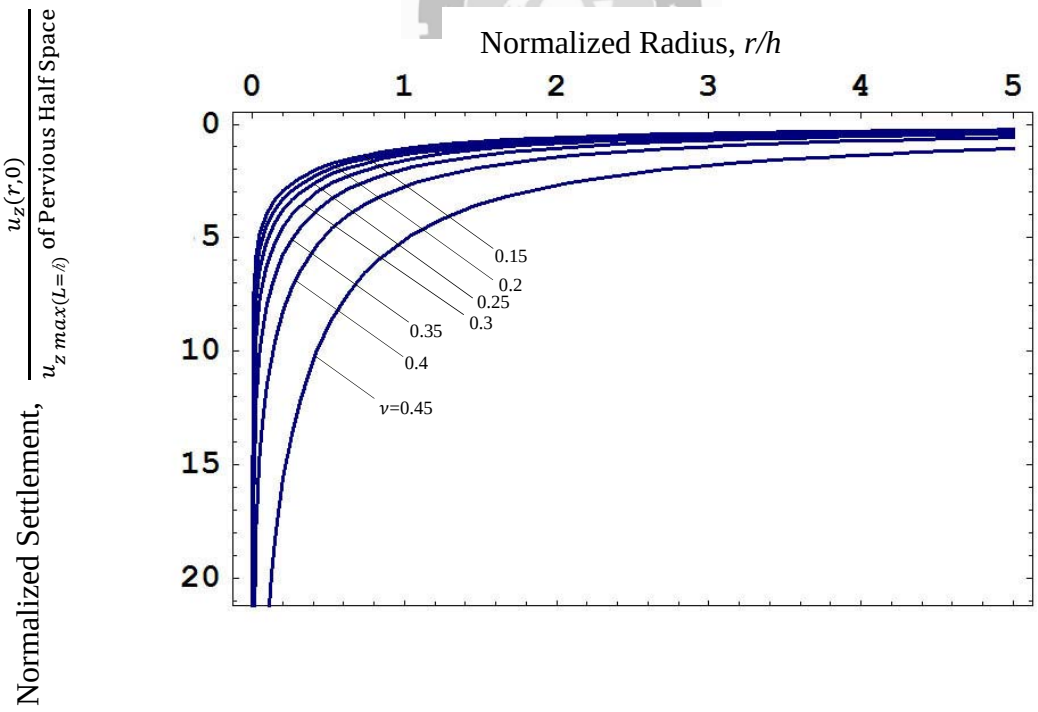

圖 4.58 地表模擬為不透水情況時線狀抽水所引致之無因次化地表沉陷量

(L/h = 1，ν = 0.15~0.45)

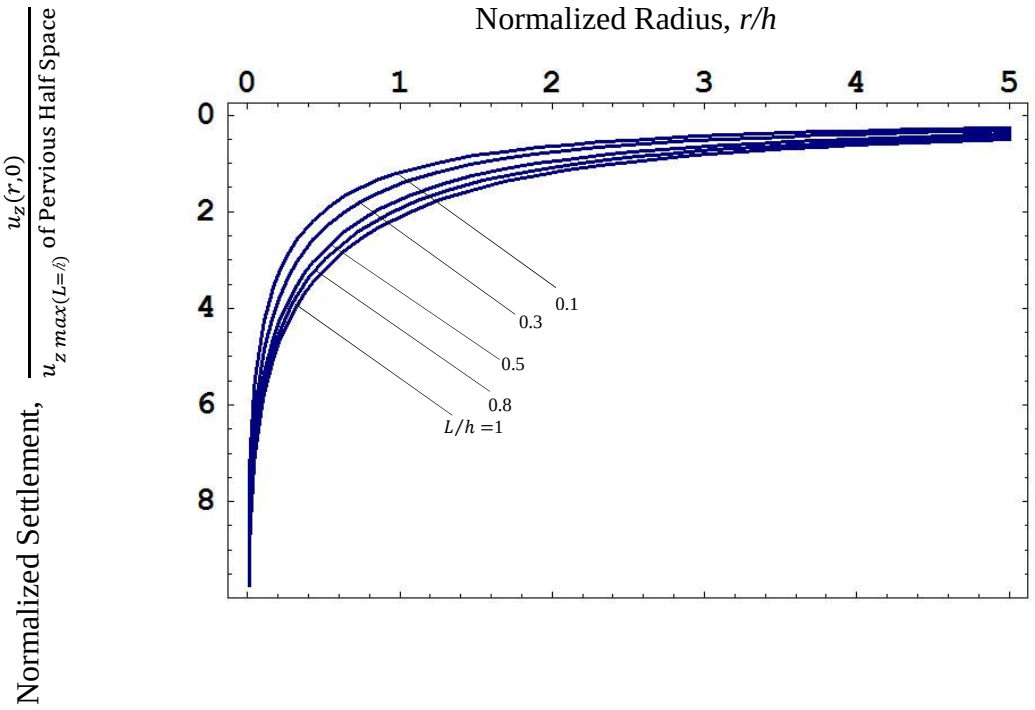

圖 4.59 地表模擬為不透水情況時線狀抽水所引致之無因次化地表沉陷量

(ν = 0.15，L/h = 0.1~1)

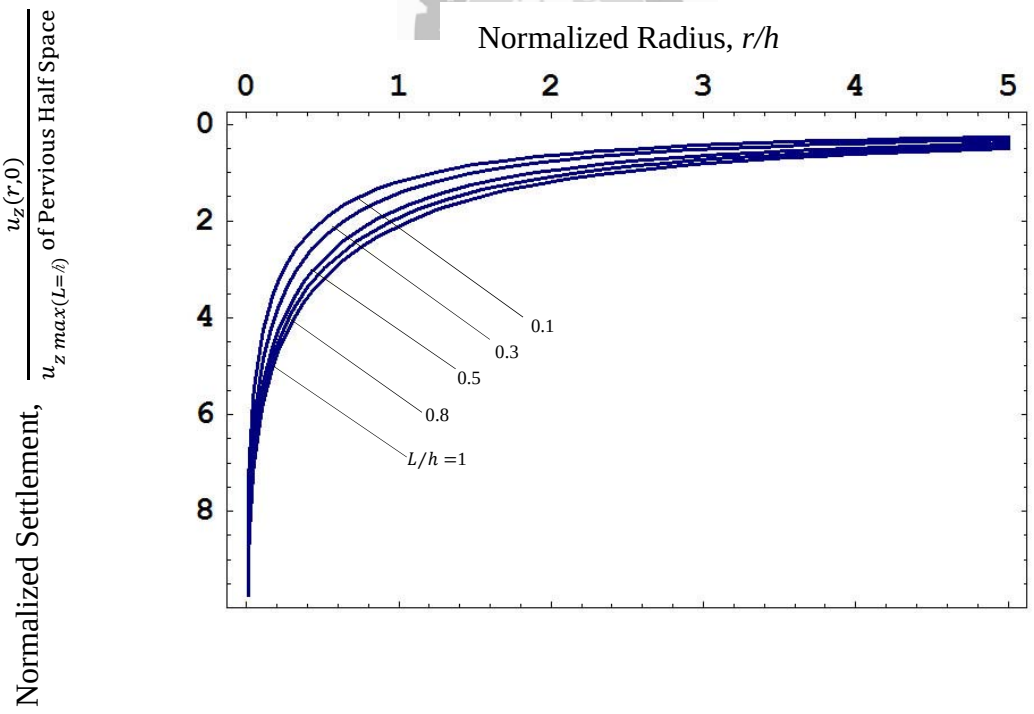

圖 4.60 地表模擬為不透水情況時線狀抽水所引致之無因次化地表沉陷量

(ν = 0.2，L/h = 0.1~1)

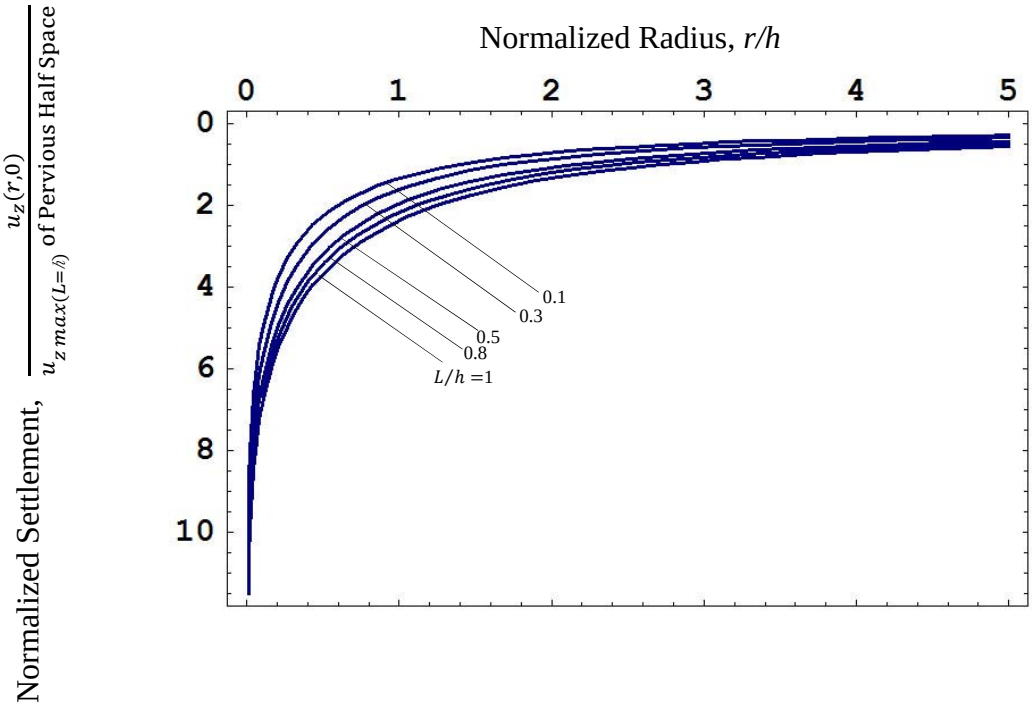

圖 4.61 地表模擬為不透水情況時線狀抽水所引致之無因次化地表沉陷量

(ν = 0.25，L/h = 0.1~1)

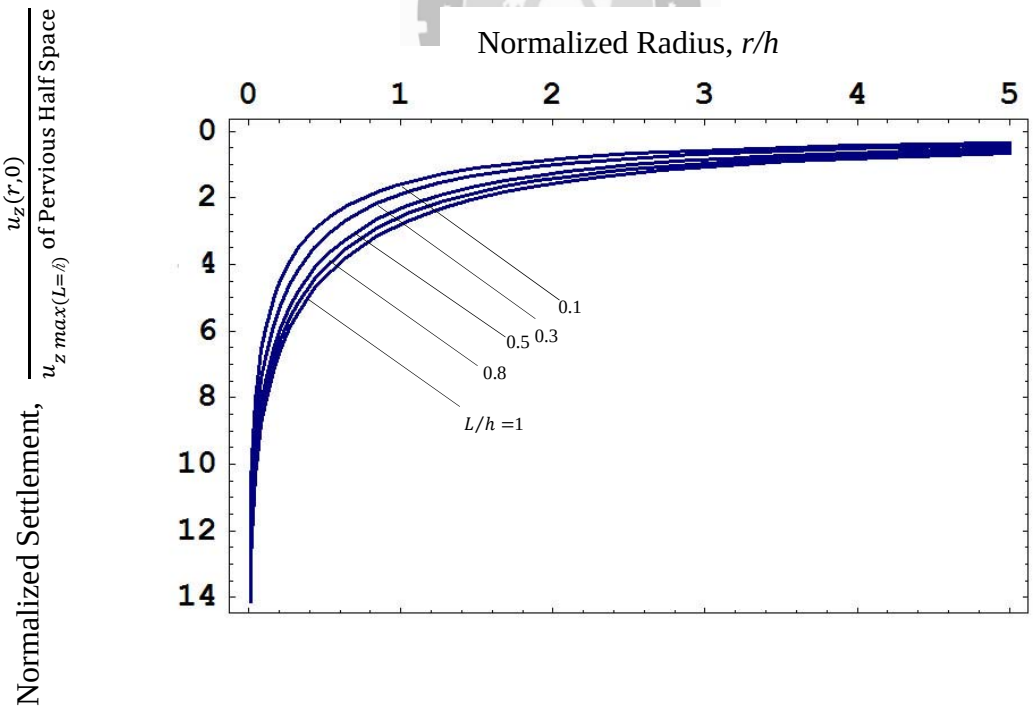

圖 4.62 地表模擬為不透水情況時線狀抽水所引致之無因次化地表沉陷量

(ν = 0.3，L/h = 0.1~1)

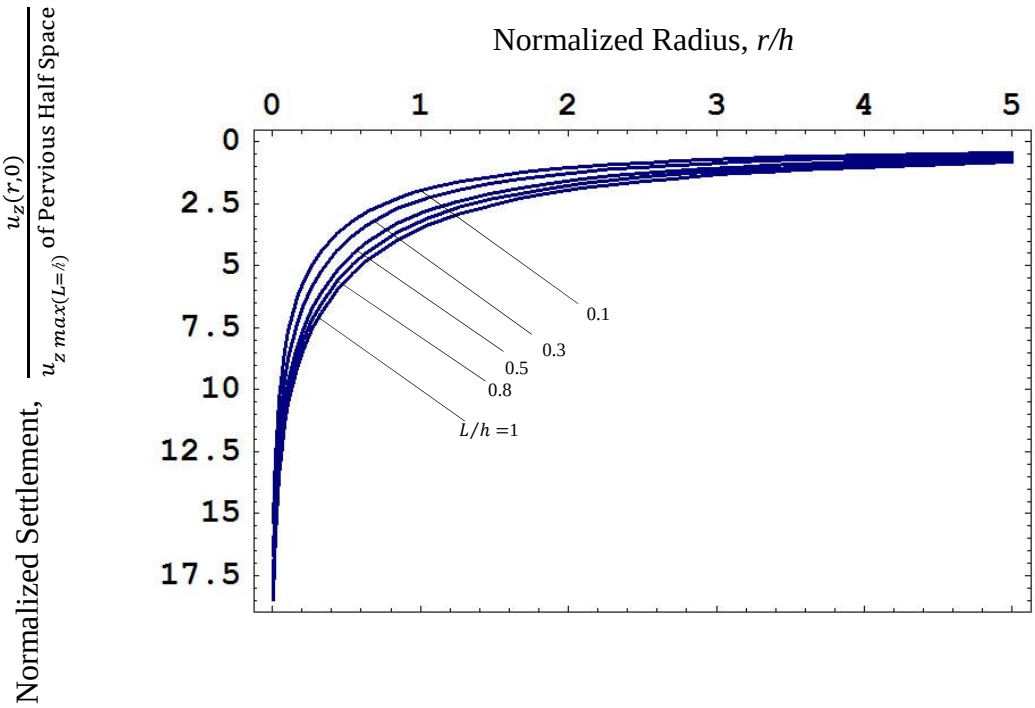

圖 4.63 地表模擬為不透水情況時線狀抽水所引致之無因次化地表沉陷量

(ν = 0.35，L/h = 0.1~1)

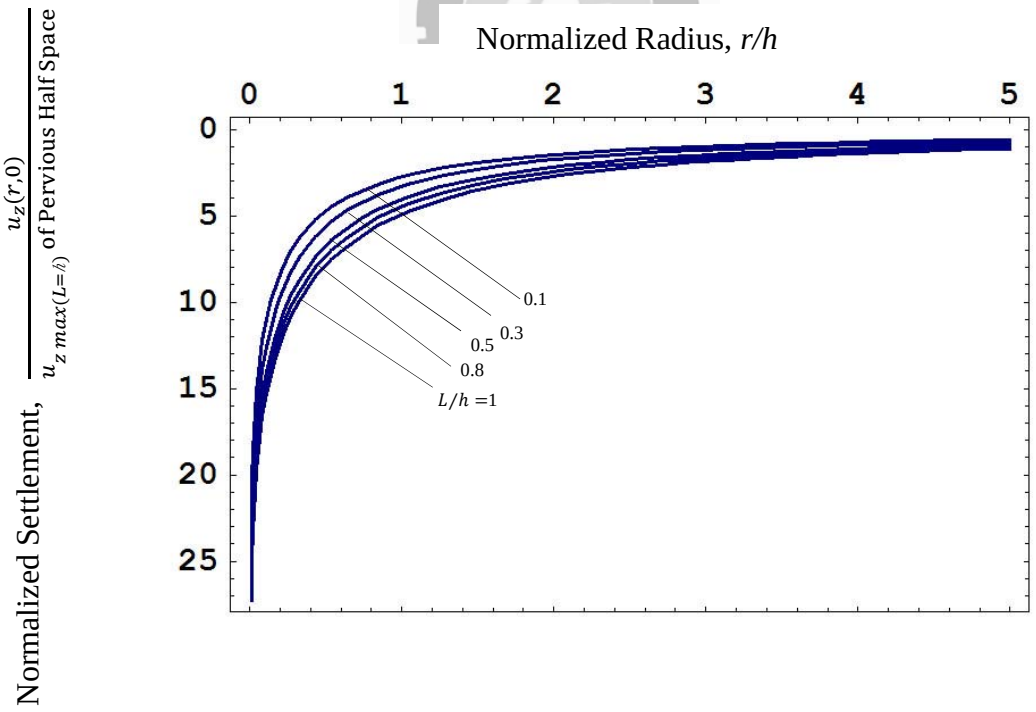

圖 4.64 地表模擬為不透水情況時線狀抽水所引致之無因次化地表沉陷量

(ν = 0.4，L/h = 0.1~1)

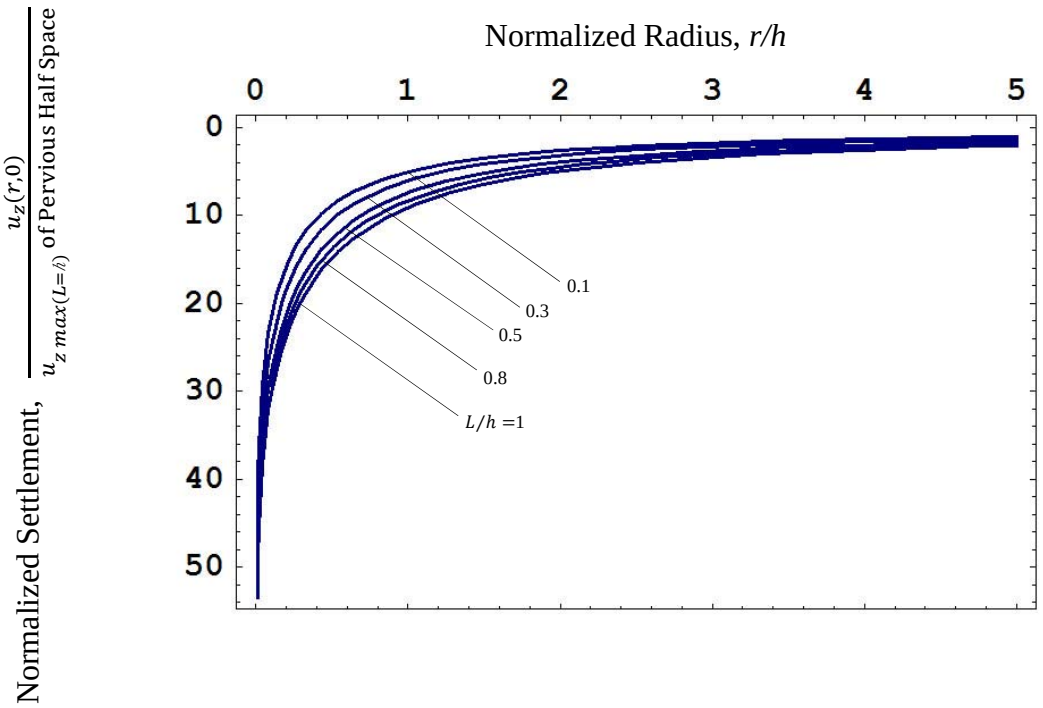

圖 4.65 地表模擬為不透水情況時線狀抽水所引致之無因次化地表沉陷量

(ν = 0.45，L/h = 0.1~1)

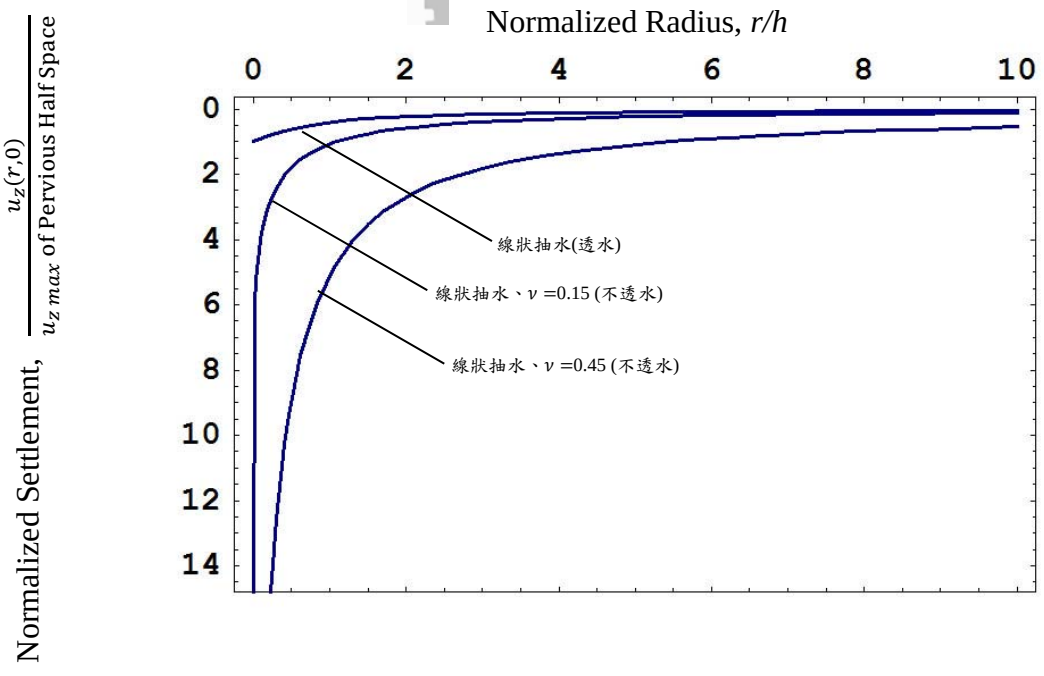

圖 4.66 地表模擬為透水與不透水情況時線狀抽水問題無因次化地表沉陷量比較圖

(L/h = 1)

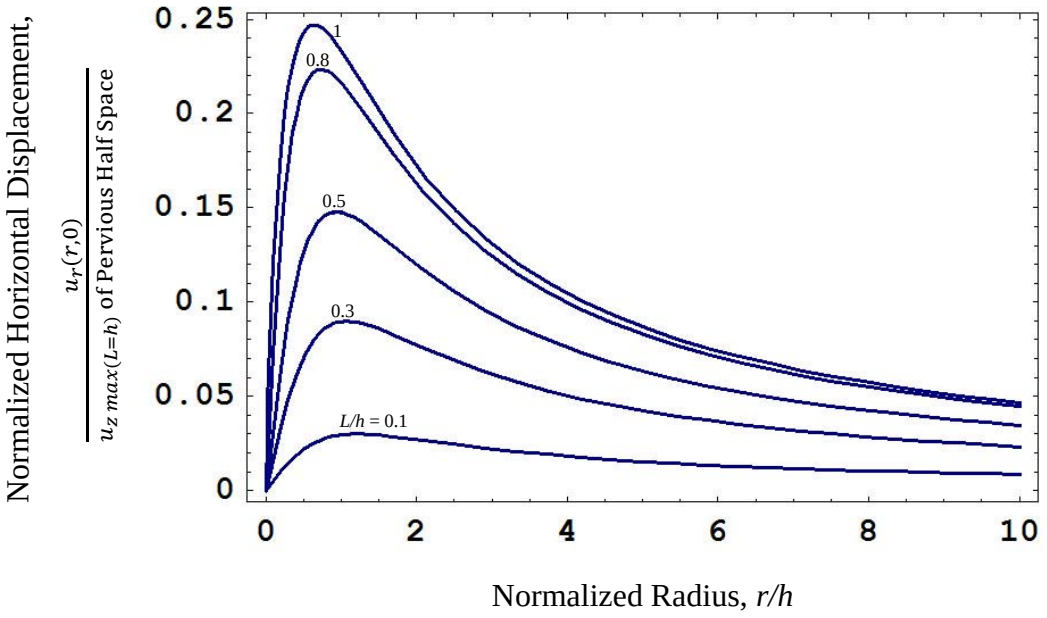

圖 4.67 線狀抽水所引致之無因次化地表水平位移曲線圖

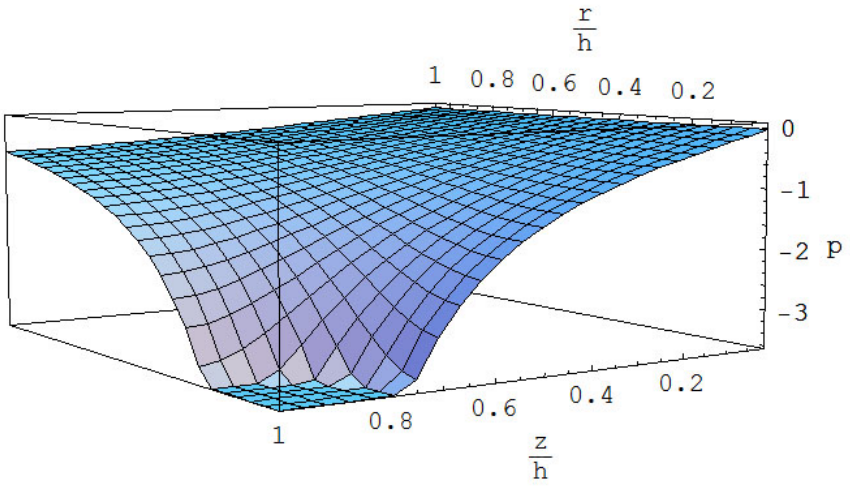

(a)立體圖

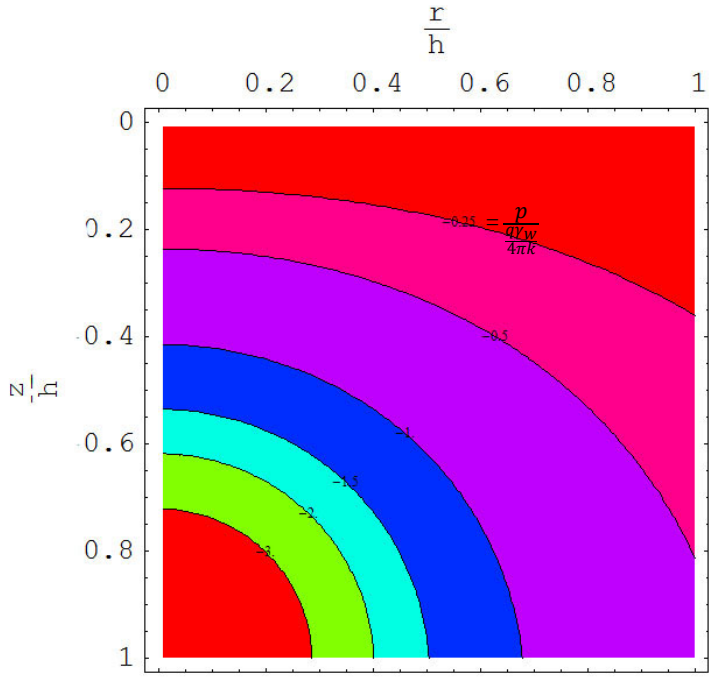

(b)平面圖

圖 4.68 地表模擬為透水邊界時點抽水所引致之無因次化孔隙水壓等值曲線圖

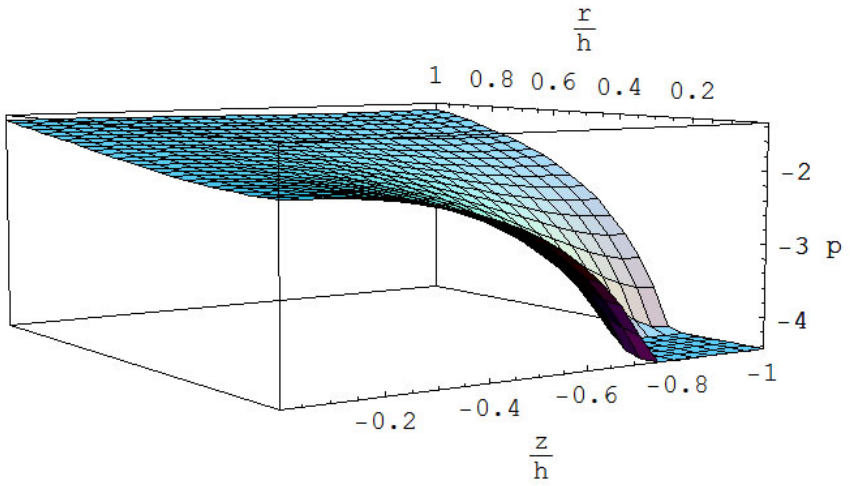

(a)立體圖

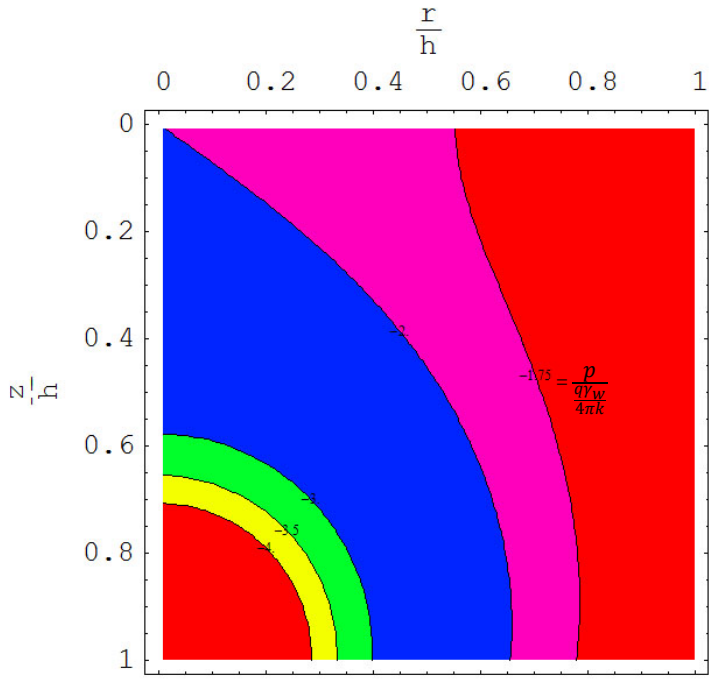

(b)平面圖

圖 4.69 地表模擬為不透水邊界時點抽水所引致之無因次化孔隙水壓等值曲線圖

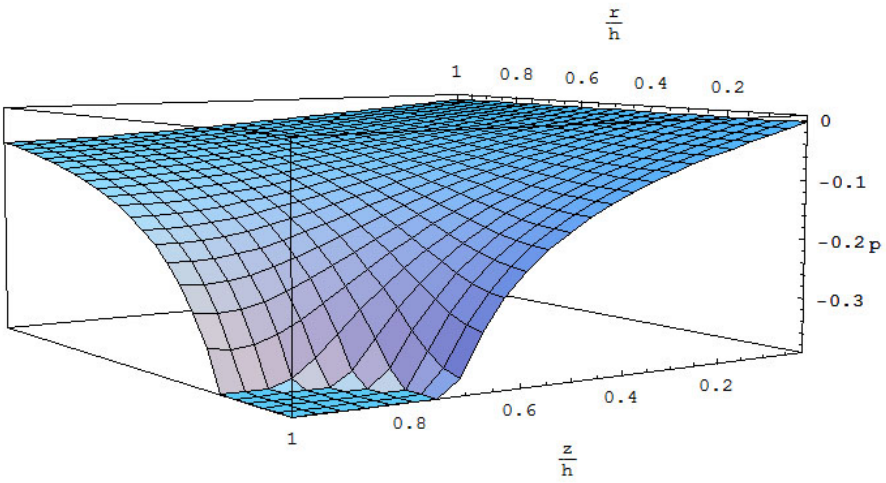

(a)立體圖

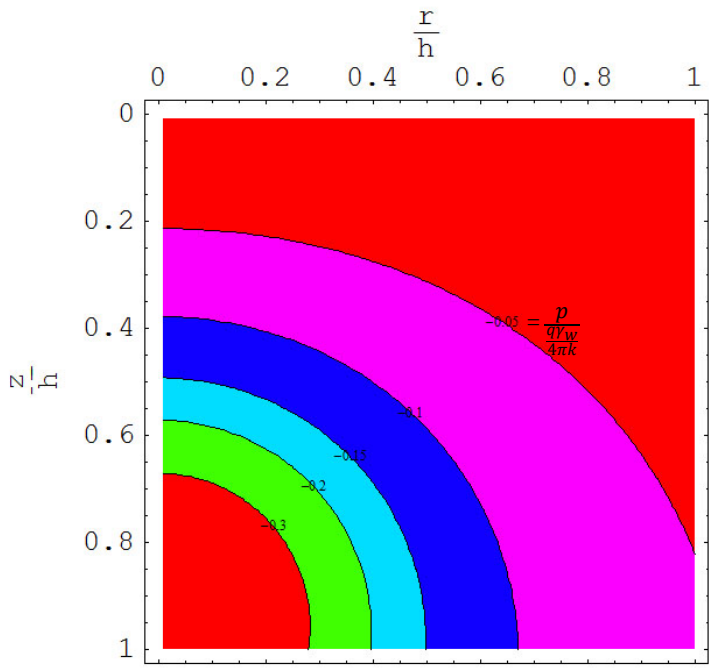

(b)平面圖

圖 4.70 地表模擬為透水邊界時線狀抽水所引致之無因次化孔隙水壓等值曲線圖（L/h = 0.1）

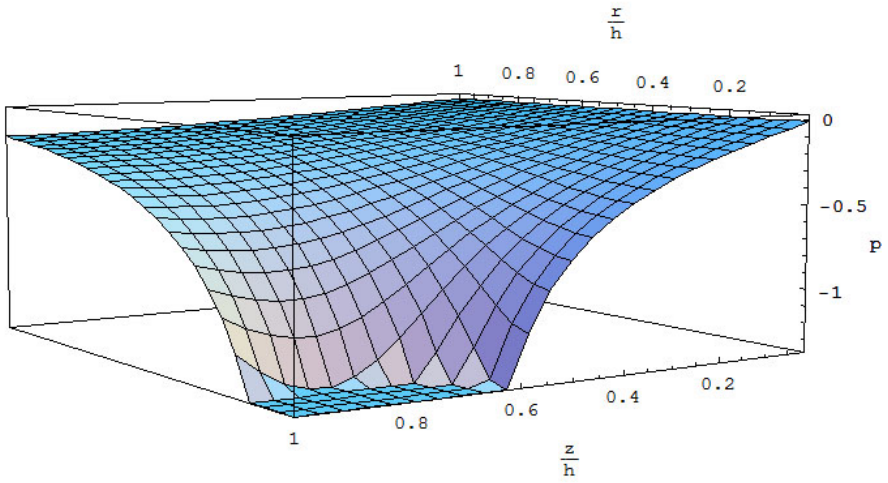

(a)立體圖

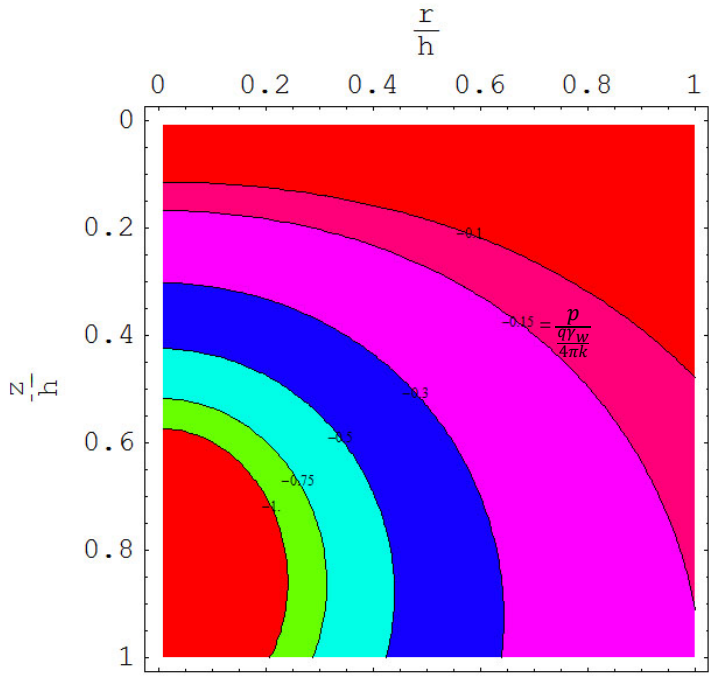

(b)平面圖

圖 4.71 透地表模擬為透水邊界時線狀抽水所引致之無因次化孔隙水壓等值曲線圖（L/h = 0.3）

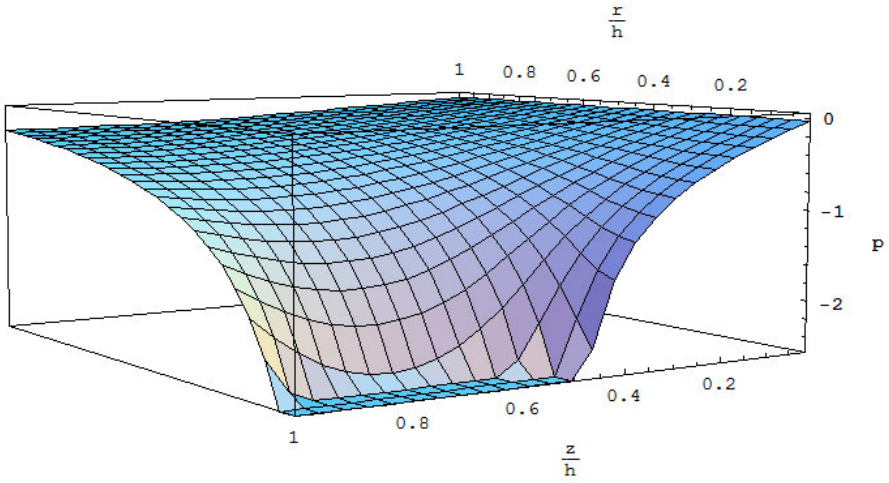

(a)立體圖

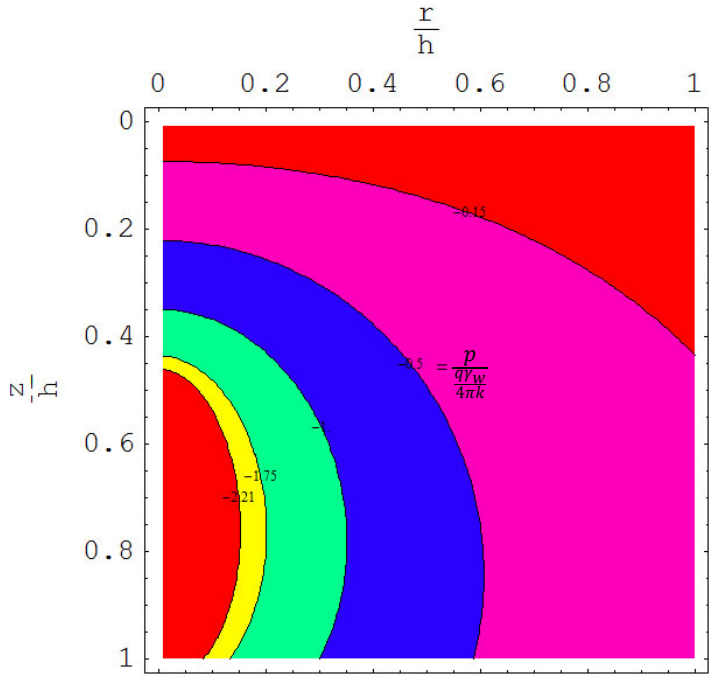

(b)平面圖

圖 4.72 地表模擬為透水邊界時線狀抽水所引致之無因次化孔隙水壓等值曲線圖（L/h = 0.5）

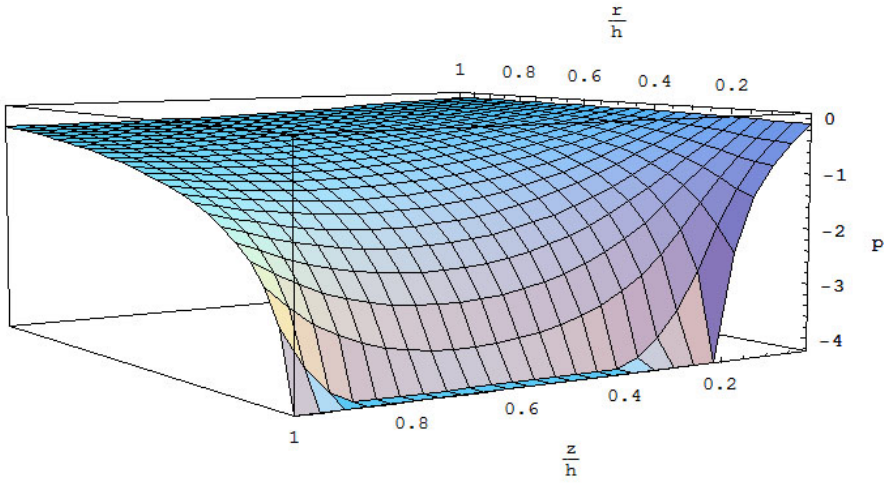

(a)立體圖

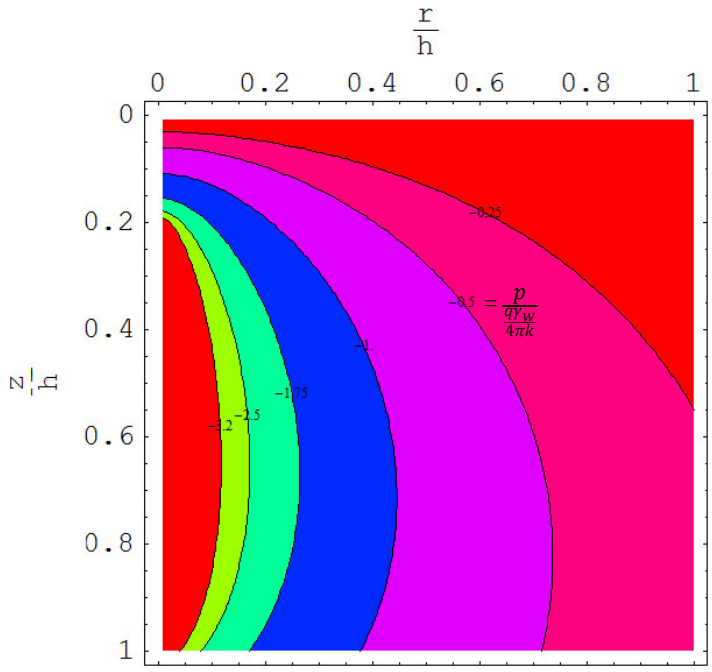

(b)平面圖

圖 4.73 地表模擬為透水邊界時線狀抽水所引致之無因次化孔隙水壓等值曲線圖（L/h = 0.8）

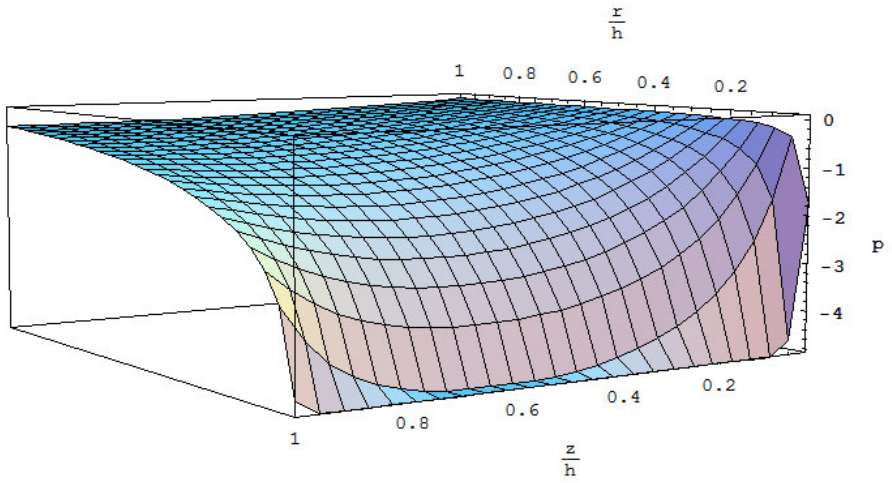

(a)立體圖

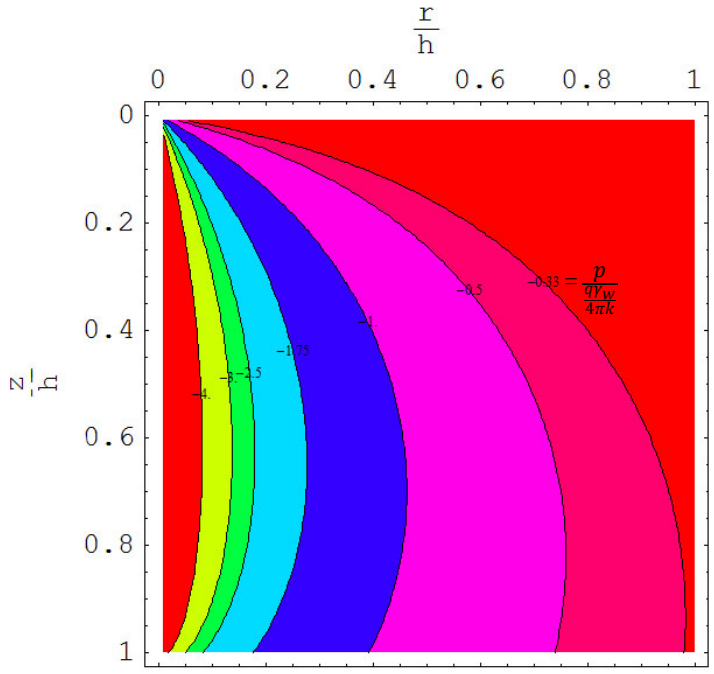

(b)平面圖

圖 4.74 地表模擬為透水邊界時線狀抽水所引致之無因次化孔隙水壓等值曲線圖（$L/h = 1$）

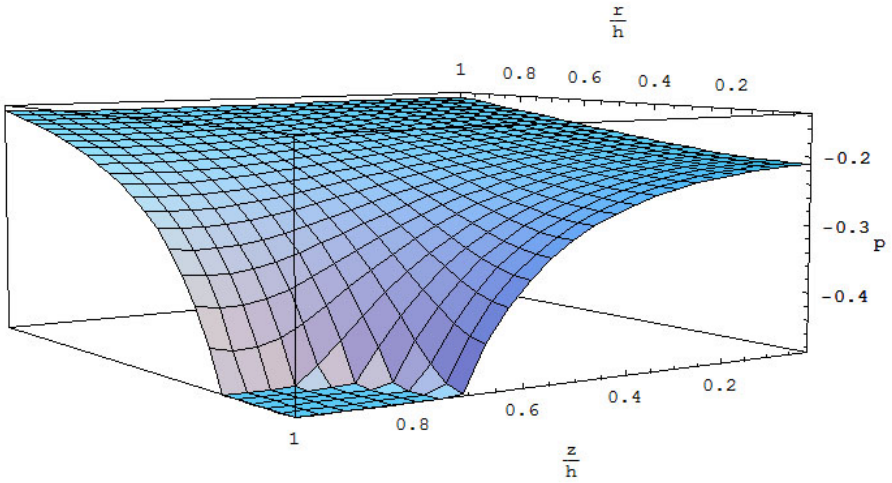

(a)立體圖

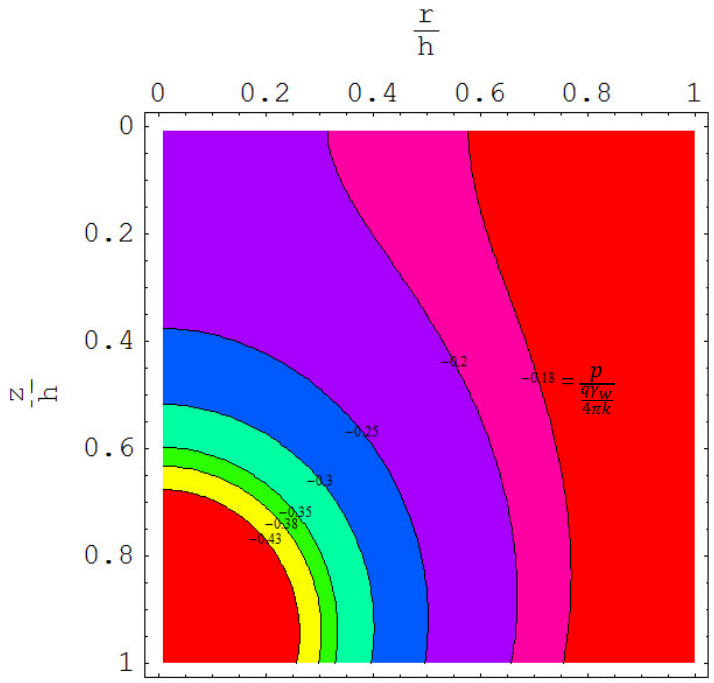

(b)平面圖

圖 4.75 地表模擬為不透水邊界時線狀抽水所引致之無因次化孔隙水壓等值曲線圖（L/h = 0.1）

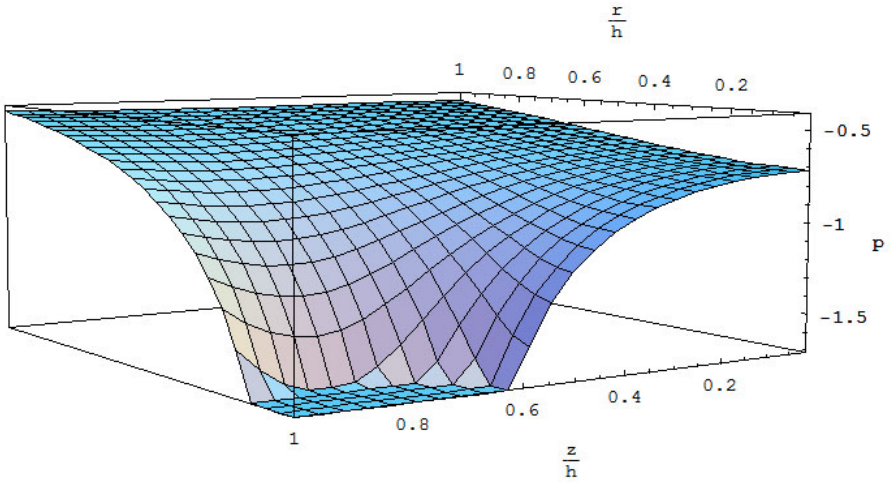

(a)立體圖

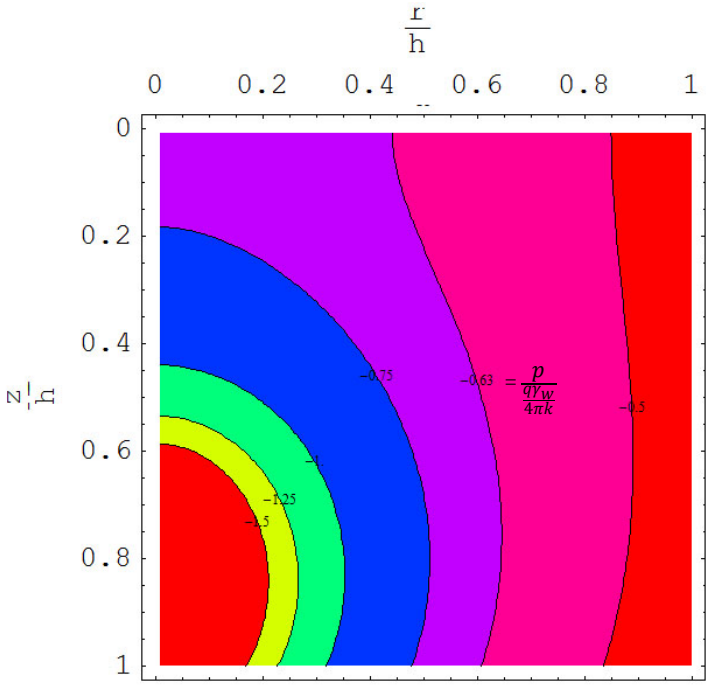

(b)平面圖

圖 4.76 地表模擬為不透水邊界時線狀抽水所引致之無因次化孔隙水壓等值曲線圖（L/h = 0.3）

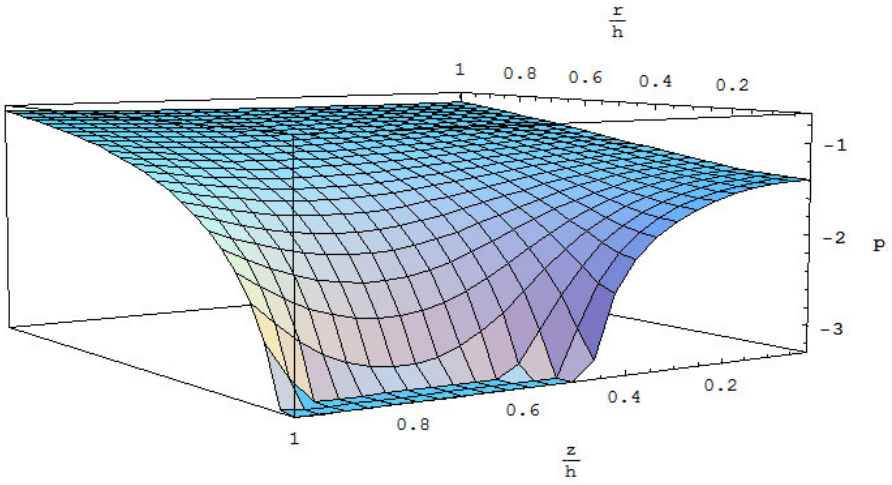

(a)立體圖

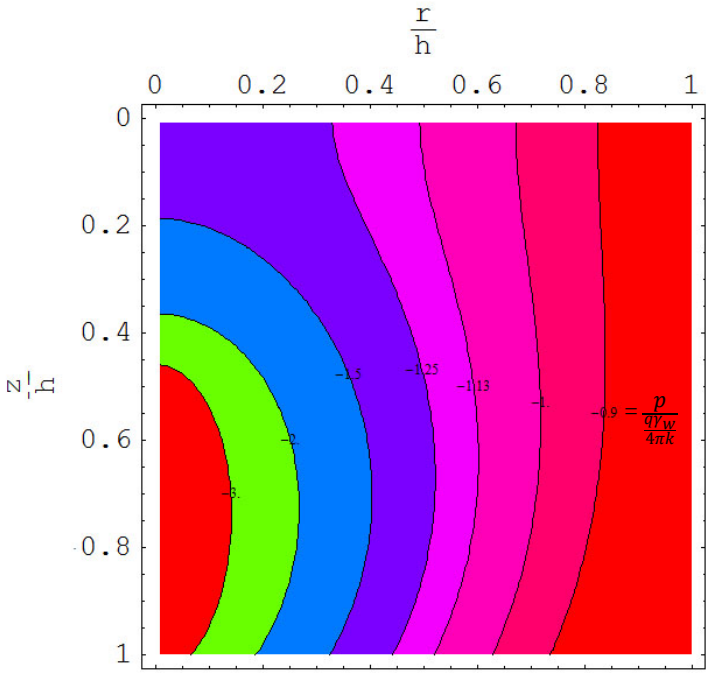

(b)平面圖

圖 4.77 地表模擬為不透水邊界時線狀抽水所引致之無因次化孔隙水壓等值曲線圖（L/h = 0.5）

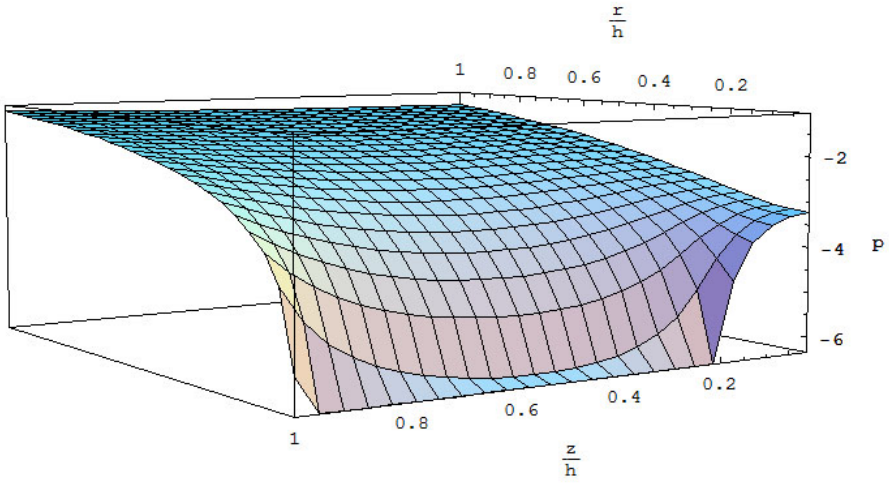

(a)立體圖

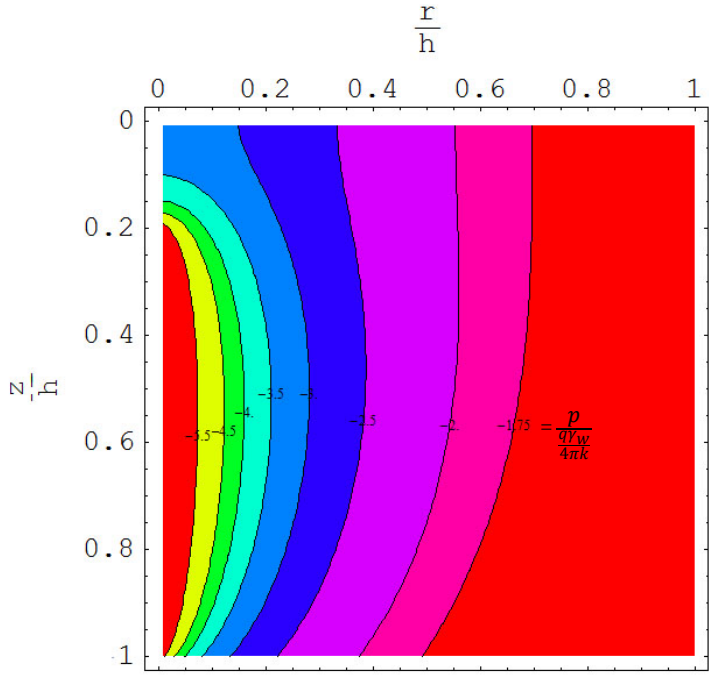

(b)平面圖

圖 4.78 地表模擬為不透水邊界時線狀抽水所引致之無因次化孔隙水壓等值曲線圖（L/h = 0.8）

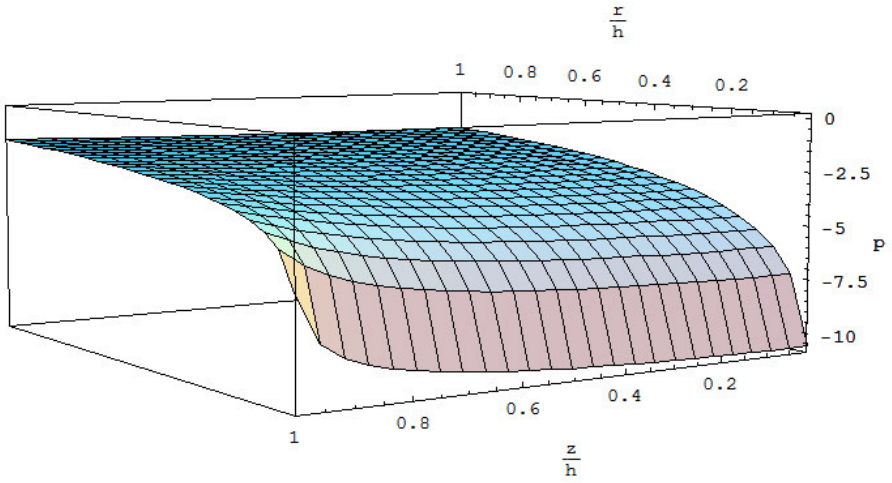

(a)立體圖

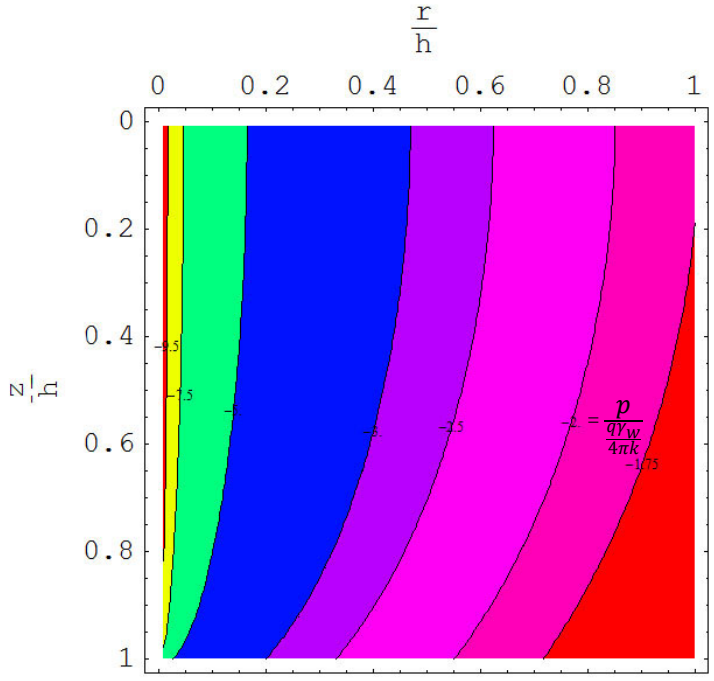

(b)平面圖

圖 4.79 地表模擬為不透水邊界時線狀抽水所引致之無因次化孔隙水壓等值曲線圖（$L/h = 1$）

第五章 結論與建議

5.1 結論

本文旨在用數學模擬方式，探討抽水所引致的地表邊界沉陷量、水平位移量與超額孔隙水壓等，係採用 Biot 三維壓密理論建立基本方程式，將抽水行為模擬為點抽水和線狀抽水兩種情況，並將地表邊界模擬為透水和不透水兩種滲流邊界條件。研討過程中有引用點抽水問題之基本解，再對其進行線積分的運算，推導出線狀抽水所引致之壓密沉陷行為。經由參數影響分析得知，在相同參數條件下，基礎地層柏松比ν、地表滲流邊界條件、取水長度與井深之比值參數等皆對地層壓密沉陷行為有不同程度的重要影響。經仔細研究與討論後，獲得以下結論：

1. 含水層柏松比對抽水所引致壓密行為有重要的影響：本研究是將地層柏松比ν分別模擬為 0.15、0.2、0.25、0.3、0.35、0.4、0.45、0.4999 等八種情況，當含水層之柏松比變大時，地層較容易產生變形，因此會反映出較大之地表沉陷。
2. 就取水長度L與井深h的比值之影響而言：本研究分別模擬L/h為 0.1、0.3、0.5、0.8、1.0 等五種情況，當取水長度L與井深h的比值L/h增加時，地表沉陷量也呈增加的現象，這是因為取水長度L增加時，抽水量也會增加，故壓密沉陷量也跟著增加。
3. 關於地表滲流邊界條件之影響而言：地表模擬為不透水情況下所引致的地表沉陷會較大，這是因為當地表面模擬為不透水邊界時，抽水所引起之負的超額孔隙水壓無法消散，含水層之有效應力因而升高，壓密沉陷之效應變大，故所導致的地表沉陷量會變大。
4. 關於將抽水行為模擬為點抽水和線狀抽水時的數值結果之差異性：比較過程中是考慮點抽水的抽水量等於所對應之線狀抽水的抽水量（且L/h考慮為 1），基於此可知，點抽水與線狀抽水所引起的最大沉陷量會相同，但於地表大多數位置上，點抽水所引起的沉陷量會較大。這是因為在相同抽水量的考量下，點抽水所產生的超額孔隙水壓會較大，導致其地層有效應力上升較多，所產生的壓密沉陷量亦

會較多之故。

5. 抽水所引起的地表水平位移量會在水井邊逐漸升高後逐步降低：這是因為單井抽水所引起的地表水平位移是一軸對稱問題，故地表面在對稱點上之水平位移量應為零；另外，含水層遠處受抽水擾動的影響很小，故地表遠處之水平位移量亦很小，因此抽水所引起的地表水平位移量會在水井邊逐漸升高後逐步降低。另外，線狀抽水時，地表最大水平位移發生位置約位於$r/h=1$的位置上，此與點抽水所引致的地表最大水平位移是落在$r=\sqrt{\phi}h\backsimeq 1.272h$位置上之結論相當接近。

5.2 建議

基於以上研究成果，擬對未來提供一些研究方向與建議：

1. 本文係探討地層力學行為與滲流性質皆模擬為等向性之線彈性飽和多孔介質，未來可朝向地層力學行為與滲流性質皆模擬為橫向等向性情況加以探討。
2. 本研究僅考慮點抽水與線狀抽水行為，未來可以朝面狀抽水甚至圓柱狀抽水行為所引致的壓密沉陷加以探討，使結果更符合真實抽水情況。
3. 後續之研究可考慮進行視窗程式設計，讓使用者僅需輸入簡單之參數即可快速求得三維壓密沉陷之各項結果，以利研究成果之工程應用與推廣。

參考文獻

丁崇峰、黃輝煌、宋長虹、許榮庭、林政偉，「地下水超抽量推估方法-彰雲地區為例」，中國土木水利工程學刊，第 18 卷，第 1 期，第 37-49 頁 (2006)。

行政院經濟建設委員會，「愛台 12 建設總體計畫」，行政院 98 年 12 月 2 日院臺經字第 0980073417 號函核定通過，共 168 頁，http://www.cepd.gov.tw/m1.aspx?sNo=0012702 (2013/1/21 瀏覽)。

行政院環境保護署，「民國 99 年環境水質監測年報」，共 118 頁，http://wq.epa.gov.tw/WQEPA/Code/Report/ReportList.aspx (2013/1/21 瀏覽)。

呂志宗，「多孔介質彈性力學之基本解與壓密沉陷解析」，博士論文，國立成功大學土木工程研究所 (1991)。

杜富麗，「抽水所引致的壓密沉陷問題之解析」，碩士論文，中華大學土木工程學系碩士班 (1993)。

宜蘭縣政府，「宜蘭縣土壤及地下水汙染整治業務網」，http://works.ilepb.gov.tw/01003/download/new_t/20050824_2.html (2012/9/22 瀏覽)。

柳志錫、杜富麗、洪偉嘉，「超抽地下水引起之地層下陷問題探討」，財團法人工業技術研究院能源與環境資源研究所 (2003)。

侯伊浩、李振誥、龔文瑞、沈岡陵、陳忠偉、陳冠位，「地下水標準對地層下陷模式建構之影響」，嘉南學報，第 36 期，第 203-215 頁 (2010)。

涂凱嵐，「管線因垂直裂縫所引致地層位移與超額孔隙水壓變化之研究」，碩士論文，中華大學土木工程學系碩士班 (2010)。

洪維恩，「數學運算大師 MATHEMATICA 4.0」，碁峰資訊股份有限公司 (2001)。

施俊如，「孔洞開挖後軟弱地盤之沉陷行為」，碩士論文，國立中央大學土木工程學系碩士班 (2000)。

徐年盛、江崇榮、汪中和、劉振宇、劉宏仁、黃建霖，「地下水系統水平衡分析與補注源水量推估之研究」，中國土木水利工程學刊，第 23 卷，第 4 期，第 347-357 頁 (2011)。

陳文福，「台灣的地下水」，遠足文化事業股份有限公司 (2005)。

單信瑜，「台灣地下水資源使用與水質現況」，2005 水環境教育教師研習活動，共

74 頁 (2005)。

湯珠孝，「應用地下水位歷線分析法推估屏東平原補注量及抽水量之探討」，碩士論文，國立屏東科技大學土木工程系碩士班 (2010)。

曾柏領，「抽水所引致彈性壓密沉陷之基本解及其在管線破裂問題上之應用」，碩士論文，中華大學土木與工程資訊學系碩士班 (2007)。

曾鈞敏，「地下水超抽引致地層下陷之三維解析研究」，博士論文，國立臺灣大學土木工程研究所 (2009) 。

彭清源，「抽水所引致壓密問題數值解析與近似展開理論之應用」，碩士論文，中華大學土木工程學系碩士班 (1997)。

馮寶蓮，「地下水井抽水量推估之研究-以台南縣後壁鄉、安定鄉及高雄縣大樹鄉、林園鄉為例」，碩士論文，國立高雄第一科技大學環境與安全衛生工程系碩士班 (2006)。

辜樹仁，「中國下沉中」，天下雜誌，第 492 期，第 146 頁(2012)。

張正緯、黃良雄、蔡東霖、郭遠錦，「三維地下水模式之發展與應用」，中國土木水利工程學刊，第 21 卷，第 2 期，第 169-181 頁 (2009)。

經濟部水利署，「地下水觀測網」，http://140.112.190.183/gw-districts.php (2012/9/22 瀏覽)。

經濟部水利署，「高屏大湖(第一階段工程)可行性研究」，經濟部水利署委託中興工程顧問股份有限公司，ISBN: 9789860167740 (2008)。

經濟部水利署,「地層下陷防治資訊網」,http://www2.water.tku.edu.tw/Sub91/index.aspx (2012/9/6 瀏覽)。

經濟部水利署，「全球資訊網，基本水利資訊 -- 地層下陷」，http://www.wra.gov.tw/ct.asp?xItem=48094&CtNode=7670 (2013/1/21 瀏覽)。

經濟部水利署，「全球資訊網，檔案下載 -- 水文技術組」，http://www.wra.gov.tw/ct.asp?xItem=25696&ctNode=5487&comefrom=lp (2012/11/3 瀏覽)。

經濟部水利署，「地層下陷防治智識服務計畫」，經濟部水利署委託國立成功大學計畫案，ISBN: 9789860220261 (2009)。

經濟部水利署、國立成功大學，「地層下陷防治服務團」，http://www.lsprc.ncku.edu.tw/index.aspx (2012/9/6 瀏覽)。

經濟部水利署南區水資源局，「高屏大湖工程計畫-地下水文監測追蹤與檢討評估(99年度)總成果報告」，經濟部水利署南區水資源局委託國立屏東科技大學計畫案，ISBN: 9789860269727 (2010)。

Biot, M.A., 'General theory of three-dimensional consolidation,' *Journal of Applied Physics*, Vol. 12, No. 2, pp. 155-164 (1941).

Biot, M.A., 'Theory of elasticity and consolidation for a porous anisotropic solid,' *Journal of Applied Physics*, Vol. 26, No. 2, pp. 182-185 (1955).

Booker, J.R. and J.P. Carter, 'Analysis of a point sink embedded in a porous elastic half space,' *International Journal for Numerical and Analytical Methods in Geomechanics*, Vol. 10, No. 2, pp. 137-150 (1986).

Das, B.M., *Advanced Soil Mechanics*, 3rd ed., Taylor & Francis, 567p (2008).

Das, B.M., *Fundamentals of Geotechnical Engineering*, 2nd ed., Taylor & Francis, 566p (2005).

Freeze, R.A., 'Social Decision Making and Land Subsidence,' *Proceeding of the Sixth International Symposium on Land Subsidence*, Ravenna, Italy, pp.24-29 (2000).

Imakiire, T. and M. Koarai, 'Wide-area land subsidence caused by the "The 2011 off the Pacific coast of Tohoku Earthquake",' *Soils and Foundations*, In press (2012).

McDonald, M.G. and A.W. Harbaugh, 'A modular three-dimensional finite-difference ground-water flow model,' Book 6, Chap. A1, *U.S. Geological Survey Techniques of Water-Resources Investigations*, 586p (1988).

McDonald, M.G. and A.W. Harbaugh, 'Programmer's documentation for MODFLOW-96, an update to the U.S. Geological Survey modular finite difference ground-water flow model,' *U.S. Geological Survey Open-File Report 96-486*, 220p (1996).

Skempton, A.W., 'Correspondence,' *Geotechnique*, Vol. 10, No. 4, p. 186 (1960).

國科會補助計畫衍生研發成果推廣資料表

日期:2013/01/27

國科會補助計畫	計畫名稱: 典型抽水所引致三維壓密沉陷解析
	計畫主持人: 呂志宗
	計畫編號: 100-2221-E-216-025- 學門領域: 大地工程

無研發成果推廣資料

100 年度專題研究計畫研究成果彙整表

計畫主持人：呂志宗	計畫編號：100-2221-E-216-025-
計畫名稱：典型抽水所引致三維壓密沉陷解析	

成果項目			量化			單位	備註（質化說明：如數個計畫共同成果、成果列為該期刊之封面故事...等）
			實際已達成數(被接受或已發表)	預期總達成數(含實際已達成數)	本計畫實際貢獻百分比		
國內	論文著作	期刊論文	0	0	100%	篇	
		研究報告/技術報告	0	0	100%		
		研討會論文	0	0	100%		
		專書	0	0	100%		
	專利	申請中件數	0	0	100%	件	
		已獲得件數	0	0	100%		
	技術移轉	件數	0	0	100%	件	
		權利金	0	0	100%	千元	
	參與計畫人力（本國籍）	碩士生	1	0	100%	人次	
		博士生	0	0	100%		
		博士後研究員	0	0	100%		
		專任助理	0	0	100%		
國外	論文著作	期刊論文	1	0	90%	篇	Lu, John C.-C. and Feng-Tsai Lin, 2013, ’ Golden Ratio in the Green’s Functions of Poromechanics and Thermomechanics,’ International Journal of Modelling and Simulation, ISSN: 0228-6203, Accepted for Publication. (This work is supported by the National Science Council through grant NSC81-0410-E-216-503 & NSC100-2221-E-216-025.) (EI)
		研究報告/技術報告	0	0	100%		
		研討會論文	2	0	100%		1. Lu, John C.-C. (Session Chair) and Feng-Tsai Lin, 2012/6/25~27, ’ Modelling of a Buried Deep Horizontal Line Heat Source in a Cross-Anisotropic

							Thermoelastic Medium,' Proceedings of the 20th IASTED International Conference on Applied Simulation and Modelling, CD ISBN: 978-0-88986-925-7, Napoli, Italy, pp. 150-157. (This work is supported by the National Science Council through grants NSC100-2221-E-216-025.) (EI) 2. Lu, John C.-C. (Session Chair) and Feng-Tsai Lin, 2012/6/25~27, 'Modelling of Consolidation Settlement Due to a Circularly Symmetric Fluid Sink,' Proceedings of the 20th IASTED International Conference on Applied Simulation and Modelling, CD ISBN: 978-0-88986-925-7, Napoli, Italy, pp. 107-113. (This work is supported by the National Science Council through grants NSC100-2221-E-216-025.) (EI)
		專書	0	0	100%	章/本	
	專利	申請中件數	0	0	100%	件	
		已獲得件數	0	0	100%		
	技術移轉	件數	0	0	100%	件	
		權利金	0	0	100%	千元	
	參與計畫人力（外國籍）	碩士生	0	0	100%	人次	
		博士生	0	0	100%		
		博士後研究員	0	0	100%		
		專任助理	0	0	100%		

其他成果 (無法以量化表達之成果如辦理學術活動、獲得獎項、重要國際合作、研究成果國際影響力及其他協助產業技術發展之具體效益事項等，請以文字敘述填列。)	1. 建立國際學術聲望方面：藉由投稿國際期刊及參與國際學術會議，極有助於建立國際學術聲望。例如，計畫執行期間於 2012/6/25~27 前往義大利拿坡里參加國際學術會議「The 20th IASTED International Conference on Applied Simulation and Modelling 時，即被邀請擔任分組會議之主持人。另外，這一年半以來，亦曾被許多 EI/SCI 期刊之主編邀請審稿，邀請審稿之期刊至少包括「International Journal for Numerical and Analytical Methods in Geomechanics」、「Advances in Water Resources」、「Chinese Physics Letters Review」和「Heat Transfer」等。 2. 人才培育方面：指導參與本計畫案之兼任研究助理謝適任同學完成其碩士論文「單井抽水所引致軸對稱彈性沉陷之研究」。 3. 本計畫之研究成果中已發表於 EI 等級期刊論文一篇、EI 等級之國際會議論文兩篇，投稿後依審查意見修訂中之 EI/SCI 等級期刊論文一篇，經初步整理後擬繼續進行投稿之論文三篇。 4. 研究成果有助於改進教學，曾獲得中華大學九十九學年度優質教材開發獎勵競賽之「第一名」的肯定。 5. 研究成果有助於改進教學，曾獲得中華大學一〇〇學年度優質教材開發獎勵競賽之「第一名」的肯定。 6. 研究成果有助於改進教學，曾獲得中華大學九十九學年度「傑出教學教師獎」的肯定。

	成果項目	量化	名稱或內容性質簡述
科教處計畫加填項目	測驗工具(含質性與量性)	0	
	課程/模組	0	
	電腦及網路系統或工具	0	
	教材	0	
	舉辦之活動/競賽	0	
	研討會/工作坊	0	
	電子報、網站	0	
	計畫成果推廣之參與（閱聽）人數	0	

國科會補助專題研究計畫成果報告自評表

請就研究內容與原計畫相符程度、達成預期目標情況、研究成果之學術或應用價值（簡要敘述成果所代表之意義、價值、影響或進一步發展之可能性）、是否適合在學術期刊發表或申請專利、主要發現或其他有關價值等，作一綜合評估。

1. 請就研究內容與原計畫相符程度、達成預期目標情況作一綜合評估

■達成目標

□未達成目標（請說明，以 100 字為限）

□實驗失敗

□因故實驗中斷

□其他原因

說明：

2. 研究成果在學術期刊發表或申請專利等情形：

論文：■已發表 □未發表之文稿 □撰寫中 □無

專利：□已獲得 □申請中 ■無

技轉：□已技轉 □洽談中 ■無

其他：(以 100 字為限)

本計畫案之各項研究成果如附錄 1~9 所示，共計包括：

1. 已發表於 EI 等級期刊論文一篇，如研究計畫成果報告之附件 1 所示。
2. 投稿後依審查意見修訂中之 EI/SCI 等級期刊論文一篇，如研究計畫成果報告之附件 2 所示。
3. 已發表於 EI 等級之國際會議論文兩篇，如研究計畫成果報告之附件 3 與附件 4 所示。
4. 研究成果經初步整理後擬繼續進行投稿之論文三篇，如研究計畫成果報告之附件 6 至附件 8 所示。
5. 出席國際會議並擔任會議主持人，如研究計畫成果報告之附件 5 所示。
6. 人才培育：指導參與本計畫案之兼任研究助理謝適任同學完成其碩士論文「單井抽水所引致軸對稱彈性沉陷之研究」，如研究計畫成果報告之附件 9 所示。

3. 請依學術成就、技術創新、社會影響等方面，評估研究成果之學術或應用價值（簡要敘述成果所代表之意義、價值、影響或進一步發展之可能性）（以 500 字為限）

1. 過量抽取地下水導致地層下陷為目前台灣及世界各國普遍遭遇的問題。為解決抽水所引致的地層下陷問題，除依賴適當的教育宣導與法規的訂定，改變國人用水習慣與觀念外，亦應從工程上之學理分析層面切入，藉以瞭解抽水所引致的地層下陷機制與沉陷結果，其關鍵課題包括抽水所引致的地層位移變化量、及地層孔隙水壓變化量等的探討，本研究已分別探討出瞬時抽水、週期性抽水、點狀抽水、圓形平面抽水及線狀抽水等各種典型抽水所引致之三維壓密沉陷之閉合解，並繪製相關之應用圖表，可有助於瞭解此一問題的關鍵影響因素及其影響結果，研究成果能提供相關主管機關做為訂立相關規範之參考依據，故研究成果極具工程應用價值。

2. 研究成果至少已發表於EI等級期刊論文一篇、EI等級之國際會議論文兩篇，投稿後依審查意見修訂中之EI/SCI 等級期刊論文一篇，尚有多篇論文準備投稿中，故研究成果極具學術價值。